Title

Hot Atom Reactive Scattering and Photodissociation Experiments with Acetylene and Ethylene

Author

Balko, B.A.

Publication Date

1991-04-01

LBL-30655

Lawrence Berkeley Laboratory
UNIVERSITY OF CALIFORNIA

Materials & Chemical
Sciences Division

Hot Atom Reactive Scattering and Photodissociation Experiments with Acetylene and Ethylene

B.A. Balko
(Ph.D. Thesis)

April 1991

Prepared for the U.S. Department of Energy under Contract Number DE-AC03-76SF00098

DISCLAIMER

LBL-30655

HOT ATOM REACTIVE SCATTERING AND PHOTODISSOCIATION EXPERIMENTS WITH ACETYLENE AND ETHYLENE

Barbara Ann Balko

Department of Chemistry
University of California

and

Chemical Sciences Division
Lawrence Berkeley Laboratory
Berkeley, CA 94720 USA

April 1991

This work was supported by the Director, Office of Energy Research, Office of Basic Energy Sciences, Chemical Sciences Division, of the U.S. Department of Energy under Contract No. DE-AC03-76SF00098.

HOT ATOM REACTIVE SCATTERING AND PHOTODISSOCIATION EXPERIMENTS WITH ACETYLENE AND ETHYLENE

by

Barbara Ann Balko

ABSTRACT

Two different experimental techniques, chemical activation and photofragment translational spectroscopy, are used to study acetylene, ethylene, and their associated radicals: C_2, C_2H, C_2H_3, and C_2H_5. The experiments are done on a molecular beams apparatus with mass spectrometric detection.

The first type of experiment uses a photolytic D atom source to look at the dynamics of the D + C_2H_2/C_2H_4 → $[C_2H_2D/C_2H_4D]^*$ → C_2HD/C_2H_3D + H substitution reactions at 20 kcal/mole collision energy. The derived product center-of-mass angular and translational energy distributions show that, for both hydrocarbons, the reaction is direct and has an exit barrier. These observations are compared with RRKM estimates of the lifetimes of the complexes.

The other type of experiment involves 193 nm photodissociation of C_2H_2, C_2H_4, and $C_2H_2F_2$. The acetylene photodissociation studies give a new measurement for the H-CCH bond energy. The H atom time-of-flight spectrum shows

structure from the formation of vibrationally and electronically exited C_2H. It is also found that internally excited C_2H preferentially absorbs a photon and dissociates to yield C_2 photofragments in high electronic states.

Both the molecular and atomic elimination channels are studied in the ethylene photolysis. For the molecular channel, it is found that three-centered elimination is preferred over four-centered; the exit barrier observed is consistent with concerted elimination. In the atomic elimination channel, the C_2H_3 that forms readily absorbs a photon to give C_2H_2 in the lowest triplet state.

The 193 nm photodissociation studies of difluoroethylene give a better understanding of the ethylene photodissociation. Both the HF and H_2 molecular elimination channels are observed. The three-centered elimination is preferred over the four-centered and HF elimination occurs more easily than H_2. H and F atoms are detected in the photodissociation as well, although the mechanism for their production cannot be completely determined.

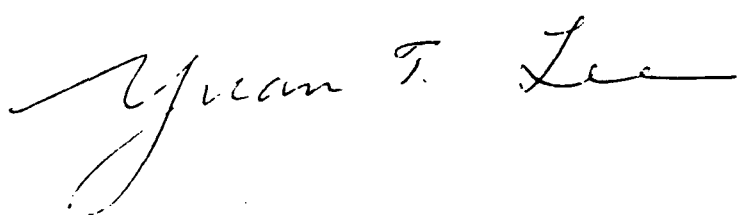

This thesis is dedicated to my parents
who made it all possible.

Table of Contents

List of Tables

Page

List of Figures

Chapter 4:

Chapter 5:

Chapter 6:

Chapter 7:

Acknowledgements

Graduate school is a difficult time in one's life. It is filled with late nights and early mornings, moments when you're sure you broke the $50,000 laser, and scientific egos. Eventually, the happy times--seeing signal and finally understanding what's going on--outweigh the bad. It's a credit to the people mentioned here and others whom I've inadvertently left out that I've been able to overcome all those barriers.

My research advisor, Yuan T. Lee, deserves a good deal of credit. His scientific knowledge, intuition, and experimental skills are legendary; I will only add that it's all true. Just as important to me, however, was Yuan's caring. He always wanted to make sure I was motivated and enjoying the science.

I was lucky to have many talented people help me on the 35" machine. Jinsong Zhang worked with me on all the experiments described in this thesis. He made the daily grind much easier and pleasant. He was always enthusiastic, ready and willing to work long hours, and had lots of ideas to improve the experiments. My training on the 35" machine came from Bob Continetti. I can't say enough about his dedication, experimental skills, and scientific knowledge. He helped make science fun and exciting again. I would also like to thank Professor Bill Jackson of UC, Davis for his

interest in the photodissociation studies that are described here. His many discussions helped us better understand the acetylene photochemistry.

My earlier years as a graduate student were spent on the A machine. Paul Weiss introduced me to molecular beams, lasers, and long hours. Jean-Michel Mestdagh was a great coworker and helped me learn to run the experiment. I finished my tenure on the A machine with Mike Covinsky; I benefitted from Mike's store of knowledge and his willingness to give me a significant role in the experiments. As I was leaving, Floyd Davis was becoming a part of the experiment; his hard work and motivation helped keep the A machine productive.

Dr. George Zimmerman at Bryn Mawr College, who was my freshman chemistry professor and later my senior research advisor, deserves much credit for starting me on my physical chemistry career. I have always admired his continual curiosity and his great love of science.

During my graduate years, I benefitted from the excellent UC, Berkeley and LBL staff. It always seemed as though the UC Berkeley machine shop could make or fix anything. Harry Chiladakis kept Giauque Hall running smoothly and taught us about cryogenic pumping. Phil Simon deserves much praise for his efforts to keep the helium liquefier in working order and making sure we weren't being overcharged for liquid nitrogen.

Ann Weightman has made working in the Lee group much easier. Her procedural knowledge and ability to break through the red tape made many of those emergency orders come through much faster and kept the pay checks flowing. I enjoyed talking with her especially when I needed to be reminded that there was a world outside of Giauque Hall.

During my time in the Lee group I had the privilege to learn from many talented people. As I'm leaving, it's exciting to watch them become professors and staff scientists. Laurie Butler and Mitchio Okumura were my first officemates and helped me through the traumatic early years of classes and prelims. Tim Minton introduced me to hiking in California and was always a good friend. Ralph Page, Alec Wodtke, Gil Nathanson, Gary Robinson, Anne-Marie Schmoltner, Xinsheng Zhao, and Eric Hinsta are also remembered for their scientific assistance and friendship.

The current Lee group members are a bright and hard-working group; I expect great things from all of them. I enjoyed collaborating with Evan Cromwell and Dr. Albert Stolow on the ethylene photodissociation. Dr. Matt Cótê was always available to answer scientific questions and give encouragement. Dr. Kim Prather has been an understanding friend and a good person to talk to about experiments past, present, and future. Pam Chu was my "neighbor" while the experiments in this thesis were carried out. It was nice to have her visit during data collection or to offer advice

when the machine was down. Pam should also be remembered for all the effort she put into setting up and keeping the microvax running in our early years at Giauque Hall and for keeping me going with hikes and other non-science activities. James Chesko deserves thanks for the time he has spent with the computer system. As I stored more and more data on the microvax, I became more and more nervous about losing it but James managed to bring my files safely through the virus attack and a crashed system disk. Good luck to the first years, Alan Bracker, Simon North, and Laura Smoliar, who show great promise and Lee group spirit. You often made me feel as though I had learned something in my time here.

Jim Myers deserves much credit for keeping me sane and happy throughout my years here. He has always been there for me; he brought me thermoses of coffee when I was working late, left flowers on my desk when I was sad, was my hiking/aerobics companion when I needed to get away, etc. We've climbed many mountains together and I hope we can climb some more.

My parents are most responsible for my obtaining my degree. Throughout my life, they have encouraged me to do the best I could and helped me in every way they could. They sacrificed much to get me where I am and I hope they will soon reap the benefits.

Finally, I would like to thank the National Science

Foundation who provided financial support for my first three years of graduate school. I am also grateful to Bryn Mawr College for the European Fellowship which assisted me in my later years. The experiments described in this thesis were supported by the Director, Office of Basic Energy Sciences, Chemical Sciences Division of the U.S. Department of Energy under Contract No. DE-AC03-76SF00098.

Chapter 1: Introduction

Choosing a title for this thesis was quite difficult in that two different types of experiments are discussed, hot atom reactive scattering and photodissociation. There is a unifying theme, however. Both experiments probe energy disposal in molecules and radicals that are important in combustion.

The D atom reactive scattering experiments with acetylene and ethylene described in Chapter 3 are an example of chemical activation in which the energy added to the system comes from the collision and the exothermicity of the addition reaction [1]. One learns about the intermediate complex, the vinyl (C_2H_2D) or ethyl (C_2H_4D), by seeing how efficiently the translational energy is randomized, estimating the lifetime, and determining whether substitution or decomposition back to the reactants is preferred. The experiments described in this thesis were carried out on the crossed molecular beams machine described

in Chapter 2. The time-of-flight (TOF) of the substitution product, C_2HD or C_2H_3D, is measured as a function of laboratory angle. Deconvolution of these spectra gives the product translational energy and center-of-mass (COM) angular distributions, $P(E_T)$ and $T(\theta)$. $T(\theta)$ reveals how long-lived the D-hydrocarbon complex is and the dynamics of the reaction. The $P(E_T)$ indicates if there is an exit barrier to the reaction and shows how efficiently the initial translational energy is transferred into internal energy. If the reaction complex is long-lived and the vibrational and rotational modes are actively involved in the energy randomization, the product energy distribution will be more statistical and the $P(E_T)$ will peak near zero when there is no exit barrier or close to the energy of this barrier if there is one. The other extreme is that the reaction is direct--the complex well does not "trap" the D atoms. In this case, the energy transfer will not necessarily be statistical and will depend on the dynamics of the reaction. Since the detected products are mass selected, it is also possible to look for other channels such as non-reactive scattering and hydrogen abstraction to see how these pathways are influenced by the complex well.

The photodissociation experiments put energy into the acetylene and ethylene molecules with 193 nm photons rather than D atom collisions. The hydrocarbon will be excited to a specific electronic state which can affect how the energy

is randomized. It is possible, however, that after the initial excitation, the molecule will internally convert to high vibrational levels of the ground electronic state; then a more statistical distribution of the initial energy would be expected, similar to what happens when a long-lived complex forms [2]. Unlike the D atoms, the photons supply enough energy to break bonds. The information from the photodissociation experiments comes from TOF spectra of the fragments. Assuming that at least some of the products are formed in the ground state and the parent molecules are internally cold, energy conservation shows that a measurement of the fastest fragment velocity will give the bond dissociation energy. Despite the relative simplicity of acetylene and ethylene (only 4 and 6 atoms), the bond strengths and heats of formation of these parents and their corresponding fragments are very poorly known [3]; any thermodynamic measurements such as those done here, then, will be of great value. In addition, in cases where the molecule dissociates to an atom, which cannot be vibrationally or rotationally excited, and a radical, the TOF spectrum will reflect the internal energy distribution in the radical fragment. The C_2H and C_2H_3 fragments are at least as poorly characterized as the corresponding parents so high resolution TOF spectra in which excited states can be seen is informative, especially for those states with low oscillator strengths. Furthermore, some of the

photofragments can spontaneously decompose or can absorb a photon and fall apart. Because of the inherent averaging involved in these secondary events, i.e. parent molecules with a wide initial internal energy range and velocity distribution will be involved, it is impossible to determine precise bond energies. One can, however, learn about the excited states of the resulting fragments and how the energy is distributed. In the photodissociation of acetylene and ethylene, there are several pathways that are thermodynamically open. Mass selection of the photofragments will show which of these channels are important.

The reactive scattering and photodissociation experiments involving C_2H_2 and C_2H_4, for the most part, probe different intermediates and products. While the reactive scattering involves the vinyl and ethyl complexes, the photodissociation experiments look at energy disposal in the C_2H, C_2H_3, and C_2H_2 photofragments. The vinyl radical is the only common intermediate, although the two experiments consider different energy regimes and excitation schemes. In the reactive scattering case, there is the exothermicity of the reaction to form the complex (~33 kcal/mole) in addition to the collision energy for a total of ~53-73 kcal/mole; in the photodissociation, there is a maximum of ~40 kcal/mole (the photon energy minus the C-H bond energy). The intermediates and fragments from both sets of

experiments, however, are all important in combustion processes [4]. The single collision conditions/well-characterized molecular beams used are quite different from the typical flame environment where reactants and by-products mix and multiple collisions can take place. To have any chance of understanding the more realistic situation, however, requires thermodynamic information as well as an understanding of energy transfer than can only come from "clean" experiments such as those described here where the individual collisions and half-collisions can be isolated. Although one normally associates oxygen reactions with combustion, H atoms are widespread in flames and have important roles because of their reactivity and typical high velocities. Acetylene and ethylene are also found in most hydrocarbon flames; acetylene, in fact, is believed to be the critical molecule in soot formation. The D atom reactive scattering experiments give an understanding of what happens when a fast moving atom collides with acetylene or ethylene. Does the radical live long enough so that it can further react or does it decompose? Competition between $C_2H_5 \rightarrow C_2H_4 + H$ versus $C_2H_5 + O_2 \rightarrow C_2H_4 + HO_2$, for example, is a determining factor in the combustion of ethane [4]. An understanding of how much energy is transferred to the hydrocarbon is also important in that it will show how internally excited the hydrocarbon becomes which will affect its further reactivity. The photodissociation experiments

provide thermodynamic information and give some idea of the fragmentation pathways and the excited states that will be involved. For example, they can show whether excited C_2H_4 is likely to fragment to $C_2H_2 + H_2$ or $C_2H_3 + H$.

The apparatus used for both the reactive scattering and photodissociation experiments is described in Chapter 2 with the emphasis on the D + hydrocarbon studies. In Chapter 3, the results of the D + C_2H_2 and D + C_2H_4 reactions are presented. In Chapter 4, the modifications required to go from reactive scattering experiments to photodissociation are discussed. Chapters 5 and 6 contain the results of the acetylene and ethylene 193 nm photodissociation. Finally, Chapter 7 describes the analogous photodissociation experiments on 1,1 and 1,2 difluoroethylene which were done to better understand the ethylene photochemistry.

References

1. For a review of chemical activation see B.S. Rabinovitch and M.C. Flowers, Quart. Rev. **18**, 122 (1964); B.S. Rabinovitch and D.W. Setser, Advan. Photochem. **3**, 1 (1964).

2. For a general discussion of photofragmentation translational energy spectroscopy see G.E. Busch and K.R. Wilson, J. Chem. Phys. **56**, 3626 (1972); A.M. Wodtke and Y.T. Lee, Advances in Gas Phase Photochemistry and Kinetics: Molecular Photodissociation Dynamics, edited by M.N.R. Ashfold and J.E. Baggott (Royal Society of Chemistry, London, 1987).

3. See, for example, D.F. McMillen and D.M. Golden, Ann. Rev. Phys. Chem. **33**, 493 (1982).

4. See, for example, C.K. Westbrook and F.L. Dryer, Eighteenth Symposium (International) on Combustion (Combustion Institute, Pittsburgh, 1981), p. 749; H. GG. Wagner, Seventeenth Symposium (International) on Combustion (Combustion Institute, Pittsburgh, 1979), p. 3; F. Kaufman, Seventeenth Symposium (International) on Combustion (Combustion Institute, Pittsburgh, 1982), p. 1.

Chapter 2: Hot Atom Reactive Scattering on the 35" Machine

1. Crossed Beams Machine

The crossed molecular beams machine used in these studies, the so-called 35" machine, is a high resolution version of that constructed by Lee et. al. [1]. The details of the design have been given elsewhere [2,3] so only a general overview of the features relevant to these experiments will be presented here. The machine supports two differentially pumped supersonic molecular beams. These beams cross under single collision conditions in the interaction region, the volume of which is determined by the slits and skimmers used to define the molecular beams. The detector rotates about this collision volume so that the angular distribution of the reaction products can be determined.

The detector consists of three differentially pumped chambers. The product molecules enter region I pass through a slit to region II, and then through another slit to region

III, the ionization chamber. The ultimate pressure in the ionization chamber is typically ~10^{-11} torr. The path length from the collision zone to the ionization region is 34 cm, the largest of this group's crossed molecular beams machines which is one factor responsible for its high resolution capabilities. In region III, positive ions are created from the product molecules by electron-impact; the ionizer design is based on that of Brink [4]. Focusing lenses facilitate transmission of the ions out of the ionizer region into the quadrupole mass spectrometer which is part of region II. The ions are accelerated to the "doorknob" held at ~-30kV which creates secondary electrons. These electrons are repelled by the same field into an aluminum coated scintillator. The resulting photons are detected by a photomultiplier tube (PMT). The doorknob/scintillator section is also part of region II.

The voltage pulses from the PMT are fed into a discriminator so low voltage pulses due to noise will not be counted. The logic output pulses from the discriminator are then amplified and sent to a multi-channel scaler (MCS) which records the signal counts in a set time interval (a maximum of 4096 channels in time intervals down to 0.1 to 0.15 μsec) [5]. The MCS is interfaced to a LSI-11/73 microcomputer through a CAMAC crate. This is the final link between the experiment and data collection.

2. Adaptation to Hot Atom Reactive Scattering

2.1. D Atom Beam (Primary Source)

The 35" machine was modified to study the D + H_2 reaction. The most significant difference from the conventional Lee group machines is the D atom source in which fast D atoms are generated by photolyzing DI. The source was designed by R.E. Continetti and the construction and considerations involved are described in detail in his thesis [2]. An overview is given here. Figure 2-1 shows the basic set-up. A home-built piezoelectric pulsed valve (0.75 mm nozzle) [3,6] is held on top of the primary source chamber. This chamber consists of two sections, an outer one and an inner one where the photolysis actually takes place. The pulsed valve nozzle fires into the inner chamber. The 248 nm output (KrF fill) of a Lambda Physik EMG 202 MSC excimer laser, is polarized with a pile-of-plates polarizer and sent into the machine through two lenses (19 and 24 cm Suprasil cylindrical lenses) that focus the laser output to a ~3x3 mm spot at the interaction region. The typical laser power is ~300 mJ/pulse before the polarizer. The laser beam is sent in perpendicular to the molecular beam and the two intersect ~3 mm below the nozzle. The photolysis chamber opens to the machine main chamber through a 3x3 mm slit. This slit collimates the D atoms produced in the photolysis region in a direction mutually perpendicular to the parent DI and laser beams and gives a

beam spread of ~7.5°. The DI pressure is adjusted to maximize the final D atom intensity at the collision region while minimizing the velocity-changing collisions experienced by the D atoms; ~140 torr was judged to be best.

The DI precursor used in these experiments is synthesized by reacting D_2 and I_2 over a platinum catalyst at ~800°C, following a procedure developed by Continetti [3]. Because of the corrosive nature of this reagent, special precautions have to be taken in its use. For example, the piezoelectric crystal in the pulsed valve had to be specially coated. The pumps in the source region also had to be protected. The inner photolysis chamber is pumped by a liquid-nitrogen cooled cyropanel as well as a 4" diffusion pump (DP) that used fomblin oil (an inert per-fluorinated polyether). The outer chamber is pumped by a cryopanel as well as a 10" DP (also filled with fomblin) backed by a corrosion resistant mechanical pump.

The photolytic beam provides D atoms with high translational energy (~95 x 10^4 cm/s and 134 x 10^4 cm/s for DI depending on the laser polarization). By photolyzing a diatomic such as DI in which neither fragment can become rotationally or vibrationally excited, one can limit the spread in product velocities to that from the distribution in initial parent internal energy. The energy broadeneing will be small because of the molecular beam expansion. DI has a fairly large cross-section at 248 nm (for HI the

cross-section is 5 x 10^{-19} cm^2 [7]). The one complication, however, is that both the ground ($^2P_{3/2}$) and excited ($^2P_{1/2}$) states of I are formed with $I/I^* \sim 1$ [8]. The electronic transitions which produce each state have different symmetries; for ground state I production, the transition moment is perpendicular to the bond while for I^*, the transition is parallel [8]. Experimentally, this makes it possible to use the polarizer to select the velocity of the D atoms and so the collision energy of the reaction.

2.2. Secondary Source

The secondary source is much simpler than the D atom (see Figure 2-1). The same type of piezoelectric pulsed valve (0.5 mm nozzle) is used. The valve is mounted in a separate chamber pumped by a 4" and a 10" DP. In the hydrocarbon experiments, neat beams with a stagnation pressure of ~300-350 torr were used. When acetylene was used, the gas was first run through a dry ice/acetone trap to remove acetone; acetone is added to acetylene cylinders to prevent decomposition. The secondary pulsed valve fires into the main chamber in the detector/D atom beam plane through a 1.5 mm diameter electroformed skimmer giving a beam divergence of 3.5°. A 15" DP with a 16" Tee attachment facing the secondary beam output at the main chamber door helps with the pumping [3].

3. Experimental Procedure

The hot D atom reactive scattering experiments consist of product TOF measurements at various laboratory scattering angles. In the hydrocarbon experiments, where the D for H substitution reaction is of interest, the selected product mass was one greater than the parent mass (C_2HD m/e = 27; C_2H_3D m/e = 29). A clock generator is used to control the experimental timing; it produces a voltage pulse at the desired frequency (typically 100 Hz). This pulse is sent to a pulse generator for shaping after which the output is split and used to control the primary and secondary pulsed valves. In the primary branch, the output frequency is divided by 2 and then used to trigger the DI pulsed valve power supply. The divided pulse is also sent to a digital delay generator, the output of which triggers the laser power supply as well as the MCS after first being sent through another pulse generator for shaping. Thus, the time between the primary pulsed valve pulse and the laser can be varied to optimize the production of D atoms but the MCS will always start counting when the laser is triggered. The secondary branch from the clock generator is not divided but sent to a digital delay generator and from there to a pulse generator for shaping before triggering the secondary pulsed valve power supply. This delay allows the timing between the D atom pulse and the hydrocarbon pulse to be changed to maximize overlap of the two pulses at the collision zone.

With this timing scheme, the primary pulsed valve runs at half the frequency of the secondary making it possible to take laser-on/laser-off measurements.

Because two iodine states are produced in the 248 nm photolysis of DI, two different velocity distributions of D atoms are observed. The TOF of the D atom beam at different laser polarizations is shown in Figure 2-2. By rotating the polarizer, it is possible to change the collision energy of the experiment, $(1/2)\mu(v_{rel})^2$, from ~20 to 40 kcal/mole so the effect of increased translational energy on the reaction can be studied. Knowing the collision energy and the exothermicity of the reaction allows one to calculate the maximum product translational energy release. Figures 2-3 and 2-4 show Newton diagrams for the D + C_2H_2 reactions at the two different collision energies assuming a ΔH of 0 kcal/mole for the substitution reactions. The D + C_2H_4 diagrams are virtually identical to those for acetylene since the D atom velocity and mass is the determining factor. For both collision energies, TOF measurements are taken at several different laboratory angles. To obtain a product angular distribution, the TOF signal is integrated at each angle.

The information that one ultimately obtains from these experiments is the relative reaction cross-section as a function of COM angle and translational energy which is frequently represented as a contour map of product flux. A

program has been developed in this group to fit the TOF data assuming an independent $P(E_T)$ and $T(\theta)$ for a reaction. The program convolutes the $P(E_T) \cdot T(\theta)$ product over the experimental apparatus function and calculates the TOF and angular distribution (in the laboratory frame) that would be expected. Through an iterative process, a $P(E_T)$ and $T(\theta)$ for the reaction can be obtained [9]. Only one significant change was required to use this program for the D atom reactive scattering experiments. The original program has a smoothing routine that takes into account the finite slit size of the cross-correlation wheel usually used to take TOF data. In these experiments, where there are no slits, this averaging is not done [10].

Use of the data analysis programs requires knowledge of the primary and secondary beam velocity and speed ratio as well as several machine constants (neutral molecule flight length, ionizer length, ion flight time constant). In these experiments, the D atom beam is characterized by recording the TOF spectra with the detector facing the source chamber and no secondary beam on (see Figure 2-2). This is done at the start of each experiment. The velocity distribution for the D atom beam can then be extracted from these TOF spectra with the appropriate Jacobian transformation (from N(t) to N(v)). The velocity distribution for the hydrocarbon beam is obtained by pointing the detector directly at the pulsed valve. A wheel with four slots (~0.8 mm wide) is mounted in

front of the detector and spun at 250 Hz to chop the beam (single shot TOF procedure). A delay is set-up between the wheel and the beam so the different parts of the pulse can be evaluated. The TOF peak position, full-width-half-maximum (FWHM), and area of the peaks from each section of the pulse are used to estimate the peak velocity and speed ratio ($V/\Delta V$) using the "traditional" 35° machine values for the detector parameters and time offsets. Because of the inherent velocity spread in the pulsed valve and the fact that the secondary beam has little effect on the reaction collision energy, a more careful measurement of the secondary beam parameters was not judged to be necessary. Figures 2-5 and 2-6 show the beam intensity versus the beam velocity for the two hydrocarbons with different beam conditions. The final values used in the analysis for both C_2H_2 and C_2H_4 are a peak velocity of 8.5×10^4 cm/s and a speed ratio of 2.5. Initially, a speed ratio of 5 was assumed which corresponds to the velocity distribution at the peak of the hydrocarbon pulsed output. The slow tail of the data, however, could not be fit unless a greater range of velocities was considered. It could not be determined if this greater velocity range was necessary because the velocity spread was truly this broad or whether this was one way of including slower collision energy reactions that were unaccounted for by the input D atom velocity distribution (see section 4.1).

The standard procedure for obtaining the detector parameters is single shot TOF [11]. The TOF spectra of the various fragments from a beam of CF_3I seeded in He are used to find the ion flight time constant. The neutral molecule flight length, effective ionizer length, and any offsets are derived from the TOF of rare gases, for which the terminal flow velocity can be predicted from $(5kT/m)^{1/2}$. The pulsed valve could not be used to obtain accurate values for the detector parameters. With the large diameter nozzle and lack of differential pumping, it was difficult to go to high enough backing pressures to obtain good expansions. Also, each part of the pulse has a characteristic velocity and speed ratio so care must be taken that the same part of the pulse is always sampled. This is especially a problem when the wheel frequency varies by even 1 to 2 Hz as it did when these measurements were taken since then the same part of the pulse will not always be chopped. The detector parameters, namely the flight path and ion flight time constant, were taken from earlier studies in which a continuous beam was used with similar detector conditions. Using these parameters along with the known DI bond energy and $I^* \leftarrow I$ spacing, the calculated D atom TOF spectrum matched the observed quite well so the true values must not deviate significantly from those used.

The secondary beam TOF procedure was used to determine if dimer formation was a problem. With a neat beam of

acetylene at ~300 torr, the dimer/monomer (m/e=52/m/e=26) ratio at the peak part of the monomer pulse was ~3 x 10^{-5}. In the later part of the pulse, the ratio was greater, ~1 x 10^{-3}. At a higher pressure of ~600 torr (the experiments were only run up to ~350 torr), the dimer/monomer ratio ranged from ~1 x 10^{-3} (peak) to 5 x 10^{-3} (late). There was no significant signal at m/e=51, a mass that the acetylene dimer would likely fragment to in the ionizer. Assuming that most of the dimer signal appears at m/e=52 or 51, then, there is < 0.1% dimer in the acetylene beam. The ethylene beam is not expected to be much different. In fact, other members of the group carried out ethylene photodissociation experiments with a similar pulsed valve and saw evidence of clustering only when the backing pressure was raised above ~500 torr or the ethylene was seeded with Ar to a total pressure of greater than 1 atm [12].

4. Problems Specific to D + C_2H_2/C_2H_4

4.1. D Atom Source

In principle, changing the secondary gas from H_2 to a hydrocarbon should have little effect on how well the D atom source functions. Problems, however, were encountered. The secondary region is physically separated from the lens/primary source section but in the initial experiments, it was found that effusive C_2H_2 was getting in the lens area and decomposing to leave a black, carbon-like deposit which

prevented the laser light from photolyzing the DI. Applying a plastic sealant to the lens tube/secondary source connection improved the situation enough so that it was possible to run experiments for a week before removing and cleaning the lens. The laser power actually reaching the DI precursor, however, would slowly decrease throughout the experiment.

A more troubling complication with the D atom source appeared later on when the data was being analyzed. The non-monoenergetic character of the D atom source confused the analysis. As shown in Figure 2-2, the polarizer does not totally eliminate the unselected D atom velocity component. In principle, this additional contribution can be handled by subtracting some fraction of the corresponding unselected polarization TOF spectrum at each angle after all the scans have been normalized to the observed laboratory angular distributions. There are two problems with this. First, it is not entirely clear how much to subtract. Since the unselected scan ideally consists of just the two pure polarization spectra, one could subtract until just before a negative dip appeared, assuming the two TOF spectra did not completely overlap. The other problem, however, makes this method somewhat questionable. Figure 2-7 shows what happens when the selected D atom TOF scan is scaled to the unselected peak. A third, broad component that results from D atom collisions in the photolysis region is present. This

underlying component makes it impossible to determine exactly how much of the unselected D atom signal to subtract since these D atoms will also react. To analyze the data, the input D atom velocity distribution can be expanded to include the values but this assumes that the $P(E_T)$ and $T(\theta)$ for scattering with these atoms is not significantly different from the main pulse. For the low collision energy data, the presence of the unselected D atoms does not have much effect, but for the higher energy scans, it means the $T(\theta)$ cannot be derived.

In addition to the opposite polarization contribution and underlying contamination, the D atom pulse contained a significant fraction of slow atoms ($\leq 60 \times 10^4$ cm/s). A large number of D atoms formed in the DI photolysis do not immediately exit the source chamber; some of these that are not pumped away will suffer thermalizing collisions with other molecules or the walls and may then leave through the slits. This is why the D atom TOF spectra shown (Figure 2-2) does not go to zero at long times. In the D + H_2 experiments, these were not a problem because of the large energy barrier to reaction. This is not the case, however, in the hydrocarbon substitution reactions. A slow signal with very little angular dependence is seen in both polarization scans. This invariance with respect to collision energy and laboratory angle suggests that this signal may be from reaction of these slow, thermalized D

atoms which are present in both collision energy experiments. The products (reactive and non-reactive) from this thermal component will appear at slow times within the reactive circles for the selected D + hydrocarbon substitution reactions. No attempt was made to model this slow signal because it was not that large and the velocity spread of the contributing D atoms was too broad.

The final problem that will be discussed is the presence of a m/e=27 and 29 (no m/e = 28 or 26!) background in the DI precursor. Looking near the primary beam with no laser and no secondary source firing, one could observe a very slow thermalized pulse related to the operation of the DI source. In the experiments, this pulse was not completely pumped out before the laser-off secondary valve fired. The problem was only significant at angles close to the primary beam (20-30° away [13]) and caused there to be more steady state background at the beginning of the laser-off TOF scan. This did not have a significant effect on the laser-off TOF shape and the scan could still be used for subtraction purposes. Freezing the DI cylinder and then pumping the noncondensables out reduced the contamination which, in any case, slowly disappeared as the cylinder was used. Most of the data collection, however, was carried out using DI that did not have this contamination since it only appeared when a newly synthesized DI sample was used. It was never determined what impurity was responsible. The one

interesting note is that the same problem was observed with a commercial cylinder of DBr.

4.2. Secondary Source

In detecting the substituted product, DCCH or HDCCHH, there was background from the C^{13} containing parent molecules (the natural abundance of C^{13} is 1.1% [14]). Because the secondary beam did not have a second region of differential pumping and was close to the interaction region (3.86 cm), both of which were required to have sufficient intensity to see reaction, there was a large amount of background at angles as far as 30° away. Since this background originates from the pulsed valve, it is temporal; a peak grows in ~1000 μsec from the time the laser fires. The temporal pulse background problem was greatest at angles ≤ 20° and ≥ 60°. The increase at angles ≥ 60° can be understood since the detector is getting closer to the secondary beam. The cause for the background rise at angles farther from the secondary source is more difficult to explain. Because the effect is present without the primary beam on, beam scattering is not responsible. Scattering off the box around the collision zone is the most reasonable explanation. When the secondary source chamber was designed for the D + H_2 experiments, this box was added to support slits to keep main chamber background out of the collision region [3]. These slits were never necessary but the box

could not easily be removed.

The reactive signal is not completely gone when the temporal background from the parent pulse begins to grown in, so a way to subtract and/or eliminate this background must be found to see the slow tail of the reactive signal. Initially, this was done by taking no-laser scans at each angle throughout an experimental run. The background pulse would then be scaled to the parent peak in the laser-on and subtracted. This subtraction method failed miserably for two reasons. The first, which was only fully realized later on, is that the laser-on signal contains a significant amount of non-reactive signal that appears at approximately the same time as the parent pulse. This non-reactive signal means that scaling the no-laser scans to the peak of the parent pulse to subtract out is not correct. The other problem is that the laser-off background scans would change shape significantly during the course of an experiment. This is probably due to a combination of factors such as changes in the pulsed valve behavior and differences in pumping speed throughout the run. Thus, when attempts were made to subtract the background signal, it was often found that the slope of the rising edge had changed.

Two approaches were taken to control the secondary source background problems. First, the overall parent background in the detector and main chamber was reduced by installing a 20K Cu cryopanel. A Koch He liquefier

circulated cold, compressed He gas which cooled the Cu panels to ~10-20K as measured with a LakeShore Cryotronics thermosensor mounted on the panel. The panel was constructed so that the detector would always face this cold surface (see Figure 2-8). This served to eliminate detector background that originates from main chamber molecules that bounce off of surfaces within the detector viewing angle. Figure 2-9 shows secondary backgrounds (no D atom beam) taken at 40° and 60° before and after the installation of the cryopanels which illustrate the two effects that the panel has. First, it significantly reduces the amount of hydrocarbon entering the detector from the pulsed valve; the ratio of peak height to detector background is reduced from 5 to 0.4 at 40° and from 10.5 to 3 at 60°. Second, the cryopanel changes the shape of the background pulse; there are less slow hydrocarbons. This is probably from the overall pumping the panel does; parent molecules that would have entered the detector after collisions with the box are instead pumped away.

After the success of the main chamber 20K panel, another one was installed in the secondary source chamber. This cut down the pulsed background somewhat and helped with the pumping but did not have the same dramatic effect. Later on an extension was added that was held between the nozzle and skimmer. This reduced the background parent pulse considerably as well as the reactive signal.

Evidently, this cold piece was cooling the skimmer and/or pulsed valve, reducing the amount of hydrocarbon reaching the collision zone, so after several unsuccessful attempts to reposition it and heat the valve, the cryoextension was removed.

The other change made to control the background was to run the secondary beam at 100 Hz and the D atom beam/laser at 50 Hz. By counting for ~11,500 μsec, a single TOF scan would consist of the laser-on signal followed by the laser-off. Separating the two and then directly subtracting them would give the signal due to the D atom beam. At most angles this subtraction was straightforward. Closer to the secondary beam, however, because the parent background pulse was so large, any slight error (<1 μsec, a fraction of a channel) in choosing the zero for the laser off signal would cause a peak or a dip to appear upon subtraction. Again, because of the slow laser correlated signal, the offset for the laser-off signal could not be determined by matching the background peaks. The time zero was finally established by taking no-laser/no-laser scans and varying the offset until the subtraction yielded a flat line.

The laser correlated signal, then, was obtained by the correct subtraction of the laser-off signal from the laser-on (see Figure 2-10a). To minimize the noise introduced by the subtraction, the laser-off signal was first fit with a polynomial. The laser correlated signal consisted of two

parts. The fast part varied with lab angle, was significantly different for the two collision energies studied, and disappeared when the parent mass was selected. The slow part, however, was essentially the same at all lab angles, at both collision energies, and was also present at the parent mass. At the lower collision energy, this product was just barely thermodynamically possible and the corresponding product expected, assuming cylindrical symmetry about the relative velocity vector, was not seen. These observations all indicate that this signal is from scattering of the hydrocarbon beam off some component in the D atom beam, perhaps slow D atoms or a secondary product (HD, D_2, H_2) produced by the laser. To study the substitution reaction signal, this slow signal needed to be subtracted away. Laser-on/laser-off scans were taken at the parent mass. To achieve the best signal for the non-reactive component, the scans from all the collision energies and angles were added (there were some differences in the slow tail but none in the rising edge). The slow signal then could be subtracted away (see Figure 2-10b). To reduce the noise added by the subtraction, the slow signal was fit with a polynomial before subtraction. This gave a good estimate of the slow edge of the reactive signal.

References

1. Y.T. Lee, J.D. McDonald, P.R. LeBreton, and D.R. Herschbach, Rev. Sci. Instrum. **40**, 1402 (1969).
2. R.K. Sparks, Ph.D. Thesis, University of California, Berkeley (1979).
3. R.E. Continetti, Ph.D. Thesis, University of California, Berkeley (1989).
4. G.O. Brink, Rev. Sci. Instrum. **37**, 857, 1626 (1966).
5. P.S. Weiss, Ph.D. Thesis, University of California, Berkeley (1986).
6. D. Proch and T. Trickl, Rev. Sci. Instrum. **60**, 713 (1989).
7. G.W. Flynn and R.E. Weston, Jr., Ann. Rev. Phys. Chem. **37**, 551 (1986) and references therein.
8. G.N.A. Van Veen, K.A. Mohamed, T. Baller, and A.E. DeVries, Chem. Phys. **80**, 113 (1983).
9. A.-M. Schmoltner, Ph.D. Thesis, University of California, Berkeley (1989) and R.J. Buss, Ph.D. Thesis, University of California, Berkeley (1979).
10. For those familiar with the GM series of programs, the subroutine Trap was removed.
11. D.J. Krajnovitch, Ph.D. Thesis, University of California, Berkeley (1983) and M.F. Vernon, Ph.D. Thesis, University of California, Berkeley (1983).
12. A. Stolow, E.F. Cromwell, and Y.T. Lee, to be

published.

13. All angles given in this thesis, unless specified, are measured with respect to the D atom beam.

14. CRC Handbook of Chemistry and Physics (CRC, Cleveland, 59th ed., 1980).

Figure Captions

Figure 2-1. Overhead view of the hot atom reactive scattering experimental configuration. The DI pulsed valve (1) sits on top of the source photolysis chamber. The polarized output of an excimer laser enters the chamber through a beam tube (2) and intersects the DI beam perpendicularly. Some of the D atoms created leave the source chamber through slits in the chamber that are mutually perpendicular to the laser and parent DI beams. The hydrocarbon (secondary) pulsed valve (3) is located in a separate chamber. This valve fires in the D atom/detector plane. A skimmer helps collimate the beam. The D atoms and hydrocarbons meet in the collision volume (4) where reaction can take place. The products are detected by a rotating mass spectrometric detector (5).

Figure 2-2. Representative TOF spectra of the D atom beam used in the experiment. The laser output is polarized (a) perpendicular or (b) parallel to the detector/D atom plane. The two scans were taken one after the other on the same day and represent the same number of laser shots.

Figure 2-3. Newton diagrams for the D(fast) + C_2H_2 → C_2HD +

H reaction. In (a), the solid line represents the maximum product translational energy and the dashed line the translational energy for elastic scattering of the C_2H_2. (b) is an enlargement of the region of interest. The laboratory angles studied were 10° intervals between 20 and 60°. The COM angle (θ) is measured with respect to the relative velocity vector. The COM product velocity (u_{HCCD}) is measured from the COM of the reaction.

Figure 2-4. Same as Figure 2-3 but for D(slow) + C_2H_2; the scales for both figures are the same. With the slower D atoms, the COM angle moves closer to the secondary beam so an additional laboratory angle, 65°, was studied.

Figure 2-5. Acetylene signal (area of TOF peak) versus beam velocity. Solid line shows the distribution for reactive scattering conditions (360 torr; 40μsec pulse width; 450 V piezo-electric pulse); the dashed line is the distribution for the high resolution photodissociation experiments described in Chapter 4 (80 torr; 100 μsec; 500V); the dotted line is the distribution for the low resolution photodissociation experiments (70 torr; 50 μsec; 400V).

Figure 2-6. Ethylene signal (area of TOF peak) versus beam velocity. Solid line shows the distribution for reactive scattering conditions (330 torr; 40 μsec pulse width; 450 V piezo-electric pulse) and the dashed line is the distribution for the photodissociation experiments described in Chapter 4 (50 torr; 50 μsec; 400V).

Figure 2-7. (a) Fast D atom TOF spectrum scaled to the slow spectrum. (b) Slow D atom TOF spectrum scaled to the fast. These show the D atom velocity spread present in the beam due to collisional broadeneing.

Figure 2-8. Enlargement of collision region (1) showing the 20K cryopanel. The panel was held against the box surrounding the collision region by pins (2) to prevent extensive heat transfer. The panel extended into the secondary source skimmer (3) so that even when at 60°, the detector would see a cold surface. The panel had extra pieces (4) to help with general main chamber pumping.

Figure 2-9. M/e = 27 background scans (no D atom beam) at (a) 40° and (b) 60°. The open circles are the data taken before the installation of the cryopanel and the solid line is the TOF scans taken after.

Figure 2-10. Background subtraction involved in the data analysis. D(slow) + C_2H_2 taken at 50° is used as an example. (a) Laser-on (open circles) and laser-off (solid line) showing the fast and slow laser correlated signal. (b) Open circles are the laser-on minus laser-off signal. Solid line is the non-reactive signal that is scaled to the slow peak/rising edge and subtracted.

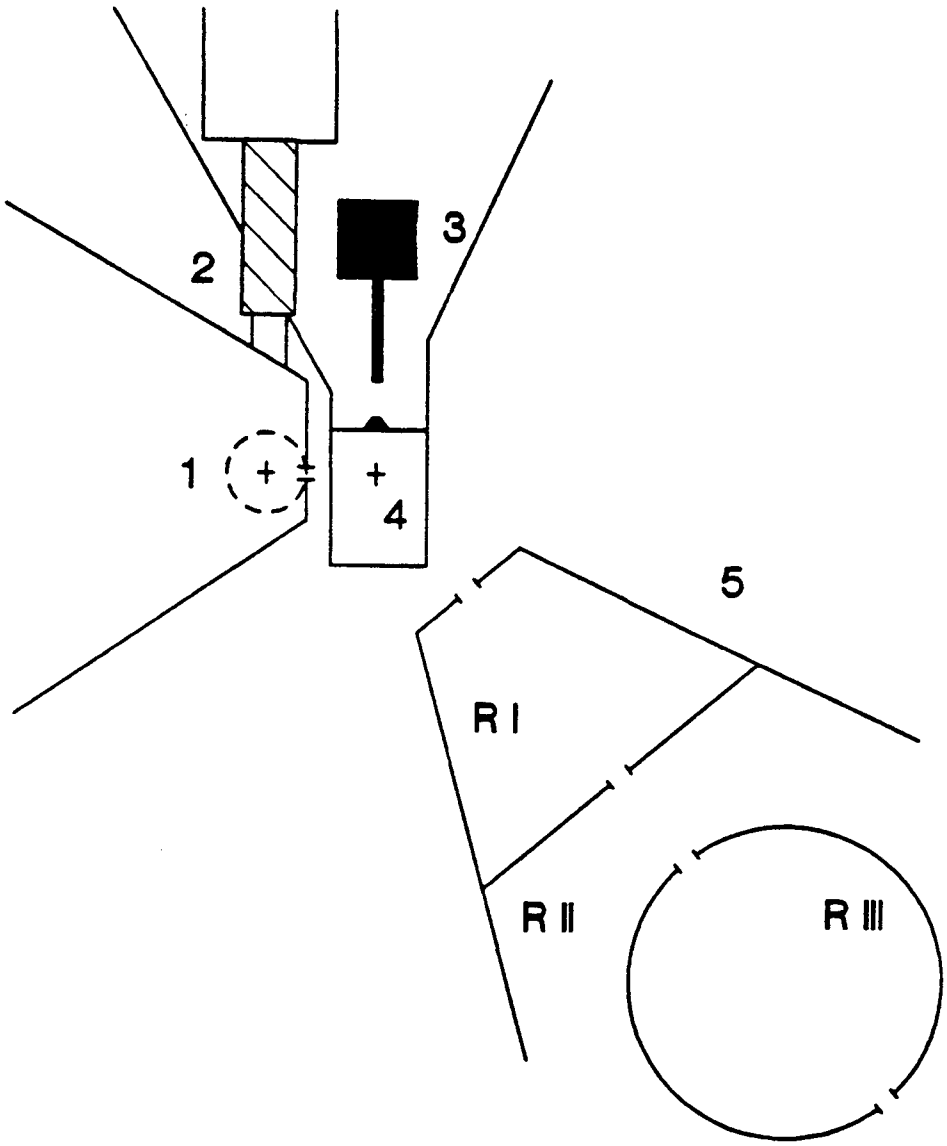

Figure 2-1

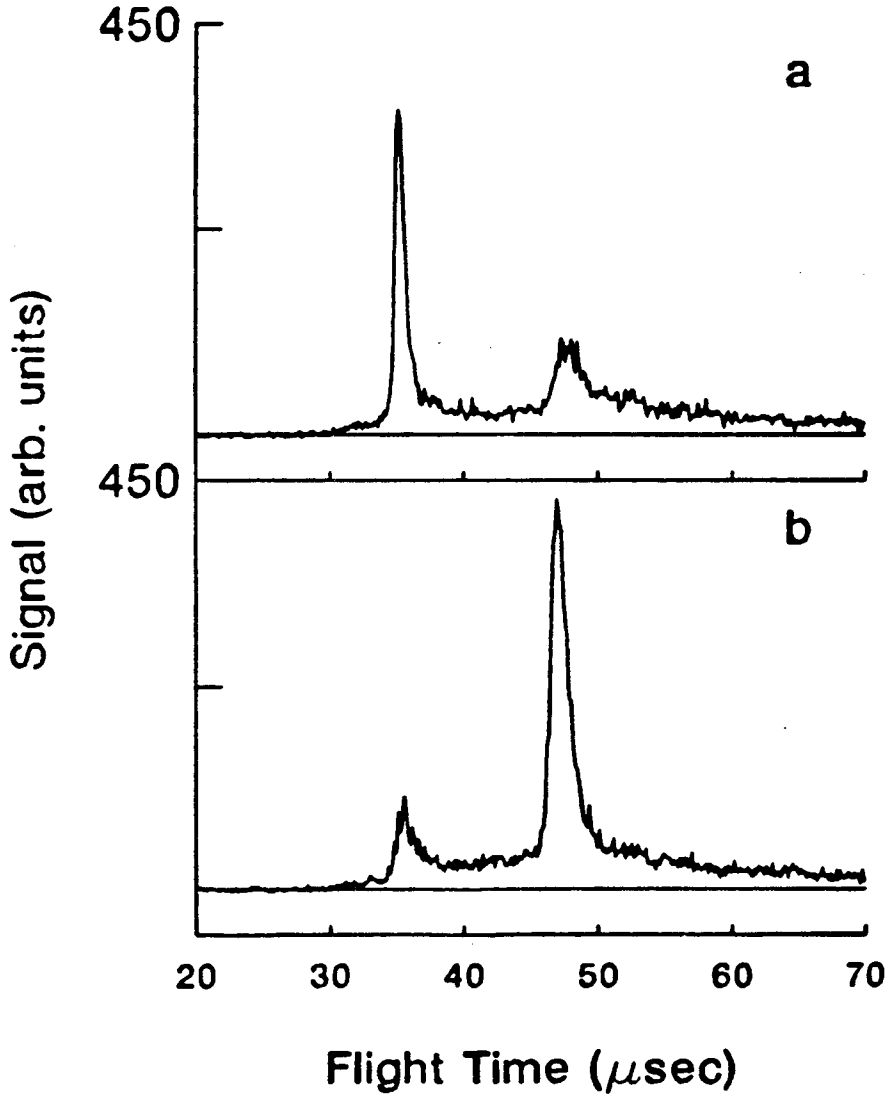

Figure 2-2

a

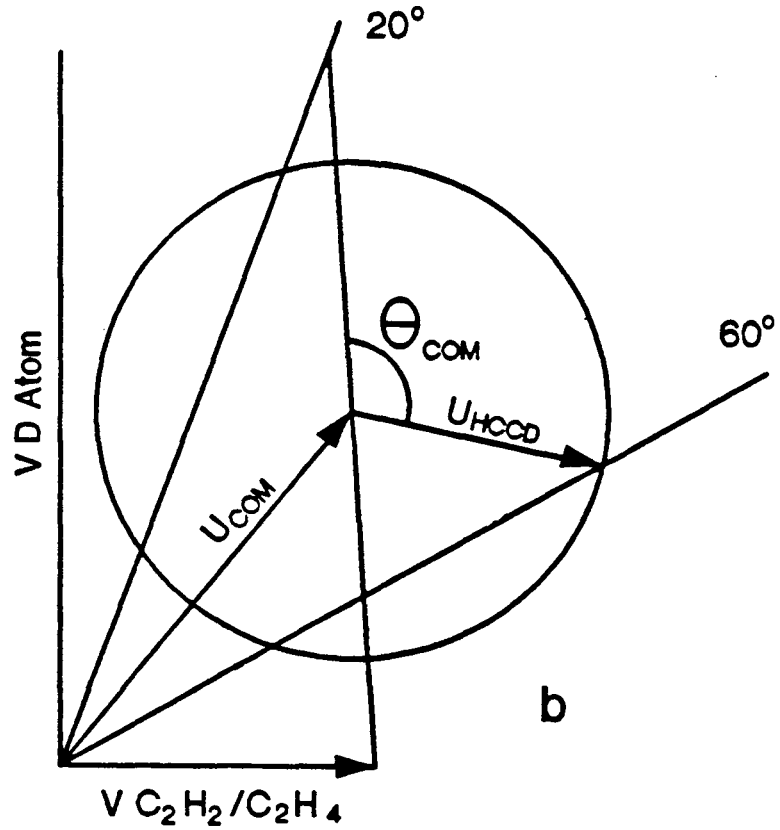

b

Figure 2-3

a

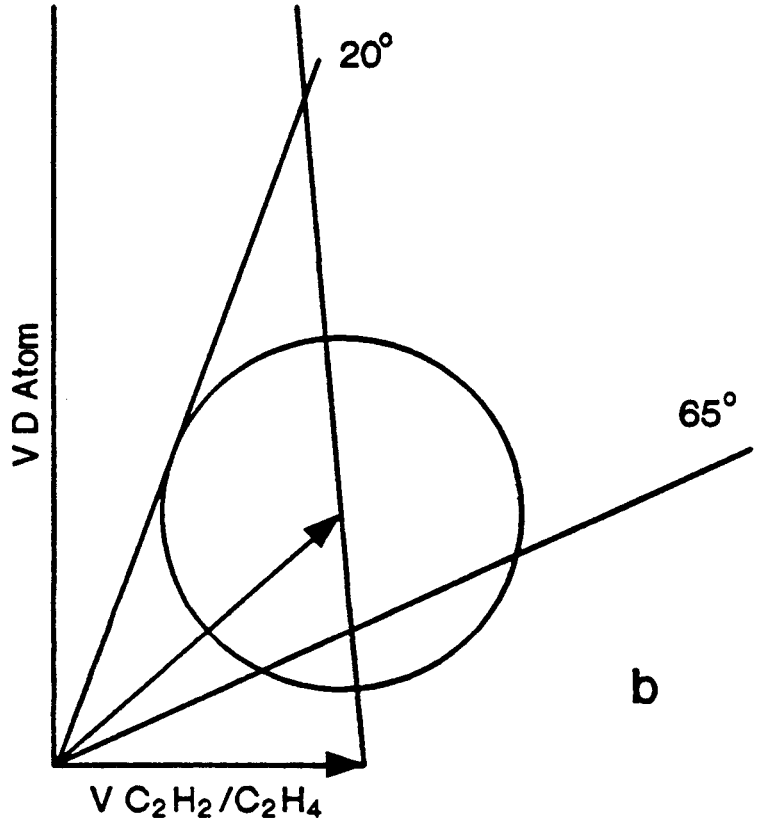

Figure 2-4

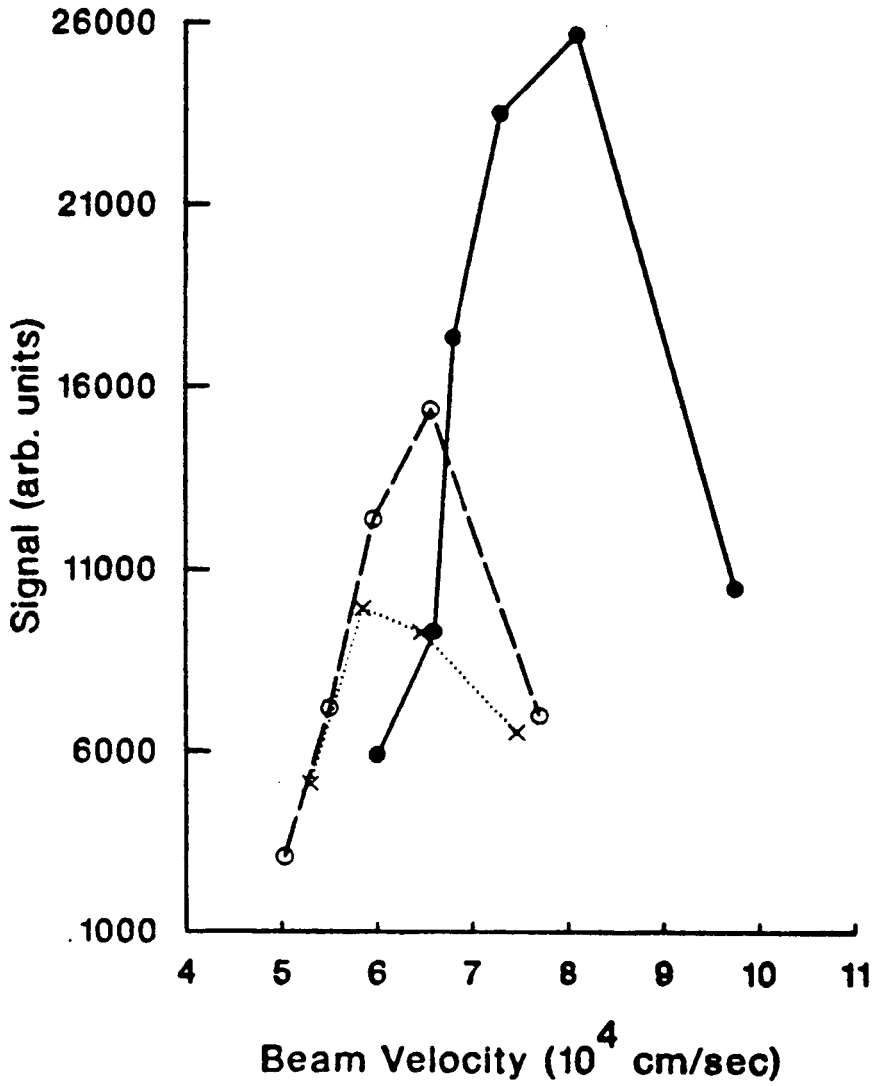
26000
21000
16000
11000
6000
1000
Signal (arb. units)
4
5
6
7
8
9
10
11
Beam Velocity (10^4 cm/sec)

Figure 2-5

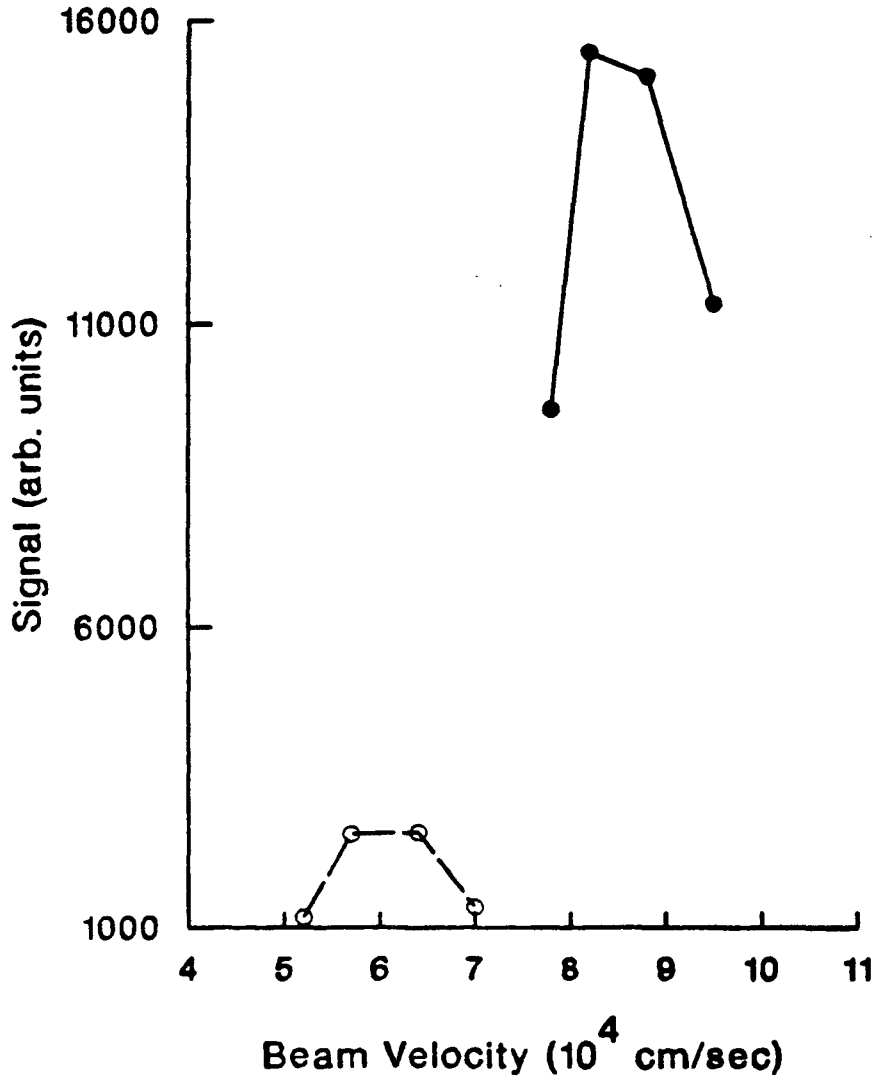
16000
11000
6000
1000
Signal (arb. units)
4
5
6
7
8
9
10
11
Beam Velocity (10^4 cm/sec)

Figure 2-6

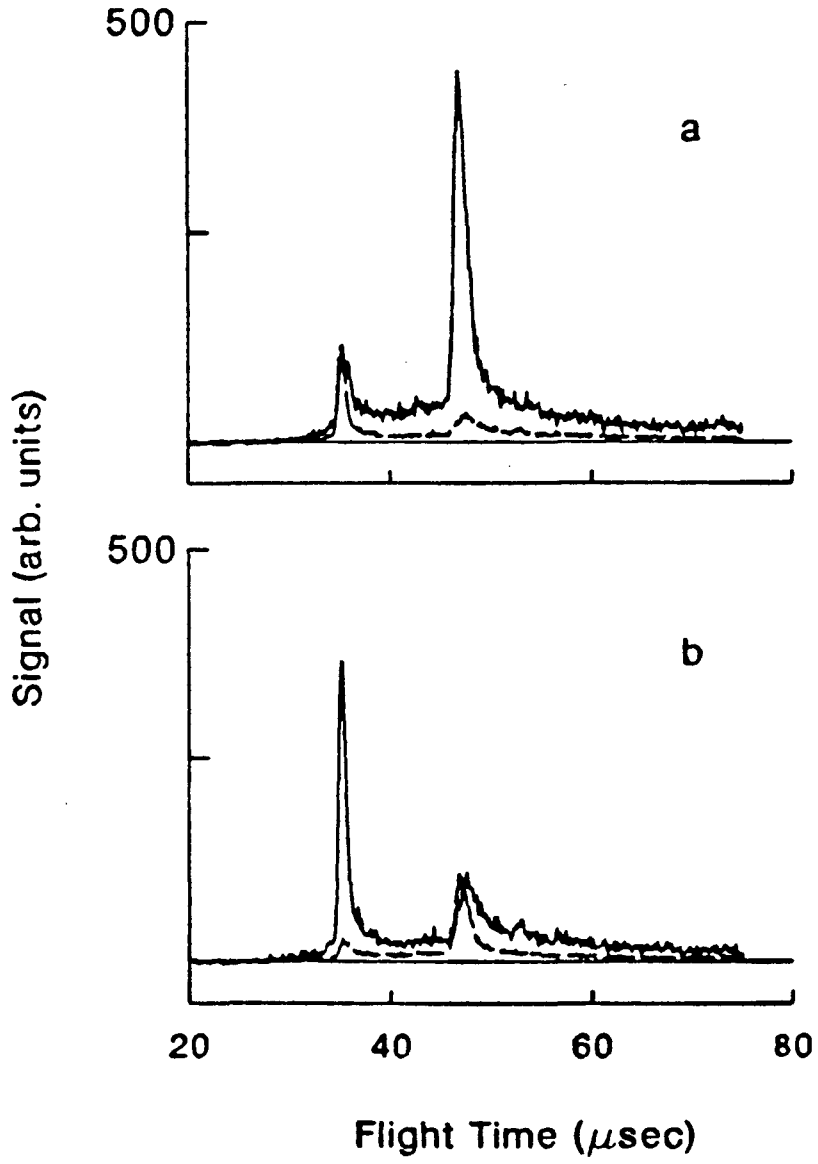

Figure 2-7

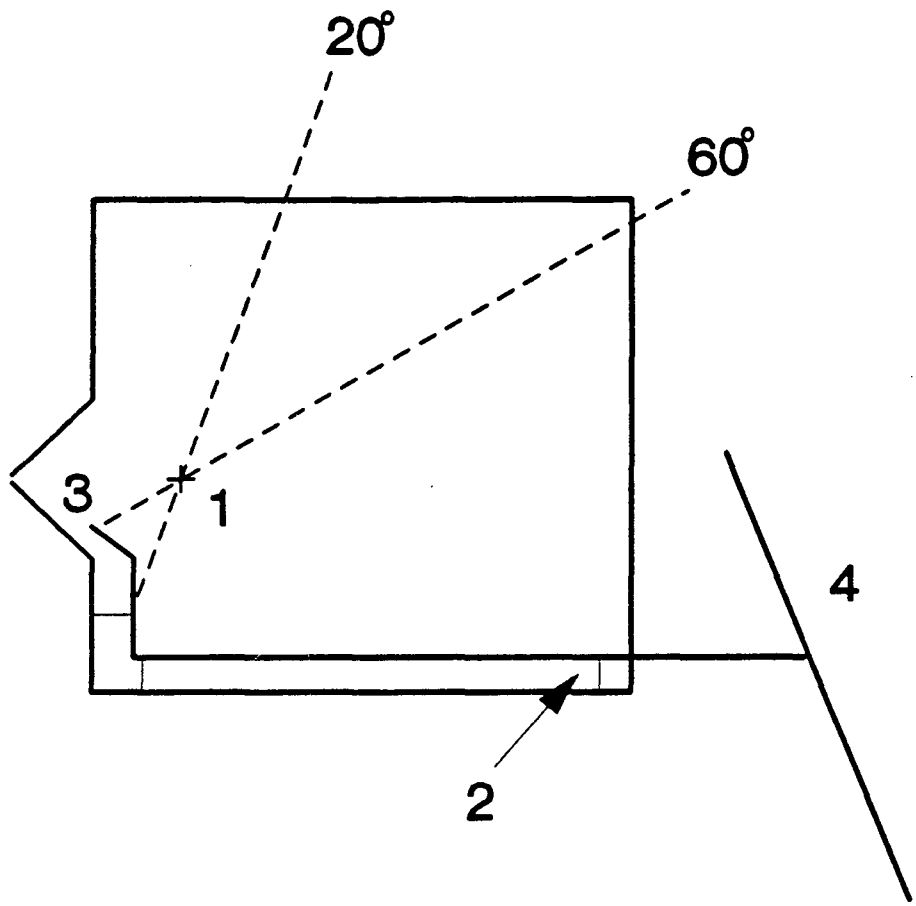

Figure 2-8

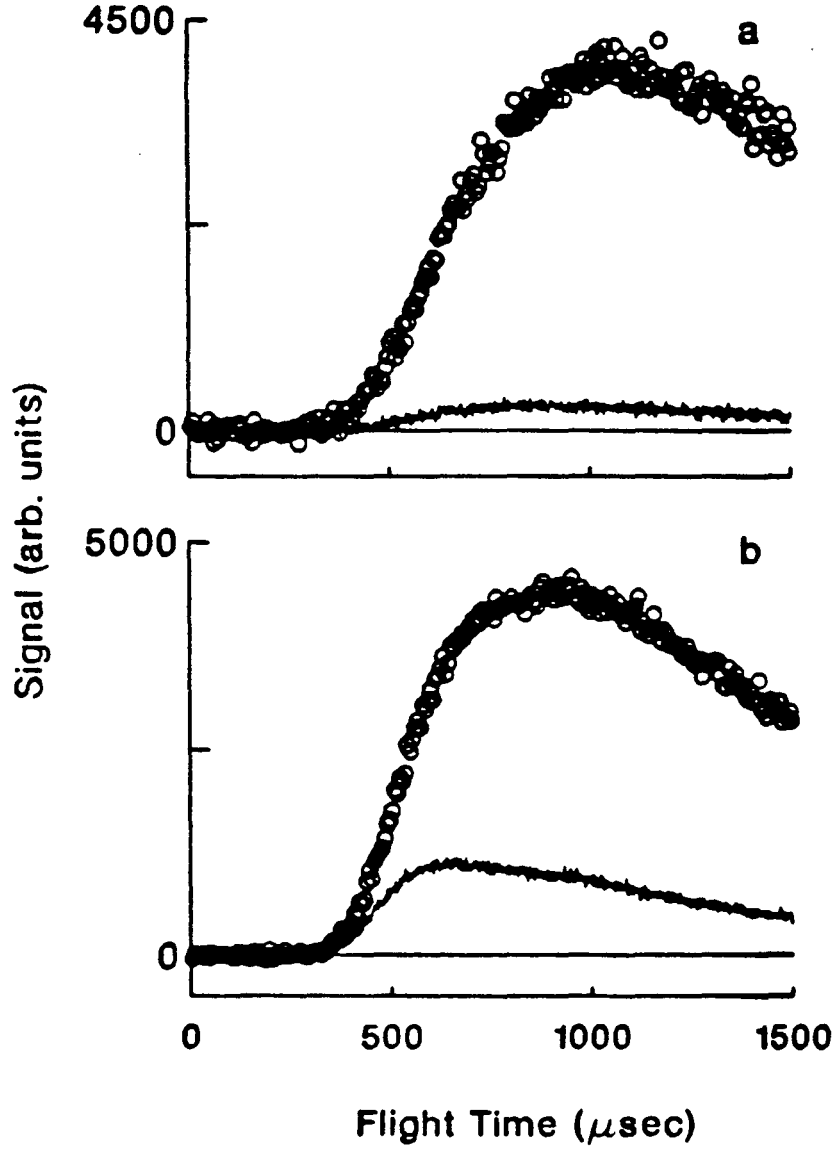
4500
a
0
5000
b
0
0
500
1000
1500
Signal (arb. units)
Flight Time (μsec)

Figure 2-9

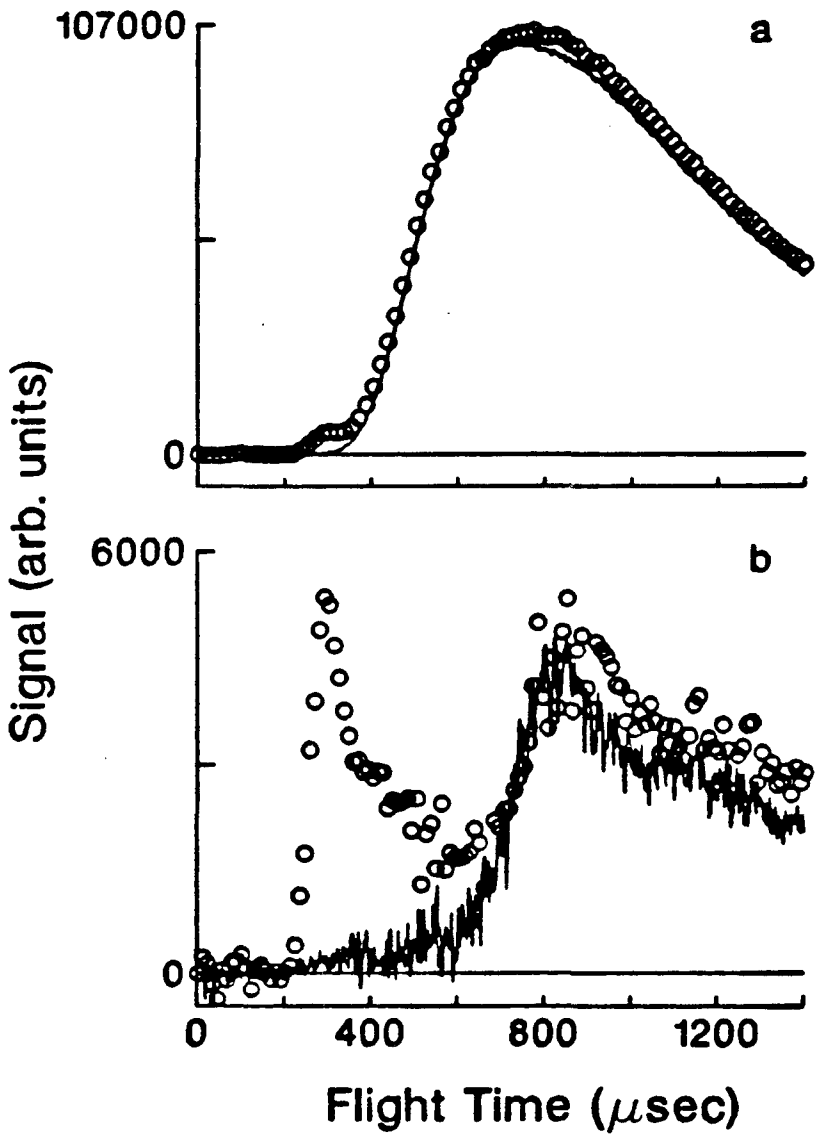
107000
a
0
6000
b
0
0
400
800
1200
Signal (arb. units)
Flight Time (μsec)

Figure 2-10

Chapter 3: D Atom Reactive Scattering with Acetylene and Ethylene

1. Introduction

Chemical activation in which an excited intermediate is produced by the collision of two reactants has been studied for some time [1]. The complex that forms can be collisionally stabilized or can decompose either into the original reactants or new products. Early measurements of the reaction rates of these various channels provided a test of statistical models of energy distribution. The effect of initial collision energy on the energy randomization in these complexes, especially at energies where the lifetime of the complex will be comparable to the rotational period is of much interest. To reach this regime in systems containing several atoms usually requires collision energies equal to the complex stabilization energy [2]; for reactions involving stable intermediates, such as the vinyl or ethyl radical, this complicates the experiment because

collision energies as high as 2 or 3 eV will be needed. With the development of photolytic ("hot") H atom sources, which can provide collision energies on the order of 1 to 3 eV, such complexes can be probed [3]. Especially promising are the recent photolytic Van der Waals HX·(molecule) experiments (where X is a halogen) in which the orientation of the H atom attack is defined by the initial Van der Waals geometry [4]. By studying how efficiently the translational energy of the fast H atom is transferred into the internal modes of the molecule it is colliding with, one learns about the energy randomization process and the nature of the potential energy surfaces of the complexes. If the vibrations/rotations of the products that are excited can be identified, even more detailed information can be extracted about the relative efficiency of different H atom approach geometries and impact parameters. Collisions in which there are reaction channels such as abstraction are even more interesting since product channels are expected to depend on approach geometries.

The collision of translationally hot H atoms with hydrocarbons, specifically acetylene and ethylene, is a good choice for chemical activation studies. First, the experiment is of practical value since the reactants and intermediates have important roles in combustion processes. Second, the intermediate radicals, C_2H_3 and C_2H_5, are quite stable [5,6]:

$$H + C_2H_2 \rightarrow C_2H_3 \quad \Delta H°(OK) = -33 \pm 1 \text{ kcal/mole} \quad (I)$$

$$H + C_2H_4 \rightarrow C_2H_5 \quad \Delta H°(OK) = -35 \pm 1 \text{ kcal/mole} \quad (II)$$

At the collision energies available in these experiments (20 and 40 kcal/mole), then, the reaction may involve a long-lived complex at the lower energy but not at the higher; it will be of interest to see to what extent the complex influences the collision dynamics. Third, two reaction channels, H abstraction and substitution, are possible. The substitution is thermoneutral. The heats of reaction for the abstraction reactions are as follows [5,6]:

$$H + C_2H_2 \rightarrow H_2 + C_2H \quad \Delta H°(OK) = 28 \pm 1 \text{ kcal/mole} \quad (III)$$

$$H + C_2H_4 \rightarrow H_2 + C_2H_3 \quad \Delta H°(OK) = 7 \pm 1 \text{ kcal/mole} \quad (IV)$$

In this chapter, the collision of fast D atoms with acetylene and ethylene is described. D atoms are used so the substitution product can be followed. The translational energy of the C_2HD or C_2H_3D product is measured as a function of laboratory angle to give the COM angular and product energy distributions. The net reactions, $D + C_2H_2 \rightarrow C_2H_2D \rightarrow H + C_2HD$ and $D + C_2H_4 \rightarrow C_2H_4D \rightarrow C_2H_3D$, will be slightly exothermic (1-2 kcal/mole) due to the differences in the zero point energies of the various isotopomers [7,8]. The barriers for addition to acetylene and ethylene are ~2.5 kcal/mole and 2.75 kcal/mole respectively [9-14]. The abstraction barrier for reaction III, 32.4 kcal/mole, is much higher [15]. A barrier at least equal to the reaction endothermicity would be expected for abstraction from

ethylene. Figure 3-1 shows a simple potential energy diagram for the substitution reactions studied. Since the two systems have similar barriers to H atom addition and the resulting complexes have approximately the same stability, the differences observed will reflect the individual geometries, the greater number of vibrational modes in the ethyl radical (15 versus 9 for the vinyl radical) and the different energetics for the abstraction channel.

The addition reactions of H + C_2H_2 and C_2H_4 and subsequent decomposition have been well studied both experimentally and theoretically. Two recent ab initio calculations have been done on the H + C_2H_2 transition state [7,15]. The H atom approaches HCCH and adds to form an intermediate with trans geometry; a bridge structure is not expected because it would involve greater repulsion with the π electrons. The transition state is generally described as loose although there is some disagreement about this point [10,15]. The term loose implies that all the complex frequencies are similar to the reactants' except for those of the new vibrations which are very low frequency; in a tight complex significant changes in geometry are required to reach the transition state [16]. More detailed trajectory studies have been done on the H + C_2H_4 addition reaction [14]. The cross-section reaches a maximum at ~40-60 kcal/mole translational energy. Increasing the kinetic energy results in collisions in which the H atom interacts

strongly with C_2H_4 but does not add because there is not sufficient time for the necessary geometry changes. Like the H atom addition to acetylene, theoretical studies have suggested that the transition state is fairly loose [6,8,10]. The major difference between H atom addition to acetylene and ethylene is that the ethylene transition state more closely resembles the initial reactants -- free radicals add to olefinic bonds easier than to acetylinic [7].

Most of the experimental work has focussed on determining the rate equations for addition at fairly high pressures where there is competition between collisional stabilization of the addition complex and decomposition [8-11,13,17-19]. While these studies provide some understanding of energy partitioning in the activated complex, the experiments are difficult to interpret dynamically because of the many collisions that occur. Single collision measurements of the product angular and energy distributions are required to compare with the trajectory and ab initio calculations that have been done and to stimulate more. Bersohn's group [20] has looked at the isotope exchange reaction of ~1 eV H atoms with deuterated acetylene, methylacetylene, ethylene, and propylene under approximately single collision conditions and measured the relative number densities of H and D atoms to determine the reaction cross sections and the product D

atom average translational energy. Based on the fraction of available energy transferred into product vibrations as a function of the number of internal modes, they concluded that long-lived complexes do not form at the collision energy studied. The experiments reported here give a more complete picture of the reaction dynamics of the substitution in that two collision energies are considered (20 and 40 kcal/mole) and the product angular distribution is measured as well as the translational energy distribution rather than just the average. This makes it possible to determine whether the average internal energy transfer to the various hydrocarbons is similar because the complexes are not long-lived or because the reactions have comparable exit barriers that funnel the transition state potential energy into translation.

2. Results

2.1. 20 Kcal/mole Collision Energy

2.1.1. $D + C_2H_2 \rightarrow H + C_2HD$

Figure 3-2 shows the summed raw signal and corresponding laser-off background from a typical run. A direct subtraction of the laser-off from the laser-on scans gives the laser correlated signal. As discussed in Chapter 2, however, this subtraction will not give the pure low energy reactive signal. First, the contribution from non-reactive scattering must be subtracted away. Integration of

the resulting reactive signal at the various laboratory angles for scans taken under similar conditions gives the uncorrected low energy angular distribution. Next, since the slow D atom beam contains some of the unselected faster D atoms, the higher collision energy signal must be removed. To do this, the TOF spectra at both energies were normalized to the uncorrected angular distributions. Then, the same fraction of the high energy spectra at each angle was subtracted from the corresponding low energy spectra. Figure 3-3 shows the accumulated raw signal and estimated high energy correction. The decision of exactly how much to subtract is somewhat arbitrary. Enough was removed so that there was no significant amount of signal at COM velocities too large to have been from reaction of the slower D atoms. It was found in the fitting, however, that the fast section of the signal, which is most affected by the subtraction, has little influence on determining the best $P(E_T)$ and $T(\theta)$. The final angular distribution is obtained by integrating the corrected spectra and is shown in Figure 3-5 along with the distribution calculated. The high energy correction, however, still does not give the true 20 kcal/mole collision energy spectra. As discussed in Chapter 2 (see Figure 2-7, for example), there is a broad, underlying component of the beam that results from collisions of the D atoms in the photolysis chamber. These D atoms can react and must be accounted for. This can be done by including these D atoms

in the input primary beam velocity distribution of the data analysis program, although this assumes that the $P(E_T)$ and $T(\theta)$ for reaction at these collision energies are similar to those for the slower D atoms. Since the contamination is fairly small and $H + C_2H_4$ trajectory studies suggest that there will be very little change in the reaction cross-section between 20 and 40 kcal/mole [14], this approximation should not be too bad.

The "pure" low energy TOF spectra are displayed as the open circles in Figure 3-4 with the solid line showing the best fit. The slow tails of the calculated spectra are consistently less than that observed; there appears to be some additional component at ~450 to 600 μsec. This signal changes very little from angle to angle and it is present at both collision energies. It is thought to be due to low collision energy events, either from the reaction of thermalized D atoms or slow hydrocarbons as was discussed in Chapter 2. The initial fits, which were done assuming a speed ratio of 5, had a much larger discrepancy between the calculated signal and the observed. It was found that decreasing the hydrocarbon speed ratio (i.e. averaging over a wider range of velocities) improved the fit considerably. Whether this is a way of including low collision energy reactions of thermalized D atoms that were not considered in the initial D atom velocity distribution or because the hydrocarbon beam spread was actually that large throughout

the experiments cannot be determined.

The $T(\theta)$ that gives the best fit (Figure 3-6) shows that the C_2HD is backward scattering (~40% change from θ = 0° to 180°) with respect to the D atom direction. The lack of forward/backward symmetry indicates that the reaction does not involve a long-lived complex. The $P(E_T)$ for the reaction is plotted in Figure 3-7. The peak occurs at ~6 kcal/mole and the average energy is ~8.3 kcal/mole which means that ~62% of the initial translational energy is transferred into internal energy.

2.1.2. $D + C_2H_4 \rightarrow H + C_2H_3D$

The summed signal and background TOF spectra from a representative experimental run where the substituted product C_2H_3D is detected are shown in Figure 3-8. Comparison with the acetylene data (see Figure 3-2) suggests that the cross-section for the ethylene substitution reaction is greater. It is difficult, however, to quantify this because the two experiments were done far apart in time (4 months). Variations in the focusing lens transmission and changes in the D atom beam intensity due to passivation changes in the DI feedline or DI corrosion of the pulsed valve undoubtedly occurred and could not be precisely measured.

Figure 3-9 shows the assumed higher collision energy correction to the summed reactive signal. Again, it should

be noted that the fast edges of the TOF spectra where this subtraction will have the most influence have little effect on the final analysis. The "pure" TOF spectra that results from the subtraction are shown in Figure 3-10. The corrected angular distribution along with that calculated is shown in Figure 3-11.

The $T(\theta)$ used in the fitting is shown in Figure 3-12. Like the $T(\theta)$ found for the acetylene reaction, it indicates that the C_2H_3D product is moderately backward scattered (also ~40% change from θ = 0° to 180°) so the ethyl radical complex must not live longer than a rotational period. The $P(E_T)$ (Figure 3-13) is also very similar to the corresponding acetylene scattering with a peak at ~6 kcal/mole and a mean energy of ~8.3 kcal/mole. One difference in the acetylene and ethylene fitting is that the input D atom velocity distribution for the latter did not have to be as broad. Possible reasons for the difference are that either not enough of the high collision energy signal was subtracted from the acetylene spectra or that the D atom beam used in the ethylene experiments was more monoenergetic. The latter is the favored explanation since as some of the problems associated with the collisional broadening contamination were apparent at the conclusion of the acetylene experiments attempts were made to improve the beam. Figure 3-14 shows a comparison of the D atom TOF spectra from the two sets of experiments which illustrates

this.

Unless the barrier to abstraction is significantly greater than the exothermicity (7 kcal/mole), the formation of C_2H_3 + HD is not thermodynamically forbidden at a collision energy of 20 kcal/mole. No reactive signal, however, was seen at m/e=27. The expected C_2H_3 + HD product can only have a maximum of ~13 kcal/mole in translation; this means the C_2H_3 will be more concentrated about the COM than the substituted product which should make it easier to detect. Thus, if there were any abstraction signal, there are no kinematic reasons to keep it from being observed. The only detection problem would be high background from dissociative ionization of the parent ethylene in the ionizer.

2.2. 40 Kcal/mole Collision Energy

2.2.1. $D + C_2H_2 \rightarrow H + C_2HD$

The laser-on/laser-off scans from a typical experimental run are shown in Figure 3-15. Subtraction of the laser-off from the laser-on data followed by the non-reactive scattering correction gives the TOF spectra shown in Figure 3-16. The same procedure used to correct for the unselected D atom contamination in the 20 kcal/mole collision energy experiment was used here to remove the low collision energy D atom contribution. The TOF spectra and assumed contribution from the low collision energy spectra

are plotted together in Figure 3-16. Subtraction yields the spectra in Figure 3-17. Unfortunately, this correction affects the height of the slow tail of the data relative to the fast peak which determines how backward scattered $T(\theta)$ is. The uncertainty in the subtraction procedure means that the COM angular distribution cannot be obtained. The $P(E_T)$ for the reaction, however, can still be derived. To a good approximation, the fast peak, which is unaffected by the subtraction, represents products with a lab velocity greater than the COM velocity. Since the product distribution should be cylindrically symmetric about the relative velocity vector the position and width of this peak contains all the information to calculate the $P(E_T)$. The fast peak was fit with the $P(E_T)$ shown in Figure 3-18. The maximum of the distribution which occurs at ~6 kcal/mole is in approximately the same position as it was in the lower collision energy experiments. The mean energy, 13.4 kcal/mole, indicates that ~68% of the initial translational energy is being transferred to internal energy of the C_2HD product.

With 40 kcal/mole in collision energy, the abstraction reaction, $D + C_2H_2 \rightarrow HD + C_2H$, is thermodynamically possible. Scans were taken about the COM angle at m/e = 25 to look for signs of the C_2H product. Because of the endothermicity of this reaction, detection of the abstraction product is kinematically favored over the substitution product; only

the larger background from dissociative ionization of the parent acetylene could obscure the reactive signal. No sign of any abstraction signal, however, was seen.

2.2.2. $D + C_2H_4 \rightarrow H + C_2H_3D$

The signal and corresponding background for detection of the substitution product for a typical experimental run are shown in Figure 3-19. As at the lower collision energy, there is more signal than for the corresponding reaction with acetylene but this cannot be quantified.

The net reactive signal along with the assumed low collision energy contribution is shown in Figure 3-20. The high energy ethylene data suffers from the same problem as the acetylene data in that this correction determines how backward scattered the calculated $T(\theta)$ will be and there is no independent means of deciding how much should be subtracted. The corrected spectra is shown in Figure 3-21 along with the fit to the fast peak calculated using the $P(E_T)$ in Figure 3-22. As at the lower collision energy, the translational energy distribution of the ethylene reaction products is quite similar to that of the acetylene. The $P(E_T)$ peak is at ~6 kcal/mole and the mean energy, 12.6 kcal/mole, implies that ~70% of the initial translational energy is transferred to the C_2H_3D internal energy.

To see if increased collision energy would open up the abstraction channel, scans were taken at m/e = 27 to look

for formation of C_2H_3. Although this product would be harder to see at the higher collision energy, it should still be easier to detect than the substitution reaction product because of the endothermicity, the only complication would be higher background. Again, no sign of the abstraction reaction was observed.

3. Discussion

The $T(\theta)$ for the 20 kcal/mole D + C_2H_2 and D + C_2H_4 substitution reactions do not show the forward/backward peaking typical of processes involving a long-lived collision complex. The vinyl and ethyl radical intermediates must live for less than a rotational period. This agrees with the conclusion drawn by Bersohn's group [20] but offers more solid evidence. Bersohn and coworkers found that the average product translational energy of various H + RD $\rightarrow$ RH + D reactions at ~1 eV collision energy was independent of the number of internal modes of the complex; they reasoned that if long-lived complexes were typical in these systems as more vibrators and rotors were added, less and less energy would go into translation because the energy would randomize statistically into all these new modes. The problem is that for reactions with an exit barrier, the potential energy tends to be released as translational energy of products as they accelerate down the barrier. This happens whether the complex lives for long

time or not [2].

The $T(\theta)$ shows that the detected product is backward scattered with respect to the D atom beam in the COM frame for both reactions. Physically, this means that the D atom collides with the C_2H_2 or C_2H_4 and before the complex formed can complete a rotation, an H atom is kicked off in a forward direction with respect to the initial D atom approach sending the substituted hydrocarbon backwards (see Figure 3-23). Very little of the original collision energy remains in translation; most (60 to 70%) must go into the internal energy of the substituted hydrocarbon product since there is not enough energy available to excite the H atom to the first electronic state. The final orbital angular momentum, L', will be less than the initial because of the decrease in reduced mass and relative velocity that the reaction involves; this means that the hydrocarbon product should be somewhat rotationally excited although this will not be too significant because of the small reduced mass of the system. For the low energy acetylene reaction, ΔL is calculated to be ~10$\hbar$ and for the higher collision energy ~14$\hbar$, assuming an impact parameter of 0.6 Å in both cases (half the carbon-carbon bond [7]). The values are comparable for the two ethylene reactions.

Overall, little difference was seen between the D + C_2H_2 and D + C_2H_4 scattering. The $P(E_T)$ for both acetylene and ethylene at the two collision energies peaks away from

zero at ~6 kcal/mole. This maximum reflects the presence of an exit barrier. The barrier measured here is the same order of magnitude as the theoretically calculated and previously measured activation energy for the H atom addition reactions (2.5 kcal/mole for acetylene and 2.75 kcal/mole for ethylene [9-14]). The $T(\theta)$'s for the two reactions at the lower translational energy are also quite similar; the structural differences between the acetylene and ethylene apparently have very little effect. Perhaps this is because it is mainly the carbon atom and associated π electrons that the D atom interacts most strongly with. The only way the two reactions really differed was in the apparent reaction cross-section. Although it could not be quantified, in the ethylene substitution experiment, the reactive signal was consistently greater than in the acetylene. This is not surprising. In Bersohn's recent study, the cross-section of the two were estimated to be 1.69 $Å^2$ and 1.85 $Å^2$ [20]. It should be noted, however, that different deuterated compounds were used than in this work. Rate constant measurements of the two addition reactions show that the ethylene absolute rate constant is higher by almost an order of magnitude [10,12]. It is thought that this is a result of better C_2H_4 charge transfer or polarization [7,12].

It is instructive to compare an estimate of the rotational periods of the vinyl and ethyl radicals with the

RRKM lifetimes for the excited radicals. The rotational period was calculated using the formula

$$\tau_{rot} = \frac{2\pi I}{L}$$

where I is the rotational moment of inertia and $L = \mu v_{rel} b$ is the orbital angular momentum from the collision [21]. It was assumed that the D atom would collide "head-on" with one of the carbon atoms as illustrated in Figure 3-23. The impact parameter, b, would then be approximately half the carbon-carbon bond length. For acetylene, r_{cc} is ~1.2 Å [7] and for ethylene, r_{cc} is ~1.3 Å [14]. This impact parameter is probably a lower limit which would make the calculated τ_{rot} an upper limit. In the reaction model where the D atom collides directly with the carbon atom on the carbon-carbon bond axis, oblate type rotation of the complex about axes perpendicular to the carbon-carbon bound should be most important. Prolate rotation about the C-C bond axis would be initiated only if the collision were off-axis. The moments of inertia for the ethyl and vinyl activated complexes have been calculated [6-8]. The average value of the two large oblate moments of inertia was used in the calculation; these were typically within 20% of each other. I for the C_2H_2D is 21 amu·Å^2 [7]. The value used for the C_2H_4D was 22 amu·Å^2. At the lower collision energy, then, the calculated rotational period for the complexes are ~1.3 x 10^{-12} sec for C_2H_2D and ~1.2 x 10^{-12} sec for C_2H_4D. The RRKM

lifetimes were calculated from the rate constants for unimolecular decomposition of the excited radicals (1/k) [22]. A program based on an RRKM algorithm of Hase and Bunker was used [23,24]. The options selected were as follows: the rotations were considered adiabatic, harmonic vibrations were assumed, and a semiclassical approximation was used in the sum and density of states calculation. The input frequencies for the DHCCH vinyl radical and D--HCCH/H--DCCH critical complexes were taken from the calculation of Harding et. al. [7]. At a collision energy of 20 kcal/mole, the estimated lifetime is ~0.4 x 10^{-12} sec (0.3 x 10^{-12} sec for the undeuterated case). Estimates of the deuterated ethyl complex and radical frequencies exist [8]. However, these were based on a complex that was later found to be too loose [6]. Since no recent frequencies for the deuterated C_2H_4D complexes and radicals could be found, Hase and Schlegel's values for C_2H_5 were used [6]; no significant differences were expected based on the acetylene calculation. The lifetime for the ethyl complex produced in the 20 kcal/mole collision is estimated to be 20 x 10^{-12} sec, significantly longer than that of the vinyl radical. A comparison of the rotational period and complex lifetime for the D + C_2H_2 reaction at 20 kcal/mole collision energy shows that only a third of a rotation will be completed before the complex breaks up. This would certainly agree with the experimental observations in which no long-lived complex was

apparent. For the D + C_2H_4 reaction, however, ~17 rotations would occur before the C_2H_4D radical decomposed. Based on this calculation, then, the D + C_2H_4 system should exhibit some type of long-lived complex behavior. This does not necessarily mean that forward/backward peaking should be observed, however. The product orbital angular momentum may not be strongly coupled to the initial angular momentum due to the light mass of the D atom; for such a system, an isotropic distribution or sideways scattering would be consistent with formation of a long-lived complex [25]. Although the $T(\theta)$ is not strongly backward scattering and so might be viewed as marginally isotropic, the similarity between the D + C_2H_2 and D + C_2H_4 systems suggests that the ethyl radical complex is only as long-lived as the vinyl radical, i.e. the ethyl complex lifetime is much less than τ_{rot}. This implies that the additional internal modes (both vibrational and internal rotation) present in the ethyl intermediate do not participate in the energy randomization and/or that the complex is tighter than has been thought so that the vibrational frequencies are really higher than those used in the RRKM calculation.

In both the D + C_2H_2 and D + C_2H_4 experiments a good deal of time was spent collecting data at the parent masses to try to understand the origin of the slow laser-correlated signal. There were no signs of significant elastic or inelastic scattering. Because of large background problems

in detecting at the parent mass, however, this type of scattering cannot be entirely ruled out. The lack of elastic and inelastic signal may imply that the substitution reactions are favored over the back reaction; once the activated complex forms, C-H bond cleavage occurs rather than C-D. This effect has been observed in the high pressure studies of acetylene and ethylene and can be predicted by an RRKM treatment. The preference for H elimination arises mainly from the lower ZPE of the deuterated hydrocarbons [8,18].

Although the higher collision energy reactions could not be well characterized, comparison of the uncorrected fast and slow D atom TOF spectra show that the substitution cross-section does not increase significantly with collision energy; the fast D atom TOF spectra clearly show the lower energy contribution. The H + C_2H_4 trajectory calculations predict this; in the 20-80 kcal/mole collision energy range, the excitation function is fairly flat [14]. Similar behavior would be expected for H + C_2H_2.

4. Conclusions

The experiments done show that at 20 kcal/mole and presumably 40 kcal/mole collision energy, the D + C_2H_2 and D C_2H_4 substitution reactions do not involve a long-lived complex. The D atom adds to the hydrocarbon and an H atom leaves in a forward direction with respect to the initial D

atom approach before the resulting complex can undergo a complete rotation. The structural differences between the acetylene and ethylene apparently have little effect on the reaction dynamics. Despite the fact that the reaction is direct, a large fraction (60-70%) of the initial translational energy is transferred to internal energy of the hydrocarbon. The $P(E_T)$'s show the presence of a small exit barrier (~6 kcal/mole) as previously predicted and observed.

Estimating the collision complex rotational period and RRKM lifetime for the D + C_2H_2 reaction at 20 kcal/mole collision energy shows that a long-lived complex would not expected to have a predominant role. Similar calculations for the D + C_2H_4 system, however, would suggest that the intermediate would be long-lived with respect to the rotational period. Although strong forward/backward peaking would not necessarily be expected, the similarity to the acetylene substitution reaction is surprising and suggests that the RRKM calculation should be critically examined. Perhaps tighter treatment of the complex is required or not all the internal modes may be actively involved in the energy randomization.

The general trends seen in the data agree with the studies that have been done under non-single collision conditions and with theoretical predictions. At both collision energies, the ethylene substitution occurs more

readily than the acetylene; this reflects the general principle that radicals add more easily to olefinic bonds. Also, no sign of significant C-D bond cleavage was detected. Because the zero point energies for C_2H_3D and C_2HD are lower than for the corresponding undeuterated molecules, this preference for H elimination is expected and has been measured previously. Finally, the reaction cross-sections at the 20 and 40 kcal/mole collision energies appear similar.

On a more practical level, the experiments have shown that the ethyl and vinyl radical complexes formed by high energy collisions will be fairly short-lived. This knowledge will be important in modeling combustion systems where C_2H_3 and C_2H_5 reactions take place. Since a large fraction of the initial translational energy is transferred to hydrocarbon internal energy, the resulting hydrocarbons may be more reactive and the H atoms less.

Finally, the experiment points out some of the limitations of using the photolytic D atom source. The collisionally broadened and thermalized D atoms produced are able to react making the data more difficult to fit. To some extent this can be corrected for in the assumed parent velocity distribution, but not if there is any strong dependence of the $P(E_T)$ or $T(\theta)$ on the collision energy. It would be best to run under conditions where there is less collisional broadening (lower DI pressure and shorter

laser/pulsed valve delay times), although this limits studies to reactions with high cross-sections. Another difficulty was caused by the presence of the unselected D atoms; a somewhat arbitrary fraction of the unselected collision energy signal had to be subtracted away. For reactions where there is a significant difference in cross-section between 20 and 40 kcal/mole collision energy, this would be much less of a problem, at least for one of the collision energies. Otherwise, it would probably be better to use a different source of D atoms such as DBr at 193 nm where there will not be two different D atom velocity ranges.

References

1. See, for example, B.S. Rabinovitch and D.W. Setzer, Advan. Photochem. **3**, 1 (1964).
2. J.M. Farrar and Y.T. Lee, J. Chem. Phys. **63**, 3639 (1975).
3. For a recent review see G.W. Flynn and R.E. Weston, Jr., Ann. Rev. Phys. Chem. **37**, 551 (1986).
4. See, for example, S. Buelow, G. Radhakrishnan, J. Catanzarite, and C. Wittig, J. Chem. Phys. **83**, 444 (1985); G. Radhakrishnan, S. Buelow, and C. Wittig, J. Chem. Phys. **84**, 727 (1986); N.F. Scherer, C. Sipes, R.B. Bernstein, and A.H. Zewail, J. Chem. Phys. **92**, 5239 (1990).
5. K.M. Ervin, S. Gronert, S.E. Barlow, M.K. Gilles, A.G. Harrison, V.M. Bierbaum, C.H. DePuy, W.C. Lineberger, and G.B. Ellison, J. Am. Chem. Soc. **112**, 5750 (1990) and references therein.
6. W.L Hase and H.B. Schlegel, J. Phys. Chem. **86**, 3901 (1982) and references therein.
7. L.B. Harding, A.F. Wagner, J.M. Bowman, G.C. Schatz, and K. Christoffel, J. Phys. Chem. **86**, 4312 (1982).
8. J.A. Cowfer and J.V. Michael, J. Chem. Phys. **62**, 3504 (1975).
9. W.A. Payne and L.J. Steif, J. Chem. Phys. **64**, 1150 (1976).

10. K. Sugawara, K. Okazaki, and S. Sato, Bull. Chem. Soc. Jpn. **54**, 2872 (1981).

11. R. Ellul, P. Potzinger, B. Reimann, and P. Camilleri, Ber. Bunsenges. Phys. Chem. **85**, 407 (1981).

12. S. Nagase and C.W. Kern, J. Am. Chem. Soc. **102**, 4513 (1980).

13. J.H. Lee, J.V. Michael, W.A. Payne, and L.J. Stief, J. Chem. Phys. **68**, 1817 (1978).

14. W.L. Hase, D.M. Ludlow, R.J. Wolf, and T. Schlick, J. Phys. Chem. **85**, 958 (1981).

15. S. Nagase and C.W. Kern, J. Am. Chem. Soc. **101**, 2544 (1979).

16. D.R. Herschbach, Disc. Faraday Soc. **55**. 233 (1973).

17. K. Kowari, K. Sugawara, S. Sato, and S. Nagase, Bull. Chem. Soc. Jpn. **54**, 1222 (1981).

18. D.G. Keil, K.P. Lynch, J.A. Cowfer, and J.V. Michael, Int. J. of Chem. Kinetics **VIII**, 825 (1976).

19. P.D. Lightfoot and M.J. Pilling, J. Phys. Chem. **91**, 3373 (1987).

20. G.W. Johnston, S. Satyapal, R. Bersohn, and B. Katz, J. Chem. Phys. **92**, 206 (1990).

21. See treatment in G.N. Robinson, Ph.D. Thesis, University of California, Berkeley (1987).

22. P.J. Robinson and K.A. Holbrook, Unimolecular Reactions (Wiley, New York, 1972).

23. W.L. Hase and D.L. Bunker, Quantum Chemistry Program

Exchange, University of Indiana, Bloomington, Indiana)

24. L.J. Butler, Ph.D. Thesis, University of California, Berkeley (1985); L.J. Butler group meeting hand-out.

25. W.B. Miller, S.A. Safron, and D.R. Herschbach, Dis. Faraday Soc. **44** 108 (1967).

Figure Captions

Figure 3-1. Simple potential energy diagram of the D atom substitution reaction in acetylene and ethylene. The small (~ 2 kcal/mole) H atom addition barrier is shown as well as the slight exothermicity due to differences in the zero point energies of the reactants and products.

Figure 3-2. Uncorrected C_2HD TOF spectra from a typical experimental run for the $D + C_2H_2 \rightarrow H + C_2HD$ reaction at 20 kcal/mole collision energy. The open circles show the reaction signal and the solid line is the laser-off background. (a) 30°, (b) 40°, (c) 50°, and (d) 60°.

Figure 3-3. C_2HD reactive signal for the 20 kcal/mole collision energy. The open circles are the accumulated laser-on minus laser-off signal after the non-reactive contribution has been subtracted. The solid line shows the unselected D atom correction. (a) 30°, (b) 40°, (c) 50°, and (d) 60°.

Figure 3-4. C_2HD TOF spectra at 20 kcal/mole collision energy. The open circles are the "pure" reactive signal after the unselected D atom contribution has

been subtracted. The solid line is the calculated fit using the $T(\theta)$ and $P(E_T)$ in Figures 3-6 and 3-7. (a) 30°, (b) 40°, (c) 50°, and (d) 60°.

Figure 3-5. Laboratory angular distribution of the C_2HD reactive signal ($D + C_2H_2 \rightarrow H + C_2HD$) at 20 kcal/mole collision energy. The open circles/dashed line represent the corrected experimental distribution while the solid circles/solid line show the distribution calculated from the best $T(\theta)$ and $P(E_T)$.

Figure 3-6. COM angular distribution ($T(\theta)$) used to fit the 20 kcal/mole $D + C_2H_2 \rightarrow H + C_2HD$ TOF data in Figure 3-4.

Figure 3-7. $C_2HD + H$ product translational energy distribution ($P(E_T)$) for the 20 kcal/mole collision energy used it fit the data in Figure 3-4.

Figure 3-8. Uncorrected C_2H_3D TOF spectra from a typical experimental run for the $D + C_2H_4 \rightarrow H + C_2H_3D$ reaction at 20 kcal/mole collision energy. The open circles show the reaction signal and the solid line is the laser-off background. (a) 30°, (b) 40°, (c) 50°, and (d) 60°.

Figure 3-9. C_2H_3D reactive signal for the 20 kcal/mole collision energy. The open circles are the accumulated laser-on minus laser-off signal after the non-reactive contribution has been subtracted. The solid line shows the unselected D atom correction. (a) 30°, (b) 40°, (c) 50°, and (d) 60°.

Figure 3-10. C_2H_3D TOF spectra at 20 kcal/mole collision energy. The open circles are the "pure" reactive signal after the unselected D atom contribution has been subtracted. The solid line is the calculated fit using the $T(\theta)$ and $P(E_T)$ in Figures 3-12 and 3-13. (a) 30°, (b) 40°, (c) 50°, and (d) 60°.

Figure 3-11. Laboratory angular distribution of the C_2H_3D reactive signal ($D + C_2H_4 \rightarrow H + C_2H_3D$) at 20 kcal/mole collision energy. The open circles/dashed line represent the corrected experimental distribution while the solid circles/solid line show the distribution calculated from the best $T(\theta)$ and $P(E_T)$ (see Figures 3-12 and 3-13).

Figure 3-12. $T(\theta)$ used to fit the 20 kcal/mole $D + C_2H_4 \rightarrow H + C_2H_3D$ TOF data in Figure 3-10.

Figure 3-13. $C_2H_3D + H$ $P(E_T)$ for the 20 kcal/mole collision

energy used it fit the data in Figure 3-10.

Figure 3-14. TOF spectra of the D atom parent beam for the acetylene (solid line) and ethylene (dashed line) experiments. This may explain why the ethylene TOF data seemed to have fewer contamination problems.

Figure 3-15. Uncorrected C_2HD TOF spectra from a typical experimental run for the $D + C_2H_2 \rightarrow H + C_2HD$ reaction at 40 kcal/mole collision energy. The open circles show the reaction signal and the solid line is the laser-off background. (a) 30°, (b) 40°, (c) 50°, and (d) 60°.

Figure 3-16. C_2HD reactive signal for the 40 kcal/mole collision energy. The open circles are the accumulated laser-on minus laser-off signal after the non-reactive contribution has been subtracted. The solid line shows the unselected D atom correction. (a) 20°, (b) 30°, (c) 40°, and (d) 50°.

Figure 3-17. C_2HD TOF spectra at 40 kcal/mole collision energy. The open circles are the "pure" reactive signal after the unselected D atom contribution has been subtracted. The solid line is the calculated fit using the $P(E_T)$ in Figure 3-18. (a) 20°, (b) 30°, (c)

40°, and (d) 50°.

Figure 3-18. C_2HD + H $P(E_T)$ for the 40 kcal/mole collision energy used it fit the data in Figure 3-17.

Figure 3-19. Uncorrected C_2H_3D TOF spectra from a typical experimental run for the D + C_2H_4 → H + C_2H_3D reaction at 40 kcal/mole collision energy. The open circles show the reaction signal and the solid line is the laser-off background. (a) 30°, (b) 40°, (c) 50°, and (d) 60°.

Figure 3-20. C_2H_3D reactive signal for the 40 kcal/mole collision energy. The open circles are the accumulated laser-on minus laser-off signal after the non-reactive contribution has been subtracted. The solid line shows the unselected D atom correction. (a) 30°, (b) 40°, and (c) 50°.

Figure 3-21. C_2H_3D TOF spectra at 40 kcal/mole collision energy. The open circles are the "pure" reactive signal after the unselected D atom contribution has been subtracted. The solid line is the calculated fit using the $P(E_T)$ in Figure 3-22. (a) 30°, (b) 40°, and (c) 50°.

Figure 3-22. C_2H_3D + H $P(E_T)$ for the 40 kcal/mole collision energy used it fit the data in Figure 3-21.

Figure 3-23. Simplified view of the D + C_2H_2 and D + C_2H_4 reactions. The D atom collides "head-on" with the carbon atom and the H atom is eliminated in a forward direction with respect to the initial D atom.

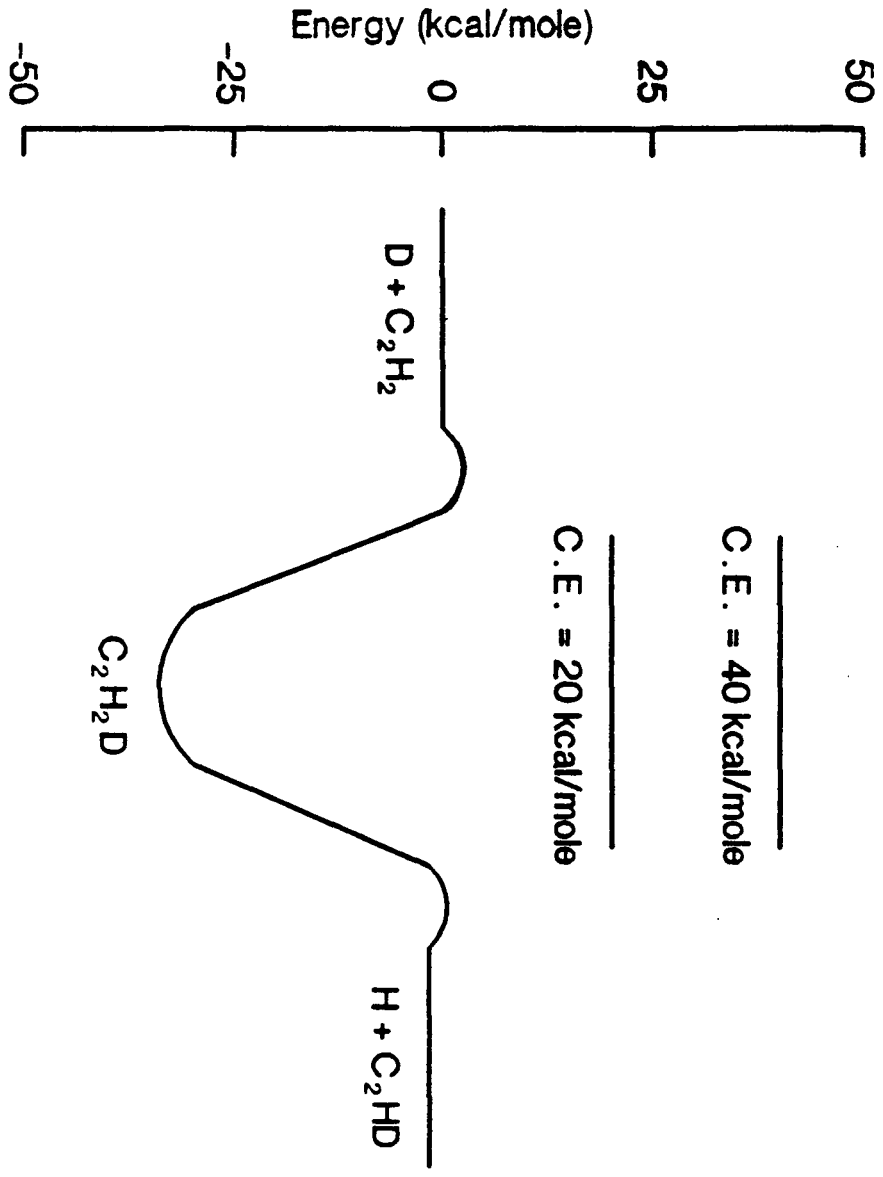
Energy (kcal/mole)
-50
-25
0
25
50
D + C2H2
C2H2D
H + C2HD
C.E. = 40 kcal/mole
C.E. = 20 kcal/mole

Figure 3-1

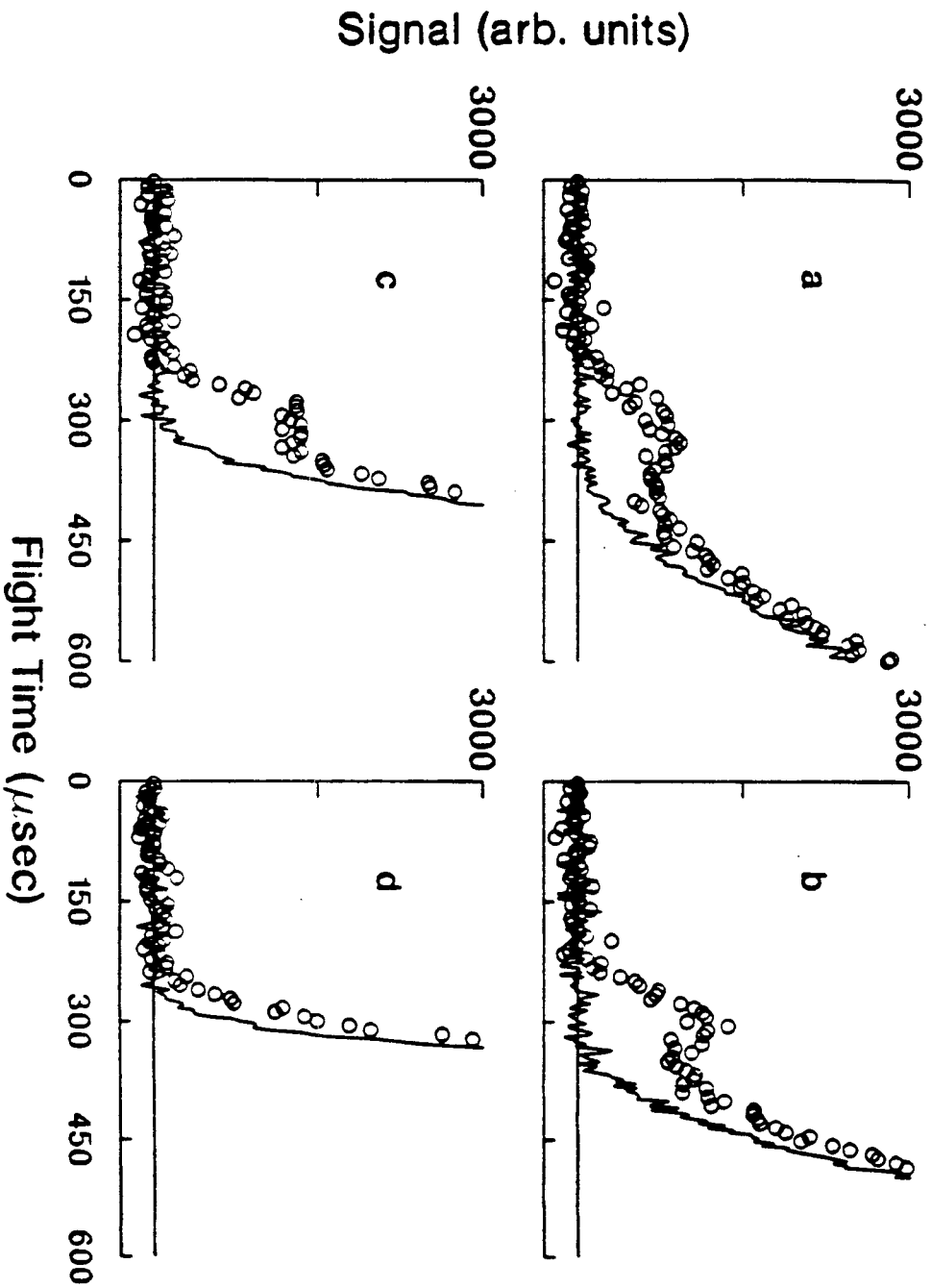

Figure 3-2

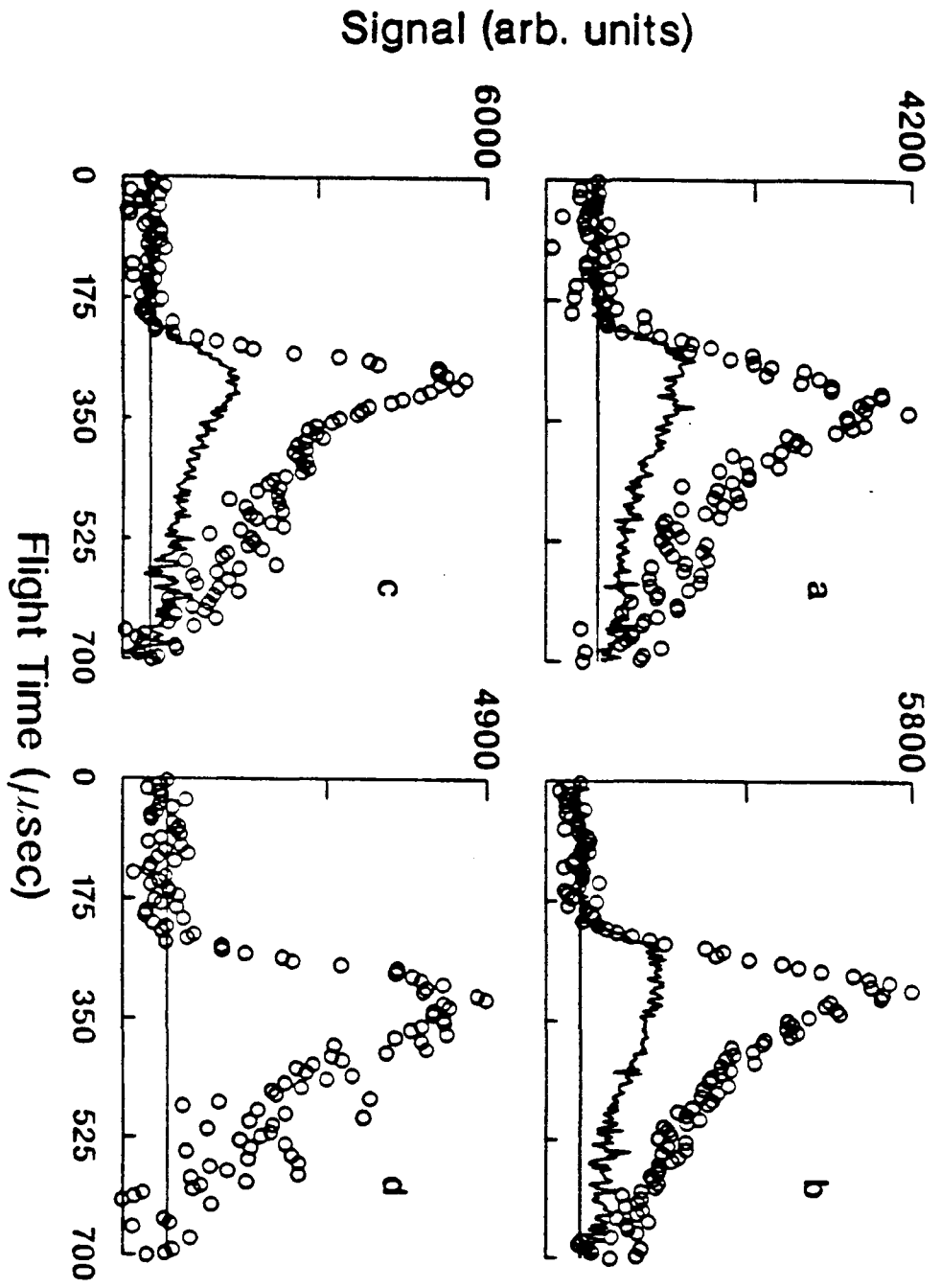
Signal (arb. units)
4200
a
5800
b
6000
c
4900
d
0
175
350
525
700
Flight Time (μsec)

Figure 3-3

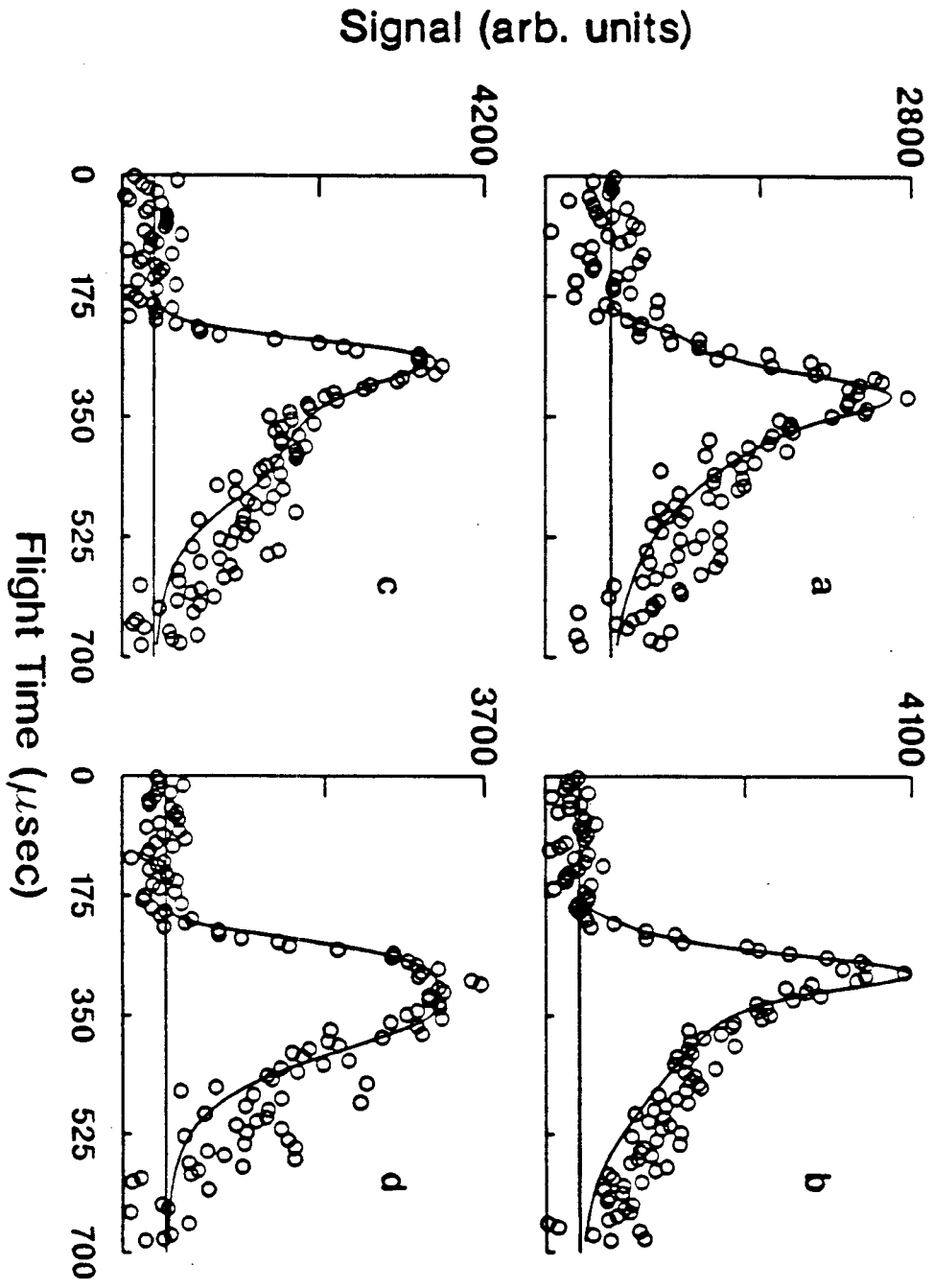
Signal (arb. units)
2800
4200
4100
3700
0
175
350
525
700
Flight Time (μsec)
a
b
c
d

Figure 3-4

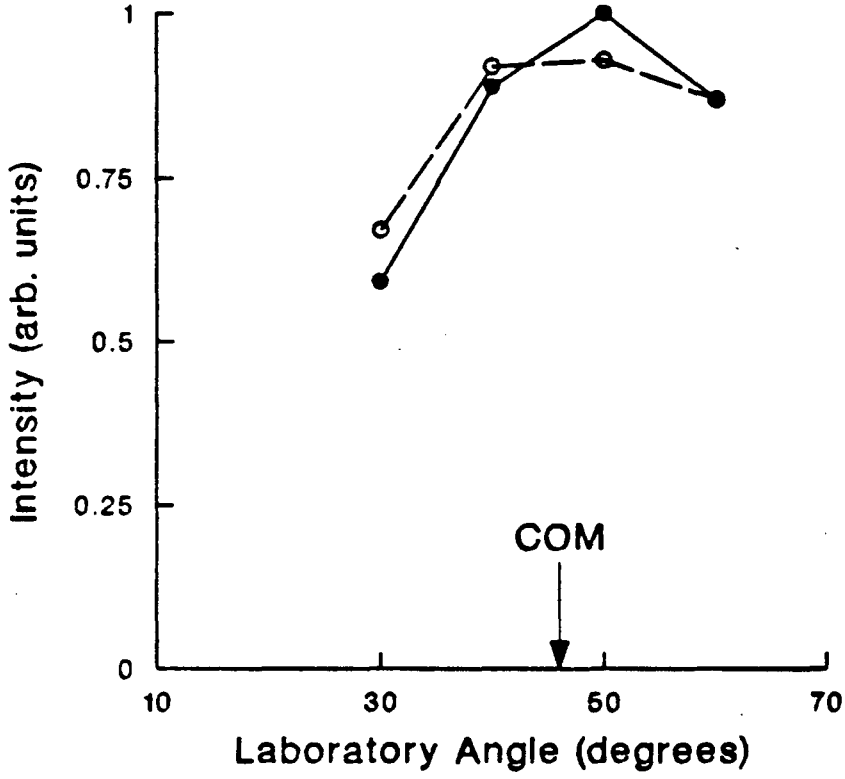
1
0.75
0.5
0.25
0
Intensity (arb. units)
COM
10
30
50
70
Laboratory Angle (degrees)

Figure 3-5

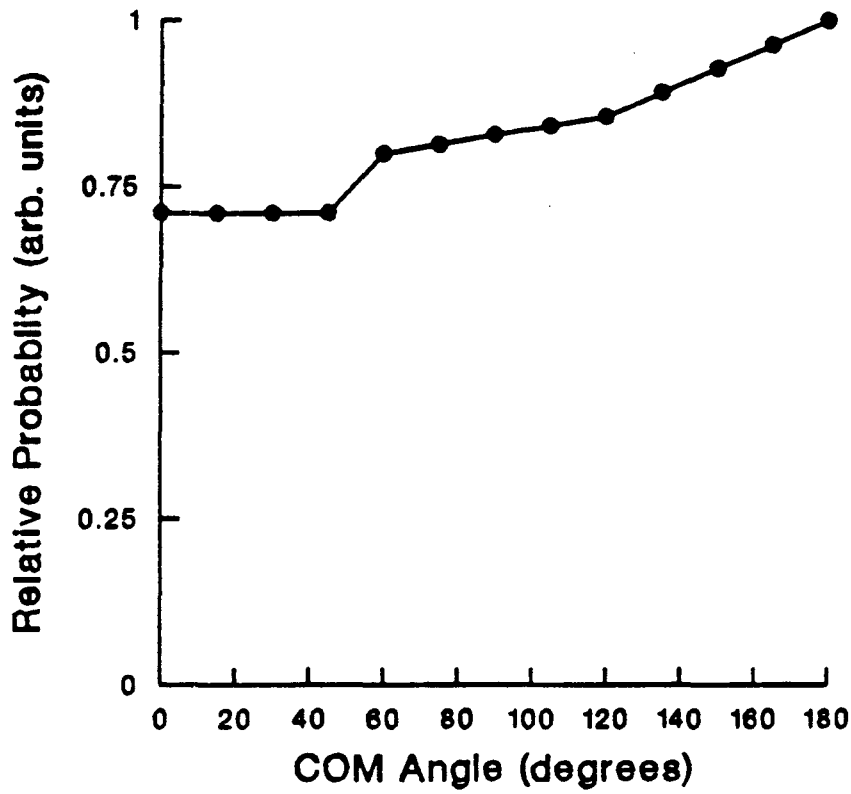
Relative Probability (arb. units)
1
0.75
0.5
0.25
0
0
20
40
60
80
100
120
140
160
180
COM Angle (degrees)

Figure 3-6

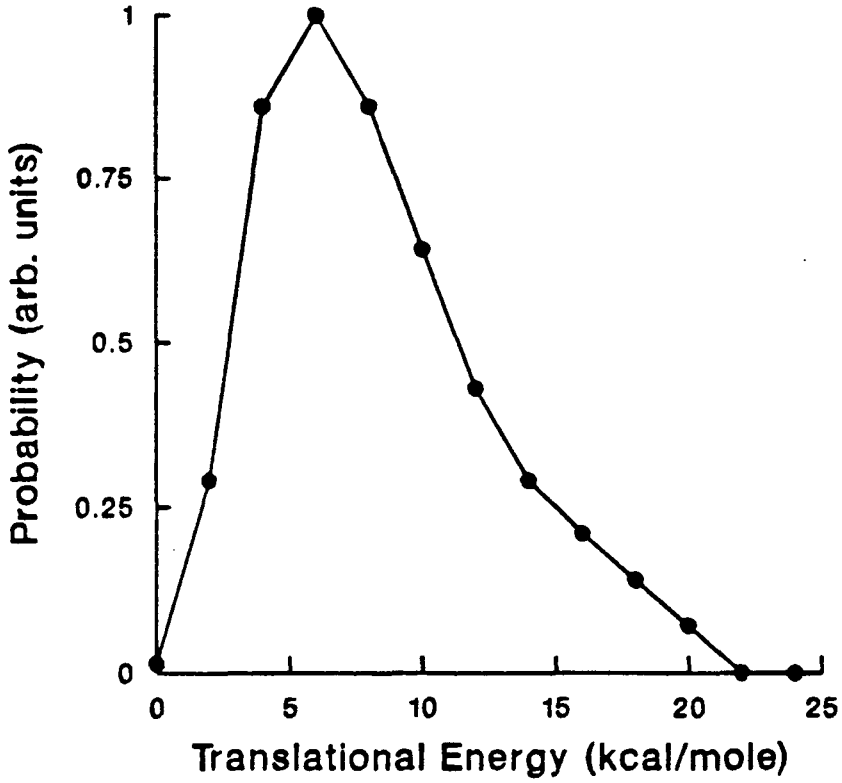
Probability (arb. units)
1
0.75
0.5
0.25
0
0
5
10
15
20
25
Translational Energy (kcal/mole)

Figure 3-7

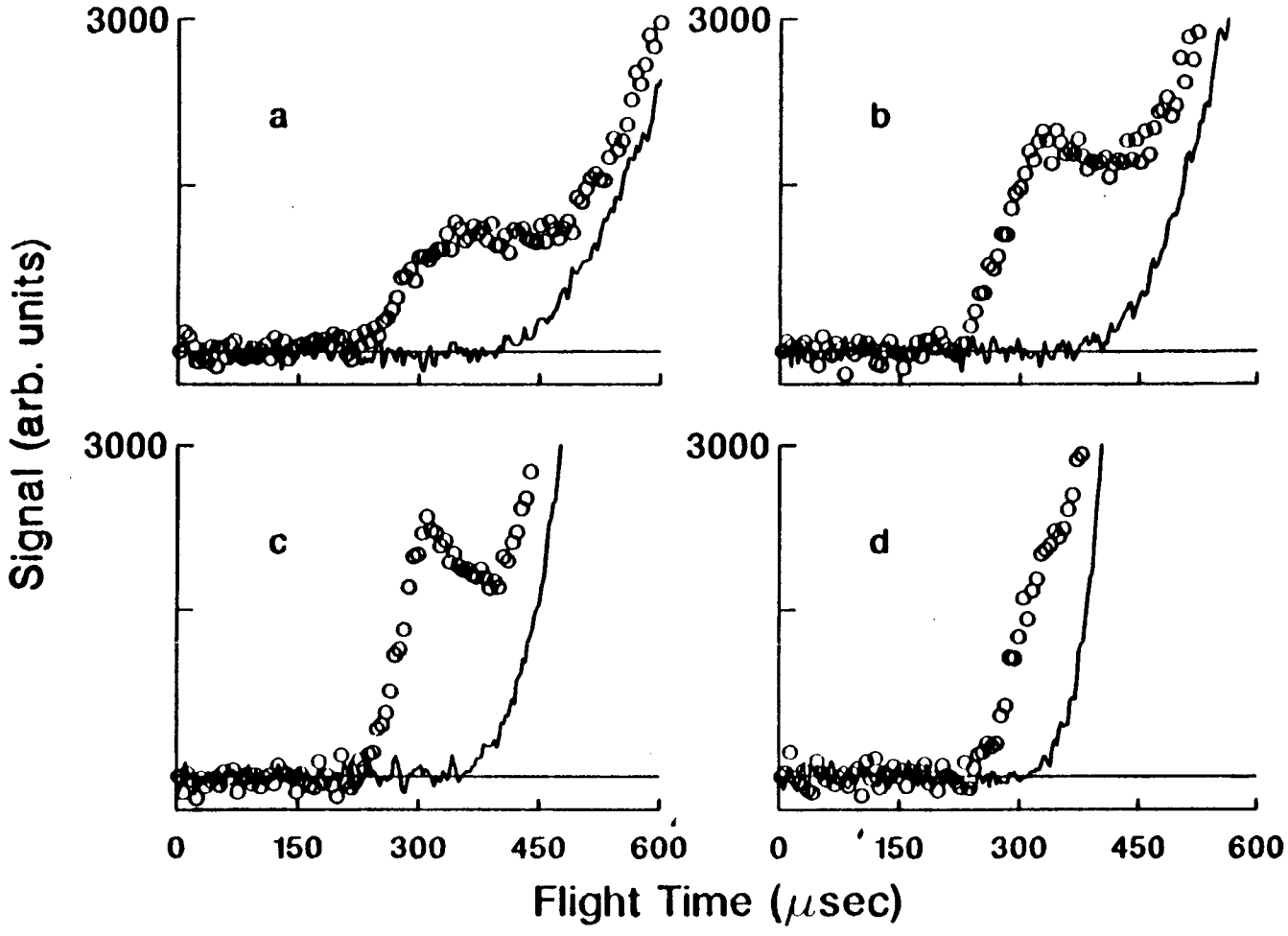
3000
a
3000
b
3000
c
3000
d
Signal (arb. units)
0
150
300
450
600
0
150
300
450
600
Flight Time (μsec)

Figure 3-8

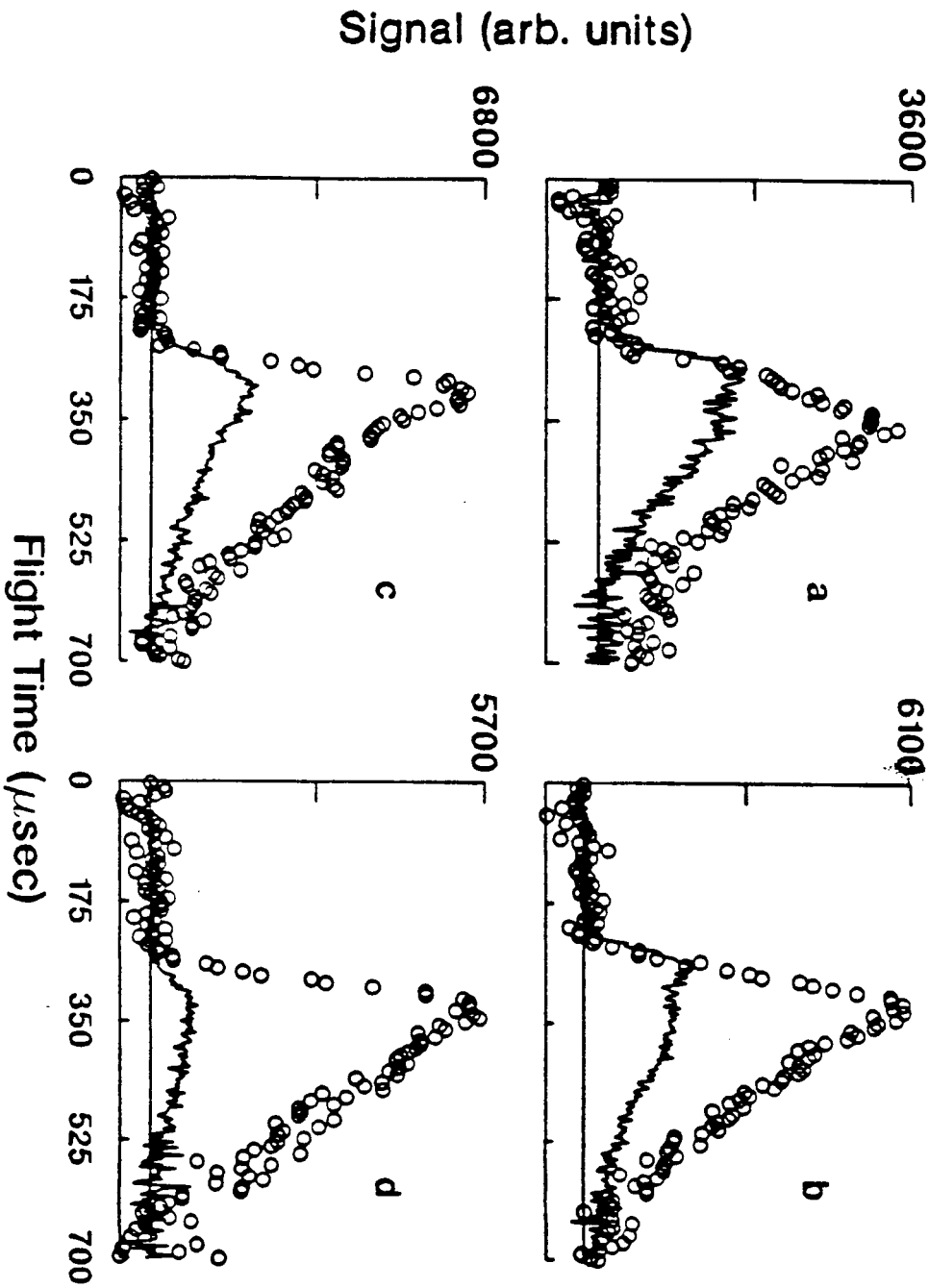
Signal (arb. units)
3600
6800
5700
6100
0
175
350
525
700
Flight Time (μsec)
a
b
c
d

Figure 3-9

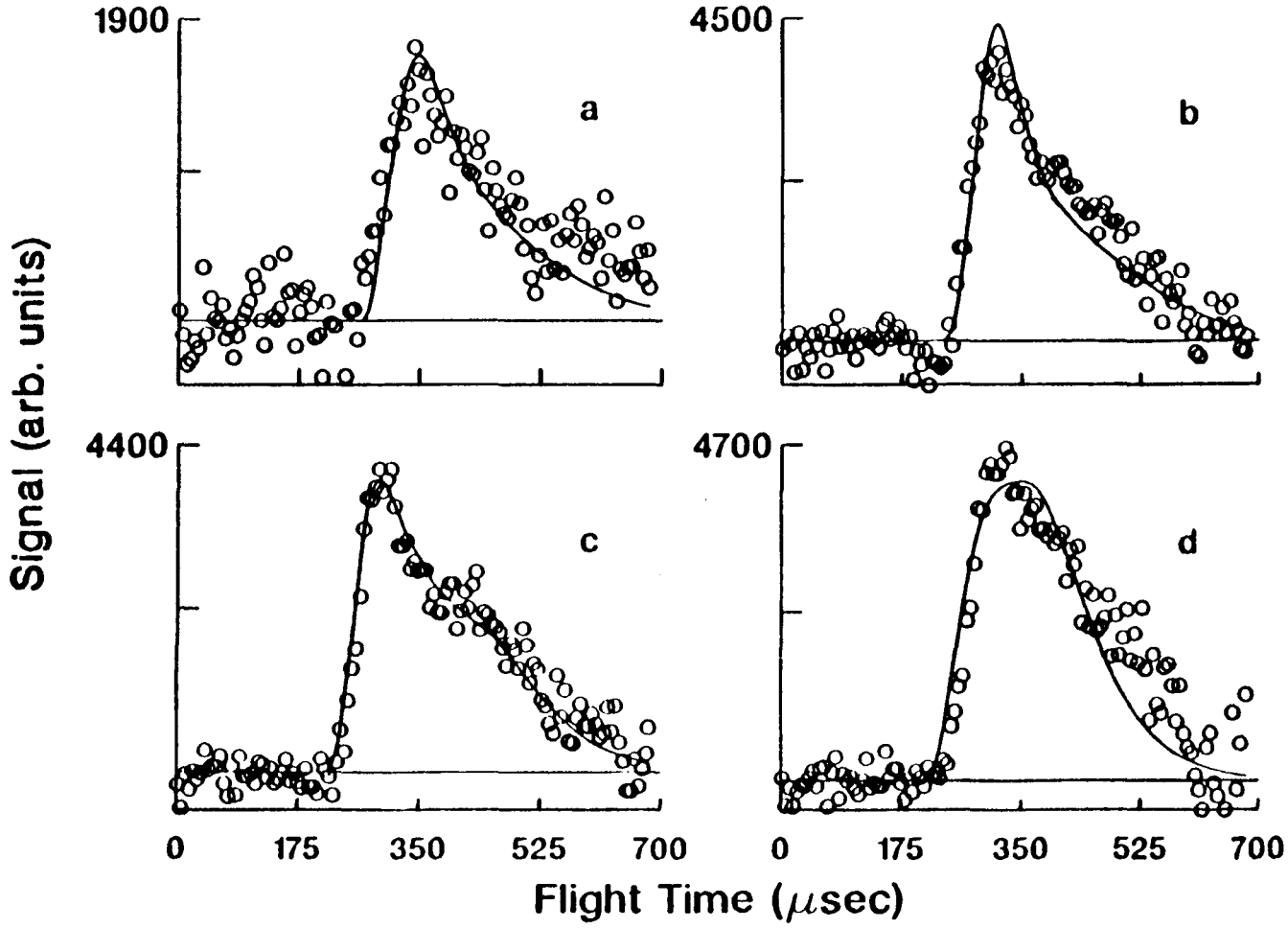
1900
a
4500
b
4400
c
4700
d
Signal (arb. units)
0
175
350
525
700
0
175
350
525
700
Flight Time (μsec)

Figure 3-10

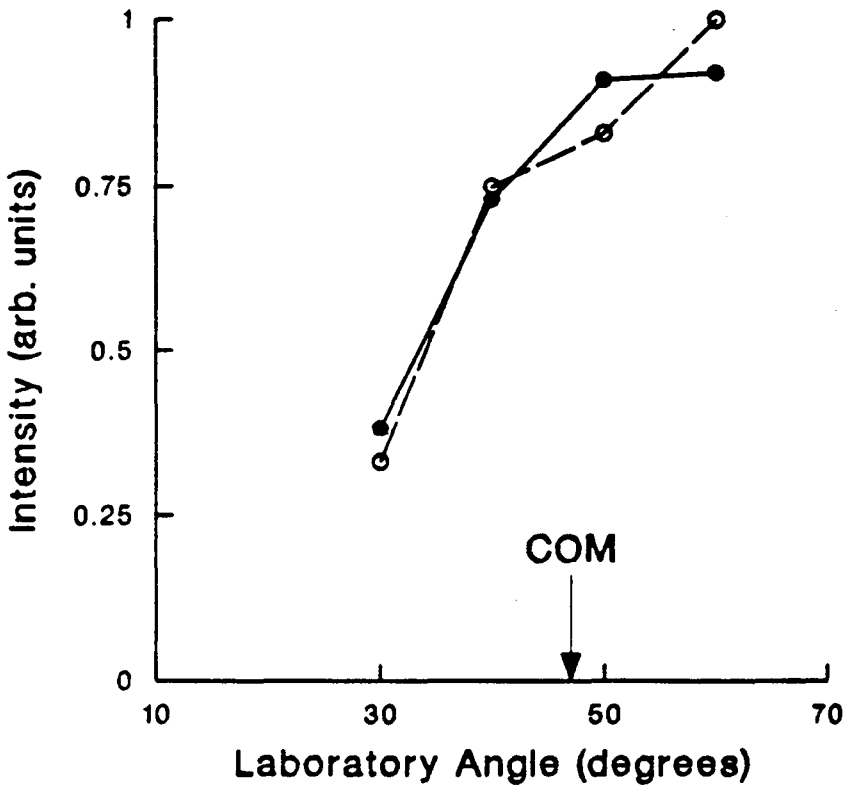
1
0.75
0.5
0.25
0
Intensity (arb. units)
COM
10
30
50
70
Laboratory Angle (degrees)

Figure 3-11

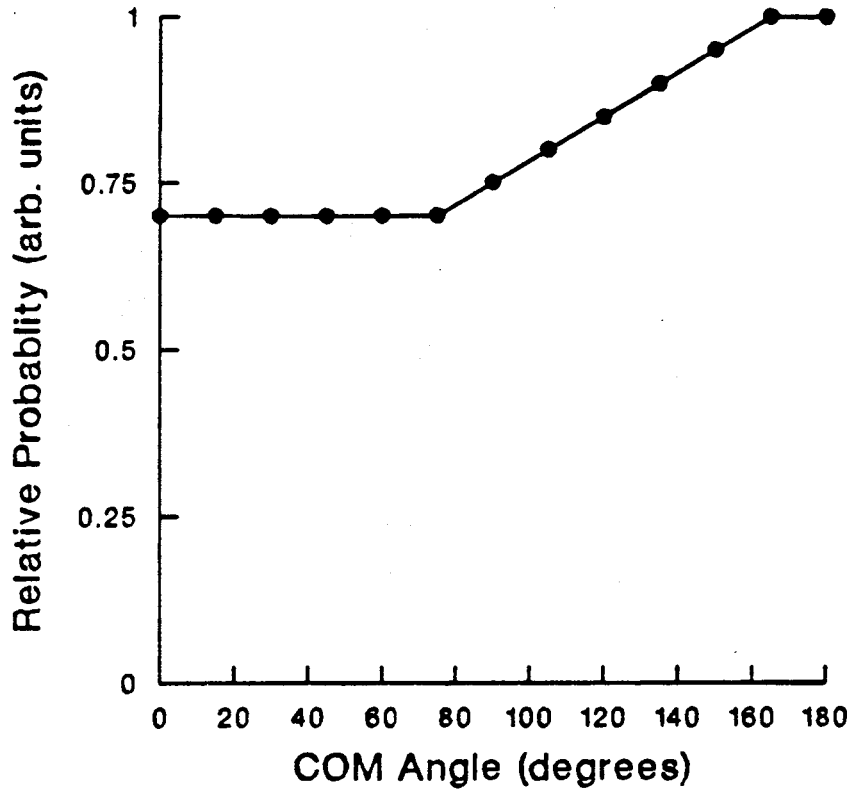
Relative Probablity (arb. units)
1
0.75
0.5
0.25
0
0
20
40
60
80
100
120
140
160
180
COM Angle (degrees)

Figure 3-12

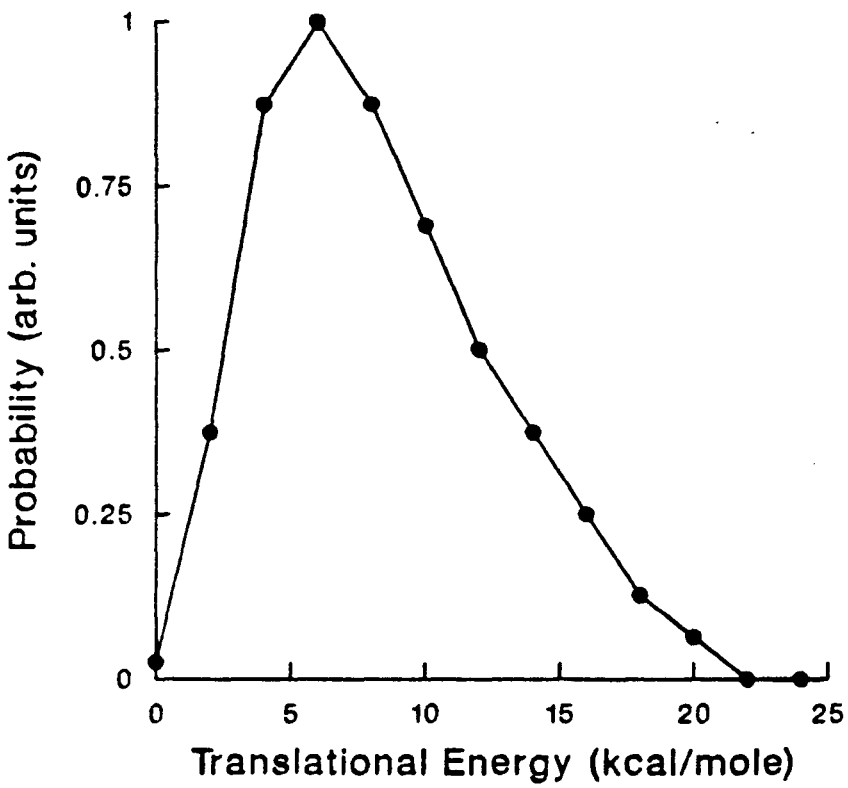
Probability (arb. units)
1
0.75
0.5
0.25
0
0
5
10
15
20
25
Translational Energy (kcal/mole)

Figure 3-13

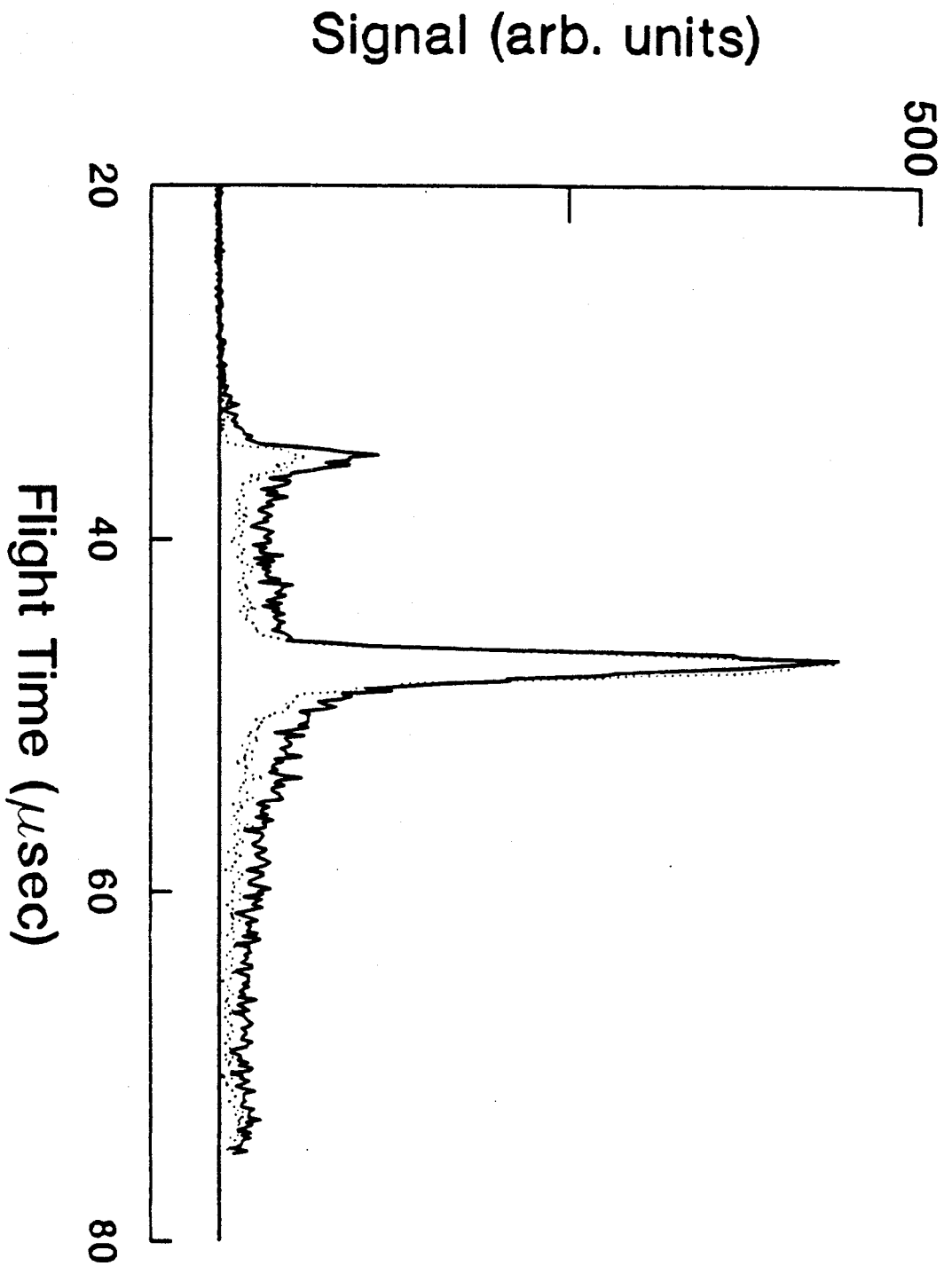

Figure 3-14

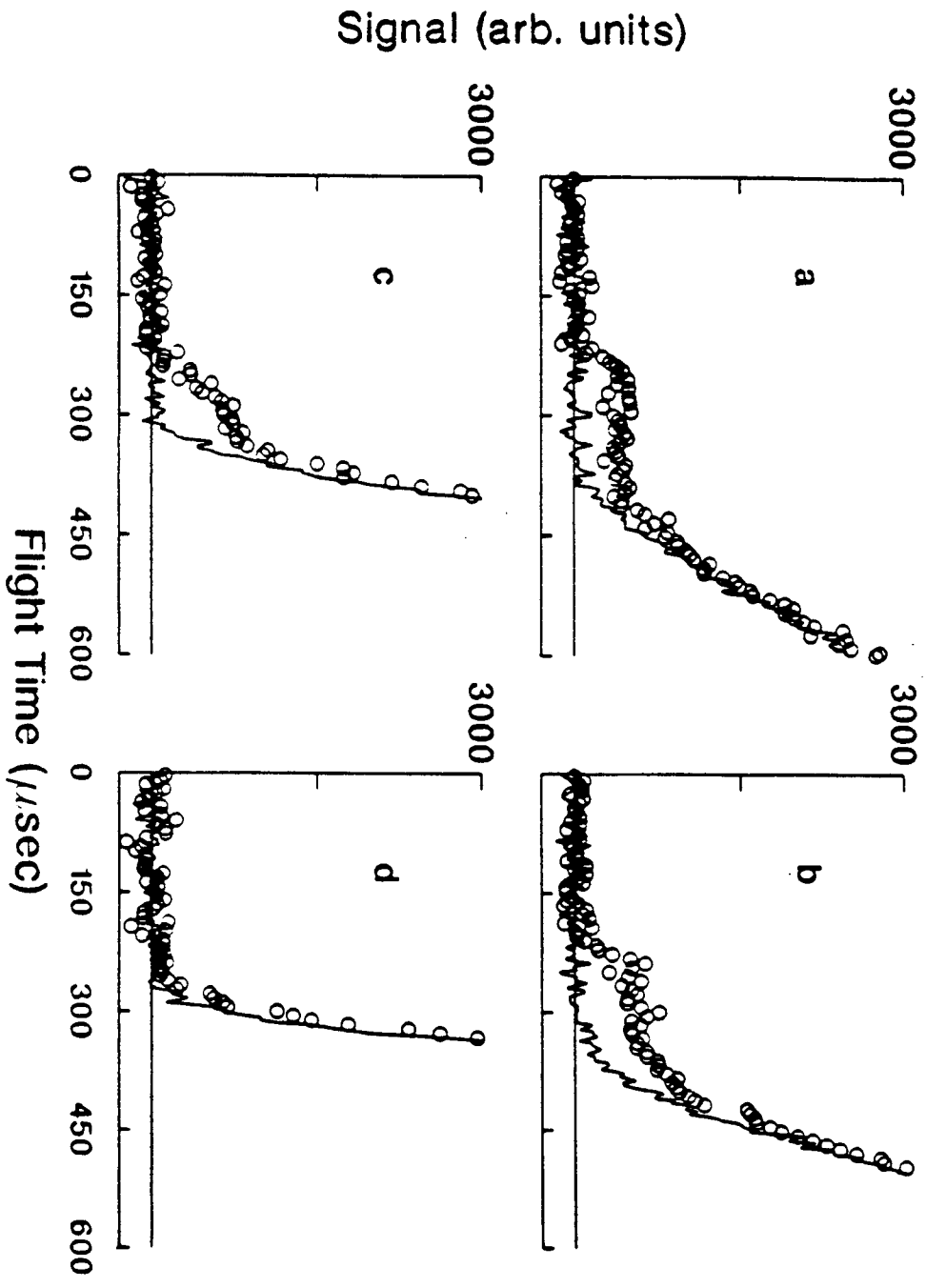
Signal (arb. units)
3000
a
e
3000
b
3000
c
3000
d
0
150
300
450
600
Flight Time (μsec)

Figure 3-15

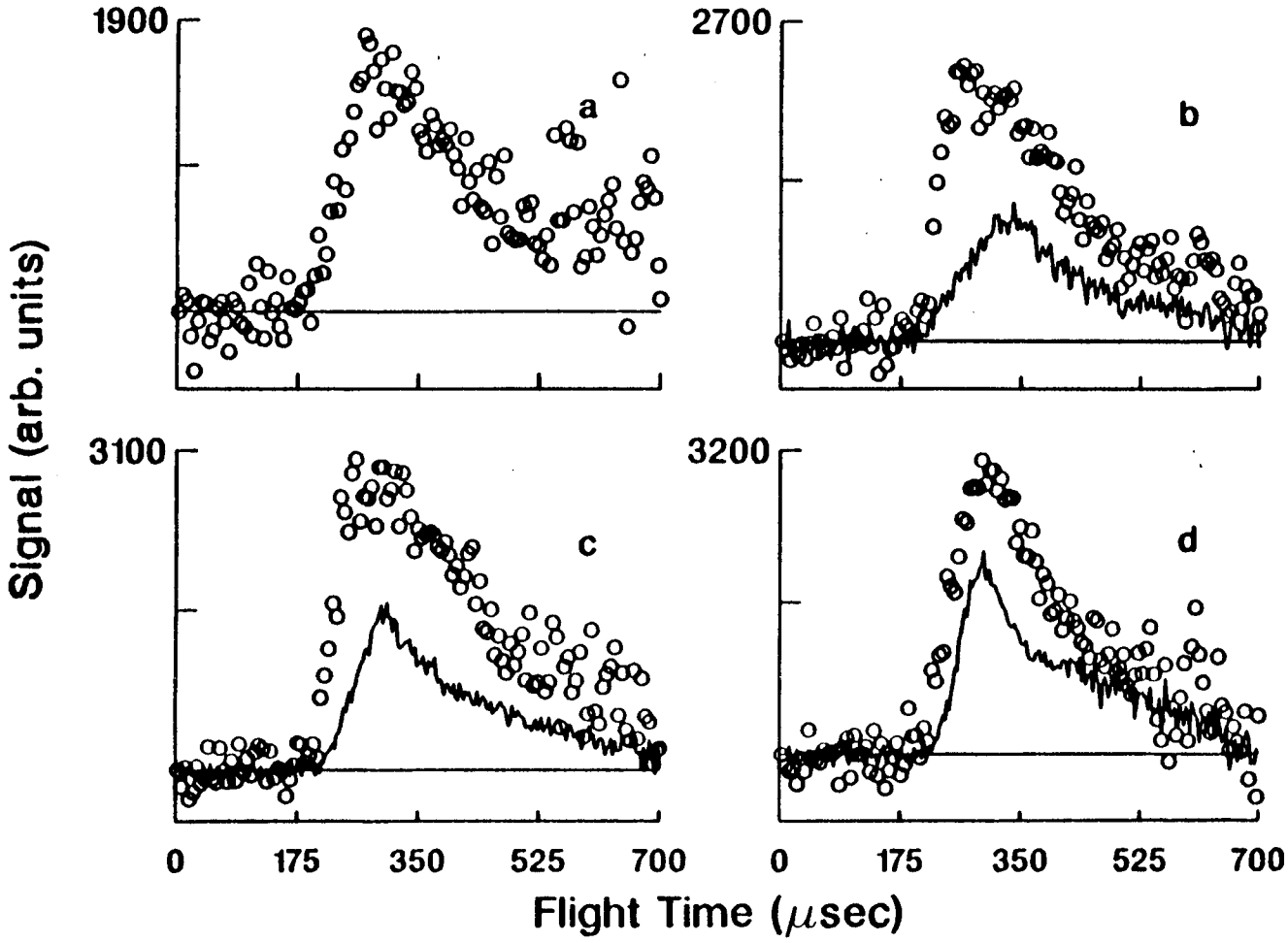
1900
2700
3100
3200
a
b
c
d
Signal (arb. units)
0
175
350
525
700
Flight Time (μsec)

Figure 3-16

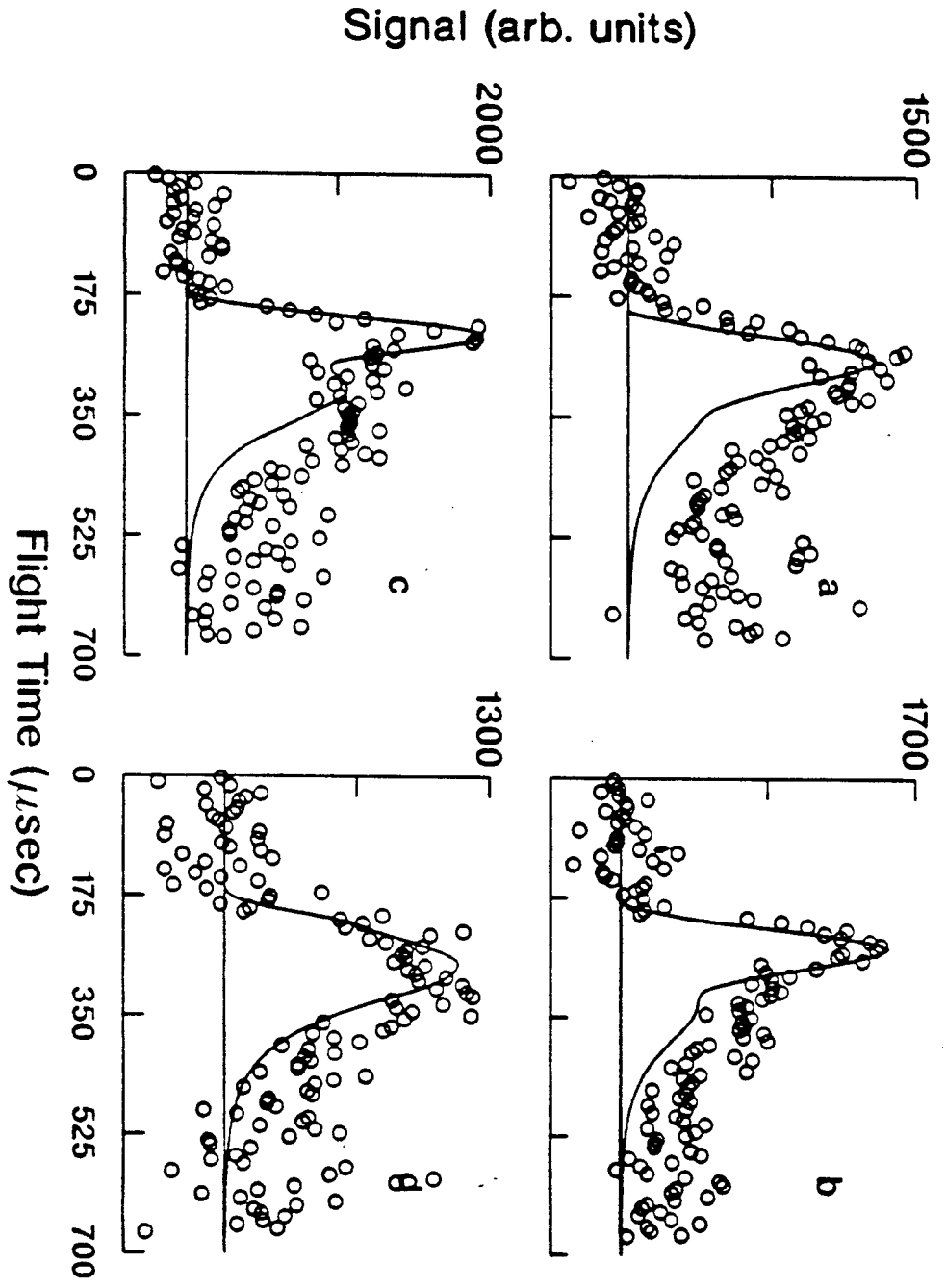
Signal (arb. units)
1500
2000
1700
1300
0
175
350
525
700
Flight Time (μsec)
a
b
c
d

Figure 3-17

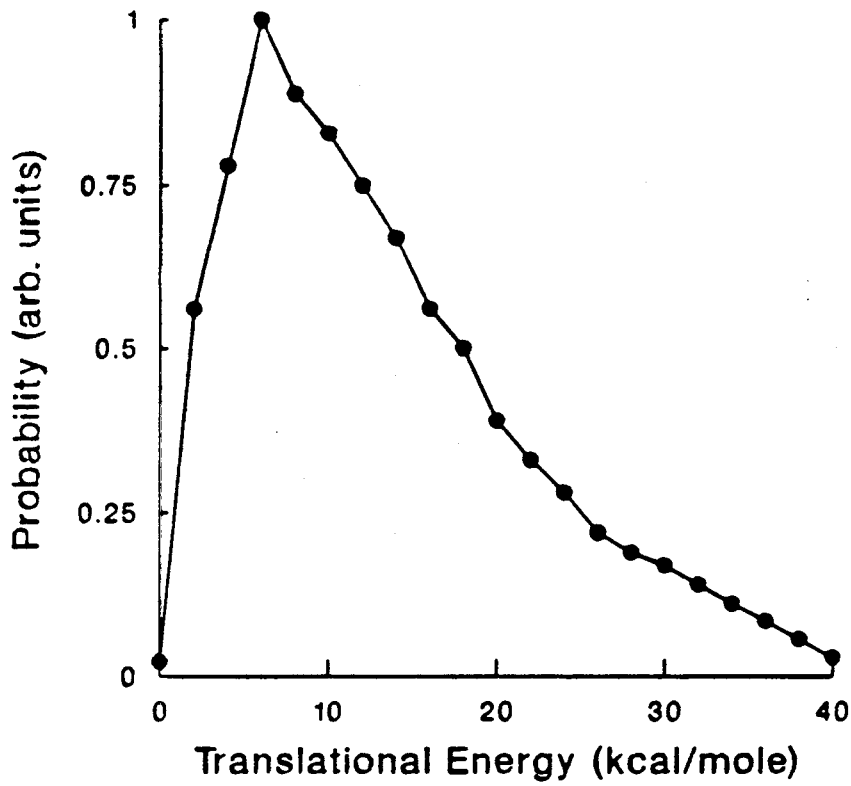
Probability (arb. units)
1
0.75
0.5
0.25
0
0
10
20
30
40
Translational Energy (kcal/mole)

Figure 3-18

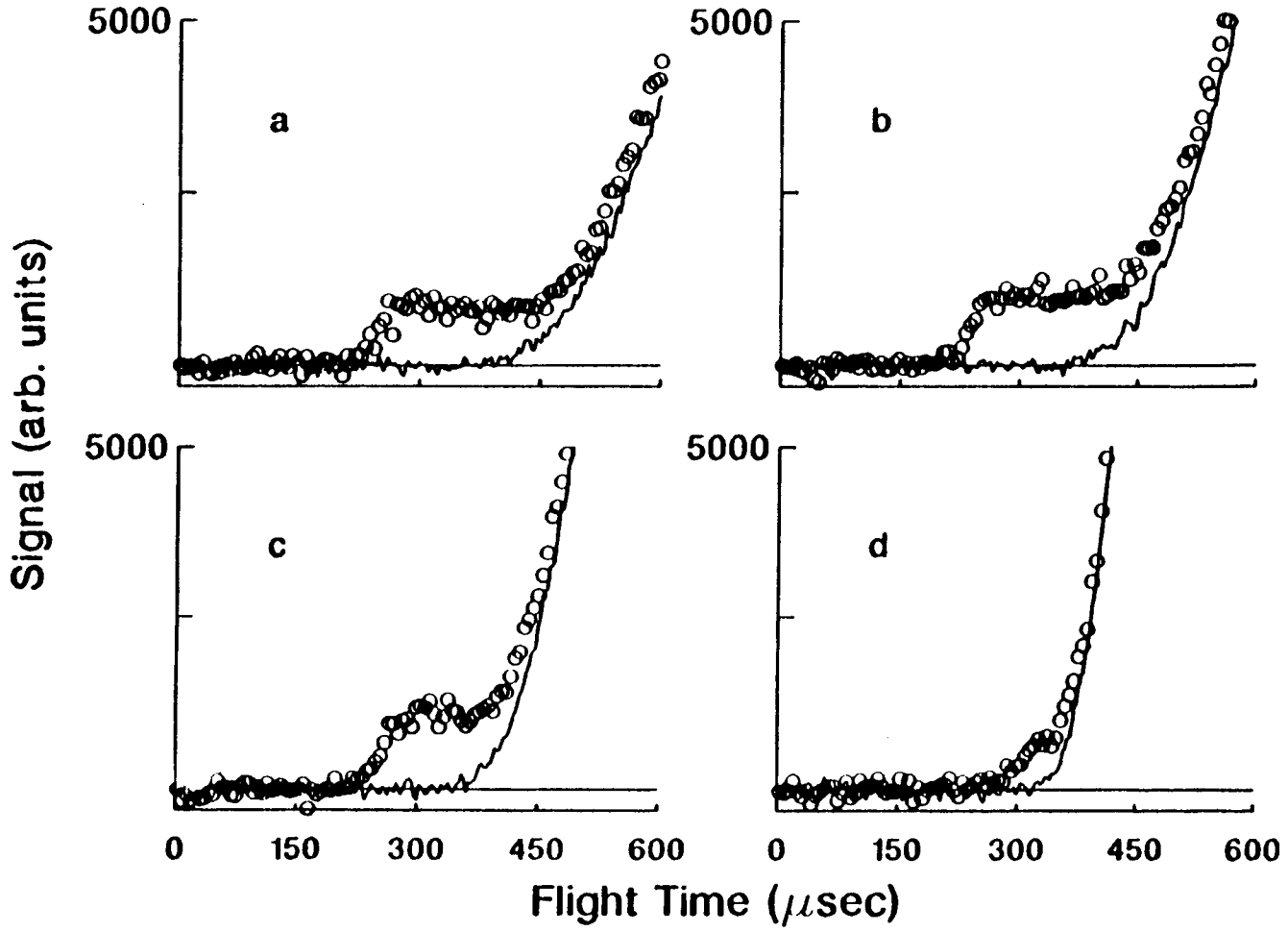
5000
a
5000
b
5000
c
5000
d
Signal (arb. units)
0
150
300
450
600
0
150
300
450
600
Flight Time (μsec)

Figure 3-19

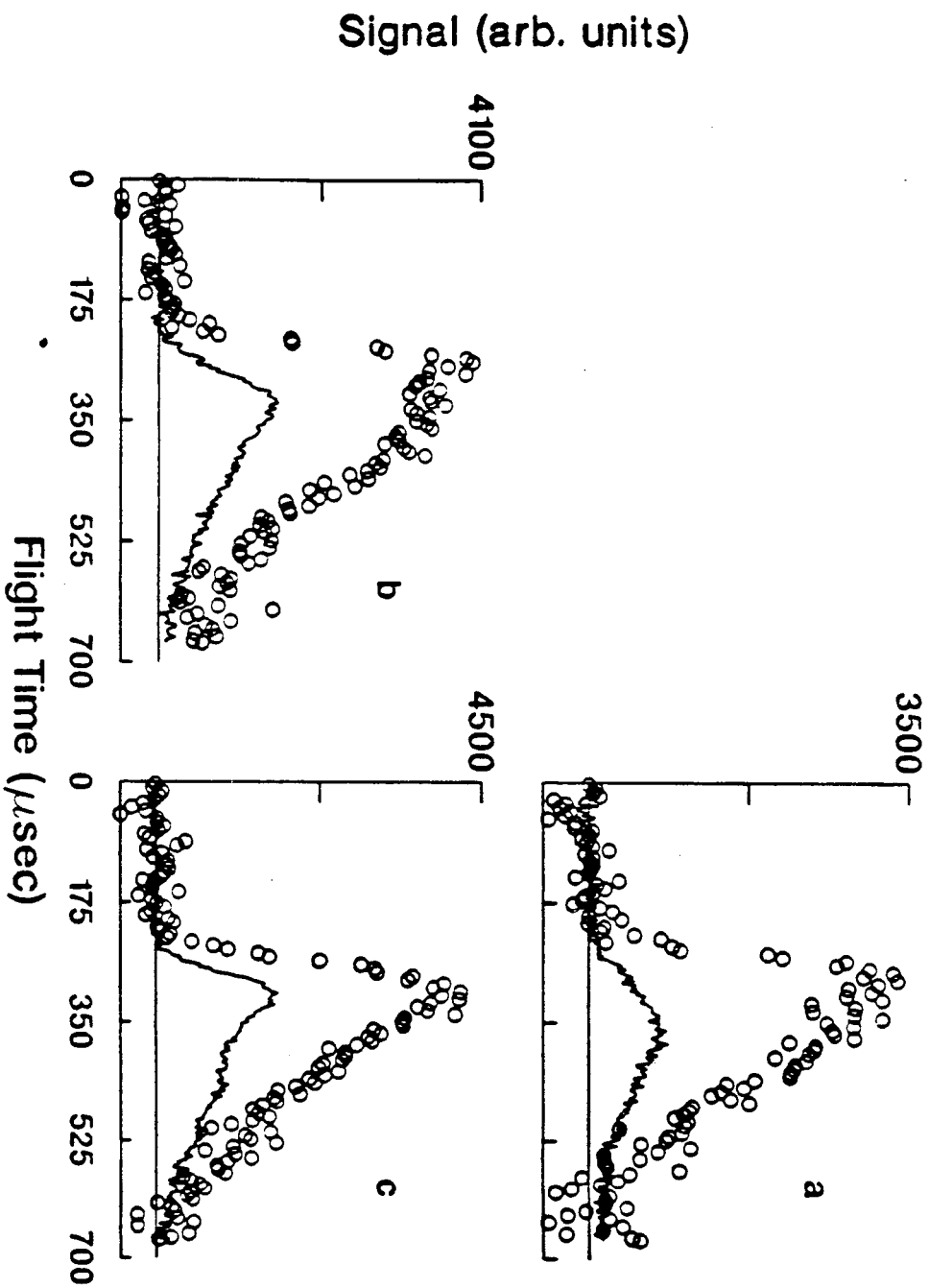
Signal (arb. units)
4100
0
175
350
525
700
b
4500
0
175
350
525
700
c
3500
a
Flight Time (μsec)

Figure 3-20

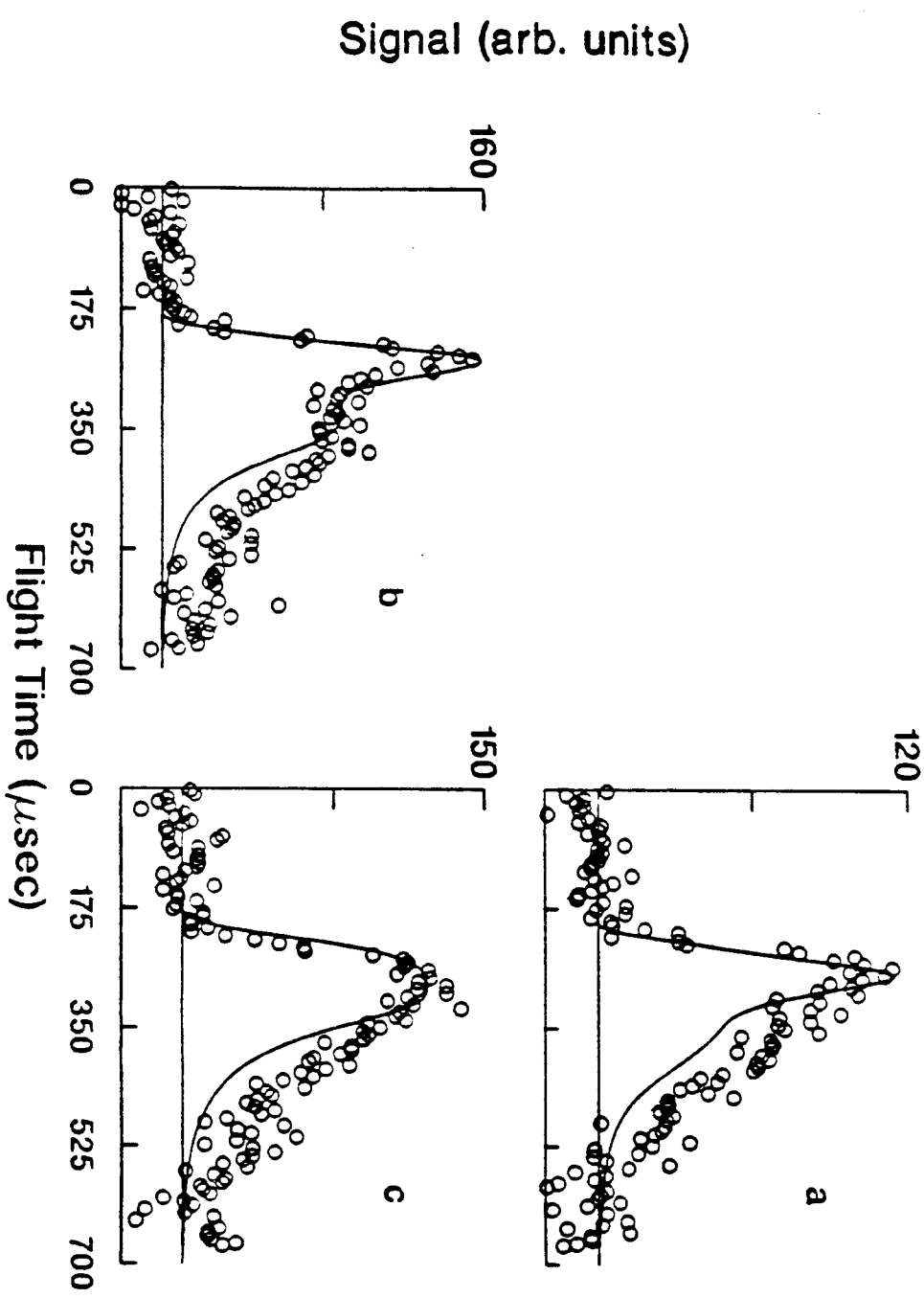
Signal (arb. units)
160
0
175
350
525
700
b
150
0
175
350
525
700
c
120
a
Flight Time (μsec)

Figure 3-21

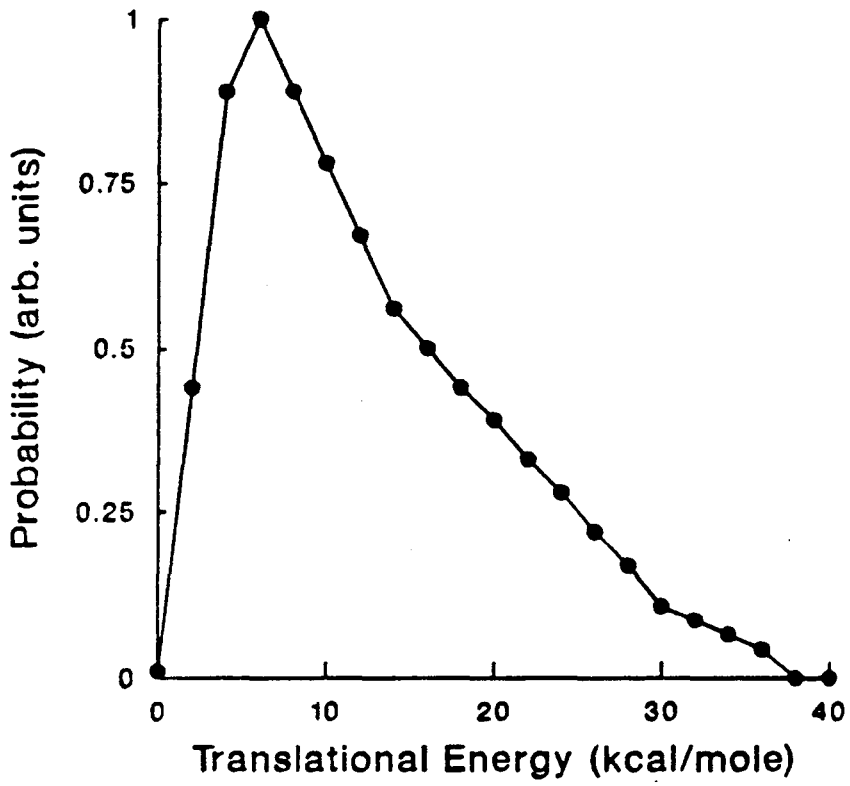
Probability (arb. units)
1
0.75
0.5
0.25
0
0
10
20
30
40
Translational Energy (kcal/mole)

Figure 3-22

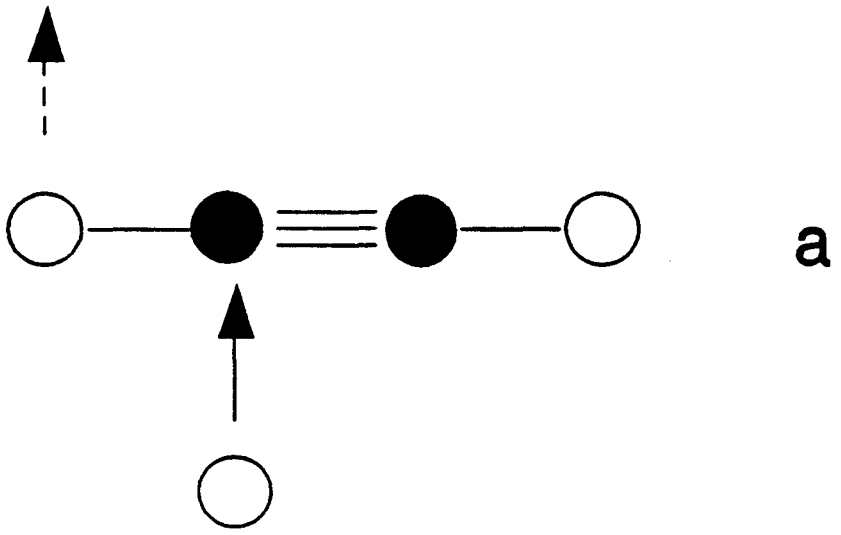

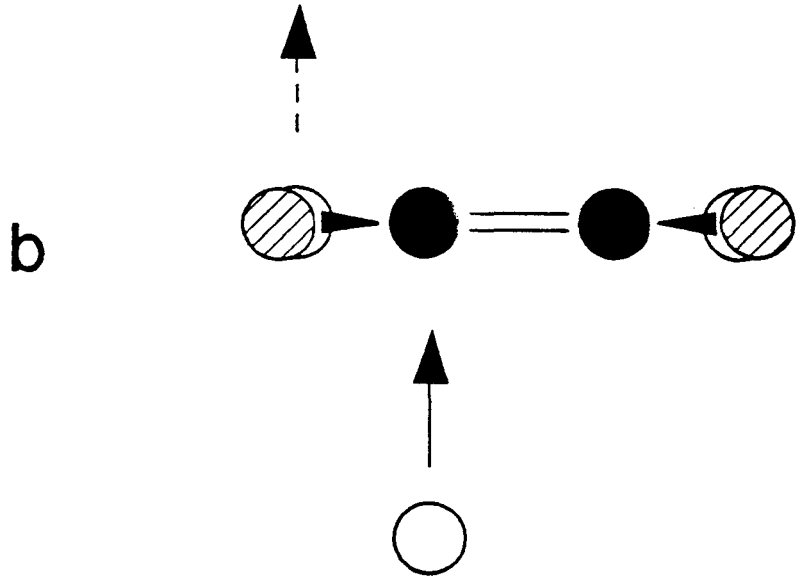

Figure 3-23

Chapter 4: Photodissociation Experiments on the 35" Machine

1. Experimental Configuration

The photolytic D atom source used in the reactive scattering experiments is a natural choice for photodissociation studies since the DI can be replaced by the molecule of interest. The pulsed valve will still fire into the photolysis chamber with the laser intersecting it perpendicularly. Since the photolysis chamber slits only allow fragments traveling perpendicular to the parent beam and laser to be detected, however, the detector must always be positioned facing these slits. A schematic of the experimental set-up is given in Figure 4-1. Because the COM velocity will be perpendicular to the detector direction, only fragments with a velocity greater than the COM can be detected; to ensure that the entire translational energy range is sampled, then, the faster photoproduct, which will always be the lighter one, must be detected in these studies. Figure 4-2a shows a representative Newton diagram

that illustrates this.

Photodissociation experiments using the 35" machine have several advantages over the more standard photolysis studies on machines such as the Lee group Rotating Source Machine (RSM). A comparison of the Newton diagrams for each type of experiment (Figure 4-2) shows that detection of the faster products improves the resolution because the distribution in parent beam velocity and angle will have little affect on the fragment velocity. This has the added advantage of allowing less well-defined but much higher intensity parent beam to be used, reducing the counting time in low signal experiments. In addition, since product detection will always be perpendicular to the parent beam and occurs in a region separate from the photolysis chamber, there is less background caused by the dissociative ionization of parent molecules.

2. Source Conditions

2.1. Molecular Beam

Since it is the photofragments that are of interest in the photodissociation experiment, several changes in beam conditions are required. The stagnation pressure of the neat parent beam must to lowered to ~30-75 torr and the pulse width shortened to 50 μsec to avoid thermalizing collisions involving the photofragments in the photolytic region; these were acceptable when the fragment beam was

used in reactive scattering and beam intensity was a more critical concern. In fact, to obtain even higher TOF resolution, a skimmer is inserted between the pulsed valve and photolysis region. The fragments produced then suffer fewer collisions before being detected because of the lower number density in the laser interaction region; in addition, since the nozzle-laser distance is increased from 0.3 cm to 2.3 cm (3 to 23 nozzle diameters), the parent molecules will be better cooled decreasing any effects from photolysis of hot parent molecules.

With these source conditions, dimer formation is not thought to be a problem. Clustering effects start to become important for $P_od > 10$ torr·cm (where P_o is the stagnation pressure and d is the nozzle diameter) [1] and in these experiments, $P_od \leq 7.5$ torr·cm. As discussed, looking directly at the acetylene beam with a backing pressure of ~300 torr showed that the beam consisted of less than 0.1% dimers. Ethylene clustering effects were observed only when $P_o \gtrsim 500$ torr or when the beam was seeded with Ar [2]. TOF spectra were taken at several different pressures to check for effects that would scale with the rate of dimer formation, P_o^2d [1]. No quadratic increase in signal was seen as the pressure was raised and no section of the spectrum changed significantly.

2.2 Photolysis Laser

The laser set-up used in the photodissociation experiments also had to be changed slightly from the reactive scattering experiments because a switch from 248 nm photons to 193 nm (ArF gas fill) was necessary. The hydrocarbons in these studies have virtually no absorption at 248 nm. In fact, 193 nm is just at the rising edge of the absorption curves. The wavelength change required using different focussing lenses to obtain a spot size ≈3 x 5 mm; the 19/24 cm cylindrical lens combination was replaced with a 30 cm spherical Suprasil lens. As in the reactive scattering experiments, the photolysis by-product buildup on the lens drops the transmission to ~70% of a new, clean lens so the actual number of photons reaching the molecular beam changes throughout the experiments. Thus all laser powers quoted are "before lens".

Since the heavier, primary products cannot be detected directly, multiphoton effects were of great concern in these experiments. For example, in the acetylene photodissociation, the H atoms detected come from either the primary process, $C_2H_2 \rightarrow C_2H + H$, or the secondary, $C_2H \rightarrow C_2 + H$. To isolate the effects due to secondary dissociation processes, the laser power was varied from ~20 mJ/pulse to ~235 mJ/pulse [7×10^{24} to 8×10^{25} photons/cm^{2}sec for the 20 nsec laser pulse]. The low laser powers were attained by placing 1 or 2 wire mesh screens in front of the laser output; each screen reduced the laser output by a factor of

three.

3. Background Considerations

The switch from reactive scattering to photodissociation studies on the 35" machine meant that the 20K cyropanels could no longer be effectively used to help reduce the detector background since the detector would always face the primary beam hole in the cryopanel. Instead, steady state background was controlled by gating the detector with a 2-slot wheel as was done in the D + H_2 experiments [3]. The wheel was positioned as close to the detector as possible; a teflon tube with a length slightly less than the distance between the wheel and the detector was held in the opening to reduce the number of molecules that enter from the main chamber. The wheel was spun at 25 Hz which exposes the detector for ~400 μsec from the initial laser firing, enough time for all photoproducts to enter.

The wheel, however, could only reduce steady state background in the detector. Temporal background problems from the use of the pulsed valve were also present in the photodissociation studies as they were in the reactive scattering. When the pulsed valve fires into the photolysis chamber, not all the molecules/fragments are removed. Many suffer collisions and eventually work their way out through the slits and enter the main chamber. This long, slow effusive-like hydrocarbon pulse can undergo dissociative

ionization in the detector and will appear in the recorded TOF spectra at many small masses. Because the photofragment signal is much faster that the peak of the background pulse, in these studies background subtraction is practical; a laser-off spectrum can be recorded, fit with a polynomial, and then subtracted from the laser-on spectrum (see Figure 4-3). The very low energy tail (<3 kcal/mole) of the $P(E_T)$, however, is generally regarded as suspect because of this temporal background.

The last background problem that was encountered was not experienced in the reactive scattering experiments and is somewhat unique to 35" photodissociation. At the low quadrupole RF voltages necessary for mass selection of the light fragments, there is a problem with laser RF pick-up causing a time dependent variation in the transmission of the quadrupole mass filter. For long, low-signal runs at times $\leq$ 50 μsec, large fluctuations in the background appeared whenever the laser was running. Unfortunately, these modulations usually appeared in the rising edge of the photofragmentation signal which is used to determine bond energies. The initial solution was to record backgrounds with the laser flagged but running and then subtract this modulation signal away (see Figure 4-4). Later, it was found that putting an RF power line filter (Corcom EMI 10VR7) on the mass spectrometer controller AC input line would essentially eliminate this noise.

4. Calibration

To fit the data, the parent beam velocity and spread as well as the detector parameters--ion flight time, effective ionizer length, neutral molecule flight length, and any offset--must be known. Information about the parent beam was obtained after the experiments were completed using a 4-slot TOF wheel with the pulsed valve in the secondary beam position (see Chapter 2). It should be noted that although the pulsed valve conditions were the same as those used during the experiments, the beam geometry (nozzle-skimmer distance, proximity to cold shields, etc.) was not the same. This was not of too much concern because, as discussed, looking perpendicular to the parent beam and detecting the fast products means that knowing the exact parent beam velocity is not critical. The measurements of the parent beam velocities and speed ratios for the gases photodissociated are given in Table 4-1 (see Chapter 2). These values are for the part of the pulse with the highest number density. This should be the section photodissociated since the laser/pulsed valve delay is varied to maximize signal.

The uncertainty in the detected product arrival time from the spread in parent beam velocity could be calculated and compared with the spread in product arrival time expected from the finite ionizer length/photolysis volume (see Table 4-2). As expected, for the fast section of the

TOF spectra, the variations in the parent beam velocity are not as important as the spread in the neutral flight path. In fact, the only cases where the parent beam uncertainty is important is for the slow tails of the heavier photofragments (namely F and HF in the $C_2H_2F_2$ photodissociation) where there are other more serious background problems.

As discussed, in the reactive scattering experiments, the detector parameters, as discussed, were taken from previous, continuous beam calibrations. The detector conditions, however, were changed dramatically in the photodissociation studies where fragments with small ionization cross-sections had to be detected. To maximize the signal, a very positive grid voltage (100 eV) and very negative extractor voltage (-1072 eV) were used. These changes have a significant effect on the ion flight time and offset. The detector could be calibrated by switching to continuous beams or by measuring TOF spectra of the photodissociation of an appropriate compound under the experimental conditions. The latter method was used. The compounds of choice were HI and DI for the same reasons that make them a good hot atom source--no sequential dissociation, large absorption cross-section, and no fragment vibrational/rotational excitation [4]. In addition, the H-I and D-I bond energies [5], as well as the $I^*_{1/2} \leftarrow I_{3/2}$ spacing [6], are well known. Using the

experimental conditions, TOF spectra for the photolysis of a mixture of HI and DI synthesized in the lab [3] was measured. The forward convolution data analysis program developed by X. Zhao [7] was used to fit the spectra with the detector parameters treated as the unknowns. An input $P(E_T)$ was generated using the known bond energies, iodine atom excitation energies, and an assumed initial parent rotational distribution; the program averaged this over the experimental apparatus function. With fine adjustments in the detector parameters, good fits to the TOF spectra were obtained. Figure 4-5 shows the H and D atom spectra from the photodissociation of skimmed and unskimmed beams of HI and DI under the typical experimental conditions. The solid line is the best fit TOF spectra using a rotational temperature of 100K. It should be noted that the fits are not sensitive to this rotational temperature; the peak width is mainly due to the ionizer length. These TOF spectra point out the differences between using and not using the skimmer. As would be expected, the skimmer spectrum is narrower; without the skimmer to help define the beam, the photolysis region is larger so there is more spread in the fragment flight length.

5. Experimental Protocol

All the photodissociation experiments followed the same general procedure. TOF spectra were taken of the molecules

of interest at several different laser powers to determine the extent of the secondary dissociation problem. Laser-off scans were regularly measured throughout each experiment to be later subtracted from the signal. To analyze the data, the forward convolution data analysis program [7] was used. A trial product translational energy distribution, $P(E_T)$, is averaged over experimental parameters to obtain a fit to the laboratory TOF. Through an iterative process, the $P(E_T)$ that best fits the experimental TOF is obtained. The program can also be used to fit any secondary dissociation processes observed. With this option, one chooses the internal energy range of primary products that undergo secondary dissociation and then gives the $P(E_T)$ for the secondary process.

References

1. D.R. Miller in Atomic and Molecular Beam Methods: Volume 1, ed. by G. Scoles (Oxford University Press, New York, 1988), p 14.

2. A. Stolow, E.F. Cromwell, and Y.T. Lee, to be published.

3. R.E. Continetti, B.A. Balko, and Y.T. Lee, J. Chem. Phys. **93**, 5719 (1990); R.E. Continetti, Ph.D. Thesis, University of California, Berkeley (1989).

4. G.W. Flynn and R.E. Weston, Jr., Ann. Rev. Phys. Chem. **37**, 551 (1986).

5. K.P. Huber and G. Herzberg, Molecular Spectra and Molecular Structure: IV. Constants of Diatomic Molecules (Van Nostrand Reinhold Company, New York, 1979).

6. M.W. Chase, Jr., C.A. Davies, J.R. Downey Jr., D.J. Frurip, R.A. McDonald, and A.N. Syverud, JANAF Thermochemical Tables, Third Edition (Journal of Physical and Chemical Reference Data, New York, 1986).

7. X. Zhao, Ph.D. Thesis, University of California, Berkeley (1988).

Tables

Table 4-1. Parent Beam Characteristics.

Gas	No Skimmer 25-50 torr 400V/50μsec			Skimmer 70 torr 500V/100μsec		
	$V_o/\Delta V$	V_o cm/s	% Ideal[1]	$V_o/\Delta V$	V_o cm/s	% Ideal[1]
C_2H_2	4.5	6.0×10^4	73	5.5	6.5×10^4	80
C_2H_4	4	6.0×10^4	71			
$C_2H_2F_2$ (cis)	5	4.6×10^4	83			
HI/DI[2]	4.5	3×10^4	75			

1. Ideal is calculated using $(7kT/m)^{1/2}$ for linear molecules and $(8kT/m)^{1/2}$ for non-linear polyatomics.

2. No TOF spectra were taken of the HI and DI parent beams. V_o was estimated assuming 75% of the ideal velocity was attained in the expansion. A typical speed ratio was used.

Table 4-2. Comparison of Contributions to Arrival Time Uncertainty.

Gas	m/e	E_T kcal/ mole	Arrival Time (μsec) Slow V_o	Arrival Time (μsec) Fast V_o	Arrival Time (μsec) Path 38.5 cm	Arrival Time (μsec) Path 39.5 cm
$C_2H_2F_2$	H	2	97.3	97.8	96.3	98.8
		65	17.6	17.7	17.4	17.9
	H_2	2	140.1	141.6	139	142
		32	36.1	36.1	35.6	36.5
	F	7	282	296	284	291
		24	153	155	152	156
	HF	4	395	435	406	417
		80	90.7	91.0	89.8	91.9
C_2H_4	H	2	98.5	99.5	97.8	100.3
		40	22.5	22.5	22.2	22.8
	H_2	8	71.9	72.4	71.3	73.1
		80	23.9	23.9	23.6	24.2
C_2H_2	H	3	80.6	81.0	79.7	81.7
		16	35.2	35.2	34.8	35.7
HI	H	78	16.1	16.1	15.9	16.3
		56	18.9	18.9	18.7	19.2
DI	D	78	23.6	23.6	23.3	23.8
		56	27.5	27.5	27.2	27.8

1. For $C_2H_2F_2$, C_2H_4, C_2H_2, and HI/DI the limits of the velocity range are 3.6 to 5.5 x 10^4 cm/sec, 4.5 to 7.5 x 10^4 cm/sec, 4.7 to 7.3 x 10^4 cm/sec, and 2.3 to 3.7 x 10^4 cm/sec respectively.

Figure Captions

Figure 4-1. Side view (a) and top-view (b) of the experimental arrangement. The piezoelectric pulsed valve (1) is used to create the hydrocarbon beam. The valve fires into the photolysis chamber (2). For the high resolution spectra, the beam passes through a skimmer (3) mode. A 4" DP (4) as well as liquid nitrogen cooled cryopanels (5) pump the chamber. The 193 nm output of the excimer laser (6) passes through a focusing lens (7) and perpendicularly intersects the hydrocarbon beam (8). The photoproducts (9) pass out of the differential chamber and travel 39.0 cm to the detector (10) where they can be ionized in the electron impact ionizer. A chopping wheel (2) is used to gate the detector to help reduce background.

Figure 4-2. (a) Representative Newton diagram for a photodissociation experiment on the 35" machine; the system shown is $C_2H_2 \rightarrow C_2H + H$. 16 kcal/mole is the translational energy of the fastest products and 3 kcal/mole is the lower limit for most of the observed product. The diagram shows that since the detection direction is perpendicular to the parent beam only the lighter product can be observed. (b) Newton diagram for the $C_2H_2 \rightarrow C_2H + H$ half reaction in which the

heavier product is detected as was done on the RSM. Comparison of the two diagrams shows that the 35" experiment will be much less affected by variations in the parent beam.

Figure 4-3. Representative high resolution H atom TOF spectrum showing the raw data (open circles) as well as the polynomial fit to the laser-off signal (solid line). For most of the systems studied, this background correction has very little effect on the region of interest.

Figure 4-4. Representative high resolution H atom TOF spectrum showing the raw data (open circles) with the RF pickup modulation spectrum (solid line).

Figure 4-5. H/D atom TOF spectra from HI/DI photolysis for calibration purposes. Open circles are the raw data and the solid line is the calculated fit. Photodissociation of (a) HI with no skimmer used (b) HI with skimmer in place and (c) DI with skimmer in place (note the change in time scale).

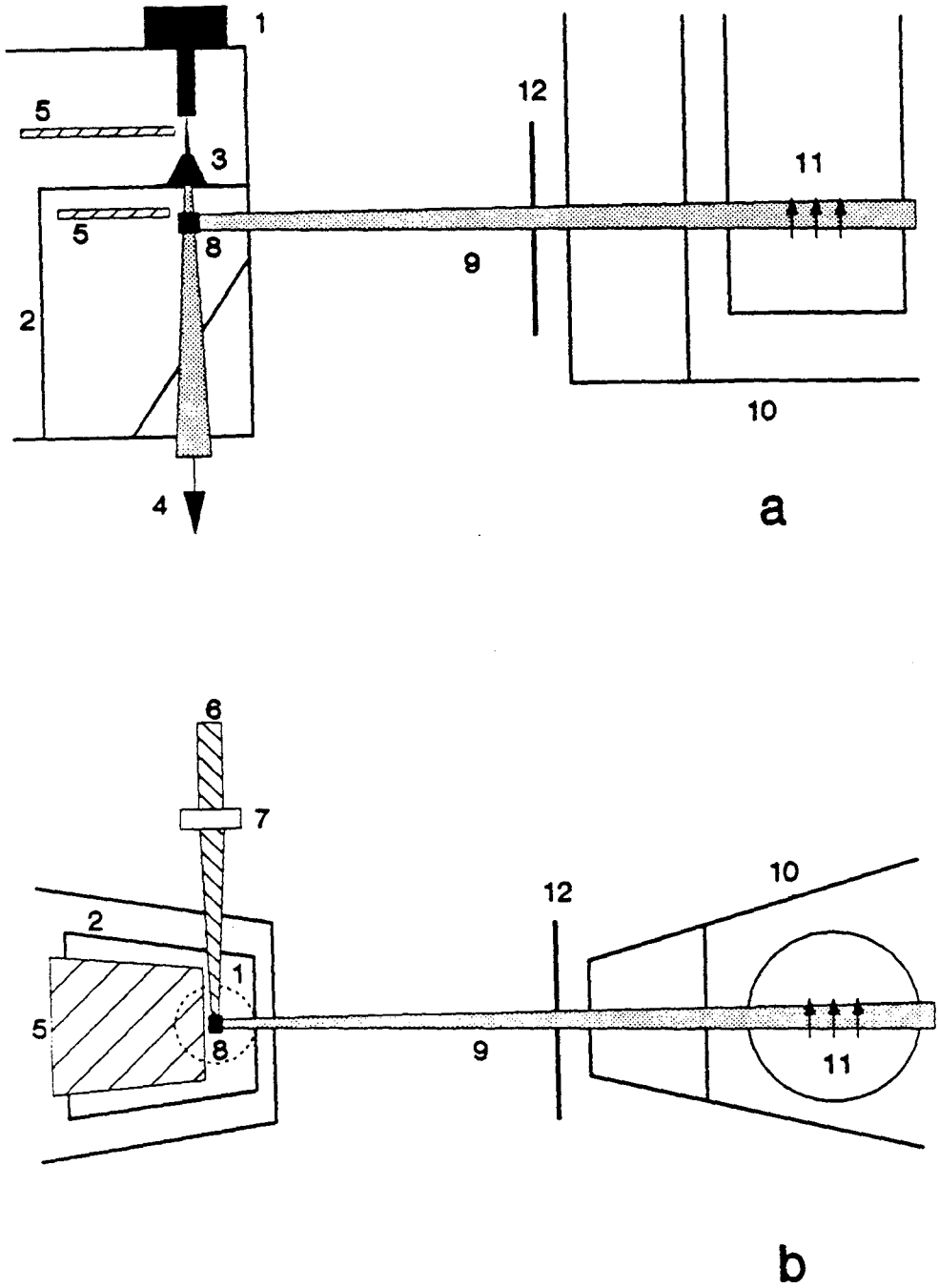

Figure 4-1

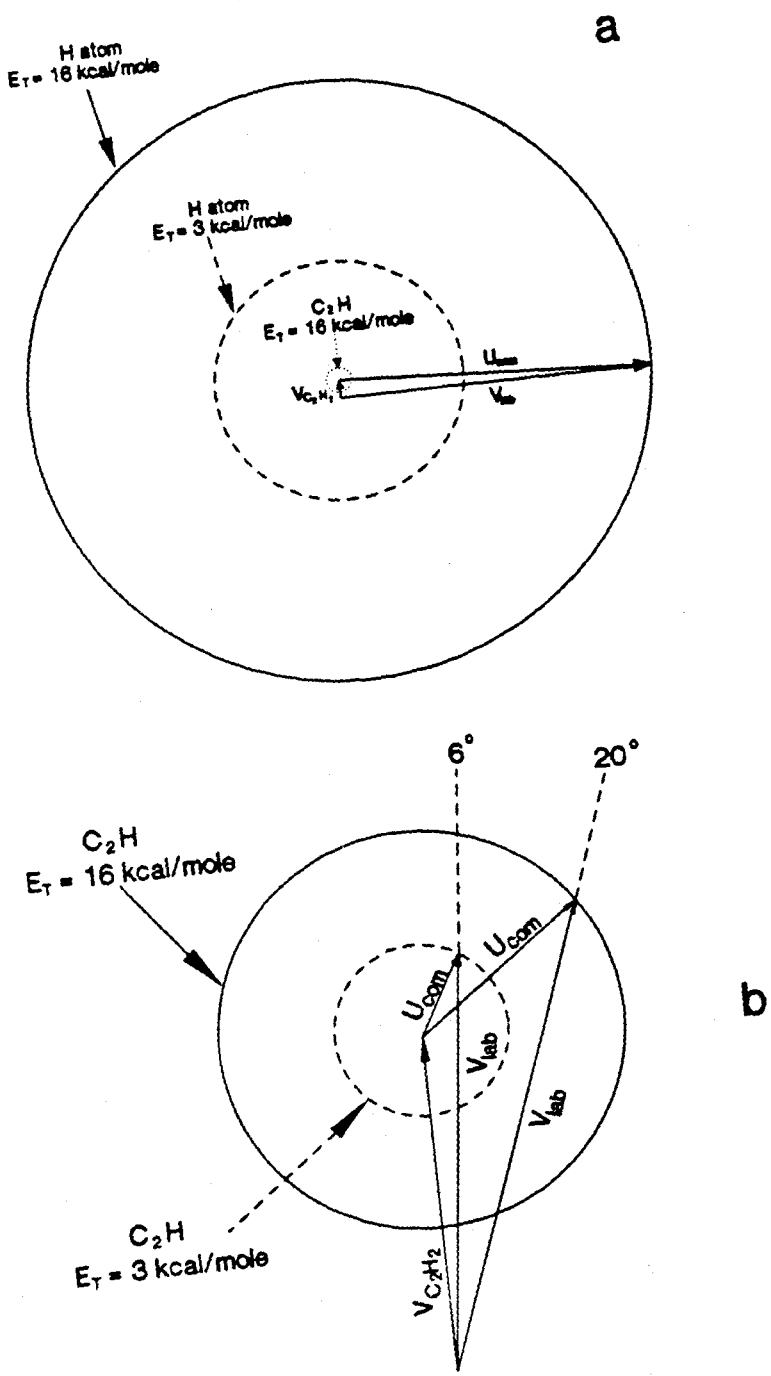
a
H atom
E_T = 16 kcal/mole
H atom
E_T = 3 kcal/mole
C_2H
E_T = 16 kcal/mole
U_{com}
V_{lab}
6°
20°
C_2H
E_T = 16 kcal/mole
U_{com}
U_{com}
V_{lab}
V_{lab}
C_2H
E_T = 3 kcal/mole
$V_{C_2H_2}$
b

Figure 4-2

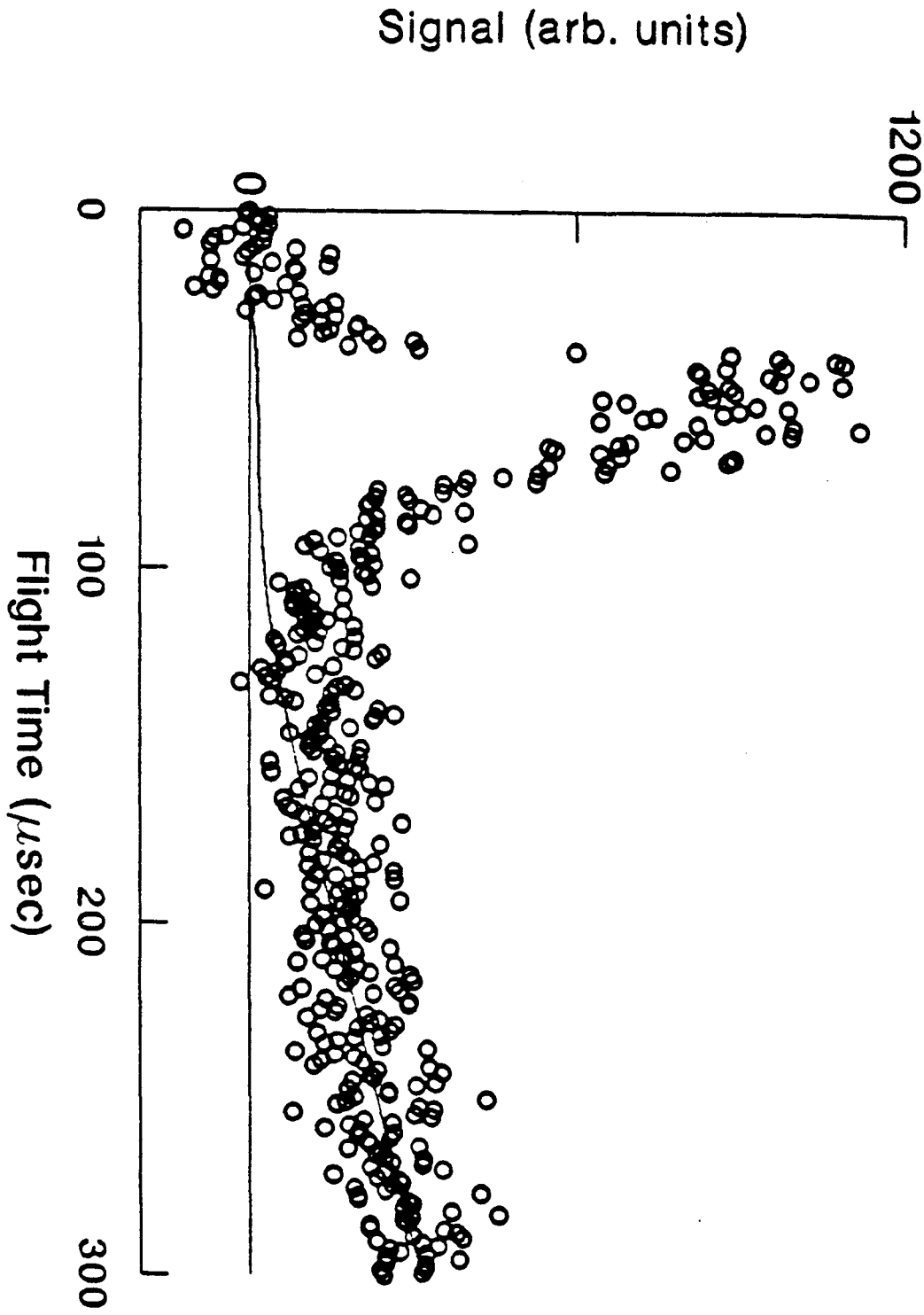

Figure 4-3

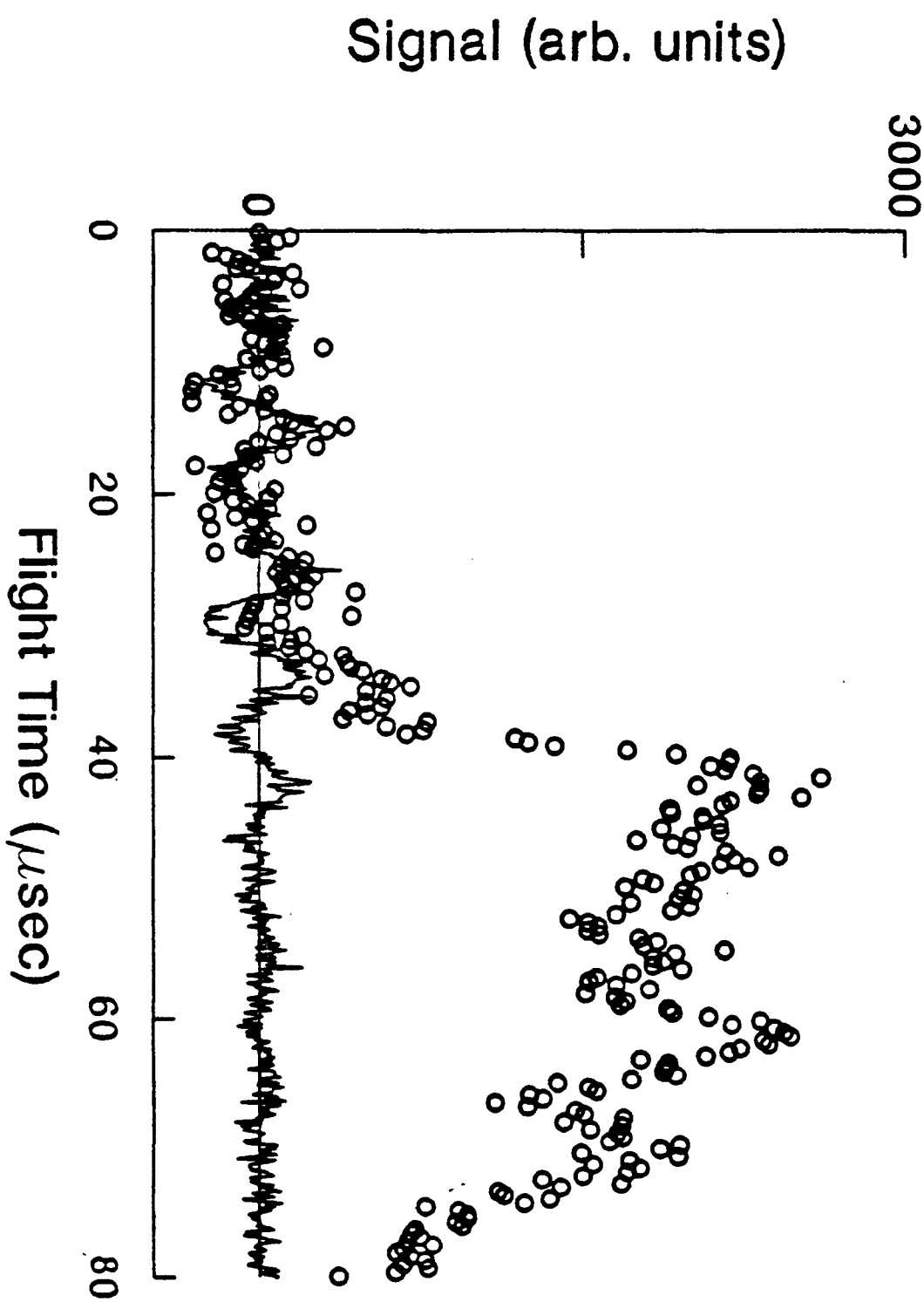

Figure 4-4

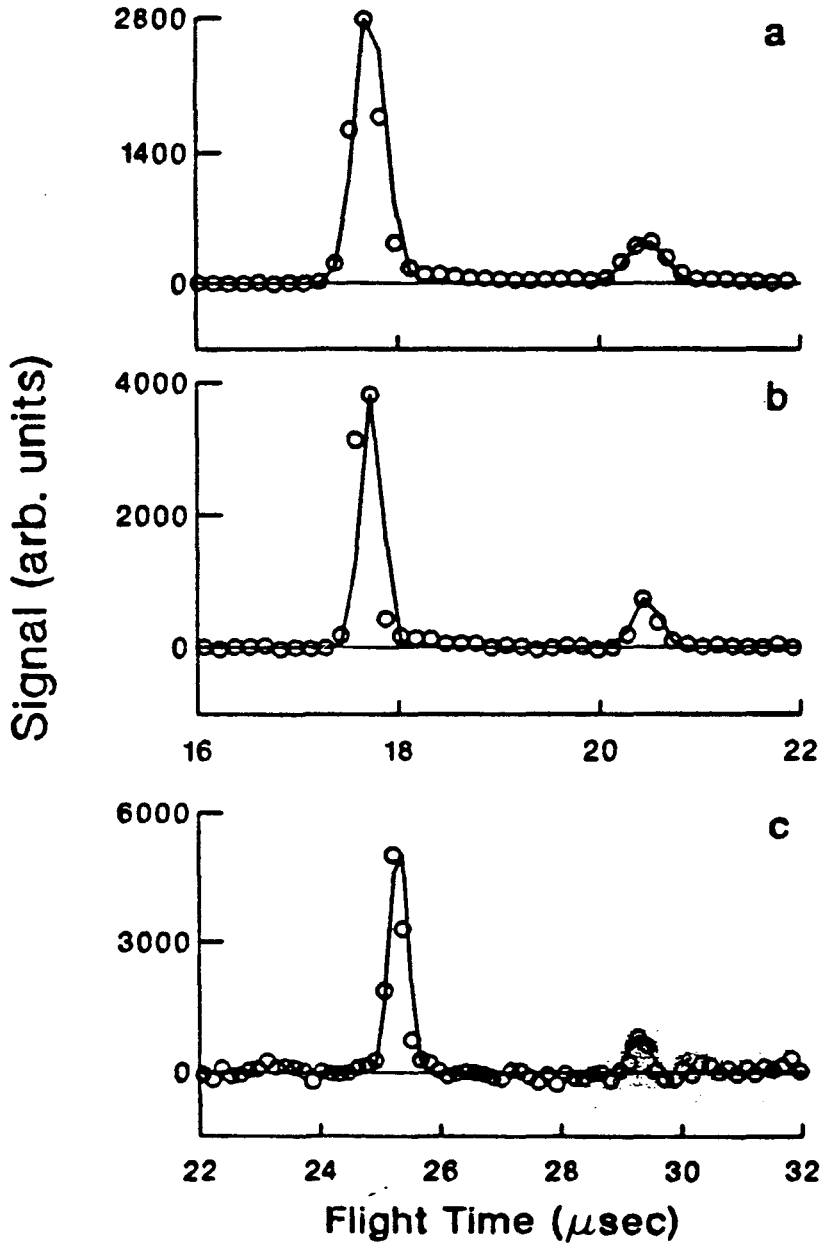
2800
1400
0
a
4000
2000
0
b
16
18
20
22
6000
3000
0
c
22
24
26
28
30
32
Signal (arb. units)
Flight Time (μsec)

Figure 4-5

Chapter 5: Photodissociation of Acetylene at 193 nm

1. Introduction

There is a scarcity of basic knowledge about acetylene and the ethynyl radical which must be remedied because of their critical role in combustion processes [1]. Photofragmentation translational spectroscopy is one way to do this. This technique has the capacity to determine bond energies and can be used to derive information about the excited electronic and/or vibrational states of the resulting radicals. It should come as no surprise, then, that Alec Wodtke in this group studied the 193 nm photodissociation of C_2H_2 on the RSM by measuring the TOF spectrum of the C_2H and C_2 fragments. Wodtke and Lee found an upper bound to the HCC-H bond energy of 132 ± 2 kcal/mole, were able to resolve vibrational and electronic structure of C_2H, and derived information about the dynamics of the dissociation process [2]. Subsequent experiments confirmed Wodtke and Lee's bond energy [3,4]. Recently,

however, two groups [5,6], using different techniques, reported HCC-H bond energies significantly lower than Wodtke and Lee's which initiated a flurry of experimental [7,8,9] and theoretical studies [10-13] (see Table 5-1). As one of the lower bond energies was based on the measurement of the H atom translational energy distribution via the Doppler profile [5], it was decided to directly measure the velocity distribution of H atoms using the molecular beam photofragmentation technique for comparison. Since the experimental set-up can be calibrated for precise velocity measurements of H atoms by photolyzing well-characterized hydrogen halides, any questions regarding systematic errors should be eliminated. The detection of H atoms on the 35" machine should also result in better TOF resolution since it would be less affected by variations in the parent beam or parent beam dissociative ionization.

The C_2H_2 photodissociation is one instance where having the ability to obtain high resolution TOF spectra is worthwhile. The C_2H fragment is not expected to be significantly rotationally excited. The parent C_2H_2 molecules in the beam produced by a supersonic expansion through the nozzle should have a very low rotational temperature which means rotational excitation of the C_2H fragment can only come from the recoil of the H atom leaving the C_2H. Owing to the light mass of the H atom and a relatively small exit impact parameter, the torque exerted

to the C_2H product is expected to be small, especially when the H atoms depart with low translational energies. This means that the peaks in the TOF spectrum corresponding to various vibrational and electronic energy levels will not be smeared out Seeing the internal energy distribution of the C_2H fragments from the C_2H_2 dissociation is especially interesting because of the multiple potential energy surfaces involved [2] and the confusion of states in the C_2H system [14]. In addition, the extensive coupling between the C_2H A and X electronic states means that the Born-Oppenheimer approximation, a standard assumption in many photodissociation models, is not appropriate [15].

193 nm is a convenient wavelength to use for these studies. The experiment can measure the bond dissociation energy since absorption of a single photon provides 147.9 kcal/mole, enough to break the C-H bond and excite the C_2H fragment but not the H atom. Acetylene does not absorb very strongly at longer wavelengths (> 200 nm) but at 192.86 nm, the 155K cross-section is a reasonable 2×10^{-19} cm^2 [16]. It is also known that the 193 nm absorption is to the ν_3 = 10 (the C-H bending vibration) of the trans-bent ^1A_u excited state [17-19]. Exciting only one, well-studied state simplifies the interpretation of the experiment.

Some information is available about the 193 nm photodissociation of acetylene. Figure 5-1 [7,20-22] shows the products that are thermodynamically possible. At laser

intensities below 10^{26} photons/cm^{2}s, for a 20 nsec pulse duration, the primary process observed by Wodtke and Lee is [2]:

$$C_2H_2 \rightarrow C_2H + H \qquad (I).$$

It was not possible for Wodtke and Lee to determine unambiguously whether just $C_2H(X)$ formed or both the X and A states [2]. This question was cleared up in Fletcher and Leone's FTIR study of the C_2H products from the 193 nm photodissociation of C_2H_2 where they detected C_2H in both the A and X states [23].

Not enough is known about the potential energy surfaces of excited C_2H_2 and C_2H to understand why both states of C_2H form. Better potential surfaces exist for R-CN. Realizing that CN is isoelectronic with C_2H, Wodtke and Lee discussed in detail how these surfaces could be used to interpret the C_2H_2 dissociation; only their basic scheme will be summarized here [2]. There is no singlet excited state surface that correlates with $C_2H(X)$ in the range of a 193 nm photon; in the absence of other effects, then, only excited state C_2H would be produced. In the absorption, the C_2H_2 goes to the $1^1A"$ surface which correlates to formation of $C_2H(A)$ + H. Because of an avoided crossing with a higher energy surface, $2^1A"$, there is an exit barrier for this channel. On the $1^1A"$ surface, however, there exists the possibility of vibronic coupling with the repulsive portion of the $2^1A'$ surface. This state also correlates with $C_2H(A)$

+ H but because of its repulsive nature, curve hopping to the $1^1A'$ surface should be possible; it is this $1^1A'$ state that correlates with $C_2H(X)$ + H. The barrier height of the $1^1A''$ surface, to a large extent, should control the $C_2H(A)/C_2H(X)$ ratio [2]. Recent fluorescence studies that probe C_2H_2 predissociation suggest that the repulsive state that vibronically couples with $1^1A''$ is a triplet; curve hopping from this triplet to $1^3A'$ would then lead to $C_2H(X)$ [24-26]. Support for the general mechanism -- excitation to a state with a barrier, coupling to a repulsive state, and then nonadiabatic surface hopping -- comes from the isotopic studies of Cool, Goodwin, and Otis. Upon 193 nm excitation of C_2HD, they found a marked preference for the $C_2D(A,X)$ + H channel over $C_2H(A,X)$ + D. This is explained with the above mechanism; the C-H vibrational wave function has greater barrier penetration than the C-D and the higher H atom velocity, as compared to the D, allows for more nonadiabatic curve crossing [26].

No evidence has been found for the only other one photon channel thermodynamically allowed:

$$C_2H_2 \rightarrow C_2 + H_2 \qquad \text{(II)}.$$

Wodtke and Lee did not observe C_2 from this channel but estimated that the II/I branching ratio could be as much as 0.15 and the C_2 from II would still remain hidden in the signal from the C_2 formed in the secondary photodissociation of the C_2H [2].

At higher laser intensities, more channels open up. McDonald's early emission studies of the multiphoton photodissociation of C_2H_2 identified several two and three photon processes. Most ($\geq$ 90%) of the measured emission intensity was from the $C_2(A^1\Pi_u \rightarrow X^1\Sigma_g^+)$ transition. Their observations were consistent with a two photon process that proceeds via sequential elimination of two H atoms:

$$C_2H_2 \rightarrow C_2H + H$$

$$C_2H \rightarrow C_2 + H$$

Emission from $C_2(d^3\Pi_g \rightarrow a^3\Pi_u)$ was also detected but this was only a minor channel (~1% of the $A^1\Pi_u$). Based on power dependence studies, they concluded that three photons were absorbed but could not determine the mechanism. Fluorescence from $CH(A^2\Delta \rightarrow X^2\Pi)$ was recorded; this channel was also minor (< 1% of $A^1\Pi_u$). The production of $CH(A^2\Delta)$ appeared to proceed via two photon excitation of C_2H_2 -- the C_2H intermediate was not involved. Finally, emission from $C_2(C^1\Pi_g \rightarrow A^1\Pi_u)$ was reported but the signal was not intense enough (< 1% of $A^1\Pi_u$) to derive any mechanistic information [27].

Wodtke and Lee also saw evidence of multiphoton processes in their studies. The $C_2(A^1\Pi_u, {}^3\Pi_u, X^1\Sigma_g^+)$ that they detected formed via two sequential one photon absorption steps: $C_2H_2 \rightarrow C_2H \rightarrow C_2$ [2]. Recently, several more electronically excited C_2 states have been detected from the sequential 193 nm photolysis of C_2H_2. Using LIF methods,

Urdahal, Bao, and Jackson reported the formation of $C_2(a^3\Pi_u$, $d^3\Pi_g$, $A^1\Pi_u$, $C^1\Pi_g$, and $B'^1\Sigma_u^+)$ [28,29]. Goodwin and Cool detected the presence of $C_2(B^1\Delta_g)$ and $C_2(b^3\Sigma_g^-)$ in the two step photolysis of C_2H_2 [30].

The formation of some of these higher excited states of C_2 is only energetically possible if the intermediate C_2H is internally excited. In fact, by studying the change in shape of the C_2H TOF spectra with laser power, Wodtke and Lee showed that the C_2H absorption cross section was larger for more highly excited C_2H molecules [2]. From what is known about the C_2H radical excited electronic states, this is not surprising. The lowest lying electronic states for which a transition from the $^2\Sigma^+$ ground state is allowed are $^2\Sigma^+$ and $^2\Pi$. These states have vertical excitation energies of 7.32 eV and 8.11 eV, respectively. The transition energy, however, drops to the 193 nm (6.4 eV) range if one assumes that the upper state is bent in its equilibrium configuration and that the initial state's C-C bond length is greater than the equilibrium value and/or the C-C-H angle is not 180° [14,31,32].

2. Experiment

The Newton diagram representing the photodissociation of C_2H_2 with H atom detection was used as an example in Chapter 4 (Figure 4-2).

The general scheme for the photodissociation

experiments was also discussed in Chapter 4. These acetylene studies followed this general procedure. The one difference was that since the C_2H_2 gas (Matheson) used comes saturated in acetone, the gas was first passed through a dry ice/acetone trap to remove the impurity.

3. Results

3.1. Skimmed Beam/High Resolution

The major problem encountered in determining the HCC-H bond dissociation energy with the H atom TOF technique, is contamination from multiphoton and/or sequential dissociation events which can produce faster H atoms than from process I. The TOF spectrum shown in Figure 5-2a, which is mainly due to the single photon dissociative process, could only be obtained at very low laser power (~35 mJ/pulse). Despite 5.6 hrs of counting, the S/N ratio of the spectrum is still low. However, the scan is of sufficient quality to generate the fast edge of the $P(E_T)$ which can then be incorporated in fitting spectra where secondary dissociation is more of a problem.

It should be noted that the spectrum in Figure 5-2a shows a good deal of RF-pickup noise at the fast edge even though the data was collected with the RF filter installed; this is because the signal is so poor that long counting times are required which means that even slight RF modulation in the background can be observed--the filter

apparently does not remove everything. Unfortunately, after the signal accumulation, it was discovered that the background RF noise scans taken do not match the pickup signal; the filter must change the modulation.

To get sufficient S/N to resolve the vibrational and electronic states of the C_2H radical, higher laser powers (~100-150 mJ/pulse) were required. Figure 5-2b shows the spectrum after all the runs had been added (21 hours) and all background/RF noise corrections made. The solid line is the TOF calculated using the $P(E_T)$ in Figure 5-3a. The dashed line represents the products from secondary dissociation, the details of which are discussed later.

Comparing the high resolution $P(E_T)$ obtained from the H atom TOF spectra with that of Wodtke and Lee shows good general agreement (see Figure 5-3b). The vibrational/electronic resolution in this experiment, however, seems higher. Most notably, Wodtke's peak 2 appears in the $P(E_T)$ as two separate peaks; the H atom TOF spectra is very sensitive to this structure whereas Wodtke and Lee reported that adding such peaks would have little effect on the calculated TOF spectrum [2].

The other area of difference is that the $P(E_T)$ from the H atom TOF has more low translational energy product than that of Wodtke and Lee. One explanation is that highly internally excited C_2H fragments more easily in the detector than ground state C_2H; at low translational energies, this

would result in less detected C_2H (and more C_2). In the 35" experiment, C_2H should not reach the detector (see Figure 4-2a) so the H atom TOF spectra will not be affected by differential fragmentation. The other possibility is that the H atom TOF results have some slow H atom laser correlated signal--perhaps from some laser produced H atoms that, after collisions inside the photolysis chamber, eventually make their way to the detector. The latter explanation is supported by high and low C_2H_2 pressure spectra taken with no skimmer. The higher pressure scans have relatively more slow H atoms (see Figures 5-4 and 5-5). With higher pressures, more collisions can take place after the photolysis event which will tend to slow down the fast H atoms produced, resulting in a relative increase in the low $P(E_T)$ H atoms.

3.2. No Skimmer/Low Resolution

When photolyzing in the free jet, a good deal of product vibration/electronic state resolution is lost due to collisional broadening and the more undefined photolysis volume so these spectra are not as useful for determining the internal energy distribution of the primary products. The S/N ration, however, is much higher which means less counting time is necessary so laser power dependence studies become practical.

Figure 5-6 shows three low resolution H atom TOF

spectra taken at different laser powers (~60, 105, and 235 mJ/pulse). All the H atoms should be from the primary process, $C_2H_2 \rightarrow C_2H + H$, or from the secondary process, $C_2H \rightarrow C_2 + H$, based on the observations of McDonald et. al. [23]. There is much uncertainty fitting the secondary contribution. One cannot presume that all the C_2H formed has the same probability of undergoing secondary dissociation. In fact, Wodtke and Lee have suggested that more highly internally excited products absorb a photon much more readily [2]. The forward convolution fitting program used allows one to select which energy C_2H will undergo further fragmentation and so can establish limits on the internal energy requirement. For ease in calculations, the dependence of the secondary dissociation on the primary product internal energy was treated as a step function. The differences between the high and low power TOF spectra indicate that C_2H fragments formed with $E_T \geq 10$ kcal/mole do not dissociate. There is enough uncertainty in the comparison, however, that this should be considered an upper bound. In fact with the assumption that only C_2H with $E_T \leq 10$ kcal/mole would be able to fragment ($E_{T,thres} = 10$ kcal/mole), it was impossible to simulate the "dip" on the rising edge of the high power TOF spectrum. Using $E_{T,thres} = 7$ kcal/mole proved most successful and was used in fitting all the data.

The secondary $P(E_T)$ that best fits the spectra is shown

in Figure 5-7. The overall appearance--the bimodal distribution and the preference for formation of slow, highly internally excited C_2--is unquestionable. There is, however, uncertainty in the shape of the curves especially at lower translational energies, which describes the secondary products that arrive at the detector the same time primary products do, and at the maximum translational energy where it is difficult to determine exactly at what point the signal completely disappears.

Since the low resolution set-up gives much better S/N, TOF spectra at m/e=2 were taken to look for evidence of process II, the H_2 elimination channel. There was no sign of any H_2 product. It should be noted that the H_2 product is expected to arrive at ≥100 μsec so the pulsed valve background may have obscured some signal.

4. Discussion

4.1. Primary Dissociation

The fast edge of the $P(E_T)$ which correlates to ground state C_2H, begins at E_T = 17.5 kcal/mole corresponding to a bond energy of 130.4 kcal/mole. Comparing the $P(E_T)$ with that of Wodtke and Lee, however, shows that this fast edge has contamination from photodissociation of internally excited C_2H_2 ($P(E_T)$ peak labelled H) [2]. The recent work identifying C_2H vibrational and electronic states [33-40] provides an alternative to estimating where the ground state

C_2H_2 dissociation actually starts contributing, reducing the uncertainty in this bond energy measurement. The maximum translational energy of the ground state C_2H product is determined by matching the sharp structures shown as peaks 4 and 5 in the $P(E_T)$ with the known C_2H energy levels. Since an inverted vibrational distribution with selective excitation of only two higher vibrational states of the ground electronic state is not likely, it was assumed that these peaks correspond to electronically excited C_2H A(0 0 0) and A(0 1 0). The main uncertainty in the fitting (~ ± 0.5 kcal/mole) comes in deciding how much rotational excitation to include. As discussed, not much excitation is expected at this low translational energy; in their study, Fletcher and Leone calculate the average energy in rotation for the C_2H A(0 1 0) to be 0.45 kcal/mole [23]. Table 5-2 and Figure 5-8 [33-39] show the final fit. Accepting that the $P(E_T)$ peaks are correctly assigned, the C_2H ground state is associated with a product translational energy of 16.5 kcal/mole; D_0(HCC-H) then would be 131.4 ± .5 kcal/mole.

The $P(E_T)$ consists of three envelopes. Based on the assignments (Figure 5-8), the first, E_T ~ 11.5 to 16.5 kcal/mole, could only be from the C-H bending series. The next step in the $P(E_T)$, E_T ~ 8 to 11.5 kcal/mole, would be associated with the excitation of the C-C stretch. By analogy, the last grouping, E_T ~ 2 to 8 kcal/mole, should be from C_2H with the C-H stretch excited as well as C_2H in the

A state. This assignment would suggest that the C-H stretching fundamental was near 3000 - 3150 cm^{-1} (E_T = 7.5 to 8 kcal/mole). ν_1 is still a subject of controversy; currently, the only limitations placed on it are that it fall in the 3250 - 3620 cm^{-1} range [37,40]. The pattern in the $P(E_T)$ presented here indicates that the C_2H ν_1 is at the lower end of the expected values.

Since the acetylene bond energy is dependent on the correctness of the $P(E_T)$ assignment, it is important to consider other possible identification schemes especially those that would yield lower bond energies. These fits, shown in Figure 5-9, are not as satisfying as the D_0 = 131.4 kcal/mole one for several reasons. First, they all leave a peak unassigned. Jacox and Olson, however, have seen lines associated with C_2H in these regions [40] so this is not an entirely convincing argument. A more damaging point is that these fits would require a highly specific and inverted vibrational distribution. For example, with D_0 = 127.6 kcal/mole, the three strongest peaks would correspond to high X and/or A vibrational levels. While it is not surprising to find highly vibrationally excited product, such an inversion would not be expected. Finally, the fits at these lower bond energies are not as good. For D_0 = 130.4 and 127.6 kcal/mole, X(0 7 0), X(0 1 1), and X(0 0 1) do not match any peaks. This cannot be easily explained by invoking rotational excitation since not much is expected.

The association of the peaks in the $P(E_T)$ with C_2H states does more than determine the translational energy at which the ground state is formed. It also provides dynamic details of the photodissociation process. Although it is impossible to get relative weights for the C_2H states because of their extensive overlap, the general trend is that the C_2H with a large amount of internal excitation (8 to 13 kcal/mole) is preferentially formed. The C-H bend is highly excited and C_2H is found with two quanta in the C-C stretch and one in the C-H stretch. The first C_2H electronic state, $A^1\Pi_u$, is also reached. The large amount of vibrational excitation is expected (especially the C-H bend and C-C stretch) since there are significant changes in the C-C-H bond angle and C-C distance during the dissociation. It is also not surprising to find that the $C_2H(A)$ is produced since at 193 nm the C_2H_2 is excited to the $1^1A''$ state (C_s symmetry) which correlates with $C_2H(A)$ + H. In fact, to explain the formation of $C_2H(X)$, one must invoke surface hopping at a $2^1A'/1^1A'$ or a $2^3A'/1^3A'$ avoided crossing as previously discussed [2,26].

4.2. Secondary Dissociation

Two peaks are seen in the secondary $P(E_T)$. Assuming that primarily C_2H with internal energy of 9.5 to 13.5 kcal/mole (products with 3 to 7 kcal/mole in translation) will undergo secondary dissociation to C_2 + $H(^2S)$ and that

the H-CC bond energy is 116 kcal/mole [8,41], indicates that the C_2 forms with E_{Int} = 20-28 (peak 1) and 32-40 kcal/mole (peak 2). Unfortunately, because of the nature of C_2H secondary dissociation, the TOF spectra are not sensitive enough to tell unambiguously what C_2 states form. The spectra, however, do reveal some general features of the dissociation process.

One conclusion that can be drawn from the secondary dissociation fitting is that C_2H must have an E_{Int} of $\geq$ 9.5 kcal/mole to photodissociate further. This value suggests that only C_2H in the upper electronic A state and/or highly vibrationally excited ground state can absorb a photon and fragment. This would agree with the theoretical predictions of the C_2H electronic transitions possible with 193 nm excitation. As discussed, to reach the lowest allowed electronic states, the C_2H must have a non-equilibrium C-C bond length and/or be nonlinear.

The overall appearance of the secondary $P(E_T)$ shows that most of the C_2 is formed highly excited. This is probably because of the large number of C_2 electronic states available for the C_2H^* to cross into. Peak 2 most likely represents $B^1\Delta_g$ formation with the slow tail being higher vibrational levels of $c^3\Sigma_u^+$ and/or $B'^1\Sigma_g^+$. The fast edge of peak 1 could be from $b^3\Sigma_g^-$ and the slow edge from $A^1\Pi_u$. The C_2 electronic states that appear to form in the 193 nm secondary dissociation of C_2H_2, with the exception of the

$c^3\Sigma_u^+$ state, have been seen before. The new information these results provide is that more of the highly excited C_2 states (B, B', and c) form than A, a, or X.

5. Conclusion

To confirm this group's previous measurement of the HCC-H bond energy, the same approach, 193 nm photofragmentation translational spectroscopy was used, but with the H atom detected rather than the C_2H. Although H atom detection is much more difficult due to the short residence time in the ionizer and the low ionization cross-section, it has several advantages--the measurements can be well calibrated, the data can be collected at one lab angle, and the TOF spectra are not affected by small variations in the parent beam. Several years of research on C_2H vibrational and electronic states have made it possible to accurately fix the threshold translational energy of ground state C_2H from the structure of the translational energy distribution rather than from an estimate of where the signal from the dissociation of vibrationally excited C_2H_2 ends. These improvements should give confidence in the dissociation energy measured, 131.4 ± .5 kcal/mole. This bond energy agrees with Wodtke and Lee's analogous experiment and is in the range of the latest experimental and theoretical predictions. It, thus, adds more support to the "D_0(HCC-H) > 130 kcal/mole side". There was no evidence

of the faster primary H atoms as detected in Segall, et. al.'s experiment.

Although the H atom TOF spectra obtained do not have nearly the resolution found in the C_2H absorption spectroscopy studies, C_2H states that lack oscillator strength can be detected. The three vibrational envelopes one can superimpose on the $P(E_T)$ suggest that the C-H stretching fundamental is 3000 to 3150 cm^{-1}, the lower end of the currently accepted range.

Finally, this TOF study adds to the understanding of the 193 nm photodissociation dynamics of acetylene. Comparison to the known C_2H spectrum shows that both C_2H A and X are formed which is only possible if curve-crossing is important in the system. As expected from the large geometry changes involved, high vibrational levels of C_2H X and A are populated. In addition to the primary photodissociation, the results increase what is known about the two photon sequential dissociation, $C_2H_2 \rightarrow C_2H + H \rightarrow C_2 + H + H$. Highly excited C_2H molecules preferentially dissociate as theoretically predicted. The formation of electronically excited C_2 is favored probably because of the large density of these states near the second photon energy.

References

1. M.B. Colket III, Twenty-First Symposium (International) on Combustion (Combustion Institute, Pittsburgh, 1986), p. 851; C.K. Westbrook and F.L Dryer, Eighteenth Symposium (International) on Combustion (Combustion Institute, Pittsburgh, 1981), p. 749; H. GG. Wagner, Seventeenth Symposium (International) on Combustion (Combustion Institute, Pittsburgh, 1979), p. 3; T. Tanzawa and W.C. Gardiner Jr., Seventeenth Symposium (International) on Combustion (Combustion Institute, Pittsburgh, 1979), p. 564.
2. A.M. Wodtke and Y.T. Lee, J. Phys. Chem. **89**, 4744 (1985); A.M. Wodtke, Ph.D. Thesis, University of California, Berkeley, 1986.
3. H. Shiromaru, Y. Achiba, K. Kimura, and Y.T. Lee, J. Phys. Chem. **91**, 17 (1987).
4. Y. Chen, D.M. Jonas, C. E. Hamilton, P.G. Green, J.L. Kinsey, and R.W. Field, Ber. Bunsenges. Phys. Chem. **92**, 329 (1988).
5. J. Segall, R. Lavi, Y. Wen, and C. Witting, J. Phys. Chem. **93**, 7287 (1989).
6. P.G. Green, J.L. Kinsey, and R.W. Field, J. Chem. Phys. **91**, 5160 (1989).
7. K.M. Ervin, S. Gronert, S.E. Barlow, M.K. Gilles, A.G. Harrison, V.M. Bierbaum, C.H. DePuy, W.C. Lineberger,

and G.B. Ellison, J. Am. Chem. Soc. **112**, 5750 (1990).

8. B. Ruscic and J. Berkowitz, J. Chem. Phys. **93**, 5586 (1990).

9. D.P. Baldwin, M.A. Buntine, and D.W. Chandler, J. Chem. Phys. **93**, 6578 (1990).

10. L.A. Curtiss and J.A. Pople, J. Chem. Phys. **91**, 2420 (1989).

11. J.A. Montgomery Jr. and G.A. Petersson, Chem. Phys. Lett., **168**, 75 (1990).

12. C.W. Bauschlicher Jr., S.R. Langhoff, and P.R. Taylor, Chem. Phys. Lett. **171**, 42 (1990).

13. C.J. Wu and E.A. Carter, J. Am. Chem. Soc. **112**, 5893 (1990).

14. For a discussion of complexities see, for example, H. Thümmel, M. Perić, S.D. Peyerimhoff, and R.J. Buenker, Z. Phys. D. - Atoms, Molecules, and Clusters **13**, 307 (1989).

15. R.F. Curl, P.G. Carrick, and A.J. Merer J. Chem. Phys. **82**, 3479 (1985).

16. C.Y.R. Wu, T.S. Chien, G.S. Liu, D.L. Judge, and J.J. Caldwell, J. Chem. Phys. **91**, 272 (1989).

17. P.D. Foo and K.K. Innes, Chem. Phys. Lett. **22**, 439 (1973).

18. C.K. Ingold and G.W. King, J. Chem. Soc. 2702 (1953).

19. K.K. Innes, J. Chem. Phys. **22**, 863 (1954).

20. M. Douay, R. Nietmann, and P.F. Bernath, J. Mol.

Spectrosc. **131**, 261 (1988).

21. K.P. Huber and G. Herzberg, Molecular Spectra and Molecular Structure: IV. Constants of Diatomic Molecules (Van Nostrand Reinhold Company, New York, 1979).

22. M.W. Chase Jr., C.A. Davies, J.R. Downey Jr., D.J. Frurip, R.A. McDonald, and A.N. Syverud, JANAF Thermochemical Tables, Third Edition (Journal of Physical and Chemical Reference Data, New York, 1986).

23. T.R. Fletcher and S.R. Leone, J. Chem. Phys. **90**, 871 (1989).

24. N. Ochii and S. Tsuchiya, Chem. Phys. Lett. **140**, 20 (1987).

25. M. Fujii, A. Haijima, and M. Ito, Chem. Phys. Lett. **150**, 380 (1988).

26. T.A. Cool, P.M. Goodwin, and C.E. Otis, J. Chem. Phys. **93**, 3714 (1990).

27. J.R. McDonald, A.P. Baronavski, and V.M. Donnelly, Chem. Phys. **33**, 161 (1978).

28. R.S. Urdahl, Y. Bao, and W.M. Jackson, Chem. Phys. Lett. **152**, 485 (1988).

29. Y. Bao, R.S. Urdahl, and W.M. Jackson, J. Chem. Phys. **94**, 808 (1991).

30. P.M. Goodwin and T.A. Cool, J. Mol. Spectrosc. **133**, 230 (1989).

31. S. Shih, S.D. Peyerimhoff, and R.J. Buenker, J. Mol.

Spectrosc. **64**, 167 (1977).

32. S. Shih, S.D. Peyerimhoff, and R.J. Buenker, J. Mol. Spectrosc. **74**, 124 (1979).

33. W.-B. Yan, J.L. Hall, J.W. Stephens, M.L. Richnow, and R.F. Curl, J. Chem. Phys. **86**, 1657 (1987).

34. M. Vervloet and M. Herman, Chem. Phys. Lett. **144**, 48 (1988).

35. P.G. Carrick, A.J. Merer, and R.F. Curl Jr., J. Chem. Phys. **78**, 3652 (1983).

36. H. Kanamori and E. Hirota, J. Chem. Phys. **89**, 3962 (1988).

37. J.W. Stephens, W.-B. Yan, M.L. Richnow, H. Solka, and R.F. Curl, J. Mol. Struct. **190**, 41 (1988).

38. K. Kawaguchi, T. Amano, and E. Hirota, J. Mol. Spectrosc. **131**, 58 (1988).

39. H. Kanamori, K. Seki, and E. Hirota, J. Chem. Phys. **87**, 73 (1987).

40. M.E. Jacox and W.B. Olson, J. Chem. Phys. **86**, 3134 (1987).

41. A lower value for D_0(CC-H) has been determined recently by R.S. Urdahl, Y. Bao, and W.M. Jackson (submitted to Chem. Phys. Lett.). Using their 112.0 ± .8 kcal/mole would shift the assignments in Figure 5-7 to translational energies 4 kcal/mole higher and would raise the estimates of the C_2 internal energy by 4 kcal/mole.

Tables

Table 5-1. Recent Determinations of D_0(HCC-H).

Year	D_0(HCC-H) (kcal/mole)	Technique	Ref.
1991	131.4 ± .5	H atom (mass spec) velocity after dissociation	this work
1990	131 ± 1	H atom (REMPI) velocity after dissociation	9
1990	131.6 ± 1	C_2H^- + H^+ threshold thermochem. cycle	8
1990	131.3 ± .7	radical electron affinity (photoelectron spec) + gas phase acidity thermochem. cycle	7
1990	129.7	theory	13
1990	130.1 ± 1	theory	12
1990	131.54 ± .51	theory	11
1989	126.647 ± .002	SAC	6
1989	≤ 127 ± 1.5	H atom Doppler shifts after dissociation	5
1989	133.52 ± 2.3	theory	10
1988	≤ 132.3 ± .001	SEP with ZAC	4
1987	132.6 ± 1	C_2H + H^+ + e^- threshold thermochem. cycle	3
1985	132 ± 2	C_2H velocity after dissociation	2

Table 5-2. Observed C_2H States and their Positions in the $P(E_T)$.

TOF Peak	Exp. Trans. (cm^{-1})	Assignment	Ref.
	5543	X	33,34
	5403		
	5161 (from 3320 + ν_3)		33
5	4144	A(0 1 0)	15,34,35
	4108	X(0 1 2)	
	4012	X(1 1 0)	
4	3786	X(0 5 1)	15,35
	3693	A(0 0 0)	15,35,36
	3600	? ← X(0 0 0)	33,34,36
	3547		37
3	3366	? ← X(0 0 0)	37
	3299		
2a	2166	X(0 7 0)	36
	2091	X(0 1 1)	38
	1841	X(0 0 1)	39
1	372	X(0 1 0)	36

Figure Captions

Figure 5-1. Product channels thermodynamically possible in the 193 nm photodissociation of acetylene. The dashed, secondary dissociation lines represent the energy limits if the ground state and the most internally excited C_2H absorb a photon. The heats of formation and bond energies used to construct this chart are from references 7 and 20-22.

Figure 5-2. High resolution H atom spectra. Open circles are the raw data (after background corrections) and solid line is the calculated best fit. Dashed line represents H atoms from secondary dissociation. (a) Low power, 35 mJ/pulse; (b) High power, 100-150 mJ/pulse.

Figure 5-3. (a) Product translational energy distribution used to fit TOF spectrum in Figure 5-2b. (b) Wodtke and Lee's product translational energy distribution that gives the best fit to their C_2H TOF spectra.

Figure 5-4. H atom TOF spectra (low resolution) at (a) low acetylene pressure and (b) high acetylene pressure. The open circles are the raw data and the solid lines are the fit calculated using the $P(E_T)$ in Figure 5-5.

Figure 5-5. $P(E_T)$'s used to fit the H atom TOF spectra in Figure 5-4. The solid line fits the high pressure scan (b) while the dashed line fits the low pressure scan (a). The relative increase in slow H atoms at the higher pressure should be noted.

Figure 5-6. Low resolution TOF spectra. Open circles are the raw data, solid lines are the calculated best fit, and dashed lines are the secondary dissociation contribution. (a) 60 mJ/pulse. (b) 105 mJ/pulse. (c) 235 mJ/pulse.

Figure 5-7. Secondary dissociation product translational energy distribution used to calculate the best fit in Figure 5-6c. The blocks represent where the ground vibrational level of the C_2 electronic states should appear assuming C_2H with an internal energy of 9.5 - 13.5 kcal/mole (E_T = 3 - 7 kcal/mole) dissociates.

Figure 5-8. Correspondence between known C_2H states (see Table 5-2) and the product translational energy distribution. Solid lines are observed transitions (from ground state C_2H); those that have been assigned are labeled. The dashed lines are the calculated C_2H C-H bending vibrations assuming Kanamori and Hirota's 2166 cm^{-1} peak is X(0 7 0) and $\omega_e\chi_e$ = 10.1 cm^{-1} [36]. As

can be seen, C_2H X(0 0 0) is expected at E_T = 16.5 kcal/mole which would yield a D_0(HCC-H) = 131.4 ± .5 kcal/mole.

Figure 5-9. Comparison of fits of the C_2H spectrum to the H atom TOF spectrum which would give HCC-H bond energies of (a) 127.6 kcal/mole, (b) 128.7 kcal/mole, (c) 130.4 kcal/mole, and (d) 131.4 kcal/mole.

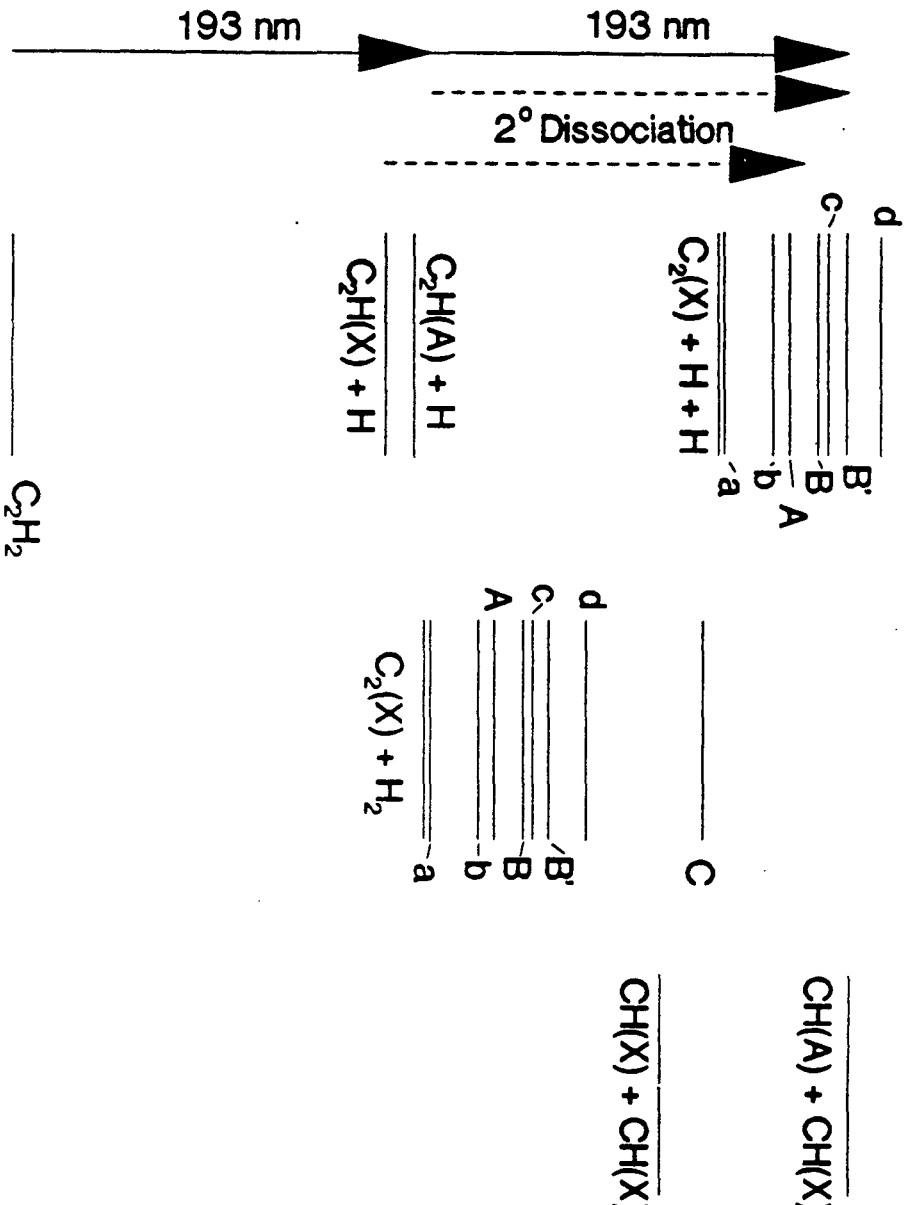
193 nm
193 nm
2° Dissociation
C2H2
C2H(X) + H
C2H(A) + H
C2(X) + H + H
a
b
A
B
c
d
C2(X) + H2
a
b
B
B'
A
c
d
C
CH(X) + CH(X)
CH(A) + CH(X)

Figure 5-1

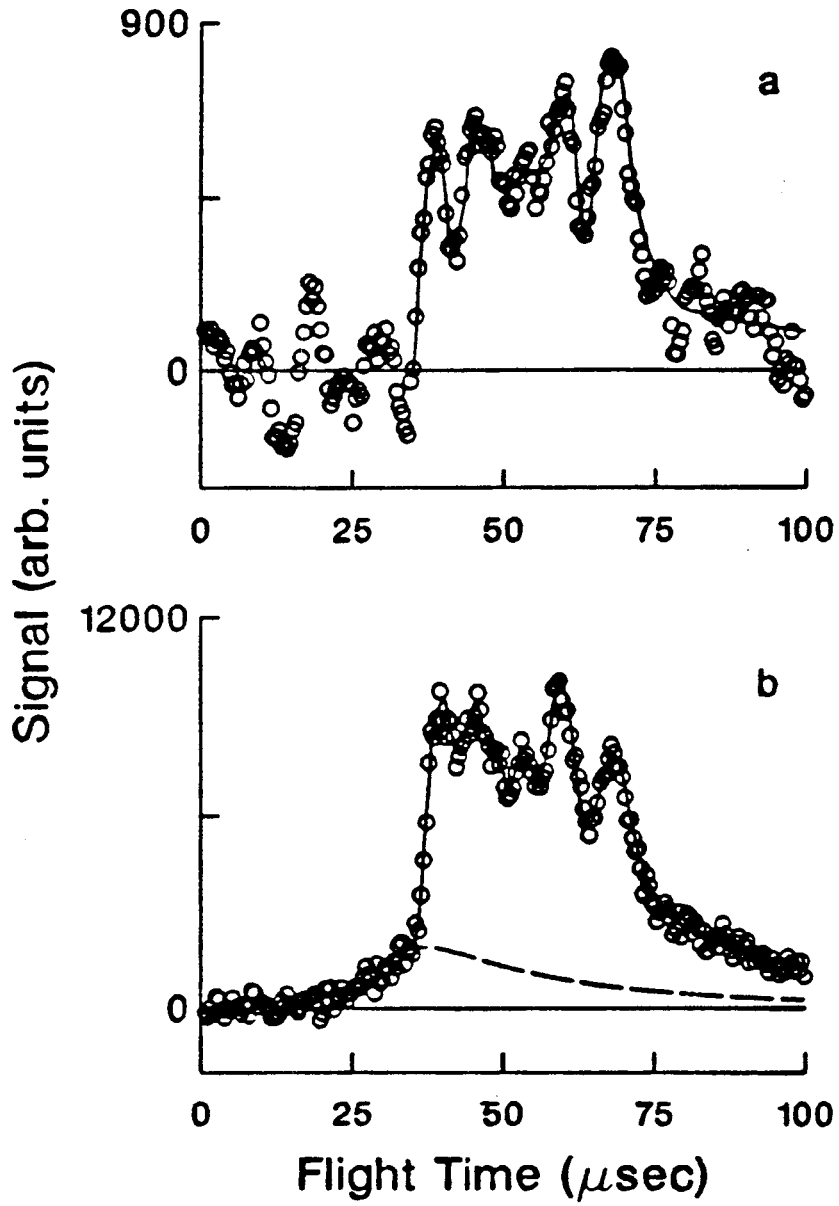
900
0
a
0
25
50
75
100
12000
0
b
0
25
50
75
100
Signal (arb. units)
Flight Time (μsec)

Figure 5-2

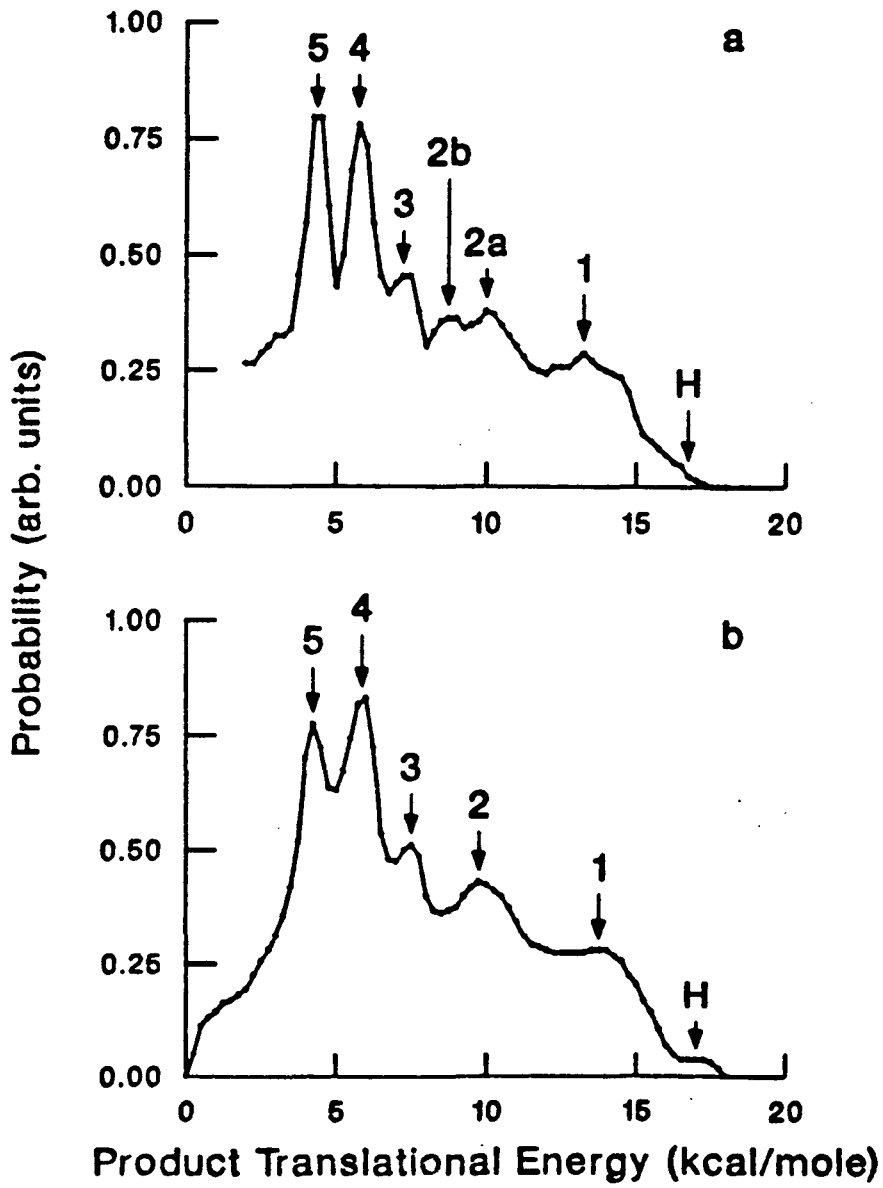
1.00
0.75
0.50
0.25
0.00
5
4
2b
3
2a
1
H
a
0
5
10
15
20
1.00
0.75
0.50
0.25
0.00
5
4
3
2
1
H
b
0
5
10
15
20
Probability (arb. units)
Product Translational Energy (kcal/mole)

Figure 5-3

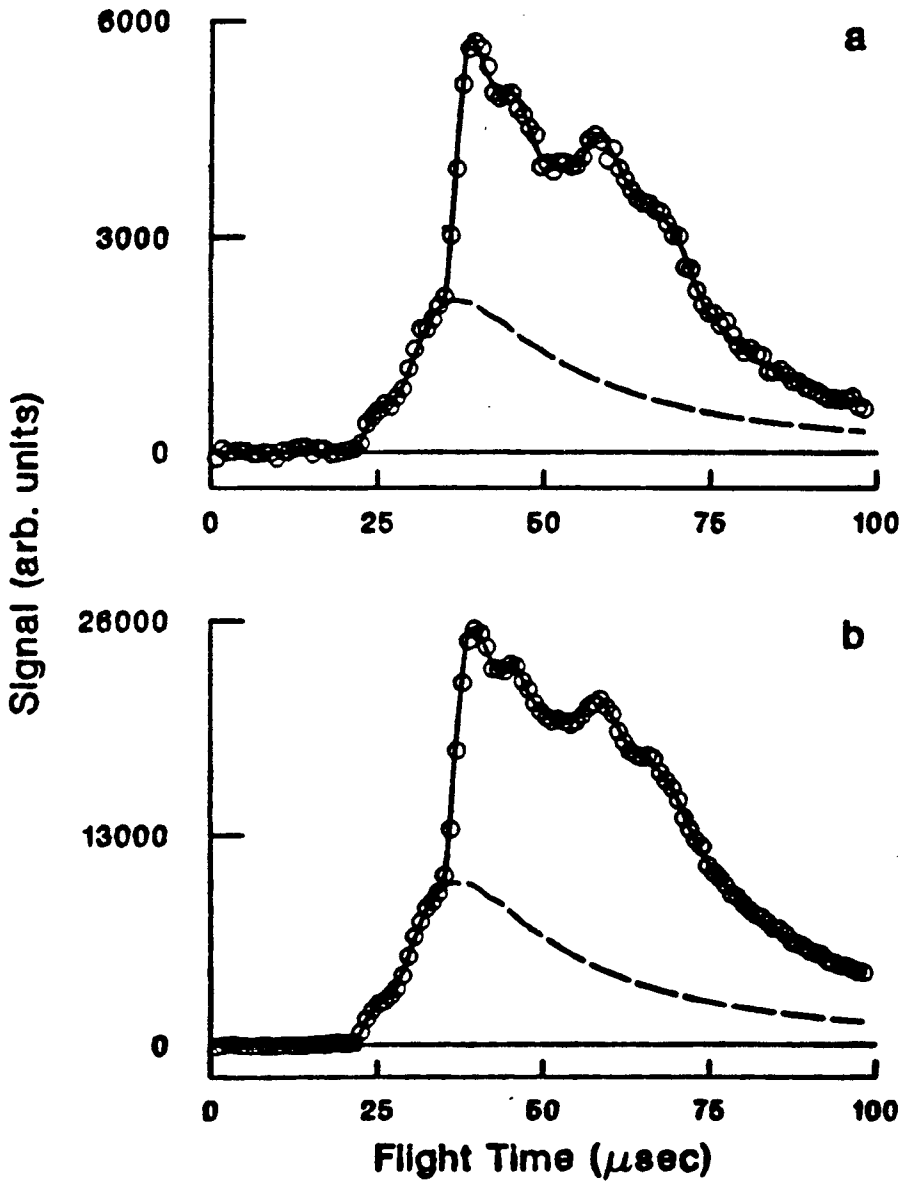
6000
3000
0
a
0
25
50
75
100
26000
13000
0
b
0
25
50
75
100
Signal (arb. units)
Flight Time (μsec)

Figure 5-4

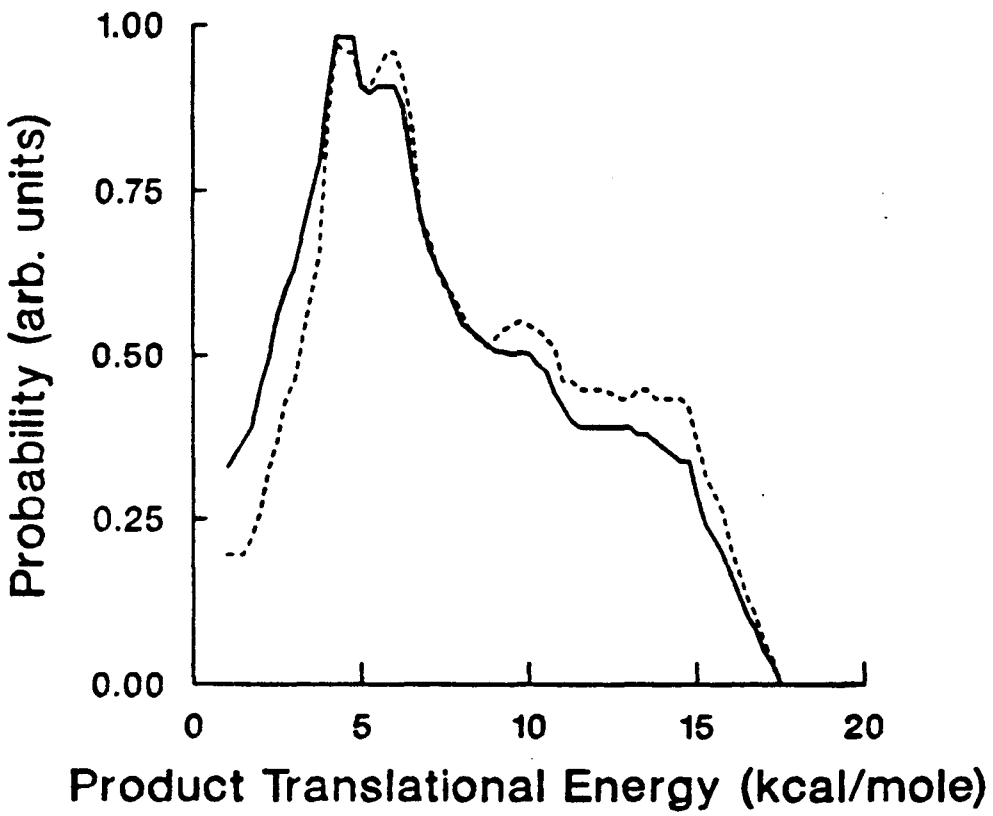
1.00
0.75
0.50
0.25
0.00
Probability (arb. units)
0
5
10
15
20
Product Translational Energy (kcal/mole)

Figure 5-5

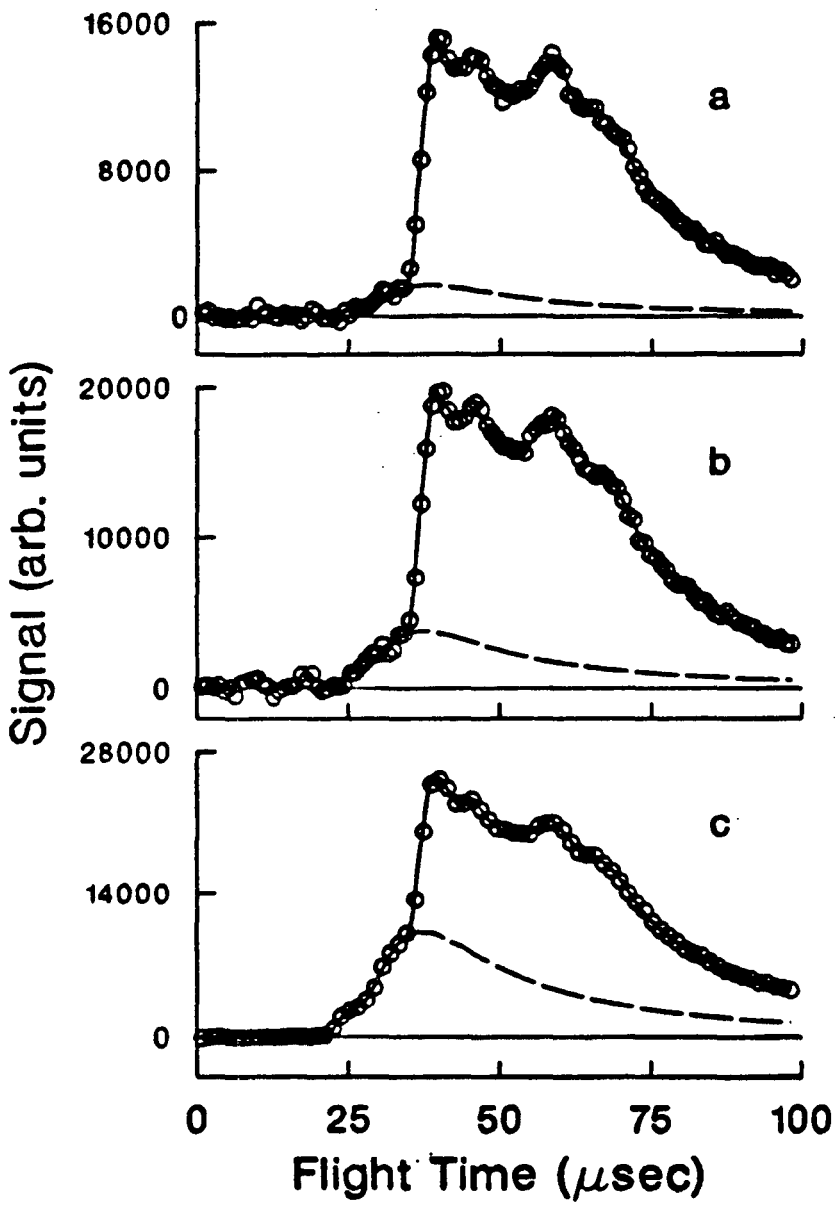
16000
8000
0
a
20000
10000
0
b
28000
14000
0
c
Signal (arb. units)
0
25
50
75
100
Flight Time (μsec)

Figure 5-6

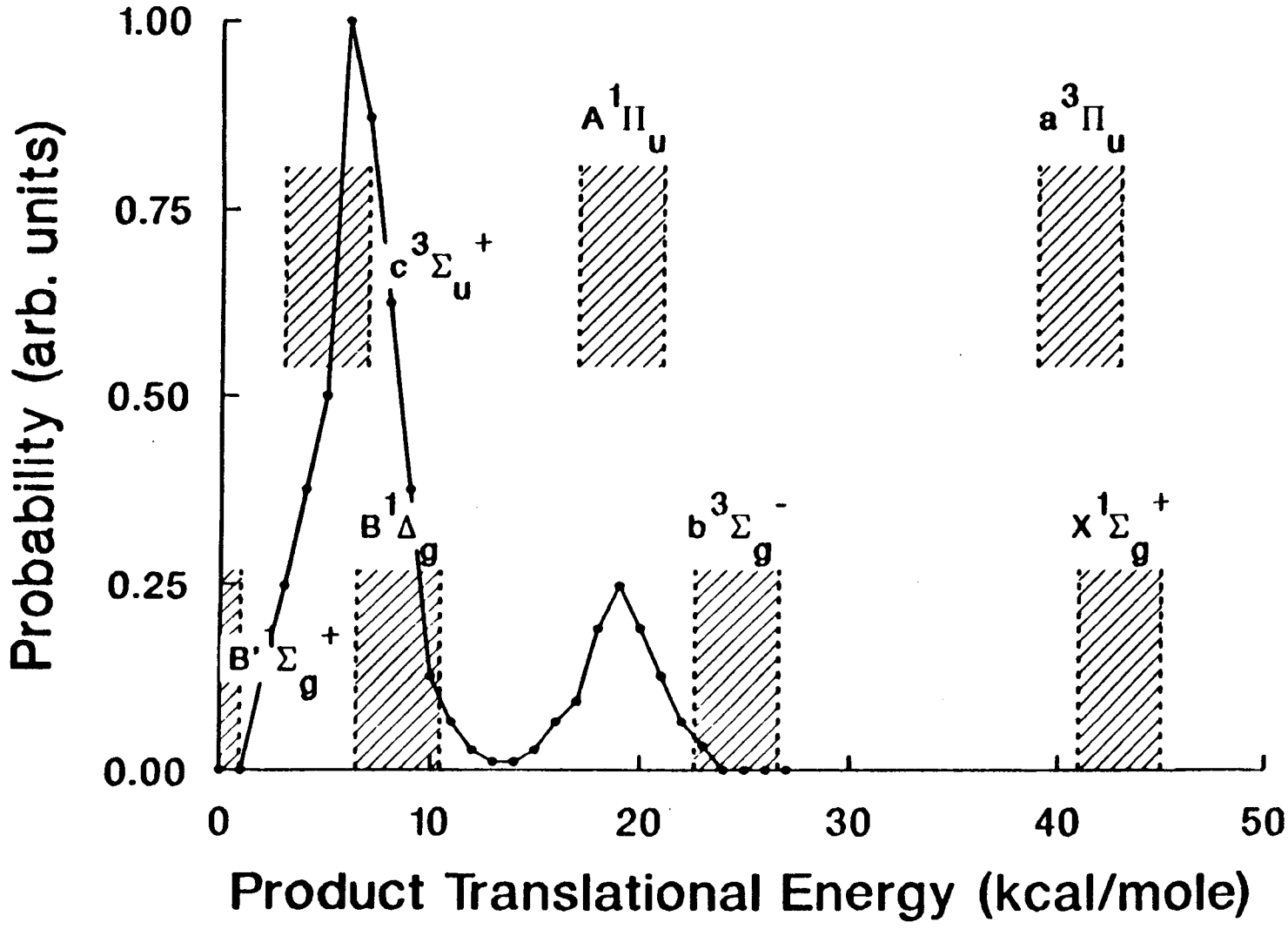
1.00
0.75
0.50
0.25
0.00
Probability (arb. units)
0
10
20
30
40
50
Product Translational Energy (kcal/mole)
A $^1\Pi_u$
a $^3\Pi_u$
c $^3\Sigma_u^+$
B $^1\Delta_g$
b $^3\Sigma_g^-$
X $^1\Sigma_g^+$
B' $^1\Sigma_g^+$

Figure 5-7

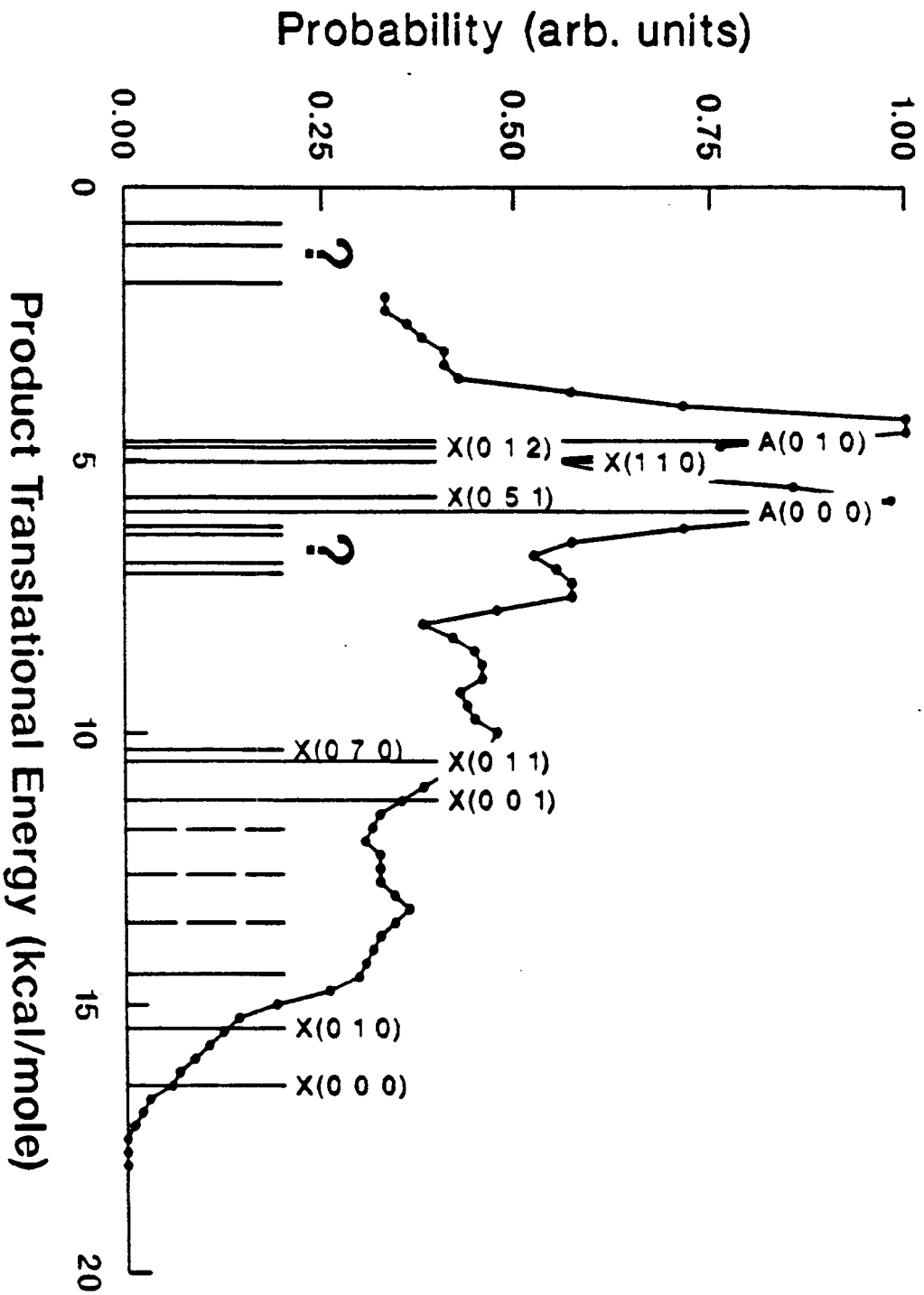
Probability (arb. units)
0.00
0.25
0.50
0.75
1.00
Product Translational Energy (kcal/mole)
0
5
10
15
20
?
?
X(0 1 2)
X(1 1 0)
A(0 1 0)
X(0 5 1)
A(0 0 0)
X(0 7 0)
X(0 1 1)
X(0 0 1)
X(0 1 0)
X(0 0 0)

Figure 5-8

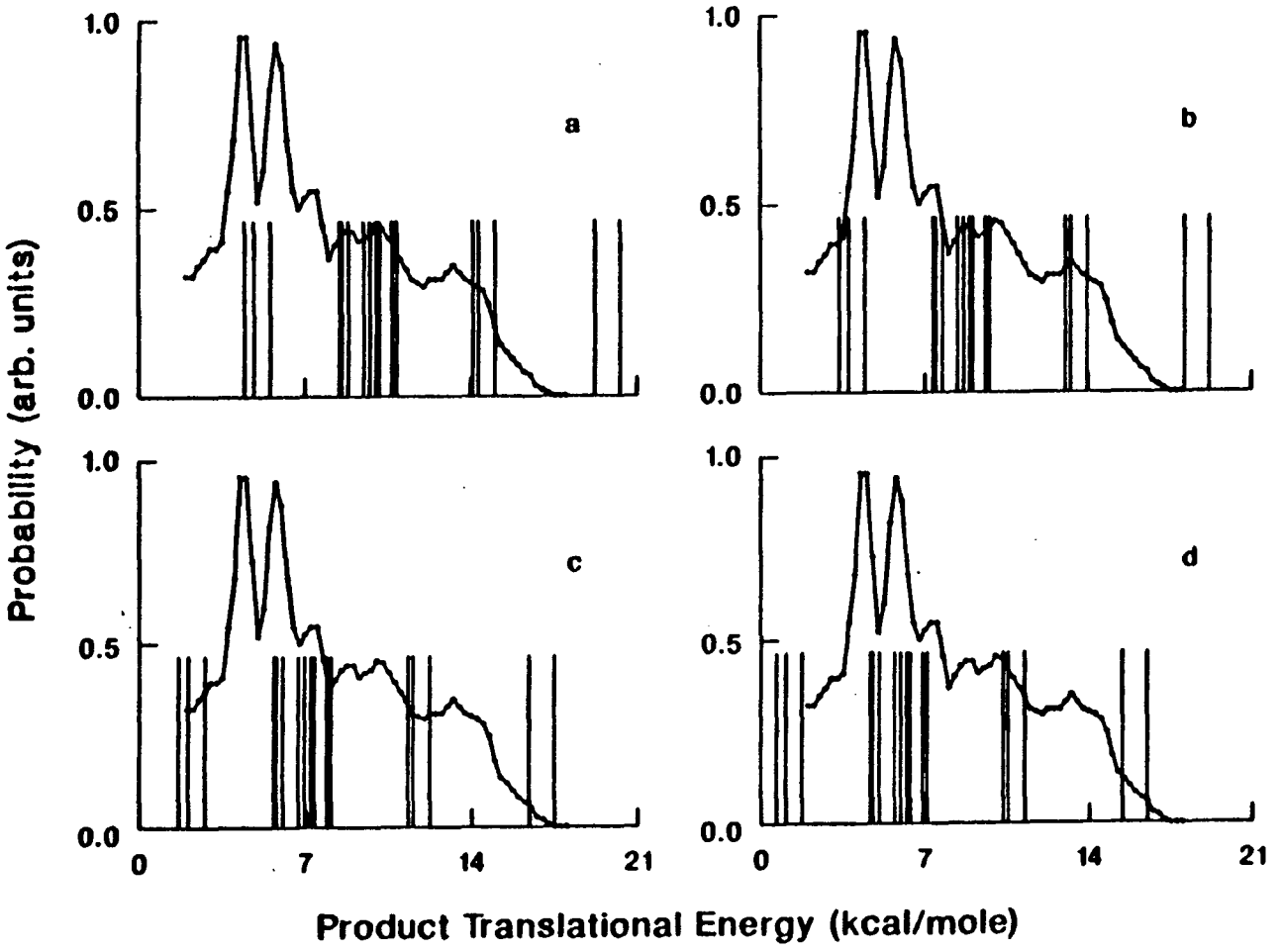
1.0
0.5
0.0
a
b
c
d
Probability (arb. units)
0
7
14
21
Product Translational Energy (kcal/mole)

Figure 5-9

Chapter 6: Photodissociation of Ethylene at 193 nm

1. Introduction

Although the photochemistry of ethylene has been studied since the 1950's, the details of the dissociation process remain uncertain [1]. A summary of the known thermodynamics is given in Figure 6-1 [2]. The earliest work was mainly concerned with identifying the primary decomposition channels [14-19]:

$$C_2H_4 \rightarrow HCCH + H_2 \qquad \text{ia}$$
$$\rightarrow H_2CC: + H_2 \qquad \text{ib}$$
$$\rightarrow C_2H_3\cdot + H \qquad \text{iia}$$
$$\rightarrow C_2H_2 + 2H \qquad \text{iib}$$

The general consensus was that atomic and molecular elimination producing H and H_2 are of approximately equal importance [17,18,19b]. In channel i, the molecular elimination, there appeared to be two different primary products, acetylene (HCCH) and vinylidene (H_2CC) [14,16]. The atomic elimination pathways, iia, single H elimination,

and iib, simultaneous loss of two H atoms, were difficult to distinguish because vinyl radicals created with vibrational energy greater than the C-H dissociation energy are apparently very short-lived with respect to further loss of an H atom [16-19]. Back and Griffiths [18] and Hara and Tanaka [19], however, "detected" stabilized C_2H_3 by observing products that could only come from reaction of the vinyl radical, so there is no question that iia occurs.

These early studies were done using different excitation sources -- alpha radiolysis [14], $Hg(^3P_1)$ sensitization [15], and 123.6 nm [16], 147.0 nm [16,17], 163.4 nm [19], and 184.9 nm [16,19b] photons. Comparison of the results shows that atomic elimination, specifically channel iib, is favored when the photon energy is increased while i(a + b) and iia decrease in importance [16,19b].

The use of isotopes in some of these early works provided additional information about the molecular elimination mechanism. It was shown that the photoexcited C_2H_4 has free rotation about the C=C bond and any pair of H atoms can participate in molecular elimination. The twisted geometry of the C_2H_4 $\pi\pi^*$ excited state [20] explains why the two hydrogens on each carbon are equivalent. No 1,2 H exchange, however, was observed except when $Hg(^3P_1)$ sensitization was used as the excitation source [15,16]. The vinylidene channel appeared to be favored over the acetylene by a ratio of approximately 3 to 2 [16]. There is

an isotope effect of ≈ 1:1.5:2 with respect to D_2:HD:H_2 elimination for both channels ia and ib, although Okabe and McNesby noted that there seems to be a slightly smaller isotope effect in ia [15,16]. This isotope effect is justified by modeling the elimination as an intramolecular abstraction or a large vibrational displacement, or by requiring a vibrationally excited ethylidene as an intermediate [15].

With the development of laser technology, more detailed measurements on the various channels in ethylene photodissociation became possible. Unfortunately, they seem to have raised as least as many questions as they have answered. Using UV flash photolysis along with 137 nm absorption spectroscopy, Fahr and Laufer explored the role of electronically excited triplet vinylidene ($^3B_2$) [21]. They found that this excited radical was a major product; the measured quantum yield was 0.75 ± 0.2. Based on appearance times, however, they concluded that neither vinylidene (ground state ($^1A_1$) or the excited $^3B_2$) nor acetylene was the direct product in molecular elimination. They hypothesized that some excited meta-stable precursor must give rise to the $^3B_2$. A gas cell photodissociation study was done recently at 193 nm that confirmed the general idea that several excited states and intermediates are involved in both channels but the authors were unable to identify exactly what these were [22]. The most recent

study, by Bersohn and coworkers, concentrated on the H atom elimination channel at 193 nm [23]; the average translational energy of H and D atoms was measured from the Doppler shift observed when the atoms were detected by laser induced fluorescence. Based on the small release of translational energy measured, they concluded that internal conversion of the excited molecule to the vibrationally excited ground electronic state occurred before dissociation.

A limited amount of theoretical work has been done on the primary ethylene photodissociation processes. Evleth and Sevin present a qualitative evaluation of two proposed molecular elimination pathways: three-centered elimination to give vinylidene and dissociation via ethylidene (CH_3CH) to form acetylene [24]. The vinylidene and ethylidene ground state products can form directly from the excited $\pi\pi^*$ state of ethylene, the state reached with 193 nm photons, or from the ground state. A later study by Raghavachari et. al. gives a more quantitative description, estimating that the activation energies for the three-centered elimination and the ethylidene channel are ~93.4 and 109.3 kcal/mole, respectively [25]. In Evleth and Sevin's analysis of the atomic elimination, it was found that to produce ground state vinyl radical, dissociation can only occur from hot ground state ethylene [24].

Applying the photofragment translational energy

spectroscopy technique in which the TOF spectra of mass-selected fragments (H or H_2) are measured, will provide more detailed information on the dynamics of the ethylene photodissociation. Since the heats of formation of acetylene and vinylidene differ by ~44 kcal/mole [2], the corresponding H_2 could differ substantially in their velocity distributions and so, in principle, the two channels can be clearly identified in the TOF spectra. Similarly, the two atomic elimination pathways will be resolved in the TOF spectra since channel iib is ~35 kcal/mole more endothermic than iia [2]. The $P(E_T)$ will also reflect whether the dissociation has an exit barrier and will show how the excess energy is partitioned. TOF spectra of the products of the photodissociation of deuterated ethylene (1,1 D_2CCH_2, cis 1,2 HDCCDH, and C_2D_4) will give additional understanding of the nature of the intermediate states involved. Specifically, they will address the question of H migration prior to dissociation. This work, together with studies by other members of this group in which the rovibrational states of H_2 produced in the 193 nm photolysis of C_2H_4 were detected, should provide a fairly clear picture of the concerted elimination of H_2 from ethylene [26].

The experiments described here should help to isolate the role of the $\pi\pi^*$ state. Many of the past studies were done at wavelengths where more than one ethylene excited

state would be involved. The photodissociation described here used 193 nm photons. Although ethylene has a small absorption cross-section at this wavelength [$\sigma \approx 2 \times 10^{-20}$ cm^2 at 193 nm [27,28]], the excitation is exclusively via a $\pi^* \leftarrow \pi$ transition to the $^1B_{1u}$ (V) excited state. The $^1B_{1u}$ state is believed to be twisted with the CH_2 groups perpendicular to each other [20].

2. Experiment

The ethylene (99.99% min stated purity from Matheson) was used neat with no purification at a stagnation pressure of ≈50 torr. To fully understand the details of the ethylene photodissociation, the following ethylene isotopomers were used: C_2D_4 (99% stated purity from Cambridge Isotope Laboratory), 1,1 D_2CCH_2 (99.1 atom % D from MSD Isotopes), and 1,2 cis HDCCDH (98.2 atom % D from MSD Isotopes).

The relevant Newton diagrams are shown in Figure 6-2. The experimental protocol is the same as for the general photodissociation experiments described in Chapter 4 with two differences. First, all experiments were done in low resolution mode (ie. no skimmer was used). Having the skimmer in place significantly decreased the S/N and did not resolve any additional structure. Second, to understand the details of the dissociation mechanism, it was necessary to develop a method for determining the relative importance of

the HD and D_2 fragments in the isotopomer photolysis. The ratios were calculated by integrating TOF spectra that were accumulated for short times (~0.25 - 0.5 hr). Only spectra taken close together in time were compared so that any changes in the detector sensitivity and beam intensity that developed over time would be reduced. The most reliable comparisons are between the various masses of products from a given isotopomer. It was difficult for spectra from the two different parent molecules to be taken next to each other in time repeatedly, so the comparisons between the 1,1 and cis 1,2 isotopomer products are more suspect.

3. Results and Analysis

3.1. Comparison of Atomic and Molecular Channels

The relative importance of the atomic and the molecular elimination channels in C_2H_4 was studied by integrating the TOF spectra of H_2 and H taken close together in time. The comparison was made at four different laser powers ranging from 120 to 220 mJ/pulse. The molecular to atomic elimination ratio was consistently 1:1 (± 0.15); no appreciable correlation between laser power and branching ratio was observed.

3.2. Molecular Elimination

3.2.1. C_2H_4

The total accumulated H_2 TOF spectrum with the

appropriate background corrections is shown in Figure 6-3. The process appears to be free of multiphoton effects, at least in the laser intensity range of these experiments; no observable change in the spectrum was seen when the laser power was varied from ~80 mJ/pulse to ~220 mJ/pulse. The $P(E_T)$ used to fit the data (see Figure 6-4) is smooth and shows no obvious vibrational structure. This is not surprising since the products that form, H_2 and C_2H_2, are expected to be vibrationally and rotationally excited because of the large changes in geometry required to form the products through three and/or four-centered elimination.

The fast edge of the $P(E_T)$ is where the acetylene products should be separated from the vinylidene. Assuming ground state vinylidene forms, the maximum translational energy expected is ~64 kcal/mole [2]. If ground state acetylene is produced, the fastest products are expected at ~108 kcal/mole [2]. The observed highest kinetic energy released, 88 kcal/mole, is between these. Internal thermal excitation of the parent C_2H_4 could contribute to some increase in the maximum translational energy. However, based on the analogous C_2H_2 photodissociation experiments (Chapter 5), this effect should only contribute a maximum of 2 kcal/mole. Since the $P(E_T)$ threshold is much greater than 64 kcal/mole, the fast tail must be attributed to acetylene formation. That the observed maximum kinetic energy is so much less than that predicted for the formation of ground

state acetylene and hydrogen implies that these products are formed vibrationally excited. It should be noted that this H_2 TOF spectrum does not mean that the acetylene channel is responsible for all the product; in fact, although the $P(E_T)$ is not bimodal, the slope dramatically increases near the maximum kinetic energy limit for vinylidene formation.

3.2.2. $C_2H_2D_2$ and C_2D_4

The TOF spectra from the photodissociation of C_2H_4 does not show convincingly whether or not vinylidene is formed. To resolve this question, the photodissociation of 1,1 and 1,2 cis deuterated ethylene was studied by measuring the TOF spectra for the D_2 and HD products. The pure H_2 spectrum could not be obtained because of contamination from D atoms produced in the atomic elimination. Both the comparison between the integrated spectra at each mass and the derived $P(E_T)$'s were used to learn about the relative importance of the acetylene and vinylidene channels.

Table 6-1 gives the relative signal of HD and D_2 from each isotopomer. Figure 6-5 shows the summed spectra used in determining the ratios to give some idea of the degree of uncertainty involved.

The relative HD and D_2 ratios from the photodissociation of the isotopomers provides important clues on the molecular elimination mechanism. First, all four H atoms cannot be equivalent, i.e. there is not

complete randomization in the excited state. If this were true, equal amounts of HD and D_2 would be formed in the photolysis of 1,1 D_2CCH_2 and cis 1,2 HDCCDH which is clearly not the case. The ratios also show that four-centered elimination to produce acetylene is not the only process that occurs. Assuming that this is the only channel, one would expect only HD products from 1,1 D_2CCH_2. However, a significant amount of D_2, as much as 50% of the HD product, was observed. The fact that 1,1 D_2CCH_2 gives more D_2 product than cis 1,2 HDCCDH suggests that three-centered elimination is likely to be more facile than four-centered.

The only mechanism that adequately explains the data is one in which both acetylene and vinylidene form from an intermediate with no appreciable H migration but with full rotation about the C=C bond. Let θ_v be proportional to the probability of forming vinylidene via three-centered elimination and θ_a be proportional to the probability of forming acetylene via four-centered elimination from each possible atomic pair. If the isotope effects for elimination to form vinylidene and acetylene are assumed equal, the following relative yields are expected (i_{HD} and i_{DD} represent the isotope effects):

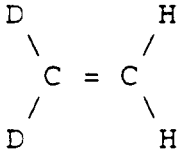

HD	$4\theta_a \cdot i_{HD}$
D_2	$1\theta_v \cdot i_{DD}$

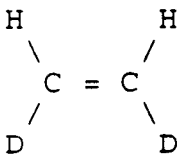

HD	$2\theta_a \cdot i_{HD} + 2\theta_v \cdot i_{HD}$
D_2	$\theta_a \cdot i_{DD}$

Based on the relative amount of HD formed from the two isotopomers, a relationship between θ_a and θ_v can be determined:

$$\frac{HD\ 1,1}{HD\ cis\ 1,2} = \frac{4\theta_a \cdot i_{HD}}{2\theta_a \cdot i_{HD} + 2\theta_v \cdot i_{HD}} \approx \frac{1}{2}\ (observed)$$

$$\therefore\ 3\theta_a = \theta_v$$

Thus, the vinylidene elimination channel is approximately three times as important as the acetylene for each possible atomic pair. Normalizing for the number of ways three-centered and four-centered elimination can occur in C_2H_4, the acetylene/vinylidene ratio should be 2:3 for C_2H_4, exactly the value previously estimated by Okabe and McNesby [16]. The mechanism and the $\theta_v = 3\theta_a$ relationship can also provide a value for the i_{HD}/i_{DD} ratio. Taking the measured ratio of HD and D_2 from 1,1 D_2CCH_2,

$$\frac{HD\ 1,1}{D_2\ 1,1} = \frac{4\theta_a \cdot i_{HD}}{\theta_v \cdot i_{DD}} \approx \frac{2}{1}\ (observed)$$

Substituting $\theta_v = 3\theta_a$, one obtains

$$i_{HD} = \frac{3}{2} i_{DD}$$

The HD to D_2 isotope effect ratio of 1.5 is exactly what was previously observed [15,16]. This gives further credibility to the proposed mechanism. Using the calculated θ_a/θ_v and i_{HD}/i_{DD}, the HD/D_2 product ratio for the cis 1,2 deuterated ethylene can also be predicted .

$$\frac{HD\ cis\ 1,2}{D_2\ cis\ 1,2} = \frac{2\theta_a \cdot i_{HD} + 2\theta_v \cdot i_{HD}}{\theta_a \cdot i_{DD}} = \frac{8 \cdot 3}{2} = 12$$

The observed ratio, $HD/D_2 = 10$, is close to the calculated value. Since the S/N of the D_2 TOF scan from the 1,2 HDCCDH is so poor, the large HD/D_2 ratio measured should be taken as conformation of the mechanism.

The acetylene/vinylidene formation mechanism derived from the HD/D_2 product ratios also provides some insight for the interpretation of the TOF spectra from 1,1 and cis 1,2 $C_2H_2D_2$. Figure 6-6 shows the TOF spectra fit with the $P(E_T)$'s in Figure 6-7. The gross differences between the spectra where 100% acetylene (HD from 1,1) and 100% vinylidene (D_2 from 1,1) are expected are consistent with the mechanism; the HD $P(E_T)$ has relatively more product at higher translational energies (50 to 80 kcal/mole). The finer details, however, suggest that there may be more to consider. The "100% vinylidene" spectrum has an energy release of ~78 kcal/mole, much greater than the available

excess energy for vinylidene formation (64 kcal/mole). The easiest explanation is that some D_2 + acetylene is forming by four-centered elimination from the 1,2 HDCCDH which is either present as an impurity or formed through extensive 1,2 H exchange in the excited state before elimination of D_2. This, however, is unlikely because the experiment shows that the 1,2 compound produces virtually no D_2. The most reasonable answer is that the D_2 is forming and leaving as the H is transferring from one carbon to the other (an ethylidene type mechanism) as illustrated in Figure 6-8. The formation of acetylene instead of vinylidene in this three-centered elimination mechanism will make the available excess energy the same as for the four-centered elimination forming acetylene.

The ethylidene type mechanism which leads to acetylene rather than vinylidene in the three-centered elimination would also help explain the differences in the rising edge of the $P(E_T)$'s of D_2 from C_2D_4 and H_2 from C_2H_4. In both the C_2D_4 and C_2H_4 photodissociation, the acetylene/vinylidene ratio is expected to be ~2:3. Figure 6-9 shows the D_2 TOF spectrum along with that calculated using the $P(E_T)$ for H_2 from C_2H_4. Although the data is noisy, the fast edges, where acetylene is expected, are clearly different; the C_2D_4 seems to have less fast D_2 + DCCD product. If some acetylene is produced from a transition state where one of the C-H bonds stretches/bends and tunnels through a

potential energy barrier to the other carbon, less acetylene would be expected when only C-D bonds are present and this type of motion will not be as facile.

3.3. Atomic Elimination

The shape of the H atom TOF spectra is extremely dependent on laser power. Figure 6-10 shows the accumulated scans taken at four different average lasers powers (40, 90, 140, and 180 mJ/pulse). In fact, it was not possible to average long enough at low enough power to obtain a pure primary distribution; product too fast to be from primary bond dissociation was always found. These secondary photodissociation processes made it impossible to use the fast edges of the H atom TOF spectra to obtain a C-H bond energy. In the further analysis of the results, then, the C-H bond energy was taken as 108 kcal/mole [2].

In fitting the TOF spectra, it was initially assumed that all the H atoms were from the combination of the primary process, $C_2H_4 \rightarrow H + C_2H_3$, and the secondary photodissociation, $C_2H_3 \rightarrow H + C_2H_2$, and that all the vinyl radicals produced had an equal probability of undergoing secondary photodissociation regardless of the extent of internal excitation. If this picture were correct, the high power experiments would yield more primary and secondary H atoms and the TOF spectra would have higher signal at all arrival times; the only change in shape would be from a

relative increase in secondary H atoms at the higher laser powers. However, as shown in Figure 6-11, TOF spectra obtained in the high power scans have significantly less slow "primary" product and more fast. There is no secondary $P(E_T)$ such that the TOF spectra at all the different powers will share the same primary $P(E_T)$. Since the primary $P(E_T)$ should not change with laser power, the dissociation process described above must be oversimplified.

Ethylene multiphoton absorption is one possible explanation for the decrease in slow H atoms and increase in fast H atoms at high laser powers. In this scheme, the C_2H_4 could absorb more than one photon at higher laser powers producing H atoms with greater translational energy. The observed disappearance of slow H atoms and appearance of more fast H atoms at high laser powers, then, is the result of the photoexcited C_2H_4 absorbing a second photon before it eliminates an H atom; the $P(E_T)$ would shift to higher translational energies simply because more energy is available for product translation. This explanation hinges on the fact that ethylene multiphoton absorption occurs at 193 nm. The cross-section for 193 nm absorption by ethylene is so small ($\sigma = 2 \times 10^{-20}$ cm^2) that even at 180 mJ/pulse (1.94×10^{18} photons/pulse$\cdot$cm^2) it is unlikely that saturation is occurring; for this scenario to work, the absorption cross-section for the second photon would have to be much greater than for the first. Not enough is known

about the multiphoton absorption of C_2H_4 to prove or disprove this. The lack of power dependence in the molecular elimination channel, however, suggests that it is not two photon absorption by C_2H_4 that gives rise to the observed power dependence in the H atom elimination.

Perhaps a better explanation for the change in shape of the primary $P(E_T)$ at higher laser powers would invoke a fast decomposition of excited C_2H_4, followed by spontaneous decomposition of internally excited C_2H_3 and competitive secondary photodissociation of the C_2H_3. This scenario is illustrated in Figure 6-12. At low laser powers, when the ethylene absorbs a 193 nm photon it will be excited by 148 kcal/mole. Since breaking a C-H bond requires ~108 kcal/mole, the resulting vinyl radical could have as much as 40 kcal/mole excess energy, which is greater than the H-CHCH bond energy (35 kcal/mole). Primary C_2H_3 products with an internal energy above 35 kcal/mole, i.e. those with $E_T \leq 5$ kcal/mole, can further dissociate with no additional photon required, producing H + HCCH with 0 to 5 kcal/mole in translation. The net result, then, will be two slow ($E_T \leq 5$ kcal/mole) H atoms from the same ethylene. At higher laser powers there is a greater chance for the vinyl radicals formed to absorb a photon rather than spontaneously decompose. Those that do absorb a photon will have more internal energy and upon fragmentation will produce faster product. The apparent difference in the low and high power

"primary" $P(E_T)$'s, then, is that at the high power fewer slow H atoms will come from spontaneous decomposition of C_2H_3 but more fast H atoms will be created from secondary absorption by the slow C_2H_3.

The two mechanisms offered to explain the effects of laser power are essentially the same except that in the latter, the vinyl radical absorbs the second photon rather than the C_2H_4. The vinyl radical absorption mechanism is preferred for several reasons. First, no multiphoton effects were seen in the H_2 elimination channel which would be expected if excited ethylene could absorb a second photon. Second, it is known that the vinyl radical absorbs at 164.7 nm and 168.33 nm [29]. Third, if it is assumed that the secondary dissociation of the slow vinyl radicals is similar to the fast, the H + C_2H_2 product falls in the right spot.

Because the H atom elimination is so complex, there are not enough breaks in the TOF spectra to uniquely determine the limits of each channel, and the secondary bond energies are not known accurately enough, the fitting procedure cannot be expected to provide the true $P(E_T)$'s. As long as these limitations are recognized, using reasonable assumptions to fit the spectra will provide some information. In the fitting procedure, four channels were considered:

$$(1)\quad C_2H_4 \xrightarrow{h\nu} H + C_2H_3$$

$$(2a)\quad C_2H_3\ (E_T > 5\ kcal/mole) \xrightarrow{h\nu} H + C_2H_2$$

$$(2b)\quad C_2H_3\ (E_T \leq 5\ kcal/mole) \xrightarrow{h\nu} H + C_2H_2$$

$$(3)\quad C_2H_3\ (E_T \leq 5\ kcal/mole) \rightarrow H + HCCH$$

In the secondary dissociation pathways in which a photon was absorbed, it was assumed that all the vinyl radicals in the internal energy range considered had an equal probability of becoming excited. The secondary product from channel (3) could, of course, contain no more than 5 kcal/mole in translation; however, in the $P(E_T)$ a maximum of 8 kcal/mole in translation was considered to account for uncertainty in bond energies. It was also assumed that the secondary $P(E_T)$ for (2a) was the same as for (2b). A primary, secondary, and spontaneous $P(E_T)$ was derived such that all the TOF spectra could be fit simply by changing the relative contribution of each channel. The final fits to the TOF are shown in Figure 6-9; Figures 6-13, 14, and 15 show the primary $P(E_T)$, secondary $P(E_T)$, and spontaneous $P(E_T)$ used.

The photodissociation of 1,1 D_2CCH_2 to give H + $HCCD_2$ gives some understanding of the effect that isotopes have on the atomic elimination. The H atom TOF spectrum calculated using the $P(E_T)$ from C_2H_4 at a similar laser power was compared to the 1,1 D_2CCH_2 H atom data. As seen in Figure

6-16, the H + $HCCD_2$ product seems to have more slow (higher internal energy) product. This is probably a result of the lower frequency C-D vibrations in the transition state [23] which allows more of the excess energy to couple into vibration.

4. Discussion

4.1. Molecular Elimination

The product ratios measured in the photolysis of 1,1 H_2CCD_2 and cis 1,2 HDCCDH as well as the TOF spectra support a mechanism in which both acetylene and vinylidene are formed. When the ethylene is excited there appears to be free rotation about the C=C bond but no significant H exchange. For each possible pair of hydrogen atoms in C_2H_4, the vinylidene formation was found to be three times as likely as the formation of acetylene. Since there are twice as many ways to produce acetylene in C_2H_4 as vinylidene, the vinylidene/acetylene product ratio was estimated to be 3/2. In the case where pure vinylidene (D_2 from 1,1 H_2CCD_2) was expected, fast product that could only have come from acetylene formation was detected. This could be accounted for by 1,2 migration of H at some point during the dissociation. The E_{act} for 1,2 H exchange, ~75.3 kcal/mole [25], is well within the available energy. Although this 1,2 H migration is related to the formation of ethylidene, the lack of extensive isotope scrambling in the

photodissociation of partially deuterated ethylene strongly suggests that it might be incorrect to think of the three-centered elimination of D_2 from 1,1 H_2CCD_2 to form acetylene as occurring through an ethylidene intermediate. The more accurate description, perhaps, is the concerted reaction involving the simultaneous migration of the H atom and the elimination of D_2 as shown in Figure 6-8.

The $P(E_T)$ for H_2 elimination from ethylene peaks well away from zero at ~22 kcal/mole which reflects a substantial exit barrier. This is quite typical of concerted elimination dissociation. For example, the $P(E_T)$'s for the concerted reactions, cyclohexene $\rightarrow$ C_2H_4 + $H_2CCHCHCH_2$ and cyclohexadiene $\rightarrow$ benzene + H_2 both peak at ~20-25 kcal/mole [30]. In concerted eliminations, when the excited molecule reaches the transition state, fast electron rearrangement often leaves the two newly formed product molecules in very close contact. As the old chemical bonds disappear and new ones form, the interaction between the products suddenly becomes repulsive. The repulsive separation converts a large fraction of the potential energy associated with the exit barrier into product translation. The fact that the three-centered elimination forming H_2 and vinylidene appears to be concerted, clearly shows that the vinylidene does not behave like a diradical in the conventional sense. The repulsive interaction of vinylidene with H_2 is more like that of a "stable molecule." The two electrons in

vinylidene must be strongly paired. This is, in fact, reflected in the heat of formation of vinylidene. The C-H bond in ethylene is known to be ~108 kcal/mole. However, breaking the C-H bond in the vinyl radical to form vinylidene, in spite of the fact that it does not involve any change in the bond order, only requires ~80 kcal/mole. This is ~28 kcal/mole less than what one expects from the simple bond additivity concept [31]. The additional 28 kcal/mole stability in vinylidene is likely to come from the energy released by the pairing of the two electrons in vinylidene.

The $P(E_T)$ obtained for the molecular elimination does not indicate whether dissociation is taking place from an electronically excited ethylene or whether internal conversion to vibrationally hot ground state ethylene precedes the dissociation. However, as will be discussed later, the translational energy distribution of simple C-H bond rupture clearly shows that a very fast internal conversion process takes place before the molecules start to dissociate.

The H_2 $P(E_T)$ from C_2H_4 photolysis contains more detailed information about the acetylene and vinylidene channels. The first electronically excited state of H_2 is out of the range of 193 nm photons. The lowest electronically excited states of acetylene ($^3B_2$ cis) and vinylidene ($^3B_2$) can form but would only appear at E_T < 29 kcal/mole and < 16

kcal/mole respectively [2]. Since vibrational and rotational excitation of both fragments is expected and a fairly significant amount has been observed in the H_2 product (an average of ~12 kcal/mole) [26], the peak of the distribution for these excited states would be expected at even lower E_T's where the $P(E_T)$ drops off. Thus, only a small percentage of the products could be formed electronically excited. Triplet vinylidene, thus, does not appear to be a major product in the molecular elimination channel at 193 nm. This is contrary to what Fahr and Laufer surmise from their flash photolysis studies of the photodissocation at much shorter wavelengths [21].

Because all acetylene + H_2 products appear at a translational energy less than 88 kcal/mole, at least 20 kcal/mole internal energy must be partitioned between the acetylene and H_2. At the translational energy at which vinylidene can just form (E_{Int} = 0 kcal/mole), the HCCH + H_2 products can have E_{Int} = 44 kcal/mole. The peak of the translational energy distribution corresponds to E_{Int} = 43 kcal/mole for the H_2CC + H_2 channel and to E_{Int} = 87 kcal/mole for the HCCH + H_2 channel. This experiment cannot identify how the internal energy is divided between hydrogen and the acetylene/vinylidene. However, the measurements carried out by Cromwell et. al. of this laboratory have shown that although H_2 is formed in rovibrational states as high as v=3/j=9, most of the H_2 is produced in v=0 and the average

internal excitation of H_2 is only ~12 kcal/mole [26]. A large fraction of the internal energy, then, must be going into vibrations and rotations of the H_2CC and HCCH since not much electronically excited triplet H_2CC and HCCH are expected to form. For a molecule with so many vibrational degrees of freedom, it is not surprising that the vibrational energy is extensively shared.

4.2. Atomic Elimination

The $P(E_T)$ obtained from the fitting process provides some important information on the dynamics of the primary process. As Figure 6-13 shows, the $P(E_T)$ peaks very close to 0 kcal/mole suggesting that the H atom elimination is a simple bond rupture with no exit barrier. It is consistent with dissociation from the ground electronic state, implying that the electronically excited ethylene internally converts to the upper vibrational levels of the electronic ground state before decomposing as has been suggested by theoretical studies [24] and Bersohn's experiments [23]. The other point apparent from the $P(E_T)$ is that most of the vinyl radical and hydrogen atom product forms with E_{Int} = 40 - 37 kcal/mole, not enough to excite the lowest electronic state of C_2H_3 ($\approx$ 53 - 57 kcal/mole [2]). The majority of the vinyl radical, then, must be produced in high vibrational levels of the ground electronic state.

The sharp rise in the fast edge of the H atom TOF

spectra with laser power as well as the velocity of the fastest products indicates that secondary photodissociation of primary products is important in the power range studied. The lowest laser intensity for which data is available is 40 mJ/pulse which corresponds to ~200mJ/cm^2 at the photolysis region.

It is difficult to obtain precise information about the secondary dissociation channels: so much averaging is inherently involved (see Chapters 4 and 5). It is also hard to discern the contribution of slow secondary products since they will appear with a velocity in the same range as the primary products. Nevertheless, the H atom TOF spectra taken do give some valuable information about the secondary events. The position of the fast edge, which is the most certain part of the spectrum, gives the maximum translational energy release. Assuming C_2H_3 with E_{Int} = 35 kcal/mole absorbs another photon and dissociates to HCCH, the ground state products should have a maximum translational energy of 148 kcal/mole. The observed maximum, however, is closer to 100 kcal/mole. If vinylidene were to form rather than acetylene, the expected maximum translational energy would be approximately 104 kcal/mole, closer to that measured. Most (~95%) of the product, however, does not appear near this threshold; it is much slower, with E_T ~15-30 kcal/mole. The relatively narrow translational energy distribution peaking at a high value

indicates that direct photodissociation from an electronically excited state is occurring. At the translational energy most of the products were observed at, there is enough internal energy for the triplet states of acetylene and vinylidene to form. The expected maximum translational energy for ground state H + $^3CCH_2$ is ≈ 56 kcal/mole and for H + ^3HCCH is ≈ 69 kcal/mole [2]. It seems likely, then, that these excited states are forming in the secondary dissociation.

The formation of triplet products implied by the secondary $P(E_T)$ is not entirely unexpected. As mentioned, Fahr and Laufer observed a significant amount of nonprimary triplet vinylidene [21]. They, however, attributed this product to the molecular elimination channel, making the assumption that the C_2H_3 would decompose to the thermodynamically favored product, HCCH. In this experiment, there was little (if any) triplet vinylidene or acetylene detected from the molecular elimination channel. Since Fahr and Laufer's results do not appear to be inconsistent with the triplet vinylidene forming from the atomic elimination channel, perhaps the metastable state they propose may be the vibrationally excited C_2H_3.

5. Conclusions

For the most part, the H and H_2 TOF studies agree with the previous work but offer a few more details. The two

major channels, the molecular and atomic elimination, were observed and were found to be of approximately equal importance. 1,1 D_2CCH_2 and 1,2 cis HDCCDH were photolyzed to understand the details of the molecular elimination channel. The product ratios and TOF spectra obtained were consistent with a mechanism in which both acetylene and vinylidene were produced in a 2 to 3 ratio for C_2H_4, there is free rotation about the C=C bond, and all H's are equally accessible but not equivalent. The D_2 TOF spectrum from 1,1 D_2CCH_2, where 100% vinylidene is expected, has some products too fast to be vinylidene; this is presumably from acetylene formation but with the elimination of D_2 from the same carbon atom. It is proposed that the H is transferring while the D_2 is leaving, through an ethylidene type intermediate. This could also explain why the D_2 TOF spectrum from C_2D_4 has less fast product (acetylene) than the C_2H_4 since it would be harder for the D to transfer than the H. The data cannot determine where along the reaction coordinate such a migration takes place or if it is responsible for all acetylene formation.

The $P(E_T)$ for the molecular elimination peaks away from zero and so indicates the presence of an exit barrier. A large fraction of the excess energy goes into internal energy of the H_2 + $HCCH/H_2CC$ products which is understandable considering the fast internal conversion of the excited molecules and the geometry changes that are

required in the excitation and dissociation. Because vibrational/rotational excitation is expected and experiments done by others in this group show that a significant fraction of this energy is in the rovibrational states of H_2 [26], very little of the acetylene and vinylidene can be formed in the lowest excited electronic states (T_1).

The studies of the atomic elimination channel were plagued by secondary dissociation even at as low laser intensity as 200 mJ/cm^2. Although this meant the C-H bond energy could not be accurately determined, important features of secondary photodissociation were explored. The best explanation for the changes in the H atom TOF spectra observed in going from low to high laser power is a competition between spontaneous decomposition and secondary photodissociation of the highly vibrationally excited vinyl radical with the latter becoming more important at high laser powers. The 193 nm dissociation begins with the absorption of a photon by ethylene. The elimination of the H atom peaks at very low translational energies suggesting simple bond rupture from the ground electronic state as theoretically predicted [24] and experimentally inferred by Bersohn's group [23]. The C_2H_3 that forms has ~0 - 40 kcal/mole in translation--not enough to go to the first electronic state ($^2A''$). Since the C-H bond energy to form acetylene is only ~35 kcal/mole, many of the C_2H_3 molecules

have enough energy to spontaneously decompose to form C_2H_2 + H with 0 to 5 kcal/mole in translation. To explain the fast H atoms seen, the C_2H_3 must also be able to absorb a second photon and decompose to H + C_2H_2. With this second photon, enough energy is available to form HCCH and H_2CC in the ground electronic state or in the lowest electronic state, T_1. The threshold for the secondary decomposition is closer to that expected for H + H_2CC suggesting that little ground state H + HCCH is produced. Based on the position of the peak in the secondary $P(E_T)$, the production of electronically excited triplet HCCH and/or H_2CC is apparently the favored pathway. The isomer that forms cannot be identified but since so little ground state acetylene is seen and Fahr and Laufer report detecting $H_2CC(^3B_2)$ as a major product in their flash photolysis studies [21] the $H_2CC(^3B_2)$ is apparently the most likely product in the secondary photodissociation of C_2H_3.

References

1. See review, G.J. Collin, Adv. Photochem. **14**, 136 (1988).

2. Not all the bond energies and heats of formation for molecules involved in the photodissociation of ethylene are well known. The following values are used: $\Delta H_f^\circ(C_2H_2)$ = 54.68 kcal/mole; $\Delta H_f^\circ(C_2H_4)$ = 14.58 kcal/mole; $\Delta H_f^\circ(H)$ = 51.6336 kcal/mole [see 3 and references therein]. $D_o(H\text{-}CHCH_2)$ = 108 ± 3 kcal/mole [see 3-5]; ΔH_{Isom}(acetylene → vinylidene) = 44 ± 3 kcal/mole [see 3,6-8]; $\Delta H(C_2H_3(^2A'' \leftarrow {}^2A'))$ = 53 - 57 kcal/mole [9,10]; H_2CC ($^3B_2 \leftarrow {}^1A_1$) = 47.6 ± .5 kcal/mole [8]; H_2CC ($^3A_2 \leftarrow {}^1A_1$) = 63.4 ± .5 kcal/mole [8]; HCCH ($^3B_2$(cis) $\leftarrow {}^1\Sigma_g^+$) = 79.1 kcal/mole; HCCH (^3B_u(trans) $\leftarrow {}^1\Sigma_g^+$) = 87.2 kcal/mole; HCCH ($^3A_2$(trans) $\leftarrow {}^1\Sigma_g^+$) = 101.7 kcal/mole; HCCH ($^3A_2$(cis) $\leftarrow {}^1\Sigma_g^+$) = 103.8 kcal/mole [11]; HCCH (^1A_u(trans) $\leftarrow {}^1\Sigma_g^+$) = 120.6 kcal/mole [12]; HCCH ($^1A_2$(cis) $\leftarrow {}^1\Sigma_g^+$) = 127.8 kcal/mole [13].

3. K.M. Ervin, S. Gronert, S.E. Barlow, M.K. Gilles, A.G. Harrison, V.M. Bierbaum, C.H. DePuy, W.C. Lineberger, and G.B. Ellison, J. Am. Chem. Soc. **112**, 5750 (1990).

4. H. Shiromaru, Y. Achiba, K. Kimura, and Y.T. Lee, J. Phys. Chem, **91**, 17 (1987).

5. A.M. Wodtke, E.J. Hintsa, J. Somorjai, and Y.T. Lee, Israel J. of Chem. **29**. 383 (1989).

6. M.M. Gallo, T.P. Hamilton, and H.F. Schaefer III, J. Am. Chem. Soc., in press.

7. Y. Chen, D.M. Jonas, J.L. Kinsey, and R.W. Field, J. Chem. Phys. **91**, 3976 (1989).

8. K.M. Ervin, J. Ho, and W.C. Lineberger, J. Chem. Phys. **91**, 5974 (1989).

9. M.N. Paddon-Row and J.A. Pople, J. Phys. Chem. **89**, 2768 (1985).

10. H.E. Hunziker, H. Kneppe, A.D. McLean, P. Siegbahn, and H.R. Wendt, Can. J. Chem **61**, 993 (1983).

11. R.W. Wetmore and H.F. Schaefer III, J. Chem. Phys. **69**, 1648 (1978).

12. K.K. Innes, J. Chem. Phys. **22**, 863 (1954).

13. S.P. So, R.W. Wetmore, and H.F. Schaefer III, J. Chem. Phys. **73**, 5706 (1980).

14. P. Ausloos and R. Gorden, Jr., J. Chem. Phys. **36**, 5 (1962).

15. A.B. Callear and R.J. Cvetanović, J. Chem. Phys. **24**, 873 (1956).

16. H. Okabe and J.R. McNesby, J. Chem. Phys. **36**, 601 (1962).

17. M.C. Sauer, Jr. and L.M. Dorfman, J. Chem. Phys. **35**, 497 (1961).

18. R.A. Back and D.W.L. Griffiths, J. Chem. Phys. **46**, 4839 (1967).

19. (a) H. Hara and I. Tanaka, Bull. Chem. Soc. Japan **47**,

1543 (1974); (b) H. Hara and I. Tanaka, Bull. Chem. Soc. Japan **46**, 3012 (1973).

20. R.J. Sension and B.S. Hudson, J. Chem. Phys. **90**, 1377 (1989).

21. (a) A. Fahr and A.H. Laufer, J. of Photochemistry **34**, 261 (1986); (b) A.H. Laufer, J. of Photochemistry **27**, 267 (1984).

22. L. Giroux, M.H. Back, and R.A. Back, Can. J. Chem. **67**, 1166 (1989).

23. S. Satyapal, G.W. Johnston, R. Bersohn, and I. Oref, J. Chem. Phys. **93**, 6398 (1990).

24. E.M. Evleth and A. Sevin, J. Am. Chem. Soc. **103**. 7414 (1981).

25. K. Raghavachari, M.J. Frisch, J.A. Pople, and P.v.R. Schleyer, Chem. Phys. Lett. **85**, 145 (1982).

26. E.F. Cromwell, A. Stolow, and Y.T. Lee, to be published.

27. P.G. Wilkinson and R.S. Mulliken, J. Chem. Phys. **23**, 1895 (1955).

28. A.J. Merer and R.S. Mulliken, Chemical Reviews **69**, 639 (1969).

29. A. Fahr and A.H. Laufer, J. Phys. Chem. **92**, 7229 (1988).

30. X. Zhao, R.E. Continetti, A. Yokoyama, E.J. Hinsta, and Y.T. Lee, J. Chem. Phys. **91**, 4118 (1989); X. Zhao, Ph.D. Thesis, University of California, Berkeley

(1988).

31. S.W. Benson, Thermochemical Kinetics (John Wiley and Sons, Inc., New York, 1968).

Tables

Table 6-1. Relative Amounts of Product Formed in the Photolysis of 1,1 D_2CCH_2 and 1,2 cis HDCCDH.

Isotopomer	D_2 m/e = 4	HD m/e = 3
1,1	0.5	1
cis 1,2	~0.2	2

Figure Captions

Figure 6-1. Heats of reaction (0K) for the various channels in the photodissociation of ethylene. The photolysis energy is 147.9 kcal/mole. Many of the molecules' heats of formation are not well known. The values used to construct this diagram are given in reference 2.

Figure 6-2. Newton diagrams for the experiment showing (a) the H_2 product velocity range for H_2 from the molecular elimination channel and (b) the H atom velocity range for the H from the atomic elimination channel. The diagrams show that since detection is perpendicular to the parent beam, only the fastest C_2H_2 product and none of the C_2H_3 can be seen.

Figure 6-3. H_2 TOF spectrum from photolysis of C_2H_4. The data was accumulated for 16.1 hrs at an average laser power of 130 mJ/pulse. The solid line is the best fit calculated using the $P(E_T)$ shown in Figure 6-4.

Figure 6-4. $P(E_T)$ for H_2 + C_2H_2 used to fit the H_2 TOF spectrum in Figure 6-3. The arrows show the maximum translational energy at which the acetylene, vinylidene, excited state acetylene, and excited state

vinylidene channels are expected.

Figure 6-5. TOF spectra from the photolysis of 1,1 D_2CCH_2 and 1,2 cis HDCCDH deuterated ethylenes. (a) and (b) show the HD and D_2 scans from the 1,1 H_2CCD_2 and (c) and (d) show the HD and D_2 scans from the 1,2 cis HDCCDH, respectively. The total accumulation times/average laser power for each are as follows: (a) 14.4 hrs at 105 mJ/pulse, (b) 17.2 hrs at 115 mj/pulse, (c) 13.8 hrs at 80 mJ/pulse and (d) 6.9 hrs at 70 mJ/pulse. The areas of these spectra have been normalized to reflect the observed relative ratios given in Table 6-1.

Figure 6-6. The TOF spectra with the best signal/noise from the deuterated ethylene experiments. These spectra have been fit using the appropriate $P(E_T)$ shown in Figure 6-7. (a) HD TOF spectrum from 1,1 D_2CCH_2; (b) D_2 TOF spectrum from 1,1 D_2CCH_2; (c) HD TOF spectrum from 1,2 cis HDCCDH.

Figure 6-7. $P(E_T)$'s used to fit the deuterated ethylene molecular elimination TOF spectra in Figure 6-6. These curves have been normalized to the same area. The solid line is for HD + C_2HD from 1,1 D_2CCH_2. The dashed line is for D_2 + C_2H_2 from 1,1 D_2CCH_2; the dotted line is for HD + C_2HD from 1,2 cis HDCCDH.

Figure 6-8. Diagram showing the ethylidene-type mechanism which can explain why acetylene + D_2 is observed in the photolysis of 1,1 D_2CCH_2. The excited ethylene (twisted) rearranges to an ethylidene-like intermediate. The 1,2 migration of the H atom occurs while the D_2 is leaving to produce D_2 + HCCH.

Figure 6-9. Open circles are the D_2 TOF spectrum from the photolysis of C_2D_4 (2.2 hrs at 80mJ/pulse). The solid line shows the "fit" using the $P(E_T)$ from C_2H_4 molecular elimination channel (Figure 6-4).

Figure 6-10. H atom TOF spectra from C_2H_4 photolysis. Solid line is the fit using the mechanism/assumptions discussed in the text. The -·- line shows the H from primary dissociation. The -···- line is H from secondary dissociation of C_2H_3 that does not have enough internal energy to undergo spontaneous decomposition; the dotted line is H from secondary dissociation of C_2H_3 that has enough internal energy to undergo spontaneous decomposition but absorbs a photon instead. Solid-dashed line is H from spontaneous decomposition of C_2H_3 to HCCH + H. Scans (a), (b), (c), and (d) were accumulated for 8.9, 7.8, 0.2, and 0.2 hrs at an average laser power of 40, 90, 140, and 180 mJ/pulse respectively.

Figure 6-11. Comparison of the H atom TOF spectra taken at high (X's) and low (open circles) laser power. The solid line is the best fit calculated using the preliminary assumptions discussed in the text. The dotted lines represent the H atoms from secondary dissociation of the C_2H_3 after absorption of a photon.

Figure 6-12. Diagram illustrating the spontaneous decomposition explanation for the change in shape of the H atom TOF spectra with laser power. The ethylene absorbs a photon (1) to produce H + C_2H_3. Some of the C_2H_3 has enough internal energy to fragment to H + HCCH (3). Otherwise the C_2H_3 can absorb a photon (2) and decompose to H + HCCH/H_2CC. As the laser power increases, the fraction of molecules undergoing spontaneous decomposition (3) decreases while the fraction that absorb a photon (2) increases.

Figure 6-13. Primary $P(E_T)$ for $C_2H_4 \rightarrow H + C_2H_3$ used to fit all the H atom TOF spectra in Figure 6-10.

Figure 6-14. Secondary $P(E_T)$ for C_2H_3 (fast) $\rightarrow$ H + C_2H_2 and C_2H_3 (slow) $\rightarrow$ H + C_2H_2 used to fit all the H atom TOF spectra in Figure 6-10. Shown are the expected maximum translational energy of the C_2H_2 + H and $^3H_2C_2$ + H products assuming the E_{Int} of the C_2H_3 is 35 kcal/mole.

The figure shows that most of the C_2H_2 product is formed in the lowest triplet state.

Figure 6-15. Spontaneous decomposition $P(E_T)$ used to fit the H atom TOF spectra in Figure 6-10. Although from the bond energies used in the thesis, H + HCCH products with E_T > 5 kcal/mole would not be expected, products with E_T up to 8 kcal/mole were considered to account for the uncertainty in this value.

Figure 6-16. H atom TOF spectrum from photolysis of 1,1 D_2CCH_2. The spectrum is fit with the same $P(E_T)$ used to fit the high power (180 mJ/pulse) H atom TOF spectrum from C_2H_4 photolysis. The H + $HCCD_2$ product clearly has more slow H atoms being formed than the H + $HCCH_2$.

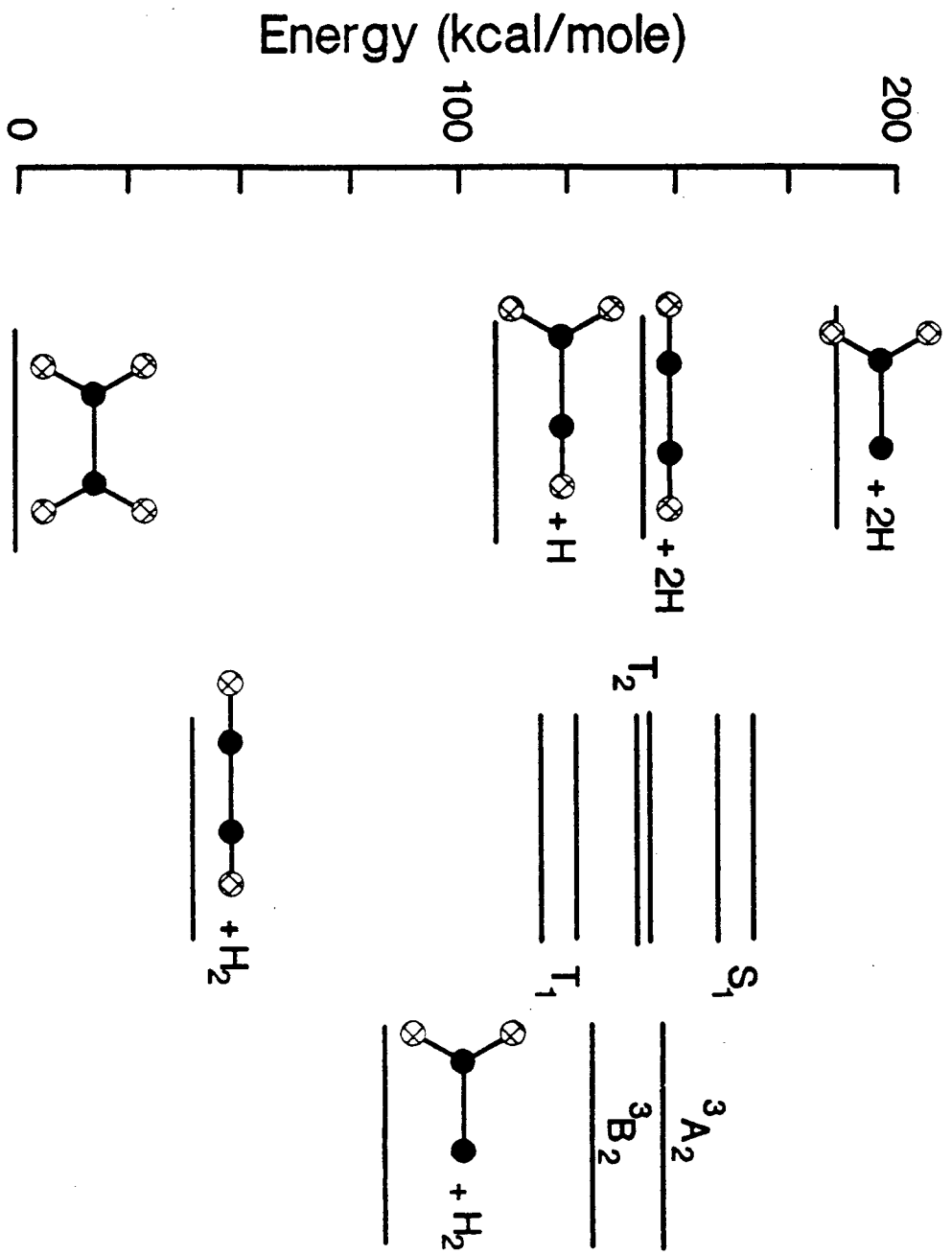

Figure 6-1

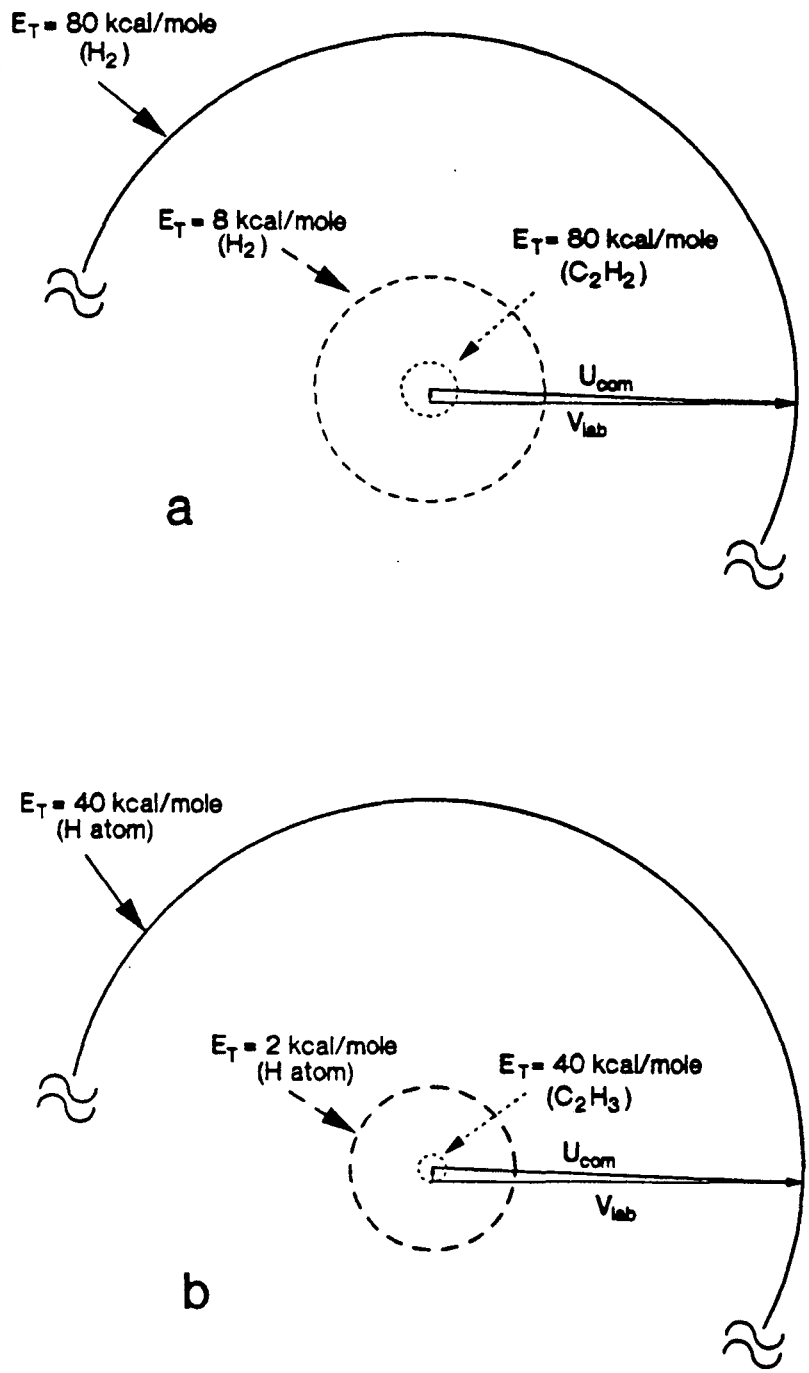
E_T = 80 kcal/mole
(H_2)
E_T = 8 kcal/mole
(H_2)
E_T = 80 kcal/mole
(C_2H_2)
U_{com}
V_{lab}
a
E_T = 40 kcal/mole
(H atom)
E_T = 2 kcal/mole
(H atom)
E_T = 40 kcal/mole
(C_2H_3)
U_{com}
V_{lab}
b

Figure 6-2

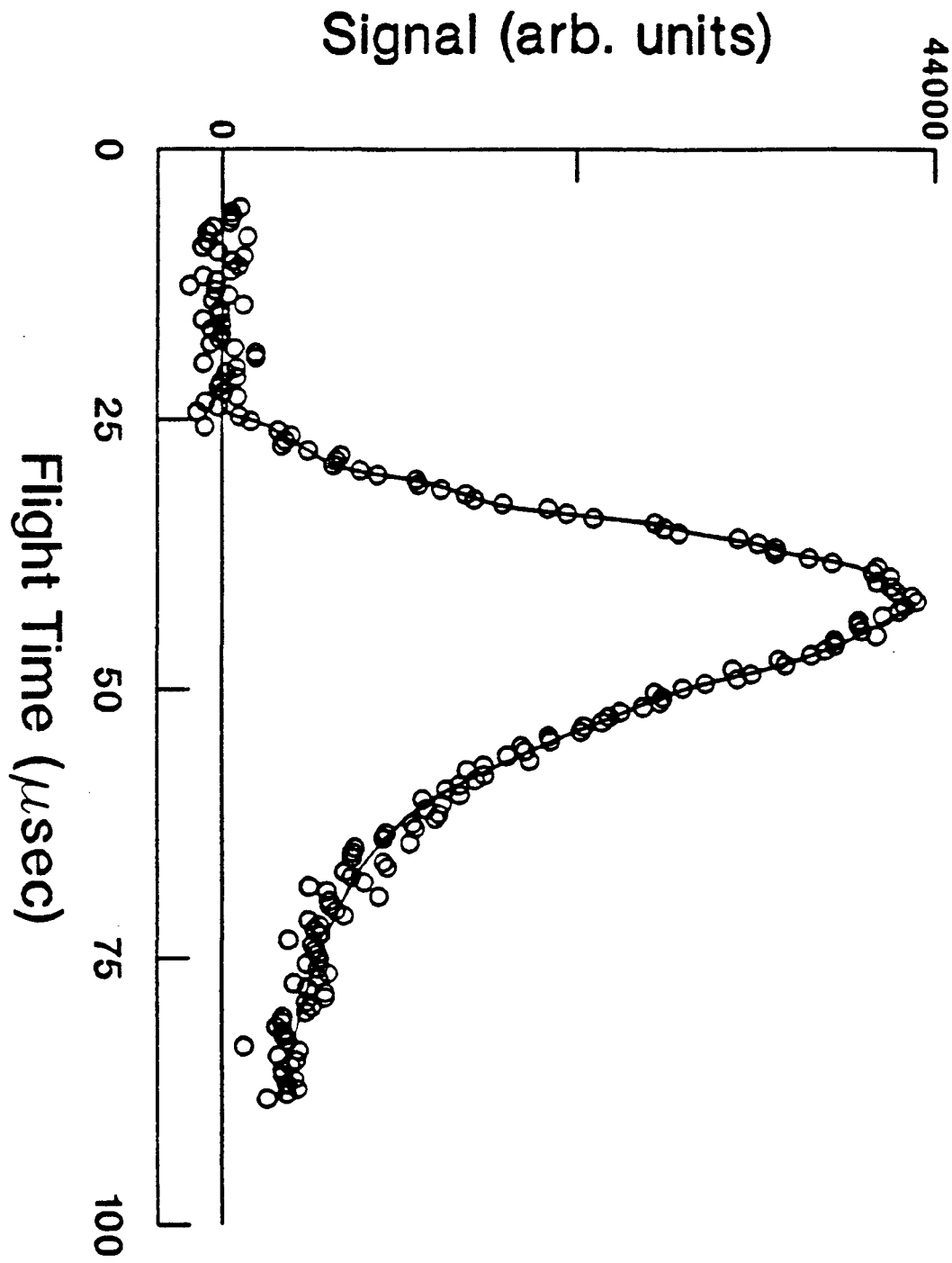

Figure 6-3

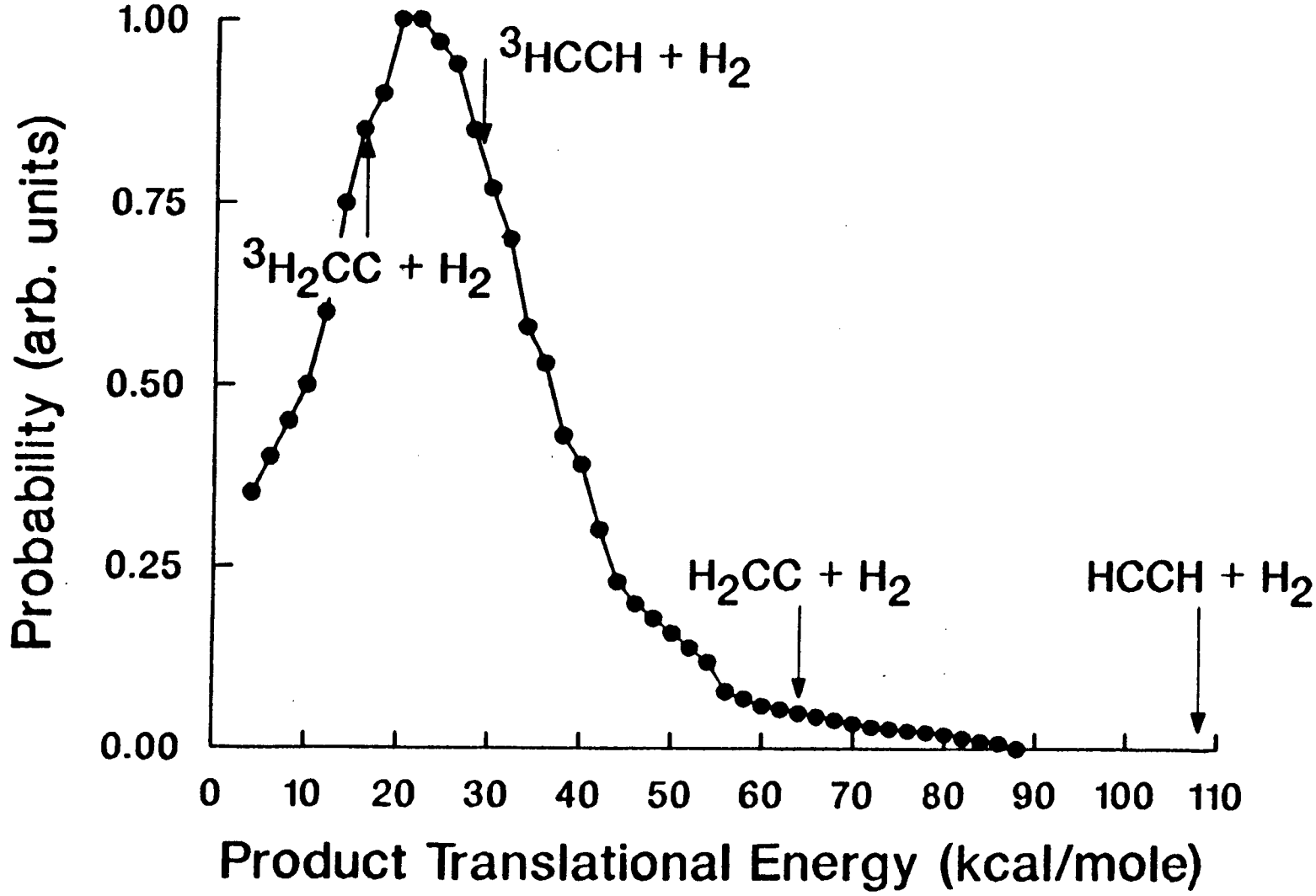
1.00
0.75
0.50
0.25
0.00
Probability (arb. units)
$^3HCCH + H_2$
$^3H_2CC + H_2$
$H_2CC + H_2$
$HCCH + H_2$
0
10
20
30
40
50
60
70
80
90
100
110
Product Translational Energy (kcal/mole)

Figure 6-4

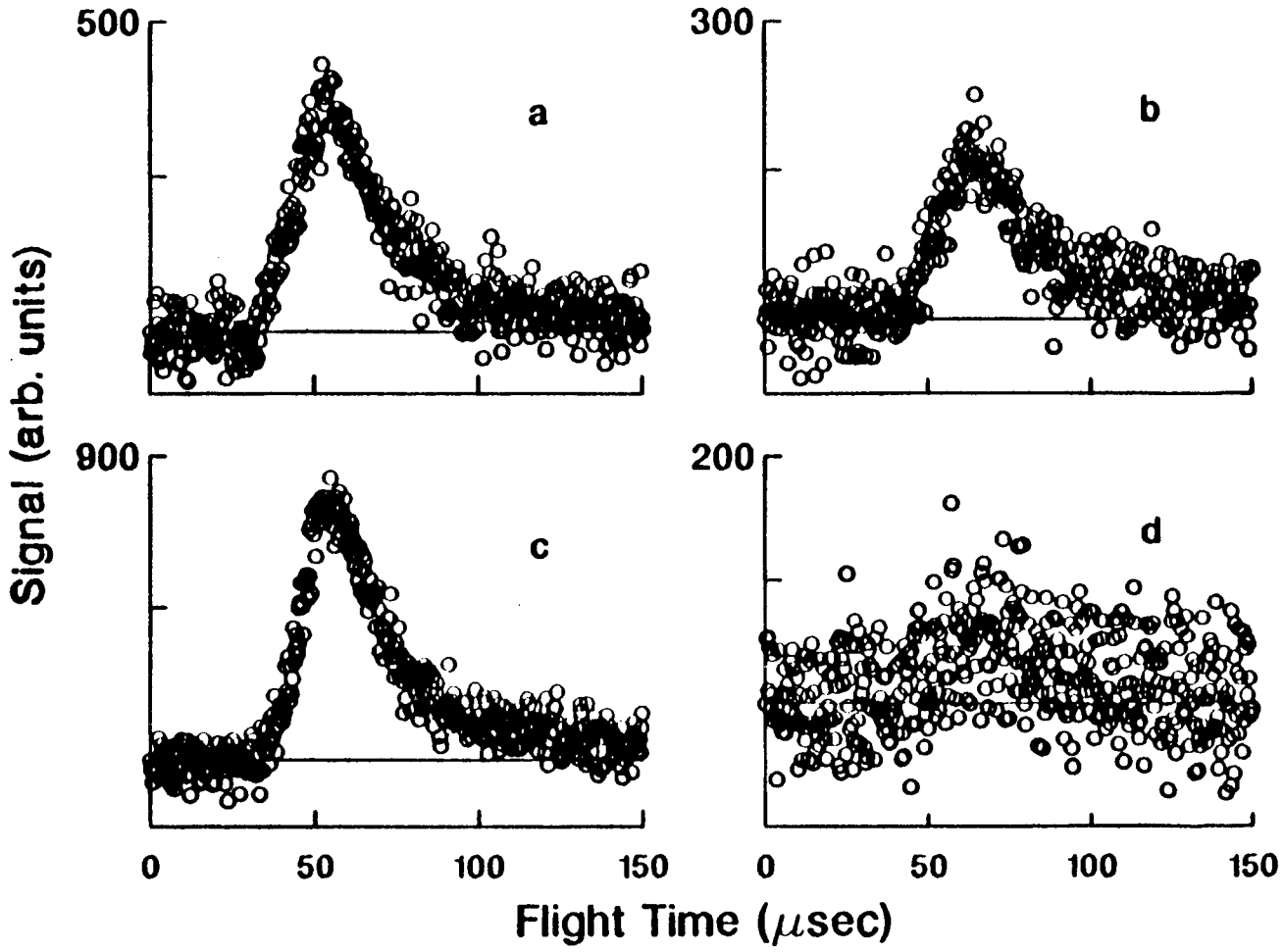
500
a
300
b
900
c
200
d
Signal (arb. units)
0
50
100
150
0
50
100
150
Flight Time (μsec)

Figure 6-5

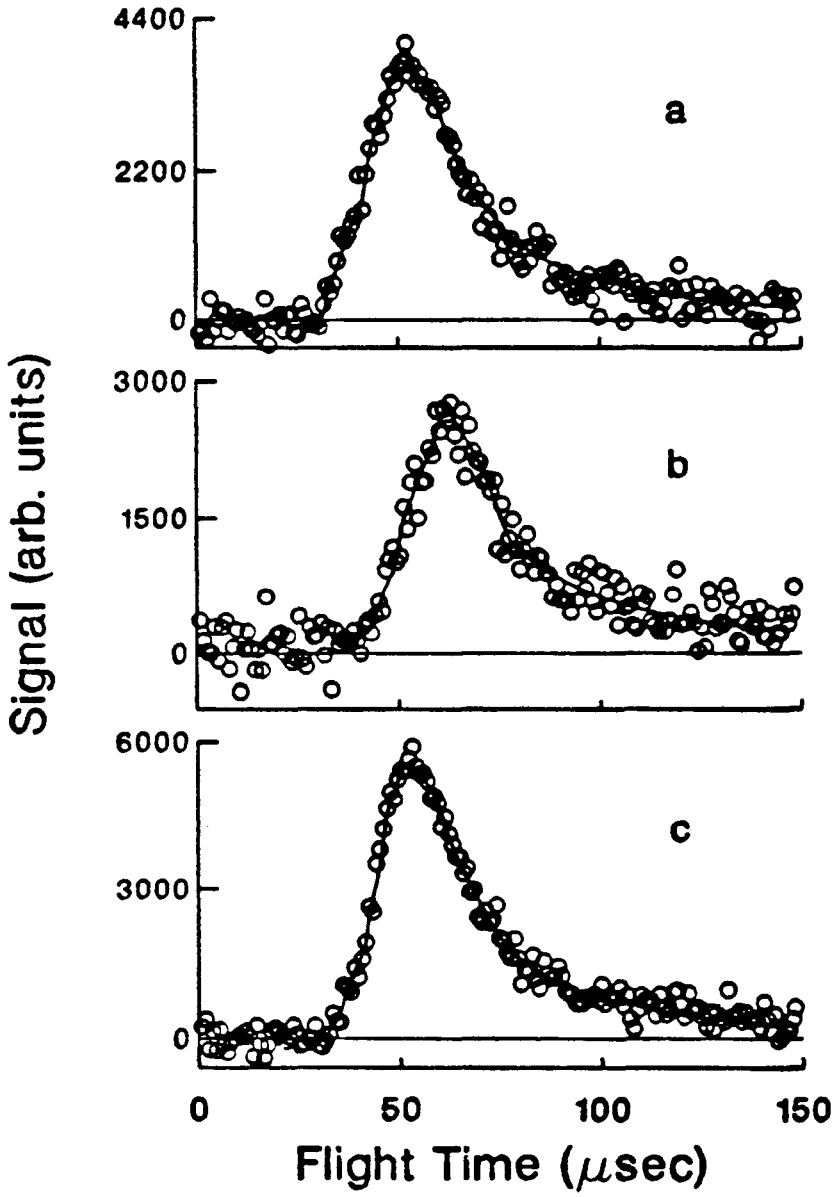
4400
2200
0
a
3000
1500
0
b
6000
3000
0
c
Signal (arb. units)
0
50
100
150
Flight Time (μsec)

Figure 6-6

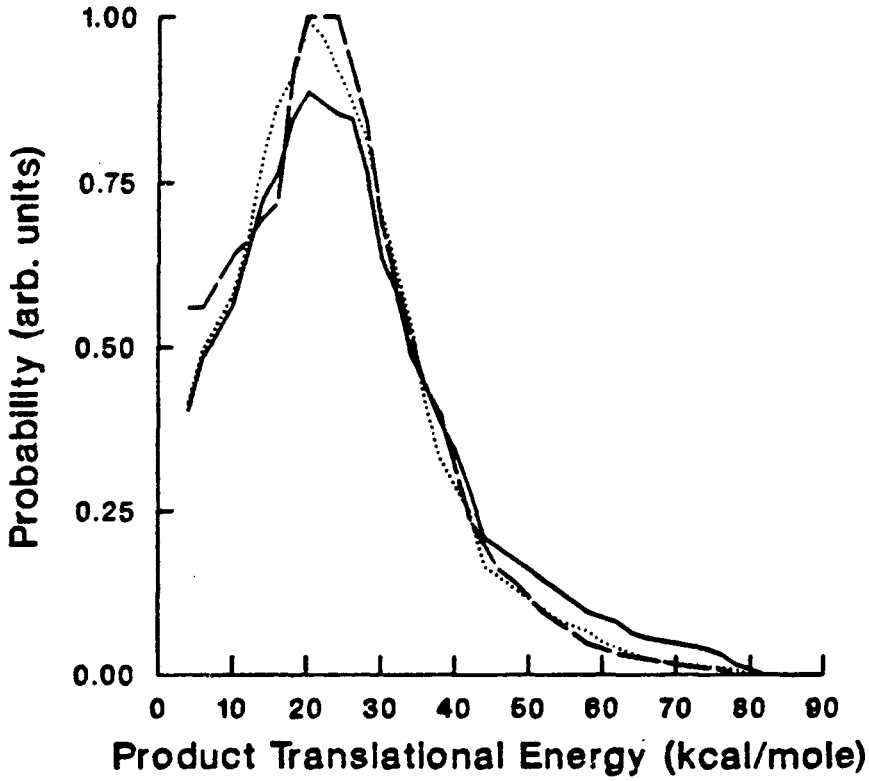
1.00
0.75
0.50
0.25
0.00
Probability (arb. units)
0
10
20
30
40
50
60
70
80
90
Product Translational Energy (kcal/mole)

Figure 6-7

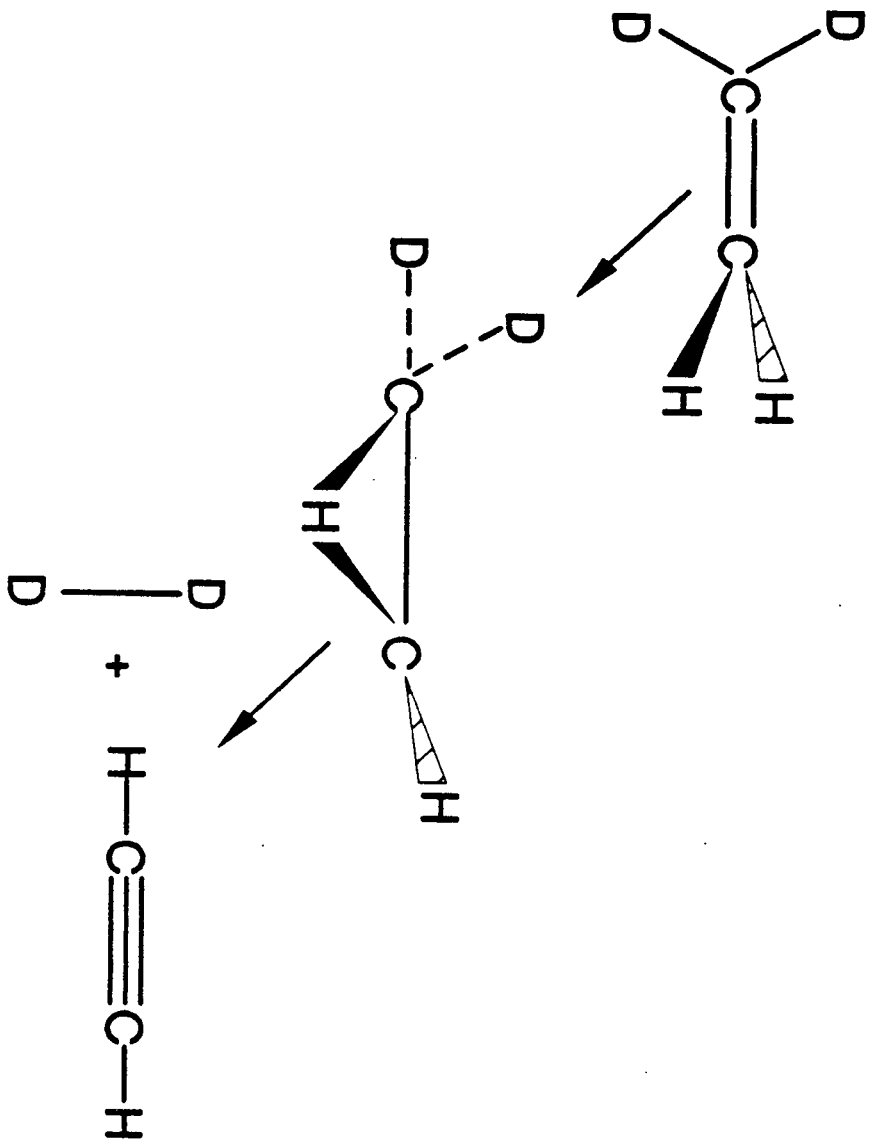

Figure 6-8

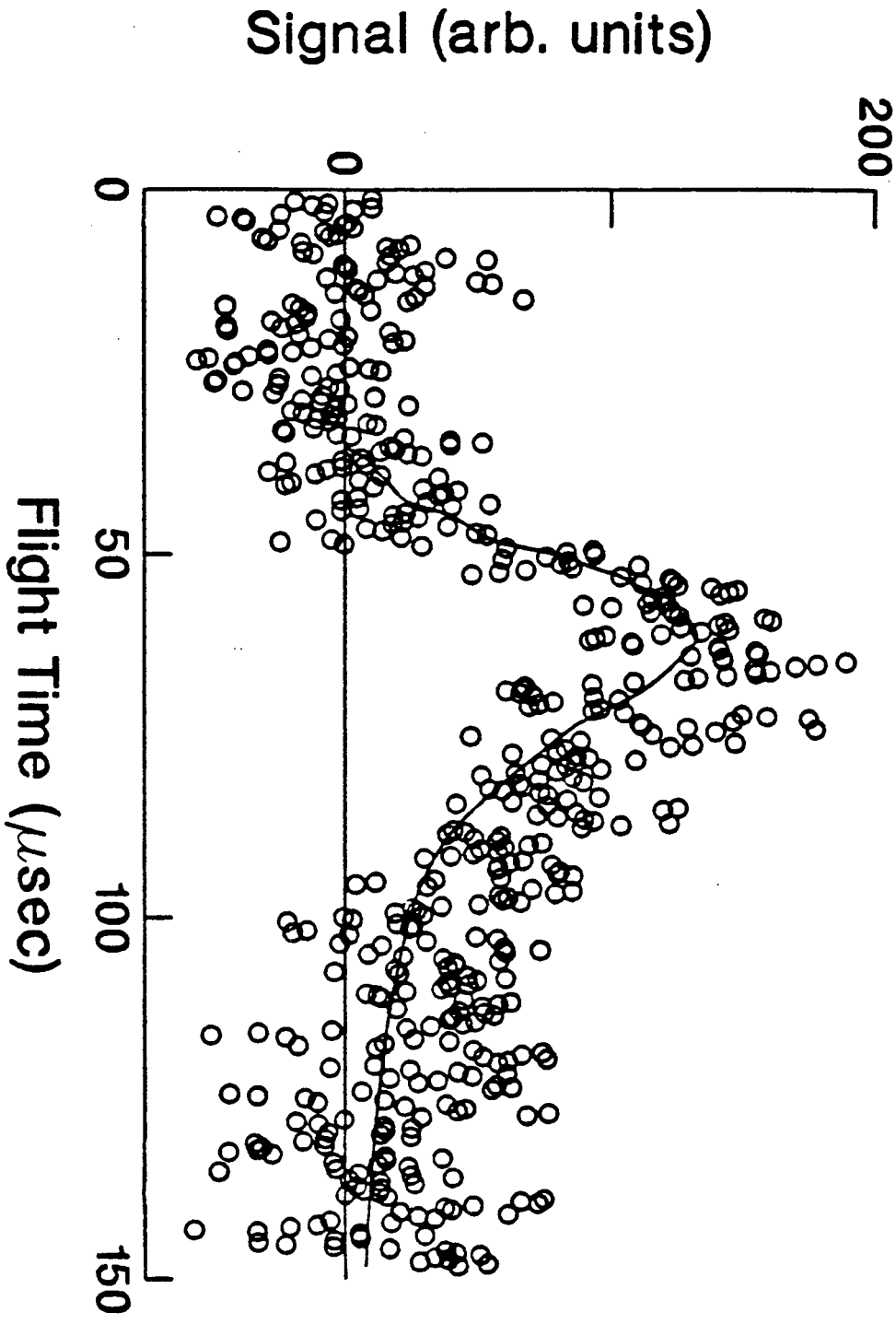

Figure 6-9

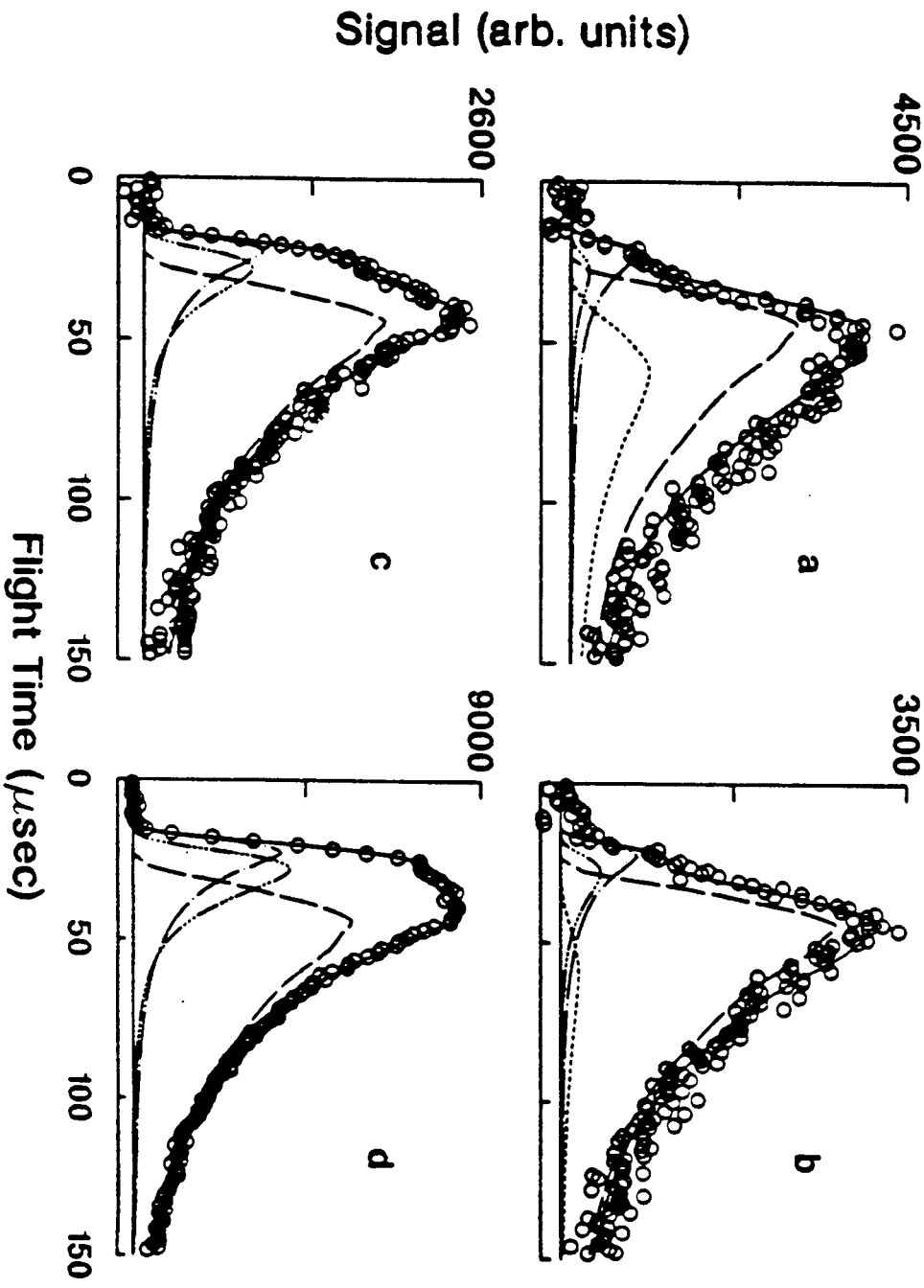
Signal (arb. units)
4500
0
a
3500
0
b
2600
0
c
9000
0
d
0
50
100
150
Flight Time (μsec)

Figure 6-10

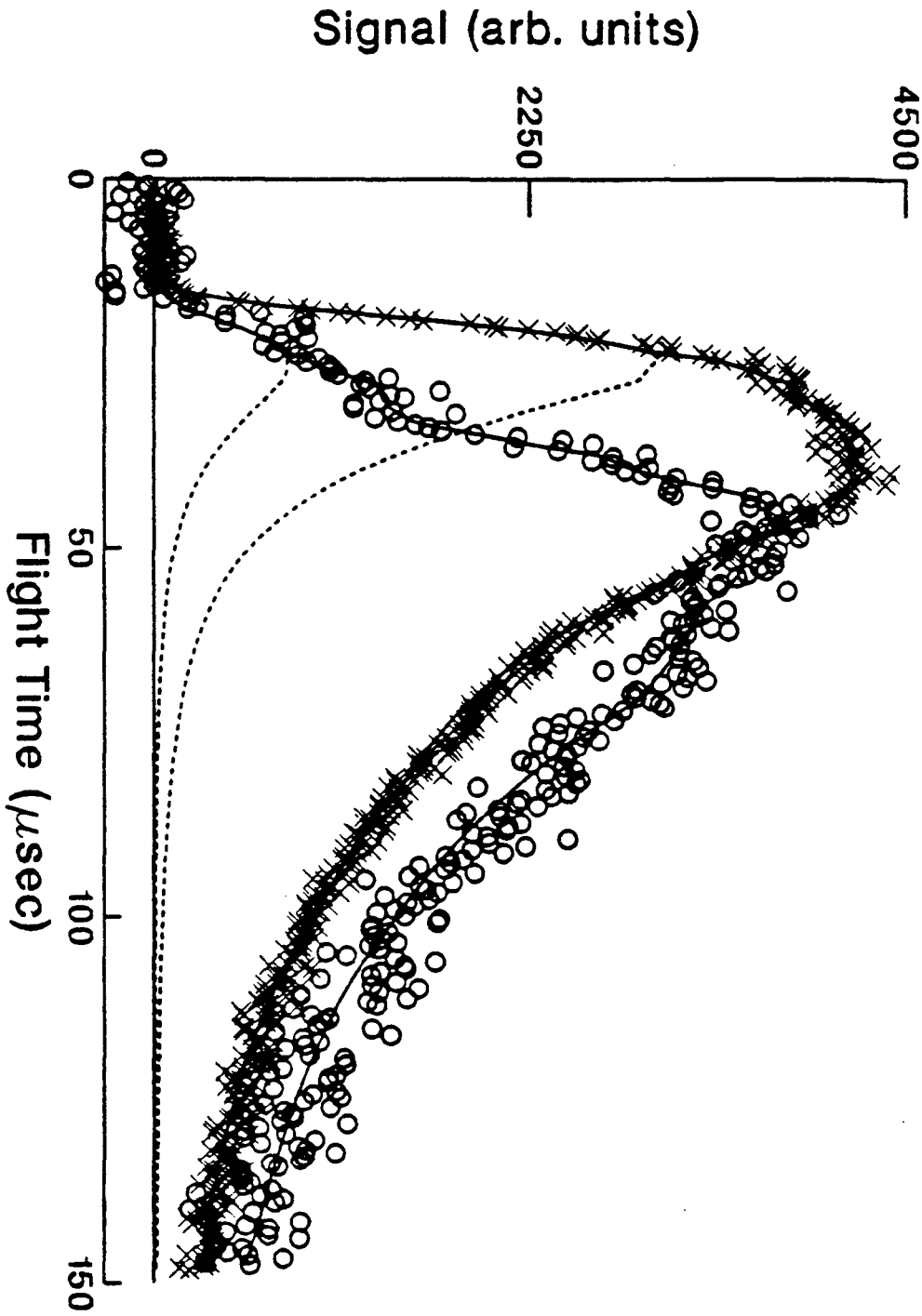

Figure 6-11

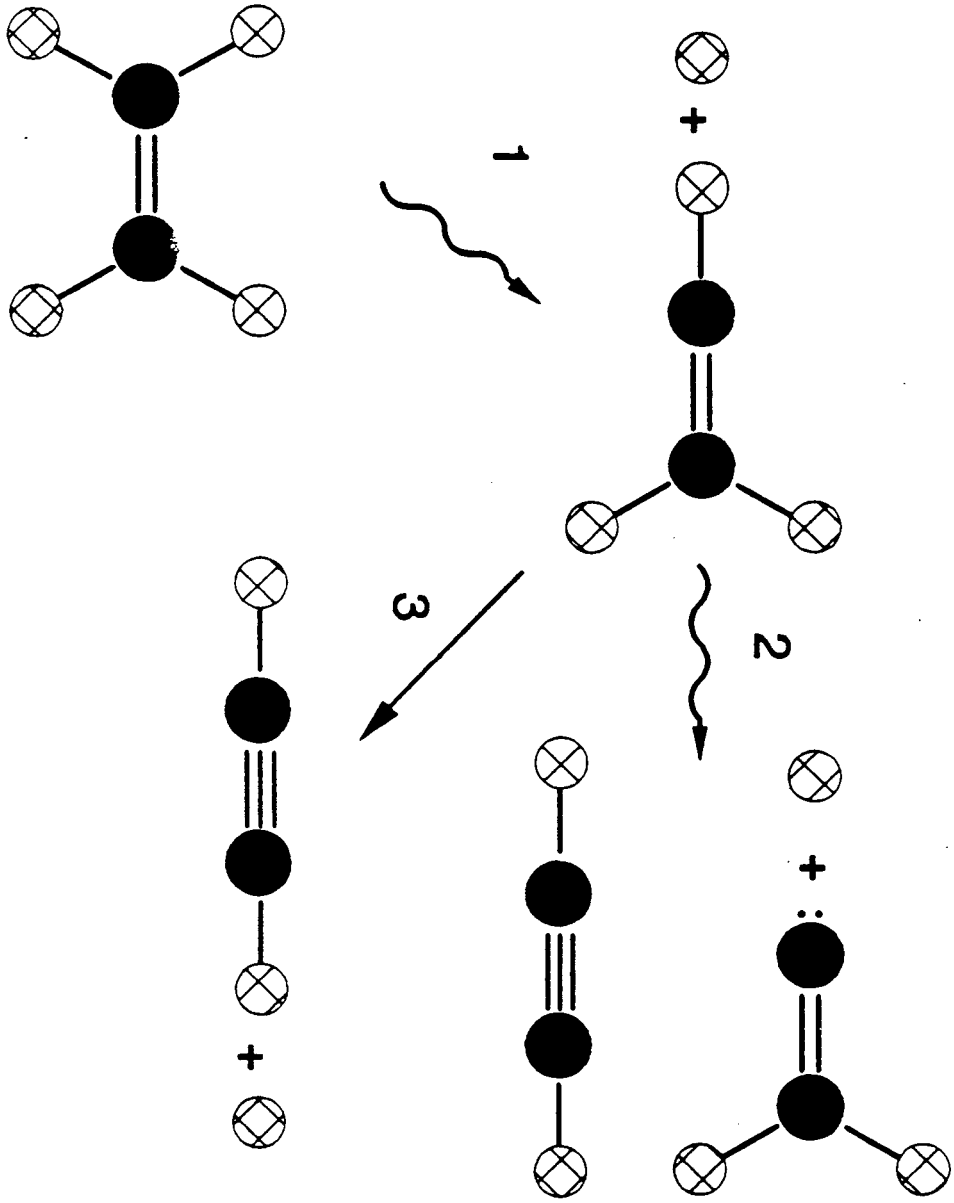

Figure 6-12

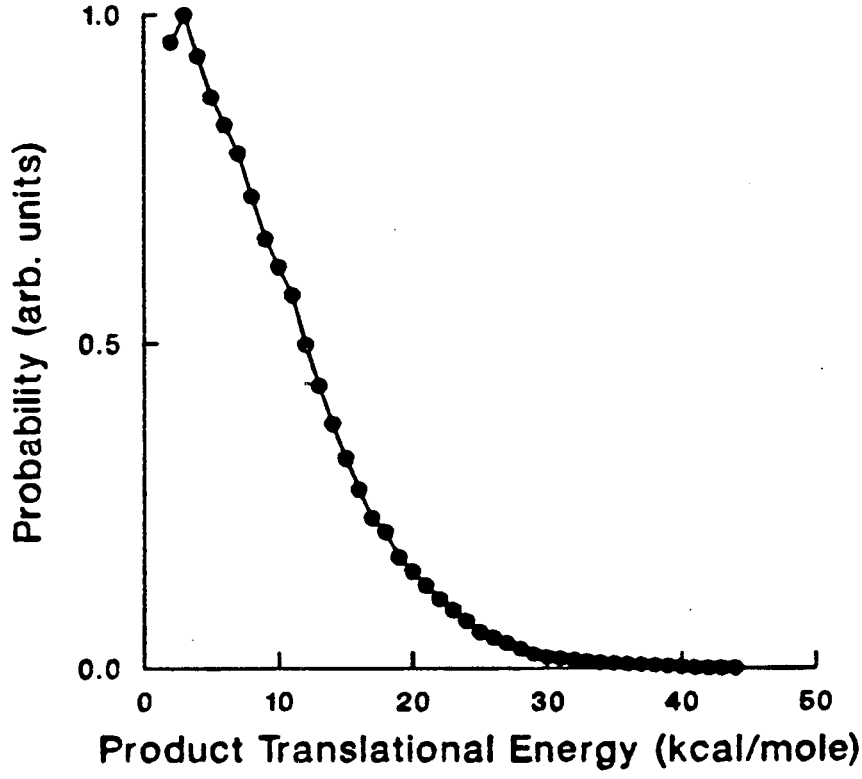
1.0
0.5
0.0
Probability (arb. units)
0
10
20
30
40
50
Product Translational Energy (kcal/mole)

Figure 6-13

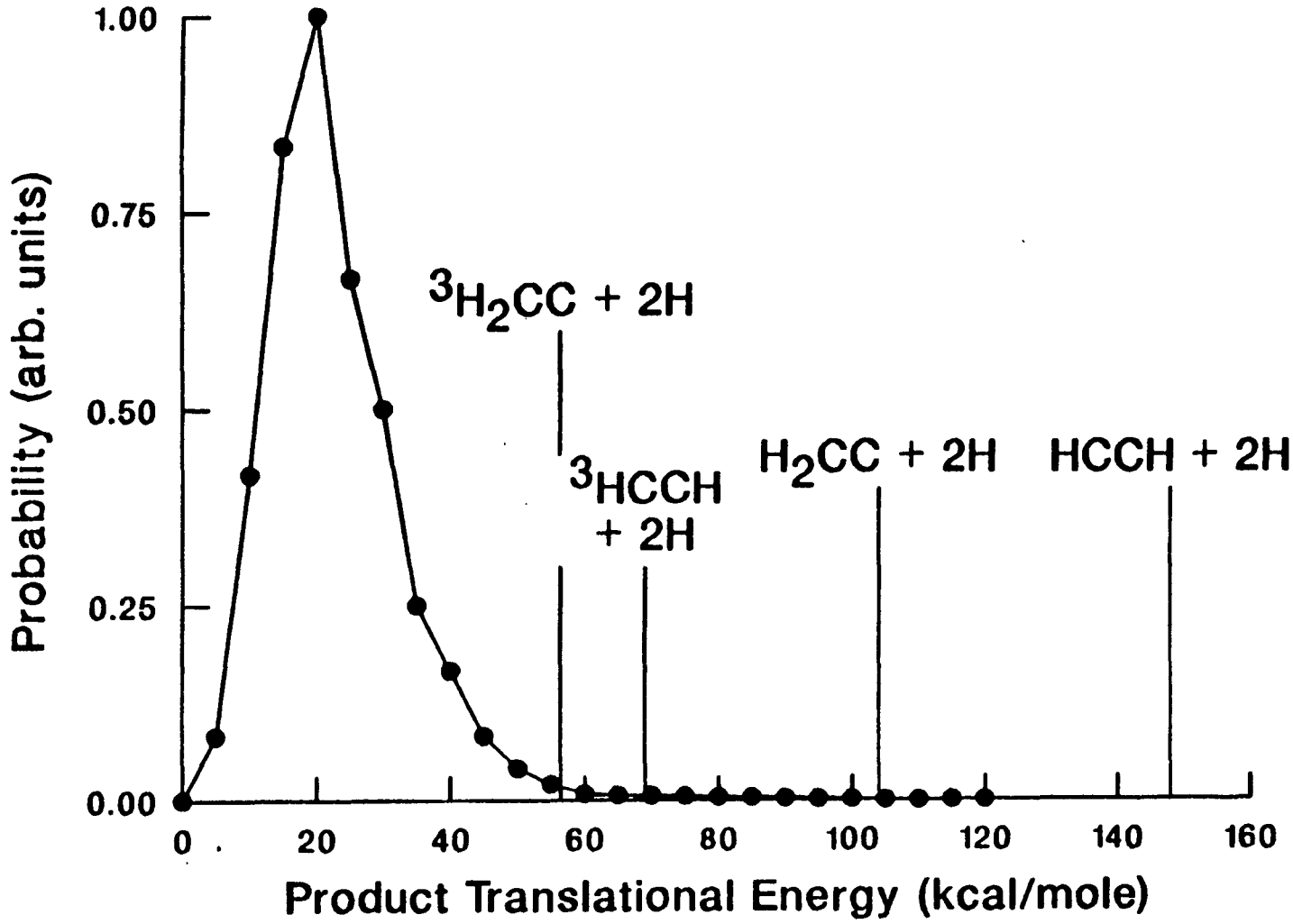
1.00
0.75
0.50
0.25
0.00
Probability (arb. units)
$^3H_2CC + 2H$
$^3HCCH + 2H$
$H_2CC + 2H$
HCCH + 2H
0
20
40
60
80
100
120
140
160
Product Translational Energy (kcal/mole)

Figure 6-14

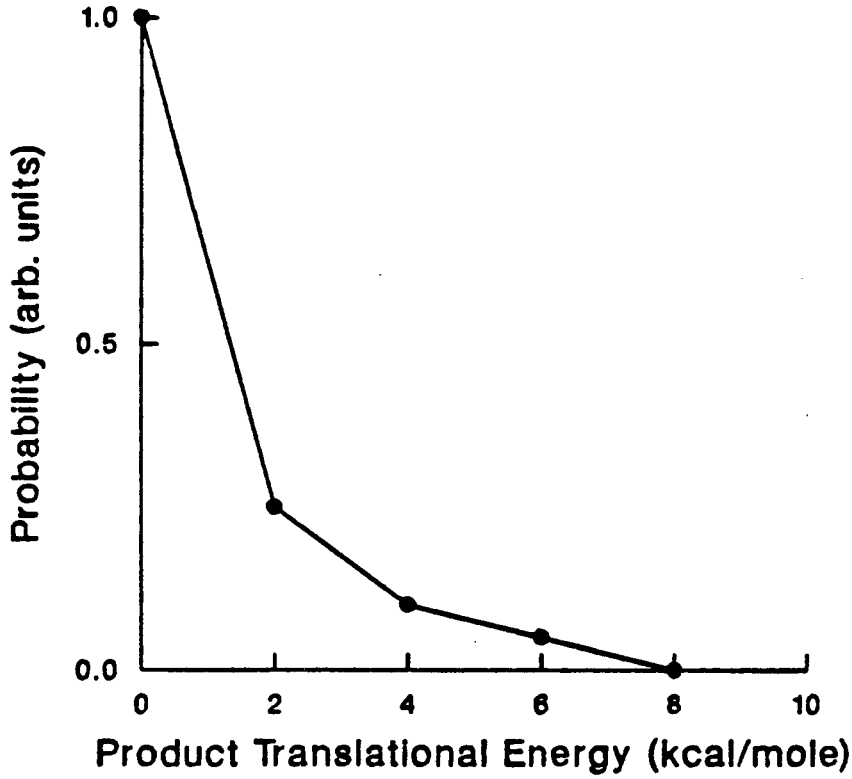
1.0
0.5
0.0
Probability (arb. units)
0
2
4
6
8
10
Product Translational Energy (kcal/mole)

Figure 6-15

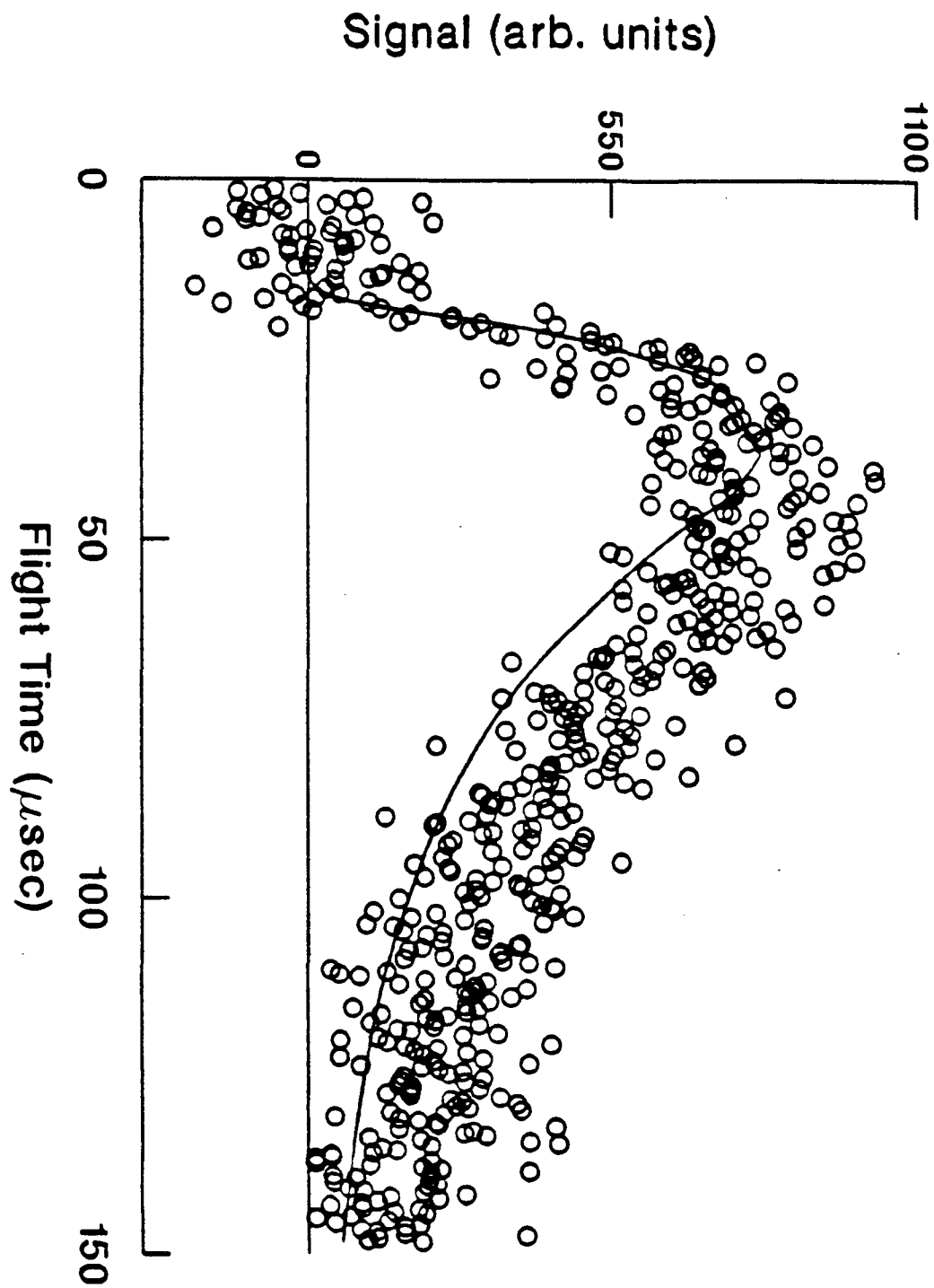

Figure 6-16

Chapter 7: 193 nm Photodissociation of 1,1 and 1,2 Difluoroethylene

1. Introduction

The photodissociation studies of 1,1 and 1,2 difluoroethylene (DFE) were initially undertaken to better understand the three- and four-centered elimination in ethylene photolysis; the DFE experiments are much easier since the 193 nm absorption cross-section for the 1,1 and 1,2 DFE's (σ ~1 to 4 x 10^{-18} cm^2) is much greater than that of ethylene [1]. The validity of the comparison between the DFE's and ethylene, however, depends on how similar the excitation/decomposition mechanisms are. Like ethylene, the DFE 193 nm absorption involves the $\pi^* \leftarrow \pi$ transition but the geometry of the DFE $\pi\pi^*$ excited state is thought to be less twisted than in ethylene [1]. The mercury triplet photosensitization work of Strausz et. al., however, showed that free rotation about the C=C bond still occurred after excitation [2], as in the ethylene system, so perhaps this

is not critical. Another difference is that a Rydberg excited state may also be important in the DFE system [1]. Nevertheless, the known DFE photochemistry is very similar to ethylene's. A matrix VUV excitation experiment [3] showed that three- and four-centered elimination of HF occurs presumably after internal conversion to the electronic ground state. As discussed in Chapter 6, ethylene photodissociation is consistent with internal conversion. H atom elimination from DFE was also seen and triplet states seemed somehow to be involved [3]. This is not unlike what was seen in the ethylene experiments since triplet acetylene and/or vinylidene was produced in the secondary photodissociation.

The DFE TOF studies also fill in some important gaps in the understanding of three- and four-centered elimination from halogenated olefins. Interest in the DFE's was particularly high in the 70's and 80's primarily because vibrationally excited HF is the primary photolysis product [2,4-6] and chemical lasers based on HF and HCl were being developed at that time [7]. As would be expected, then, these early studies concentrated on measuring the HF vibrational distributions to determine to what extent they were nonstatistical. Excitation was either via infrared multiphoton excitation [6] or Hg photosensitization [4,5] with very similar results, confirming that the electronically excited state does not have a critical role.

~11% of the energy available to the products in excess of the reaction endothermicity was transferred to HF vibrational energy in the 1,1 DFE while ~8% was transferred in the cis and trans isomers [5]. The HF vibrational distribution from the cis and trans DFE was nearly statistical while that from the 1,1 DFE was not [5]. The difference between the 1,1 and 1,2 isomers has been attributed to changes in the elimination mechanism [2,5]: in the 1,1 DFE, elimination of HF is expected to be four-centered to produce fluoroacetylene (FA) while in the 1,2 DFE, both three-centered and four-centered elimination can occur to give FA and fluorovinylidene (FV). Based on the ~40 kcal/mole [8,9] difference in the heat of formation of FA and FV, three-centered elimination would be expected to give a cooler HF vibrational distribution because the formation of FV would leave less energy available for the HF vibrations [5,6]. Another reason why the three-centered elimination is cooler is that the three-centered exit barrier is lower so there will be fewer forces acting on the separating photofragments; such forces tend to put energy into vibrations nonstatistically [5,8]. A theoretical study of HF elimination in C_2H_3F [11] found barrier heights of 81 and 80 for elimination via four-centered and three-centered intermediates. Since the endothermicity to form FV is greater than to form FA, the similar barrier heights imply a smaller exit barrier for three-centered elimination.

Little work has been done on the other channels that are thermodynamically possible. Figure 7-1 [2,8,9,12-16] shows the possible products and their energy levels with respect to the DFE's. (The values are quite uncertain (± 5-15 kcal/mole) so all three DFE isomers have been grouped together since their ΔH_f°'s only differ by ~3-4 kcal/mole.) An early shock tube study found that HF elimination was the predominant 1,1 DFE decomposition channel at low temperatures but that atomic elimination occurred at higher temperatures [12]. VUV photolysis of 1,1 and 1,2 DFE in a matrix showed no C_2H_2, C_2F_2, CF_2, or CHF indicating that H_2 and F_2 elimination as well as C-C bond fission were not important dissociation pathways [3]. Evidence of H atom elimination was seen but there was no indication of loss of an F atom.

TOF distributions of the 193 nm photoproducts of 1,1 and 1,2 DFE are measured in the experiments described here. The HF TOF spectra will complement what is already known about the HF vibrational distribution of this elimination channel; the $P(E_T)$'s should reveal the exit barrier heights for elimination from the 1,1 and 1,2 DFE isomers to show whether this is the cause for the different vibrational distributions. Since the products are selected with a mass spectrometer and photolysis is done under single collision conditions, the spectra taken at different masses may be able to probe some of the channels that have not been

studied. Finally, comparison of the TOF spectra from DFE should add to the understanding of ethylene photochemistry.

2. Experiment

These experiments were done following the procedure described in Chapter 4. Although the absorption cross-section was much higher for the DFE's then ethylene, to make sure that all the channels could be seen if they were occurring, most of the scans were taken with no skimmer. When the experiment was first done, the detector gating wheel was used to help reduce background problems. This limited detection to H and H_2 fragments since the heavier HF and F products would be slower and might not all reach the detector before the wheel closed the opening. The rest of the experiments were done without the wheel. The DFE used was from Matheson; the lecture bottles were dated 1976 so they were frozen in liquid nitrogen and pumped on to remove any noncondensable decomposition products. Comparison between the 1,1 and 1,2 DFE elimination is not quantitative because the experiments were not run close together in time; the first 1,2 DFE cylinder ran out and it took ~1 month to locate a replacement. The photodissociation channels for a given molecule should also not be rigorously compared. To go from H/H_2 detection to HF/F detection required changing the mass spectrometer High-Q head which affects the detector sensitivity. Unfortunately, the laser thyratron (an

expensive part!) failed before better calibrated TOF spectra could be recorded. The data, however, was sufficient for determining what channels were open and how the product translational energy distributions differed. It would be informative to repeat the experiments using the skimmer, fresh DFE, and making careful quantitative comparisons between the 1,1 and the 1,2 DFE ethylene and between the various elimination channels.

As discussed, photodissociation on the 35" machine is ideally suited for detecting fast, i.e. light, photoproducts. Table 7-1 shows the various products and their expected earliest arrival time assuming the ΔH values in Figure 7-1. This is useful for identifying what channels the various masses detected come from. The table shows that the H_2 and HF molecular elimination channels as well as the H atomic elimination channel should be easy to pick out of the spectra; these signals should occur much faster than any thermalized background. In addition, H atoms from the atomic elimination channel should not be confused with H atoms from dissociative ionization of other products. The F atoms from the atomic elimination, however, may be more difficult to separate from the F atoms that result from cracking of heavier products.

3. Results and Analysis

3.1. H_2 Molecular Elimination

H_2 product was seen in the photodissociation of both 1,1 and 1,2 DFE; the H_2 TOF spectra are shown in Figures 7-2 and 7-3. In both cases, the peak was fast enough that it could not come from some laser-correlated background. The H_2 TOF spectrum from the 1,2 DFE has a component that arrives after ~100 μsec; it is unlikely that this could be H_2 from the direct photodissociation of the parent. Based on previous experience with the photolysis chamber (see Chapters 4-6), a more reasonable explanation is that it results from reactions of H radicals such as H atom abstraction or H atom recombination. The effect was probably more noticeable in the 1,2 dissociation because signal is lower. The slow peak made it impossible to accurately determine the shape of the low translational energy section of the $P(E_T)$. It is difficult to quantify but there appeared to be more H_2 elimination in the 1,1 DFE. As in the ethylene system, three-centered elimination appears to be preferred over four-centered. H_2 elimination is definitely less probable than HF elimination. Much higher quality TOF spectra at m/e=20 (HF) could be obtained with significantly less counting time.

The $P(E_T)$'s used to fit the TOF spectra are plotted in Figure 7-4. The H_2 + C_2F_2 products from the 1,2 DFE are much faster than those from the 1,1. This can be seen just by comparing the TOF spectra. The maximum translational energy release for the 1,2 DFE, 64 kcal/mole, is very close to the

66 kcal/mole predicted from the enthalpy of $C_2H_2F_2 \rightarrow H_2$ + FCCF and the 193 nm photon energy. Thus, as would be expected from the ethylene studies, four-centered elimination to form difluoroacetylene (DFA) is occurring. While the 1,2 DFE H_2 TOF spectrum can be used to distinguish between DFA and difluorovinylidene (DFV) formation, it is not of high enough quality to be used to extract more exact thermodynamic values. The H_2 product from the 1,1 DFE has a maximum translational energy of ~32-38 kcal/mole. This is slightly less than the value predicted from the enthalpy of the H_2 + CCF_2 reaction, 40 kcal/mole.

In the photodissociation of ethylene, 100% vinylidene was expected in the 1,1 $D_2CCH_2 \rightarrow D_2$ + CCH_2 channel. However, D_2 too fast to be from 1,1 elimination was observed. The explanation given in Chapter 6 was that an H migrated as the D_2 left through a type of ethylidene intermediate. In the three-centered H_2 elimination channel in 1,1 DFE, however, only DFV is actually formed; there is no fast product due to the formation of DFA. The difference in the ethylene and DFE cases can be understood by realizing that F migration cannot occur as readily as H so the F atom will not transfer over as the H_2 leaves.

The maximum of the H_2 + C_2F_2 $P(E_T)$ for the 1,1 DFE occurs at ~6 kcal/mole. The fact that it is nonzero indicates the presence of an exit barrier. The peak, however, is at lower translational energy than that observed

in the H_2 molecular elimination in ethylene. One explanation is that the CCF_2 product is less stable than the CCH_2 so there is less of the closed-shell repulsion. Another possibility is that the lower C-F vibrational frequencies compared to the C-H allow more translational energy to couple into the CCF_2 product. The peak position in the 1,2 DFE H_2 TOF spectrum cannot be determined because of the slow laser-correlated signal .

That the observed maximum translational energies from the 1,1 and 1,2 DFE photodissociation to give H_2 are so close to the predicted values indicates that some of the FCCF and CCF_2 form vibrationally cold. In the ethylene molecular elimination, the maximum translational energy of the vinylidene could not be determined because of the acetylene channel. However, no ground state acetylene was detected. The fastest H + HCCH product contained 20 kcal/mole internal energy. The reason given for the high internal energy of the H_2 + HCCH products was the large distortions in geometry required. Perhaps, then, the transition state to form the H_2 + FCCF products from the 1,2 DFE is much closer to the products.

3.2. HF Molecular Elimination

The HF TOF spectra from the 1,1 and 1,2 DFE's are shown in Figures 7-5 and 7-6; Figure 7-7 shows the $P(E_T)$'s used to fit this data. The 1,1 and 1,2 DFE HF TOF spectra both have

a maximum product translational energy of ~80 to 90 kcal/mole. The expected maximum for elimination to give FA is 106 kcal/mole and to give FV is 66 kcal/mole. As would be expected, then, both isomers undergo four-centered elimination. Unlike the H_2 elimination, however, there does not seem to be much ground state fluoroacetylene formed; the fastest HF + HCCF detected must have ~16 to 26 kcal/mole internal energy (the uncertainty of the elimination reaction endothermicity is ± 15 kcal/mole). The HF four-centered elimination, thus, is much more like the four-centered H_2 elimination in ethylene. The lack of ground state product indicates that large structural changes from the transition state to product may be required.

Although the fast edge of the 1,1 and 1,2 DFE's are similar, the rest of the $P(E_T)$'s are quite different. This can also be seen directly in the HF TOF data; much of the 1,2 signal occurs at slower times than the 1,1. This difference is expected; only 1,2 elimination can occur in the 1,1 DFE while both 1,1 and 1,2 can take place in the 1,2 DFE. The 1,1 DFE $P(E_T)$, which should reflect 100% four-centered elimination, peaks away from zero indicating the presence of a substantial exit barrier. As discussed in the ethylene chapter, this is typical of dissociations producing two stable closed-shell molecules. Such a barrier is not surprising considering the changes in geometry involved. A barrier has, in fact, been used to explain the non-

statistical HF vibrational distribution in the 1,1 DFE dissociation [5].

Based on structural probability alone one would expect equal contributions from FV and FA to the 1,2 DFE $P(E_T)$. However, the ethylene photodissociation experiments showed that vinylidene formation was approximately three times as likely as acetylene so the 1,2 DFE $P(E_T)$ should have more vinylidene "character." The $P(E_T)$ peaks at or near 0 kcal/mole. This indicates that the exit barrier for 1,1 elimination, if it exits, must be much smaller than the exit barrier compared for 1,2 elimination. Again, this difference has been hypothesized to explain the more statistical HF vibrational distribution observed in the 1,2 DFE dissociation [5]. The peaking of the HF + CCHF $P(E_T)$ close to 0 kcal/mole is also the first clear evidence that the elimination is occurring from the ground electronic state. (In the ethylene photodissociation, this had to be inferred from the atomic elimination channel.) After the initial photon absorption, the electronically excited DFE must undergo internal conversion to the upper vibrational levels of the ground state. In addition, that the $P(E_T)$ peaks near 0 kcal/mole means that most of the product is forming with a large amount of internal energy, ~55 kcal/mole. This is large considering that a statistical HF vibrational distribution is expected so only ~8% of E_{avail} or ~5 kcal/mole should go into HF vibrations [5]. A good deal

of the internal energy, then, must go to the FV fragment. Again, this is consistent with the excess energy being statistically distributed in the transition state since the FV fragment has more and lower vibrational frequencies than the HF.

The three-centered elimination channel producing HF + CCHF is substantially different from that giving H_2 + CCF_2 and the D_2 + CCH_2 in the ethylene photodissociation. In the ethylene case, the $P(E_T)$ peaked at ~20-26 kcal/mole and in the H_2 elimination (1,1 DFE $\rightarrow$ H_2 + CCF_2), the peak occurred at ~6 kcal/mole. One might attribute these differences to vinylidene stability concluding that the CCH_2 must be more stable than the CCF_2 which is in turn more stable than the CCHF. An earlier infrared multiphoton dissociation study of three-centered HCl elimination in $HClCCF_2$, however, showed that most of these products formed with almost no translational energy [17]. Since the DFV is a product in this dissociation as it is in the 1,1 DFE $\rightarrow$ H_2 + CCF_2 where the $P(E_T)$ peaks away from zero, it cannot be the DFV stability that is primarily responsible; something about an HX fragment leaving must cause the high internal excitation/low translational energy. Perhaps the presence of the X atom makes the transition state looser, effectively removing any exit barrier. Another possibility is that the C-H interaction is the predominant source of product repulsion but since the COM of HX is close to the X atom,

repulsion between the separating products will transfer more energy into HX rotations, something that could not occur as readily when a homonuclear diatomic is eliminated.

3.3. F Atom Elimination

The F atom TOF spectrum from the photolysis of the 1,1 DFE isomer is shown in Figure 7-8. Since the $P(E_T)$ for 1,1 DFE $\rightarrow$ HF + C_2HF gives an excellent fit (solid line), the F atoms observed must be from HF undergoing dissociative ionization in the detector. There is no evidence for any F atom elimination.

The F atom TOF spectra from the 1,2 DFE photolysis at two different laser powers are shown in Figure 7-9. The spectra are similar to the HF m/e = 20 spectrum suggesting that the F atom crack is being detected but there is also a new, slower component. The power study confirms that a second component exists: the F atom TOF spectra change with laser power indicating that there is some secondary dissociation process going on, but the HF TOF spectrum show no such power dependence. The new component starts to arrive at ~100-150 μsec. From Table 7-1, the most likely candidates are F atoms from 1,2 DFE $\rightarrow$ F + FC_2H_2 or F atoms from a crack of HCCF after 1,2 DFE $\rightarrow$ HF + FCCH. Of course, there is a host of two photon processes than could also contribute. The lack of a F atom signal from 1,1 DFE photodissociation which should also give FCCH makes the F +

C_2H_2F channel the obvious first choice. The low power scan was fit by scaling the HF contribution for which the $P(E_T)$ is known to the fast shoulder; the rest of the signal was assumed to be from F elimination. The $P(E_T)$ obtained peaks at 10-12 kcal/mole. A nonzero peak for what should be a simple bond rupture is disturbing. The possibility that another channel is at least partially responsible for the new F atom signal must be considered.

The idea of a different channel is supported by a cursory examination of the power dependence. Increasing the laser power seemed to decrease the new F atom peak relative to the HF contribution as well as add some faster product. If the F atoms were from DFE $\rightarrow$ F + C_2H_2F, secondary photodissociation of the C_2H_2F should not change the HF to primary F atom ratio. The ratio would be expected to change, however, if the F atoms are from a crack of HCCF. If the HCCF absorbs a photon and dissociates before reaching the detector, the peak corresponding to this fragment will decrease but a new fast F atom peak from the HCCF $\rightarrow$ F + HCC will grow in. To test this idea, the $P(E_T)$ from 1,1 DFE $\rightarrow$ HF + HCCF, where the product is expected to be from four-centered elimination, was used to fit the data. The TOF of the F atom expected from the crack is much too slow. It may be that the four-centered $P(E_T)$ is different in the 1,2 DFE where there is competition with the three-centered elimination than in the 1,1 DFE where photodissociation to

acetylene is the only channel. If this were true, then one could also explain why no F atoms other than those from the HF crack were observed in the 1,1 DFE TOF spectrum.

It is clear that there are many other possible sources of F atoms. For example, consider the following scenario: 1,2 DFE → CCFH + HF followed by secondary photoabsorption by the FV, giving CCF + H; the CCF can then undergo dissociative ionization in the detector giving a F atom signal which would be slightly faster than the CCFH. This would require a power dependent H atom signal but this is observed (see next section). Because the heavier photofragments could not be detected in these experiments, the 1,2 DFE TOF spectrum cannot be completely understood.

3.4. H Atom Elimination

The H atom TOF spectra from the 1,1 and 1,2 DFE's are shown in Figures 7-10 and 7-11. The spectra consist of a slow and fast peak. The slow peak corresponds to the H atom crack of the HF photofragment. Consulting Table 7-1, the fast peak, assuming it is a primary product, can only come from H atom elimination: DFE → H + HC_2F_2. The fast edge of the spectra show a strong dependence on laser power and this effect is greatest in the 1,2 DFE. Based on the ethylene photodissociation experiments, this is not surprising; the vinyl radical formed readily absorbed a photon and lost another H atom.

The spectra were fit starting with the 1,1 DFE since it had the least interference from secondary dissociation. Some secondary products are still being formed, however, so this data cannot be used to obtain the C-H bond energy. In the fitting, it was assumed that the maximum translational energy would be ~40 kcal/mole (i.e. that the C-H bond energy is ~108 kcal/mole, approximately the C-H bond energy in ethylene [12]). The primary $P(E_T)$ obtained is shown in Figure 7-12. The $P(E_T)$ peaks close to 0 kcal/mole and is typical of that expected from a simple bond rupture. This would suggest, as did the molecular elimination results, that after the DFE absorbs the photon, it internally converts to the ground electronic state before dissociating. The higher laser energy DFE H atom TOF spectrum was then used to get some idea of the secondary dissociation $P(E_T)$. The secondary dissociation was assumed to be sequential as in the ethylene and it was further assumed that all of the C_2HF_2 formed had an equal chance of absorbing a second photon. The secondary $P(E_T)$ is shown in Figure 7-13. In the secondary dissociation of the 1,1 DFE, unless the F atom migrates, only the vinylidene form will be produced. Therefore, the maximum possible secondary product translation energy would be ~84 + E_{Int}. As was found in the ethylene secondary photodissociation, the secondary product is much slower than expected; the peak is at ~20 kcal/mole. In the ethylene case, this was attributed to formation of

triplet product. Perhaps the same is true here. In the only other study of the atomic elimination channel, the triplet quenching studies Guillory and Andrews [3], it was inferred that the triplet state of the DFE's was somehow involved. It should be noted that there are other possible sources for the secondary H atoms observed. For example, 1,1 DFE → HCCF + HF followed by secondary photodissociation of the HCCF to give CCF + H. Again, TOF spectra of the higher mass products are required to completely resolve the mechanism.

There is less H atom elimination relative to the amount of H from HF from the 1,2 isomer. This is not necessarily because more H atom elimination occurs in 1,1 DFE. It is more likely that there is more HF elimination in the 1,2 DFE because the preferred three-centered elimination can occur in this compound and/or that the HF formed in the 1,2 DFE photodissociation has more internal energy (the $P(E_T)$ peaks at 0 kcal/mole) so tends to crack more in the ionizer. A quantitative comparison of the data shows that secondary dissociation also seems to be much more predominant in the 1,2 DFE isomer. This can be attributed to the average laser power being approximately twice as great in the 1,2 scans as in the 1,1. Another possibility it that the greater power dependence is the result of secondary photodissociation of the primary product, FV. In any event, the greater power dependence for the 1,2 DFE made it much more difficult to

fit the primary H atom elimination. As a first approximation, it was assumed that the primary and secondary $P(E_T)$'s used in the 1,1 DFE fitting would also apply to the 1,2 DFE. Figure 7-11 shows that this works well, although not too much emphasis should be placed on this result because there are many other primary and secondary $P(E_T)$'s that could fit the TOF spectra. That the same primary $P(E_T)$ can be used to describe the H atom elimination from the 1,1 and 1,2 DFE's suggests that this process is not too affected by the presence of a F atom on the same carbon atom as the departing H. Of some significance is the fact that the 1,1 DFE secondary $P(E_T)$ rising edge fits the 1,2 DFE TOF spectrum quite well. Unless 1,2 F migration occurs, secondary H atom dissociation from the 1,2 DFE will leave DFA rather than the DFV as is produced in the 1,1 DFE secondary dissociation. The enthalpy of isomerization between the acetylene and vinylidene forms is ≈25 kcal/mole [13] so, in principle, the fast edge of the 1,2 DFE secondary $P(E_T)$ should be ~25 kcal/mole faster than the 1,1 DFE $P(E_T)$. This certainly would be seen in the TOF spectra. In addition, the predicted maximum kinetic energy (~109 + E_{int} kcal/mole) is much greater than that observed. The secondary $P(E_T)$, thus, suggests that some excited DFA is forming in the secondary dissociation and that the triplet DFA and DFV are very close in energy (as are the un-fluorinated compounds) or F migration can occur after the

vinyl radical absorbs a photon.

4. Conclusions

The 193 nm photodissociation of the DFE's provides more details about three-centered and four-centered elimination than could be obtained from the analogous ethylene experiments. The HF TOF spectra from the two isomers dramatically shows that three-centered elimination is preferred; the 1,2 DFE spectrum, where equal amounts of three and four-centered elimination are expected from statistics alone, bears little resemblance to the corresponding 1,1 DFE where 100% four-centered elimination must occur. The three-centered elimination of HF in the DFE peaks very close to 0 kcal/mole showing that the FV channel can have only a very small exit barrier. This should be compared with the three-centered elimination of H_2 in the 1,1 DFE peaked which is peaked at ~6 kcal/mole and that in ethylene at ~20 kcal/mole. This reveals the importance of the transition state and that HF elimination occurs from a looser critical complex. In addition, the DFE experiments added to what was known about photodissociation of these isomers. Although the HF elimination has been well studied [2-6], there was only one previous mention of the H atom elimination channel [3] and the H_2 elimination pathway has not been reported. Guillory and Andrews believed that the H elimination was preferred over F elimination [3]. F atoms

not from the cracking of HF were detected in the 1,2 DFE photodissociation but they did not seem consistent with simple bond rupture. Despite the fact that the C-F and C-H bond strengths are expected to be similar (108 versus 111 kcal/mole) [12], H atom elimination is greatly favored. Perhaps this indicates that the C-F dissociation energy of 111 kcal/mole is too low. The H atom elimination in the DFE's was very much like that in ethylene in that there was a large amount of secondary dissociation and the secondary fragments have only a very small percentage of the maximum possible translational energy. This suggests that the formation of an electronically excited state, most likely the lowest triplet, is occurring. The involvement of a triplet is not unexpected based on Guillory and Andrews triplet quenching studies. The elimination of H_2 in the DFE's was found to be similar to that of HF in the DFE's and of H_2 in the ethylene photolysis. The one difference, however, was that in the four-centered elimination, some H_2 + FCCF products were produced in the ground state. The reason espoused here is that there are less structural changes required to go from the transition state to the products. More information on the molecular geometries is needed to confirm this point.

The DFE studies here have raised several questions that should be further addressed. A more quantitative comparison between the various channels is needed. Detection of some

of the heavier fragments should prove whether or not F atom elimination is occurring and the exact mechanism for producing some of the secondary F and H atoms detected. Finally, with more accumulation time and the appropriate fragment choice, better estimates of heats of formation and bond strengths could be obtained.

References

1. G. Bélanger and C. Sandorfy, J. Chem. Phys. **55**, 2055 (1971).

2. O.P. Strausz, R.J. Norstrom, D. Salahub, R.K. Gosavi, H.E. Gunning, and I.G. Csizmadia, J. Am. Chem. Soc. **92**, 6395 (1970) .

3. W.A. Guillory and G.H. Andrews, J. Chem. Phys. **62**, 3208 (1975).

4. P.N. Clough, J.C. Polyanyi, and R.T. Taguchi, Can. J. Chem. **48**, 2919 (1970).

5. H. Watanabe, H. Horiguchi, and S. Tsuchiya, Bull. Chem. Soc. Jpn. **53**, 1530 (1980).

6. C.R. Quick, Jr. and C. Wittig, J. Chem. Phys. **72**, 1694 (1980).

7. M.J. Berry and G.C. Pimentel, J. Chem. Phys. **51**, 2274 (1968).

8. J.D. Goddard, Chem. Phys. Lett. **83**, 312 (1981).

9. M.J. Frisch, R. Krishnan, J.A. Pople, and P. v. R. Schleyer, Chem. Phys. Lett. **81**, 421 (1981).

10. M.J. Berry, J. Chem. Phys. **61**, 3114 (1974).

11. S. Kato and K. Morokuma, J. Chem. Phys. **74**, 6285 (1981).

12. J.M. Simmie and E. Tschuikow-Roux, J. Phys. Chem. **74**, 4075 (1970).

13. M.M. Gallo and H.F. Schaefer III, J. Chem. Phys. **93**,

865 (1990).

14. M.W. Chase Jr., C.A. Davies, J.R. Downey Jr., D.J. Frurip, R.A. McDonald, and A.N. Syverud, JANAF Thermochemical Tables, Third Edition (Journal of Physical and Chemical Reference Data, New York, 1986).

15. C.L. Yaws and P.-Y. Chiang, Chem. Engineering **95**(43), 81 (1988).

16. K.M. Ervin, S. Gronert, S.E. Barlow, M.K. Gilles, A.G. Harrison, V.M. Bierbaum, C.H. DePuy, W.C. Lineberger, and G.B. Ellison, J. Am. Chem. Soc. **112**, 5750 (1990) and references therein.

17. Aa. S. Sudbø, P.A. Schulz, E.R. Grant, Y.R. Shen, and Y.T. Lee, J. Chem. Phys. **70**, 912 (1979).

Tables

Table 7-1. Earliest Expected Photofragment Arrival Times for Energetically Accessible Channels.

Product	E_T Max.	Lab Velocity (10^4 cm/s)	Arrival Time (μsec)
H_2	40	127	34
H_2	66	164	27
CCF_2	40	(1)	(1)
FCCF	66	2	2335
F_2	16	11	374
HCCH	16	17	245
HF	66	44	100
HF	106	55	82
CCHF	66	19	219
HCCF	106	25	174
F	37	33	127
FC_2H_2	37	13	307
H	40	182	24
HC_2F_2	40	(1)	(1)
CH_2	24	33	127
CF_2	24	8	509

(1) COM product velocity is less than the parent DFE velocity so no product can be detected perpendicular to the parent beam.

Figure Captions

Figure 7-1. Thermodynamic diagram showing the energy levels of possible products from the 193 nm (148 kcal/mole) photodissociation of DFE. For the most part, the values are quite uncertain (± 5-15 kcal/mole) so the 1,1 and 1,2 DFE isomers have been grouped together.

Figure 7-2. H_2 TOF spectrum from the photolysis of 1,1 DFE. The scan represents 6.6 hrs counting time at an average laser power of 90 mJ/pulse. The open circles show the data and the solid line is the fit calculated using the $P(E_T)$ in Figure 7-4 (solid line).

Figure 7-3. H_2 TOF spectrum from the photolysis of 1,2 DFE. The scan represents 4.7 hrs counting time at an average laser power of 90 mJ/pulse. The open circles show the data and the solid line is the fit calculated using the $P(E_T)$ in Figure 7-4 (dashed line). The figure shows the rise in signal after ~100 μsec that is attributed to thermalized H_2 from the photolysis chamber.

Figure 7-4. $P(E_T)$'s for the DFE → H_2 + C_2H_2 channel. The solid line shows the distribution used to fit the H_2 TOF spectrum from the 1,1 DFE photolysis (Figure 7-2) which is expected to be a three-centered elimination of

H_2 to give difluorovinylidene. The dashed line is the distribution used to fit the 1,2 DFE photolysis to give H_2 (Figure 7-3); this elimination should be a four-centered process.

Figure 7-5. HF TOF spectrum from the photolysis of 1,1 DFE. This scan represents 3.3 hrs accumulation time at an average laser power of 60 mJ/pulse. The open circles show the data and the solid line is the best fit obtained using the $P(E_T)$ shown in Figure 7-7 (solid line).

Figure 7-6. HF TOF spectrum from the photolysis of 1,2 DFE. This scan represents 0.6 hrs counting time at an average laser power of 80 mJ/pulse. The open circles show the data and the solid line is the best fit using the $P(E_T)$ shown in Figure 7-7 (dashed line).

Figure 7-7. $P(E_T)$'s used to fit the DFE $\rightarrow$ HF + C_2HF channel. The solid line shows the distribution used to fit the 1,1 DFE photolysis (Figure 7-5). The dashed line shows the distribution used to fit the 1,2 DFE photolysis (Figure 7-6).

Figure 7-8. F atom TOF spectrum from the photolysis of 1,1 DFE. The scan was accumulated over 2.2 hrs at an

average laser power of 80 mJ/pulse. The open circles show the data and the solid line is the calculated spectrum using the 1,1 DFE → HF + C_2HF $P(E_T)$ shown in Figure 7-7 (solid line). The agreement shows that the F atoms observed are from the dissociative ionization of HF in the detector.

Figure 7-9. F atom TOF spectra from the photolysis of 1,2 DFE at two laser powers. The spectrum in (a) shows the low power scan which was accumulated for 0.6 hrs at an average laser power of 40 mj/pulse. The spectrum in (b) shows a high power scan which represents 0.3 hrs of counting at an average laser power of 120 mJ/pulse. The open circles in both spectra are the data. The dashed line shows the expected F atom TOF spectra from the dissociative ionization of HF (1,2 DFE → HF + C_2HF) using the $P(E_T)$ in Figure 7-7 (dashed line).

Figure 7-10. H atom TOF spectra from the photolysis of 1,1 DFE at two different laser powers. The spectrum in (a) shows the lower power scan accumulated for 1.2 hrs at an average laser power of 25 mJ/pulse. The spectrum in (b) is the high power scan which represents .6 hrs counting time at an average laser power of 70 mJ/pulse. The open circles show the data. The solid line shows the total fit. The dashed line represents the

contribution from the dissociative ionization of HF, calculated using the $P(E_T)$ in Figure 7-7 (solid line). The -···- line shows the primary H atom TOF spectrum (1,1 DFE → H + $HCCF_2$) calculated using the $P(E_T)$ in Figure 7-12. The -·- line shows the secondary H atom TOF spectrum ($HCCF_2$ → H + C_2F_2) calculated using the $P(E_T)$ in Figure 7-13 and assuming that all the C_2F_2H has an equal probability of absorbing a photon and dissociating.

Figure 7-11. 1,2 DFE high and low power H atom TOF spectra. The spectrum in (a) was accumulated over 0.8 hrs at an average laser power of 45 mJ/pulse. The spectrum in (b) was taken for 0.3 hrs at an average laser power of 130 mJ/pulse. The open circles show the data and the solid line is the total fit. The dashed line shows the H atom contribution from the dissociative ionization of HF calculated using the 1,2 DFE → HF + C_2HF $P(E_T)$ in Figure 7-7. The primary (-···-) and secondary (-·-) H atom contributions have been calculated using the same $P(E_T)$'s used to fit the 1,1 DFE H atom TOF spectra in Figure 7-10 (see Figures 7-12 and 7-13).

Figure 7-12. The $P(E_T)$ for the primary H atom elimination (DFE → H + C_2F_2H) used to fit both the 1,1 and 1,2 DFE H atom TOF spectra in Figures 7-10 and 7-11.

Figure 7-13. The $P(E_T)$ for the secondary H atom elimination, $C_2F_2H \rightarrow H + C_2F_2$, used to fit the 1,1 and 1,2 DFE H atom TOF spectra in Figures 7-10 and 7-11. It was calculated assuming that all the C_2F_2H created have an equal probability of absorbing a second photon.

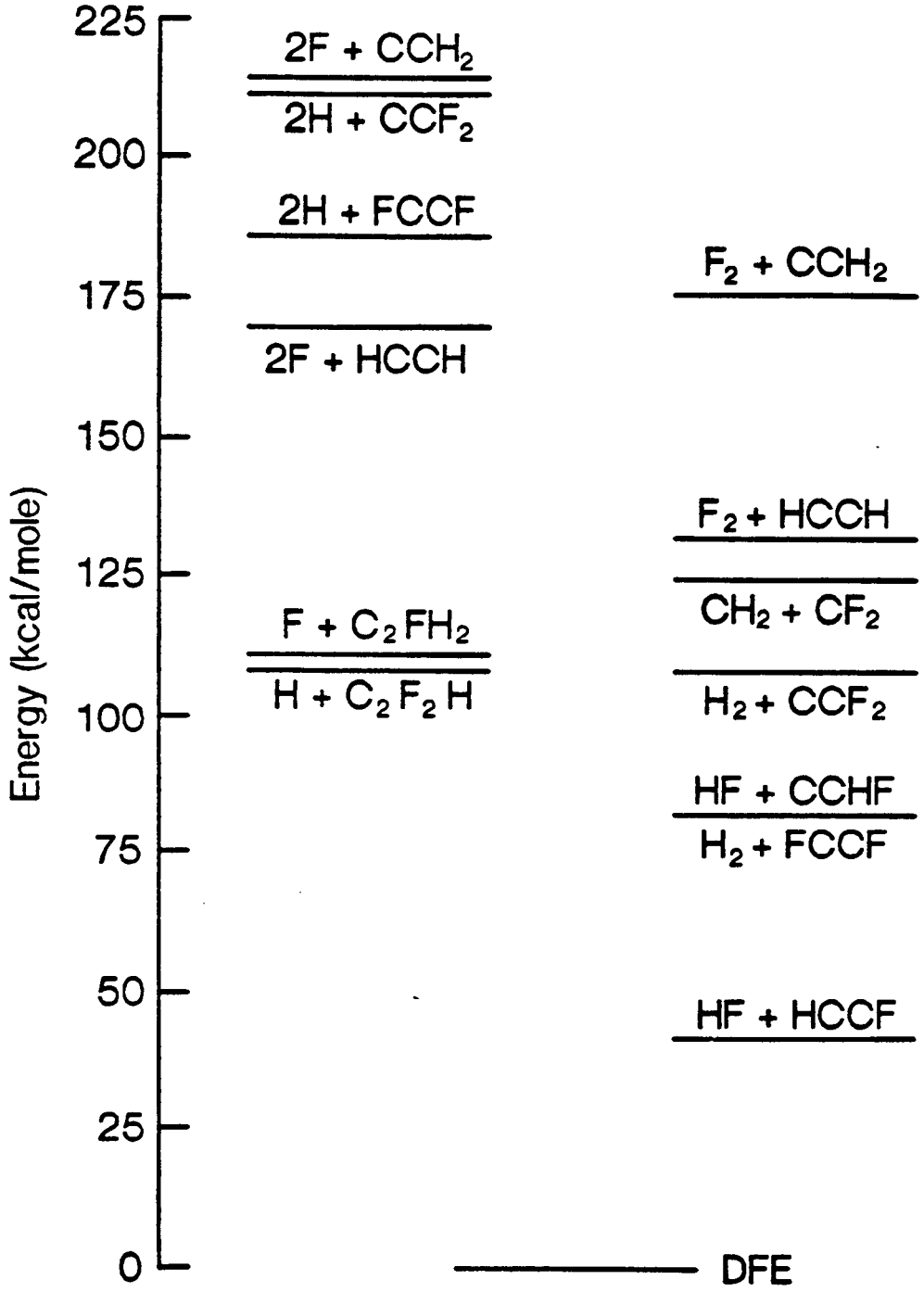
225
200
175
150
125
100
75
50
25
0
Energy (kcal/mole)
2F + CCH2
2H + CCF2
2H + FCCF
2F + HCCH
F + C2FH2
H + C2F2H
F2 + CCH2
F2 + HCCH
CH2 + CF2
H2 + CCF2
HF + CCHF
H2 + FCCF
HF + HCCF
DFE

Figure 7-1

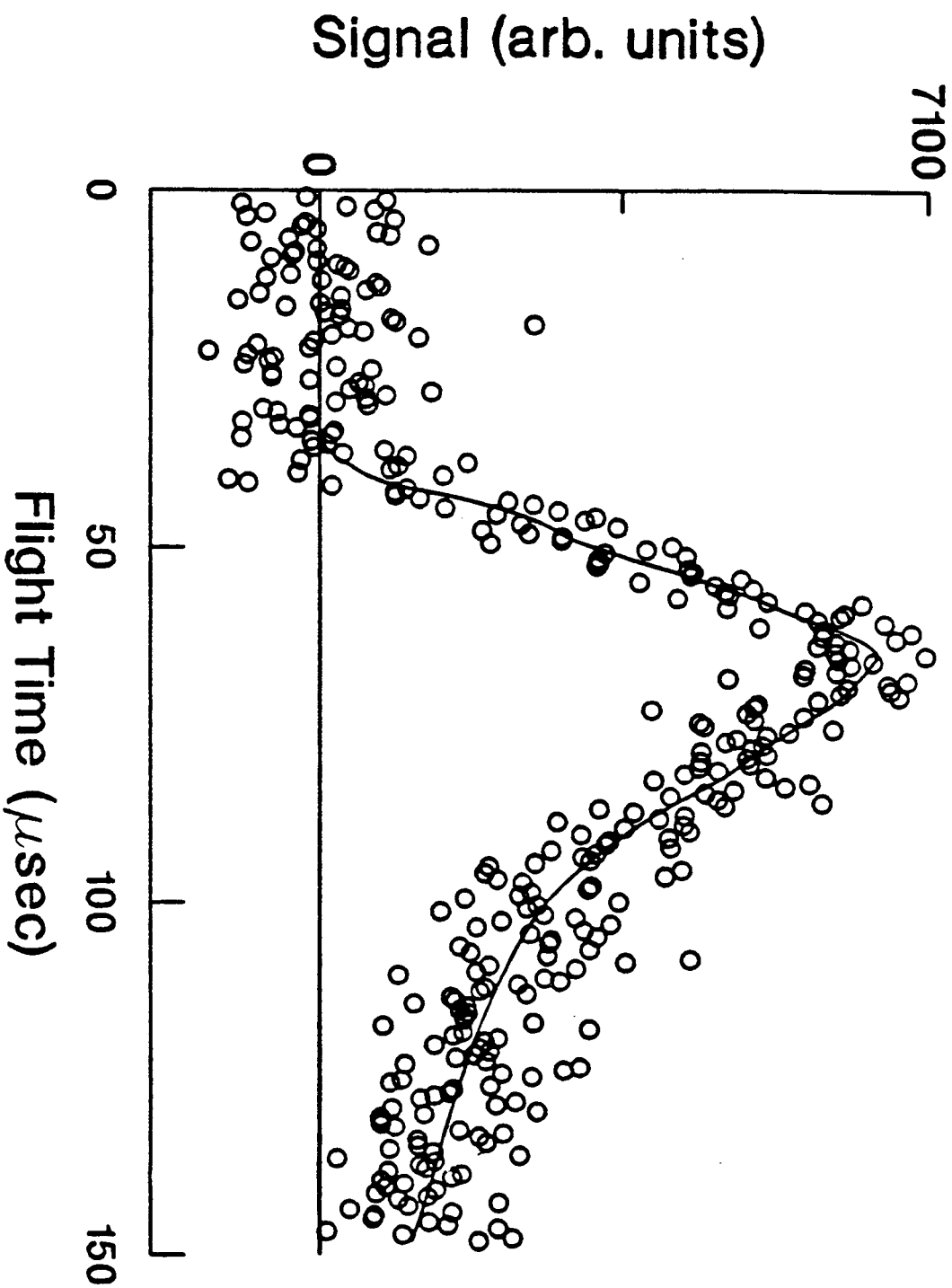

Figure 7-2

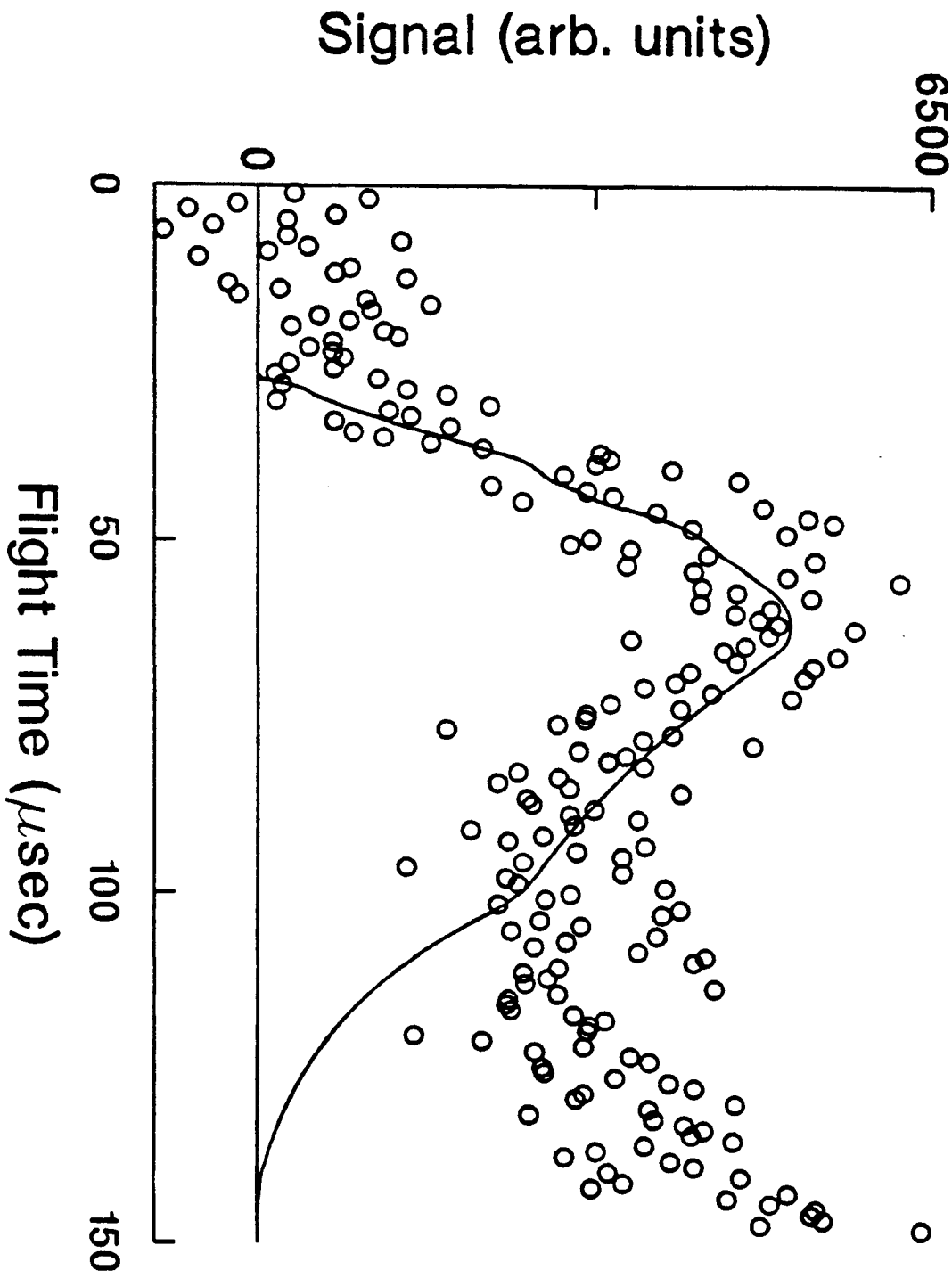

Figure 7-3

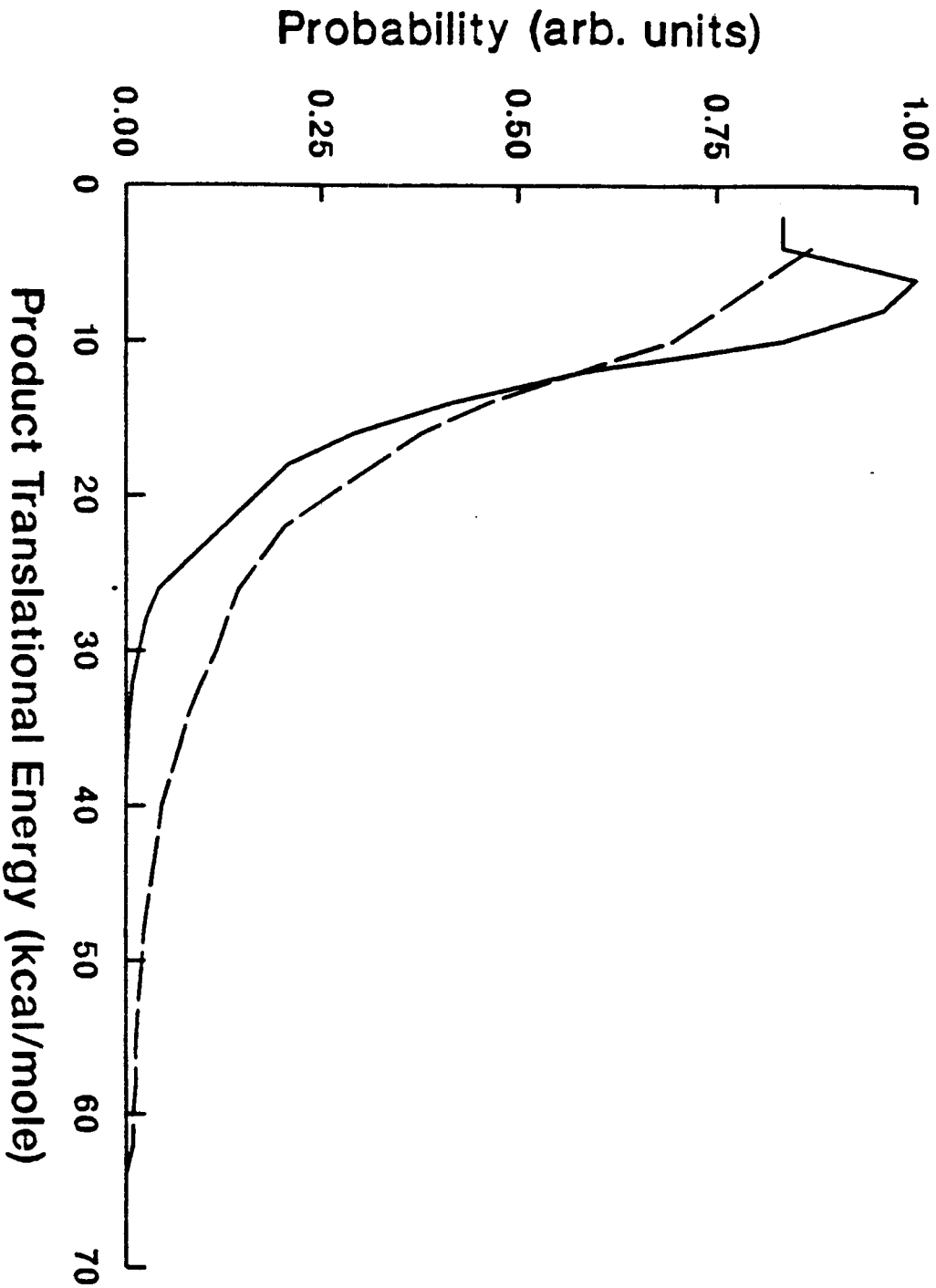
Probability (arb. units)
0.00
0.25
0.50
0.75
1.00
0
10
20
30
40
50
60
70
Product Translational Energy (kcal/mole)

Figure 7-4

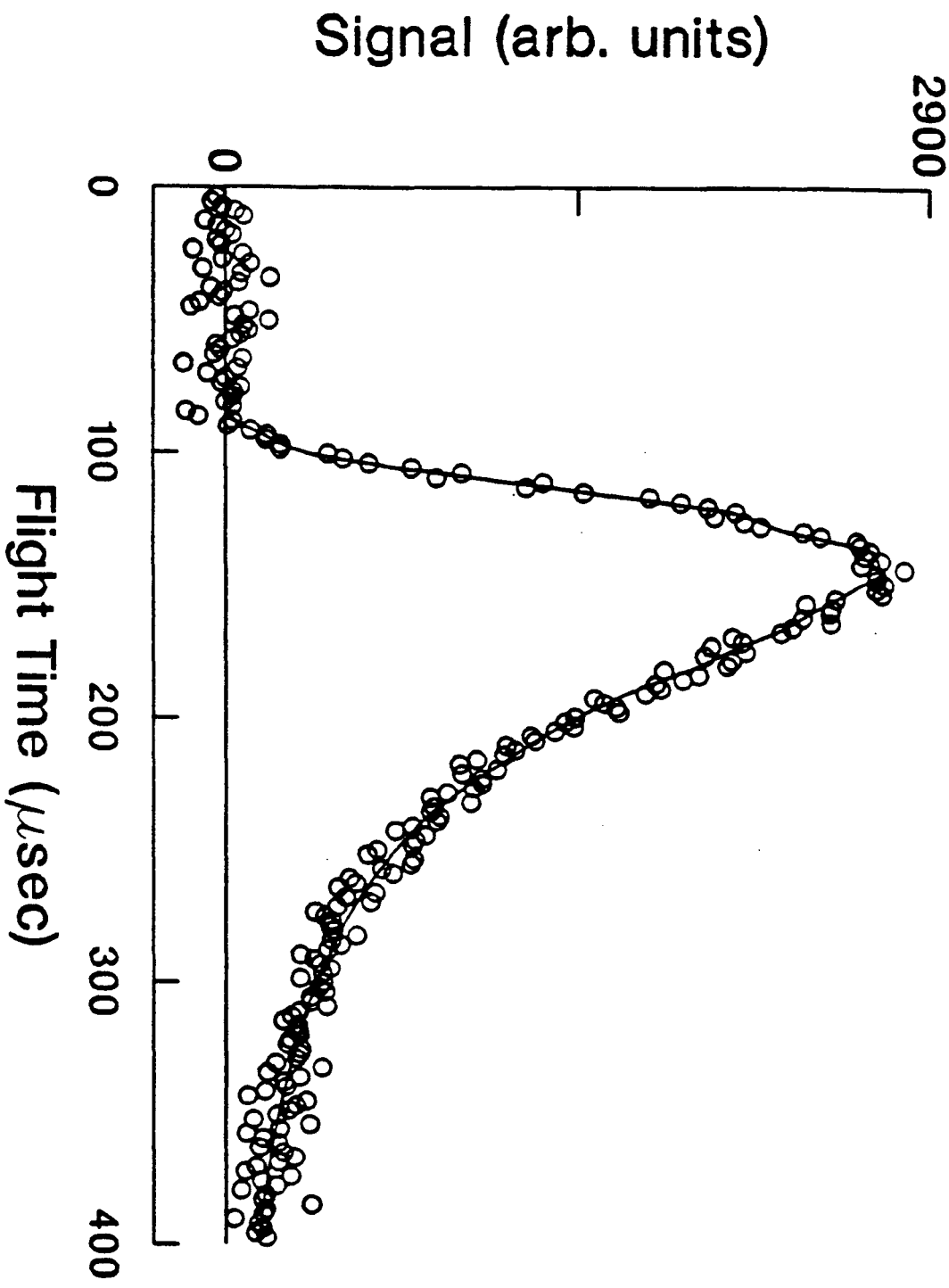

Figure 7-5

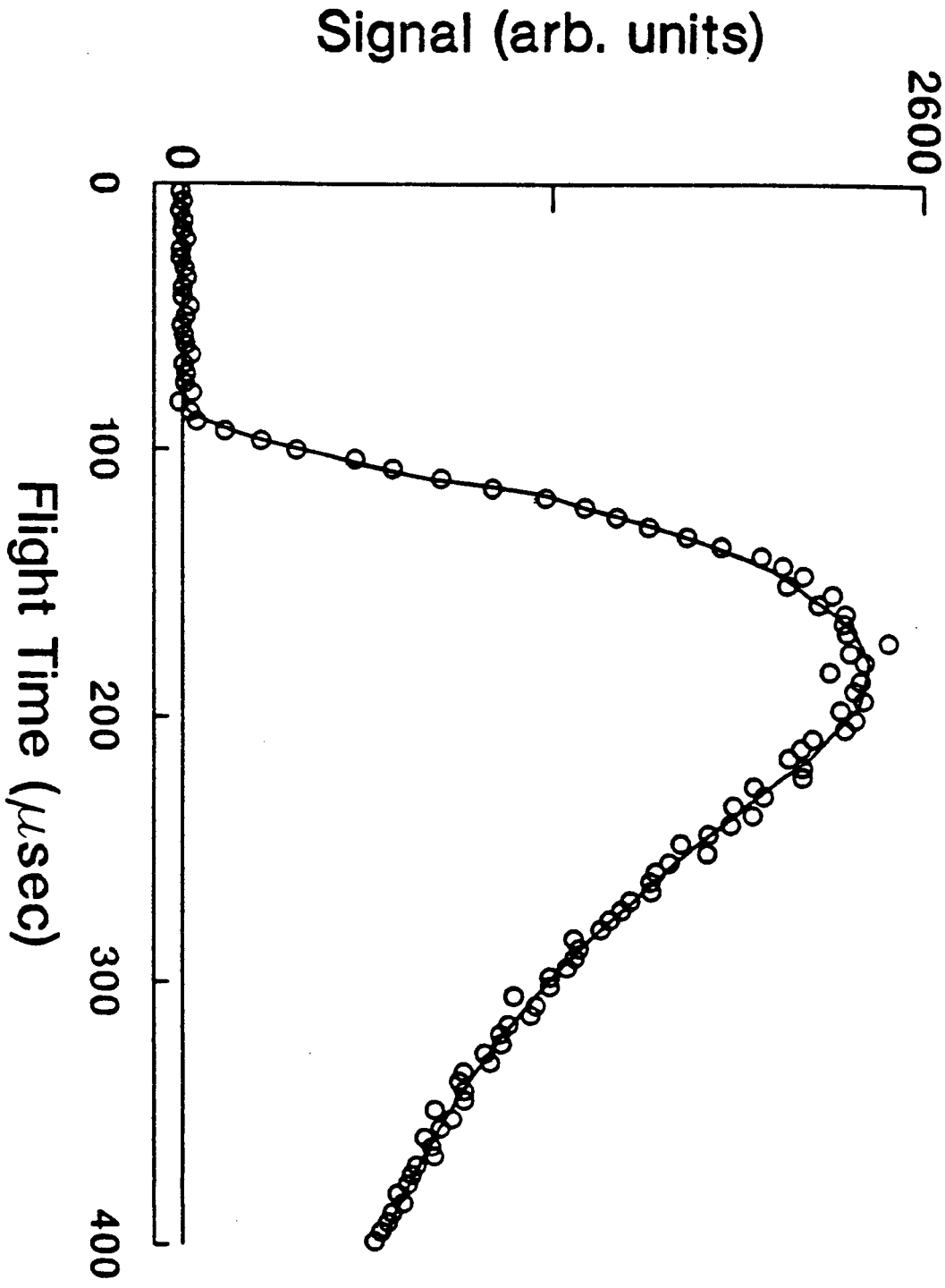

Figure 7-6

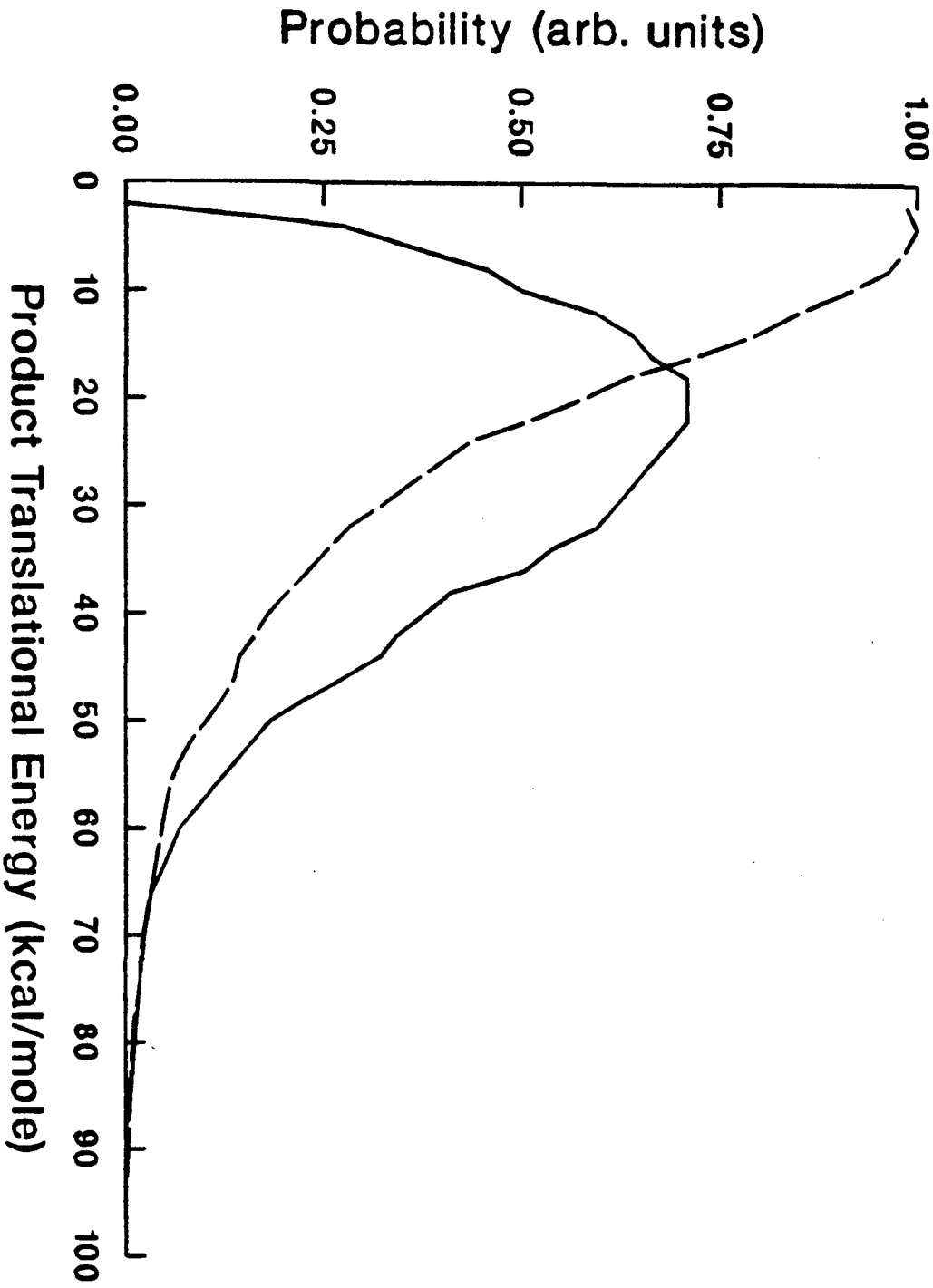
Probability (arb. units)
0.00
0.25
0.50
0.75
1.00
Product Translational Energy (kcal/mole)
0
10
20
30
40
50
60
70
80
90
100

Figure 7-7

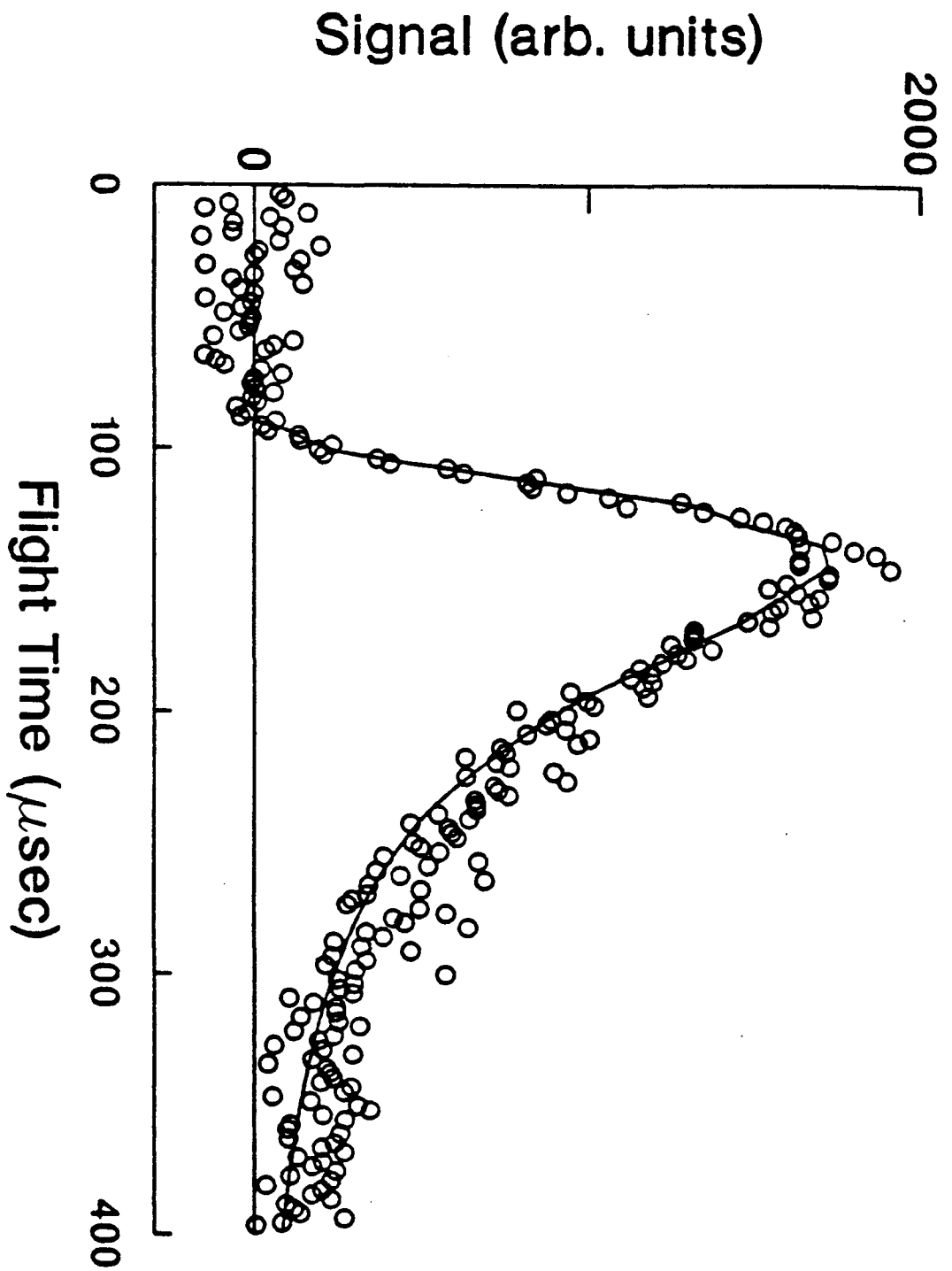

Figure 7-8

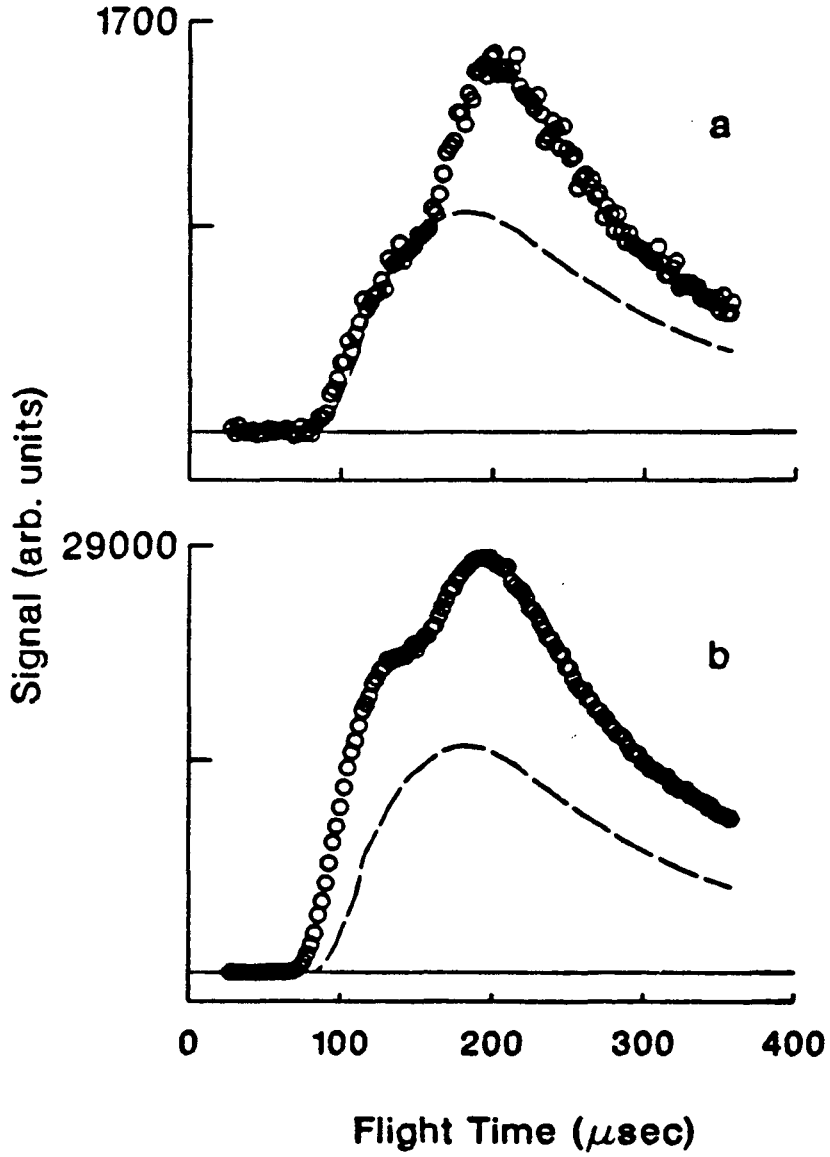
1700
a
29000
b
Signal (arb. units)
0
100
200
300
400
Flight Time (μsec)

Figure 7-9

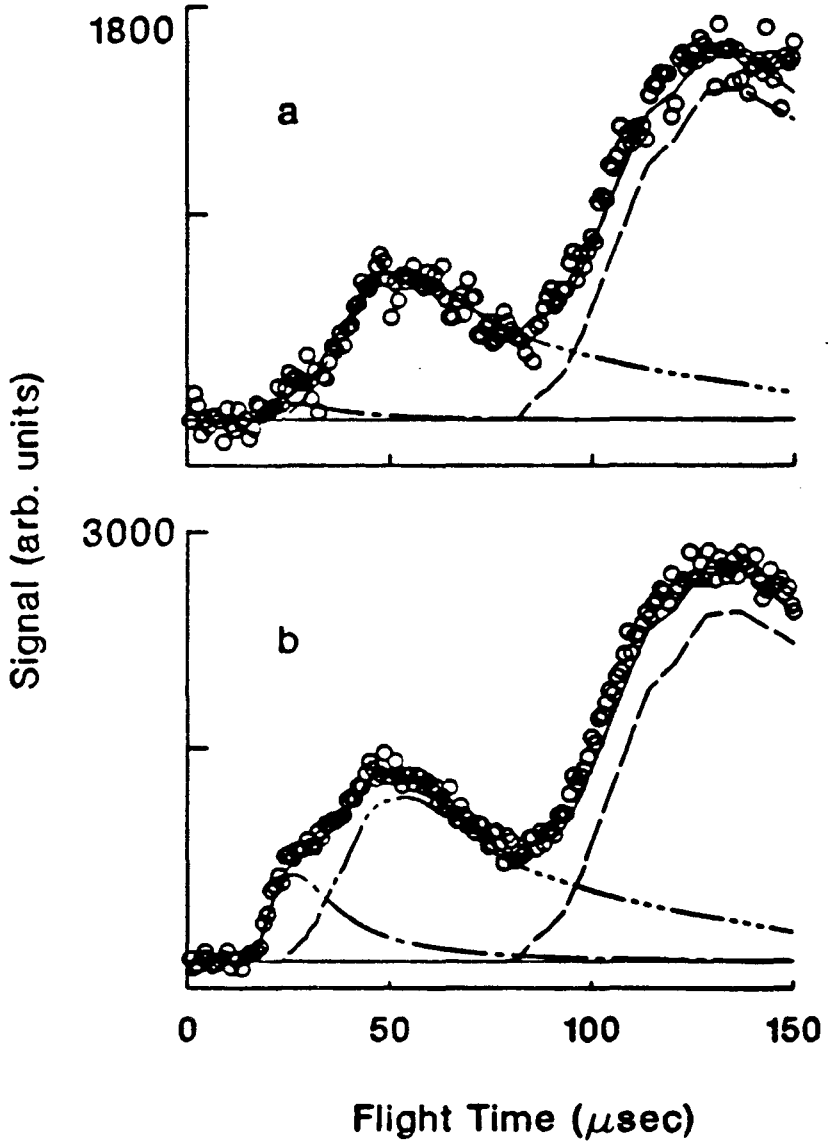

Figure 7-10

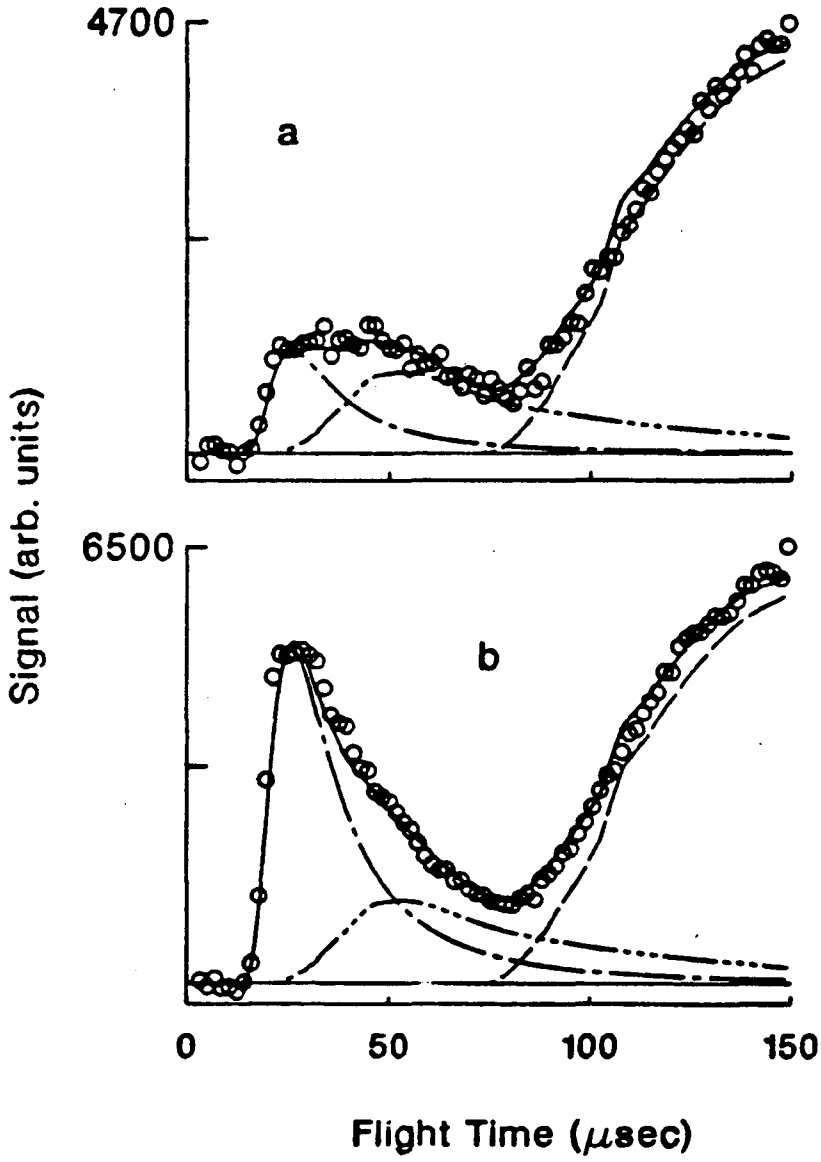

Figure 7-11

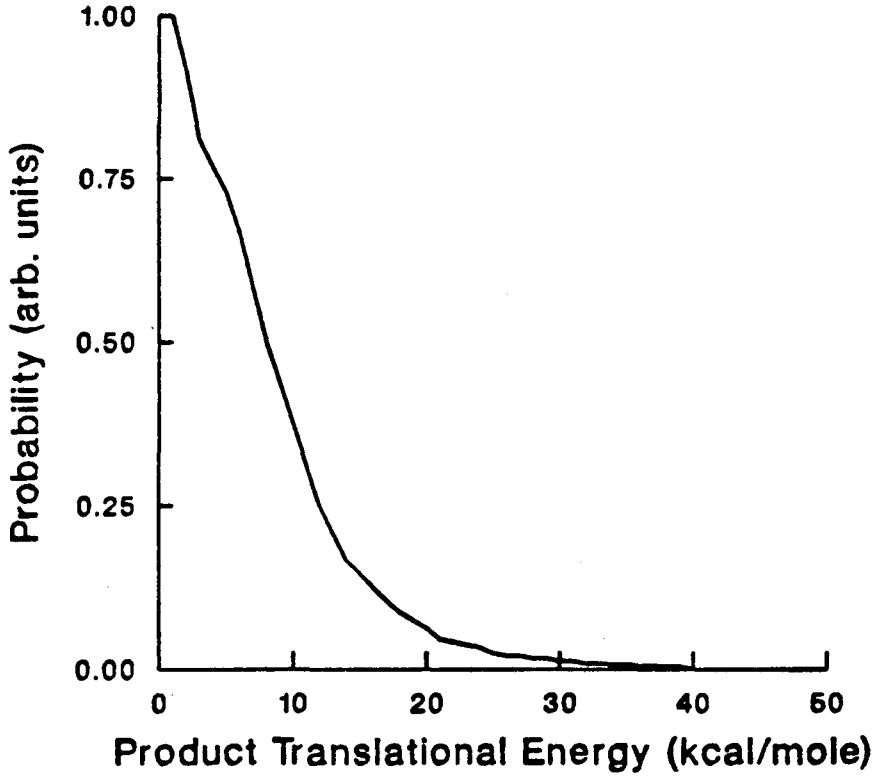
1.00
0.75
0.50
0.25
0.00
Probability (arb. units)
0
10
20
30
40
50
Product Translational Energy (kcal/mole)

Figure 7-12

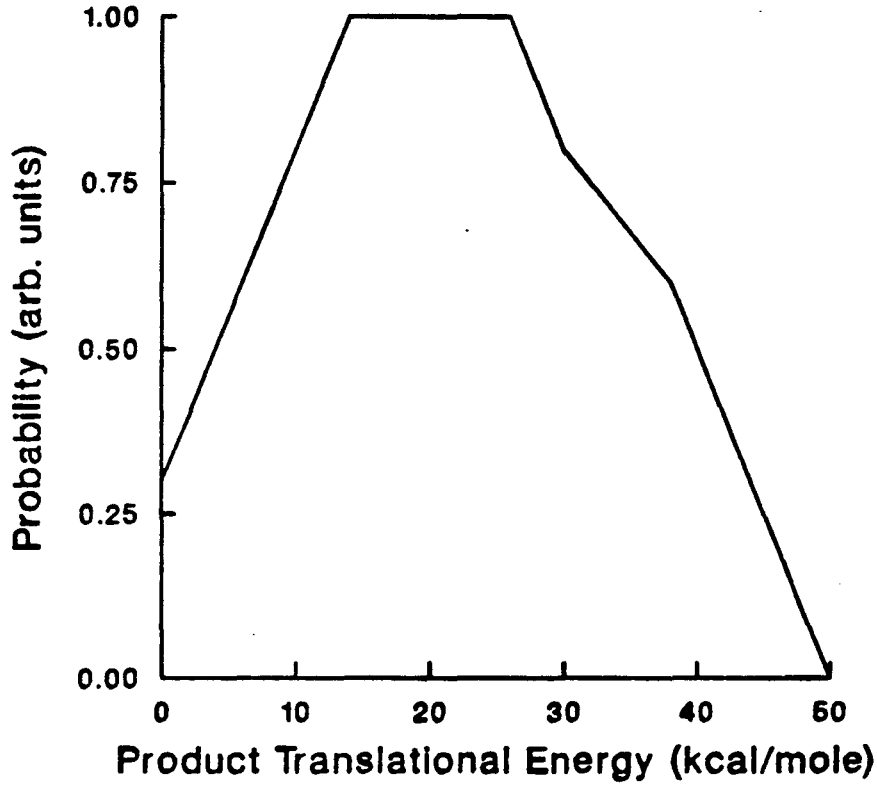
1.00
0.75
0.50
0.25
0.00
Probability (arb. units)
0
10
20
30
40
50
Product Translational Energy (kcal/mole)

Figure 7-13

LAWRENCE BERKELEY LABORATORY
UNIVERSITY OF CALIFORNIA
INFORMATION RESOURCES DEPARTMENT
BERKELEY, CALIFORNIA 94720